Loughborough University

Plasticisation Effects of High-Pressure Carbon Dioxide on Polymers

By

Salah T. Al-Enezi

A Doctoral Thesis Submitted In Partial Fulfilment of the Requirement for the Award of the Doctor of Philosophy of Loughborough University

June 2008

Loughborough University

Plasticisation Effects of High-Pressure Carbon Dioxide on Polymers

By

Salah T. Al-Enezi

A Doctoral Thesis Submitted In Partial Fulfilment of the Requirement for the Award of the Doctor of Philosophy of Loughborough University

June 2008

Abstract

This thesis examines the effects derived from the ability of high pressure carbon dioxide to soften polymers. This has potential applications in the shape forming of polymers at lower temperatures, dye impregnation and the foaming of polymers. This study was conducted in two parts: (i) mechanical measurement of polymer softening under CO_2 at high pressure, and (ii) foaming behaviour of polymers containing dissolved CO_2 during depressurisation. In the first study the softening of polymers as a function of applied CO_2 pressure and temperature was measured using a novel mechanical 3-point bend test rig. In initial experiments the temperature was slowly ramped upwards and the nominal glass transition temperature was recorded as where the central deflection suddenly begins to increase. Significant reductions in the bending onset temperatures were observed on the application of CO_2 for polycarbonate, poly(methyl-methacrylate), glycol modified poly(ethylene-terepthalate) and polystyrene, of typically 50 - 100 °C over the range of pressures applied (24 to 120 bar). The temperatures at which large scale deflection occurred were significantly higher than the onset point and this was attributed to the time taken for CO_2 to diffuse into the polymer. A model was developed to use onset and full-scale bending temperatures to estimate diffusion coefficients, assuming that full-scale bending corresponded to the centre of the strip being sufficiently plasticised by CO_2 to become rubbery. Diffusion coefficients produced by the model were of a similar order of magnitude to literature values obtained by more conventional methods. Further isothermal experiments were then performed to track the central deflection as CO_2 diffuses into the polymer. An equation for deflection versus time was derived from a diffusion analysis where it was assumed that the stiffness of the strip was only due to the glassy core region which gradually reduces in thickness as the CO_2 penetrates the strip. Diffusivities derived from this method were slightly higher than from the scanning experiments. In the second study polymer foaming was investigated using cylindrical high pressure view cell with 2 optical widows. This study differs from previous published work in that conditions were chosen to be near the glass transition temperature (T_g) of the polymer. Foaming was not observed when the polymer was initially at conditions below T_g, but was observed for initial conditions above the T_g. It was also found that more extensive foaming occurred at higher temperatures (100 °C versus 70 °C) despite less CO_2 being originally absorbed in the sample. This was attributed to lower viscosities and higher diffusivities at the higher temperature. The radius of bubbles was measured with time and the results compared against models for bubble growth. Best fits were obtained with a model where the local diffusivity and viscosity varied according to the Williams-Landel- Ferry equation, and with T_g values corresponding to the local CO_2 concentration.

Acknowledgements

This report would not have been possible without the help of God (Allah) and support of many people.

First and foremost, I would like to express my sincere and deepest gratitude to Dr. Andrew Stapley for his dedicated and excellent supervision which includes the invaluable advice, discussion, co-operation, guidance and most of all for being very understanding for my situation as student and a father at the same time.

I would like to take this opportunity to show my appreciation and deep thanks to Dr. Klaus Hellgardt and Dr. Iain Cumming who has been supportive and helpful. And also would like to extend my thanks to Mr. Chris Manning for his help and support.

I also wish to extend my gratitude to the Kuwait Institute for Scientific Research, for granting me the scholarship to pursue my PhD.

I would also like to thank my parents and last but not least, like to deepest gratitude and indebted to my wife (Ragheda Al-Shatti) and my children (Ghaida, Dana, Yousef, Mohammad, Durar and Sunan) who gave me the love, encouragement and support throughout the years of my study.

Table of Contents

List of Tables

Page

List of Figures

Page

Chapter 1 Introduction

1 Introduction

Plasticisers are commonly used in polymer processing as they lower the glass transition (softening) temperature of polymers to allow shape forming at lower temperatures. A plasticiser is a substance which when added to an amorphous material, such as amorphous polymers, makes it more flexible and easier to handle by lowering the glass transition temperature. The ability of carbon dioxide at high pressure to act as a plasticiser of certain synthetic polymers has been well documented in the literature. The non-toxic nature of supercritical carbon dioxide ($scCO_2$) and its ability to swell and plasticise polymers makes it ideal for extraction, polymerisation and processing of polymeric materials, including mechanical foaming, polymer foaming and dye impregnation. When CO_2 is incorporated into the polymer matrix it must, to be effective, interpose itself between the polymers chains, then interact with the forces, which hold the polymer chains together. The significant interactions are those due to dispersion and induction interactions, hydrogen bonding and chain entanglements.

The thermodynamics of polymer-gas mixtures, polymer supercritical fluid interaction, and the theory of glass transition in polymers induced by supercritical fluids and high-pressure gases has received much attention in recent years. The sorption of carbon dioxide and plasticisation effect on polymers has been investigated using a variety of techniques such as Fourier Transform infrared (FTIR) spectroscopy, differential scanning calorimetry (DSC) and gas sorption/gas permeation techniques. It is typically found that the application of pressures of the order of 30 bar will depress the glass transition (T_g) by slightly over 1K for each bar of applied pressure of carbon dioxide. Few studies have directly examined the effect of carbon dioxide on the mechanical properties of polymers. Mechanical properties are of prime importance when plasticisation is used as an aid to extrusion or other shape forming processes, and so if plasticisation is to be an effective for shape forming polymers the effect also needs to be demonstrated mechanically. In addition most work to date has taken place at relatively low pressures (around 40 bar).

The core of this research project is to study the behavior of polymers processing with pressure levels reaching a maximum of 120 bar of CO_2 and a maximum temperature of 160 °C. This thesis presents a novel processing of polymers subjected to high-pressure carbon dioxide and it consist of two main studies; "Polymer softening" and "Polymer foaming". In the first part of this thesis the softening temperature of four polymers is studied as a function of applied carbon dioxide pressure using a linear variable displacement transducer (LVDT) to continuously monitor the deflection of a polymer strip undergoing 3-point bending test. Four polymers were tested: polycarbonate (PC), poly(methyl-methacrylate) (PMMA), glycol modified poly(ethylene-terepthalate) (PETG) and polystyrene (PS). The main purpose is to measure how the deflection varies as a function of temperature and time for various pressures of CO_2 under isothermal and non-isothermal conditions, the nominal glass transition temperature was recorded as the onset temperature where the central deflection suddenly begins to increase. The experimental data is interpreted using deflection model that includes the diffusion of CO_2 into the polymer strip as the major factor influencing the bending behaviour. At the end of the LVDT experiments it was noticed that bubbles had formed within the samples. This prompted a second investigation into polymer foaming.

Bubble formation and foaming is caused by CO_2, previously dissolved in the polymer under pressure, to be released upon depressurisation. This has been well reported in the literature and a number of models for bubble growth have been presented. However relatively few experimental studies have been performed, and these have all taken place using polymer melts at high temperature (140 – 200 °C). It was therefore decided to study this topic further at lower temperature; beginning with observations of the samples removed from the LVDT experiments and then continuing by observing bubble formation *in situ* using a specially constructed high pressure view cell with 2 optical widows, connected to a digital still camera with a high magnification lens (60 mm) to monitor and record the bubbles growing. The experimental data are analysed by measuring bubble radii at different times during depressurisation using image analysis software. The experimental data of bubble growth is interpreted using various bubble growth models.

1.1 Objective

The main theme of this thesis is to understand and describe the interaction of CO_2 with polymers at elevated pressures in an engineering context. The specific objectives are as follows:

1. Measure the softening of polymers using direct mechanical measurement under CO_2 at high pressure.
2. Interpret the experimental data for non-isothermal (constant heating rate) and isothermal data using appropriate mathematical models.
3. Observe *in situ* the formation of bubbles in polymers in the rubbery regime under depressurization conditions (conditions that can typically be expected for extruders).
4. Model bubble growth at these conditions.

1.2 Structure of the Thesis

Chapter 2 Literature Review:

In this chapter a literature search is presented with regards to the following topics relevant to this study: the properties of carbon dioxide, the glass transition temperature in polymers, the interaction of carbon dioxide with polymers, and polymer foaming. This includes previous studies concerning the measurement of the plasticisation of polymers by high-pressure carbon dioxide. Published values of solubility and diffusion coefficient of carbon dioxide with various polymers are presented to support the modelling work later in this thesis. Finally, bubble growth models presented in the literature are discussed.

Chapter 3 Experimental Apparatus, Methods and Materials:

This chapter presents details of the two specially constructed cells used for the experiments described in this thesis. The first cell tests the softening temperature of polymers as a function of applied CO_2 pressure using a novel mechanical device, equipped with a linear variable-displacement transducer (LVDT) to continuously monitor the deflection of a polymer strip undergoing 3-point bending test. The cell is described both before and after modifications which were made halfway through the project in order to improve the accuracy and temperature response. The second cell is used to study bubble formation and polymer foaming on depressurisation using a special cylindrical view cell with 2 optical widows, linked to a digital still camera with high magnification lens to monitor and record the bubble growth. Also described are the four polymer materials which were selected (PC, PS, PETG and PMMA) which had appropriates properties over the pressure and temperatures used in the experiments.

Chapter 4 Derivations of the Mathematical Models Used:

This chapter presents the mathematical models that are used to help interpret the experimental data presented in later chapters. The polymer softening (3 point bend test) experiments are interpreted using deflection models that assume that the major factor influencing the deflection versus time profile is the diffusion of carbon dioxide into the sample. The carbon dioxide is considered to plasticise the polymer into the rubbery state above a critical concentration. The outer regions of the sample where the carbon dioxide exceed this critical concentration is assumed to have negligible stiffness. Models are developed for applying to non-isothermal (steady heating rate) and isothermal experiments.

Three models are presented for describing the growth of bubbles during polymer foaming. These models have a similar basis but differ in the assumptions made.

(i) Bubble growth is controlled only by the rate of diffusion of CO_2 into the bubble.

(ii) Bubble growth is also controlled by the extensional viscosity of the polymer (assumed constant) which requires the bubble pressure to rise above the external pressure for expansion to occur.

(iii) Bubble growth is again controlled by both diffusion and viscosity but these coefficients are varied according to the local concentration of CO_2 in the polymer and the Williams–Landel–Ferry (WLF) equation.

Chapter 5: Mechanical Measurement of Polymer Softening:

This chapter presents experimental data for polymer softening using the 3 point bend test rig. The nominal glass transition temperature was recorded as the onset temperature where the central deflection suddenly begins to increase. A first series of experiments are described in which PC, PS, PETG and PMMA samples at various CO_2 pressures are heated at a constant rate using the rig. This is followed by similar experiments on PS and PMMA after modifications to the cell to improve accuracy. The final set of experiments relate to isothermal studies using samples of PS. All the results and the measurements are compared and discussed with published data, and interpreted with the aid of the diffusion based deflection models detailed in Chapter 4.

Chapter 6 Mechanical Measurement of Polymer Foaming:

This chapter describes the experiments on polymer foaming with CO_2 and the effect of processing conditions on bubble growth. Initial investigations focus on the appearance of samples produced after depressurisation of the 3-point bend test samples. However, in order to develop a more complete understanding of bubble foaming and growth, experiments are performed in which these processes could be observed as they occur. Theses experiments are carried out in the view cell described in chapter 3 section 3.4. Photographs of specimens during different stages of the experiment are analysed using image analysis software to provide data for bubble radius versus time. In these sets of experiments only one polymer (PS) is tested to enable a more extensive study of the effect of process variables to be made. All the results and the measurements are compared and discussed with published data, and interpreted with the three bubble growth models detailed in Chapter 4.

Chapter 7 Conclusions & Recommendations:

In this chapter, overall conclusions are given, and recommendations for future work are discussed.

Chapter 2 Literature Review

2 Introduction

The most important phase change in amorphous polymer processing is the glass transition. A plasticiser (e.g. CO_2) is a substance which when added to an amorphous material, usually an amorphous polymer, makes it more flexible and easier to handle by lowering the glass transition temperature. It has been recognised for many years that the sorption of carbon dioxide results in a strong plasticisation effect on several polymers. Supercritical carbon dioxide has the ability to swell and plasticise the polymers and this makes it ideal for the extraction, polymerisation and processing of polymeric materials and many new developments have arisen out of this use of carbon dioxide. Therefore, there is a very real need to understand how supercritical carbon dioxide interacts with polymeric materials and how it may modify process operations.

In this chapter a wide literature search is conducted with regards to the following topics relevant to this study; supercritical carbon dioxide, glass transition temperature in polymers, interaction of carbon dioxide / polymers, and polymer foaming. This includes previous studies concerning the measurement of the plasticisation of polymers by high-pressure carbon dioxide. Published values of solubility and diffusion coefficient of carbon dioxide with various polymers are presented to support the modelling work later in this thesis. Finally, bubble growth models relevant to polymer foaming by carbon dioxide are discussed.

2.1 Carbon Dioxide

Carbon dioxide (CO_2) is odourless, colourless gas. Carbon dioxide is a small but important constituent of air. Exhaled air contains as much as 4% carbon dioxide. Carbon dioxide is a multipurpose material, being valued by various users for its inertness and coldness if used as dry ice. CO_2 is also non-toxic, non-flammable, non-corrosive and inexpensive. Common uses include fire extinguishing systems; carbonation of soft drinks; freezing of food products such as poultry, meats, vegetables and fruit; chilling of meats prior to grinding; refrigeration and maintenance of ideal atmospheric conditions during

transportation of food products to market; enhancement of oil recovery from oil wells; a raw material for the production of various chemicals and treatment of alkaline water. CO_2 has many commercial uses with new applications continually being created. While CO_2 may be used in either a gas, liquid, solid and supercritical fluid in a given application, it is typically converted into liquid form at approximately 250 to 300 psig (1.76 – 2.6 MPa) for economical storage and transportation. Some CO_2 is obtained from the combustion of coke or other carbon-containing fuels [Eaves 2004].

2.1.1 Properties of CO_2

Some properties of CO_2 are listed bellow in Table 2 - 1, and the phase diagram is shown in Figure 2- 1.

Table 2 - 1: Propertes of CO_2 [Eaves 2004].

Chemical Formula	CO_2
Molecular weight (kg/kmol)	44.0
Sublimation point at 1 bar, °C	-78.3
Critical temperature, °C	31.1
Critical pressure, Bar	74

The phase diagram shows the areas where carbon dioxide exists as a gas, liquid, solid or as a supercritical fluid (SCF). The curves represent the temperatures and pressures where two phases coexist in equilibrium (at the triple point, all three phases coexist). The gas-liquid equilibrium curve is known as the boiling curve. If we move upwards along the boiling curve, increasing both temperature and pressure, then the liquid becomes less dense due to thermal expansion and the gas becomes denser as the pressure rises, this can be seen in Figure 2 - 2. Finally, the densities of the two phases converge and become identical, the distinction between gas and liquid disappears, and the boiling curve ends at the critical point. Supercritical fluids are materials that are above their critical point temperature and pressure. For carbon dioxide this occurs at a temperature of 31.1 °C and a pressure of 74 bar [Taylor 1996].

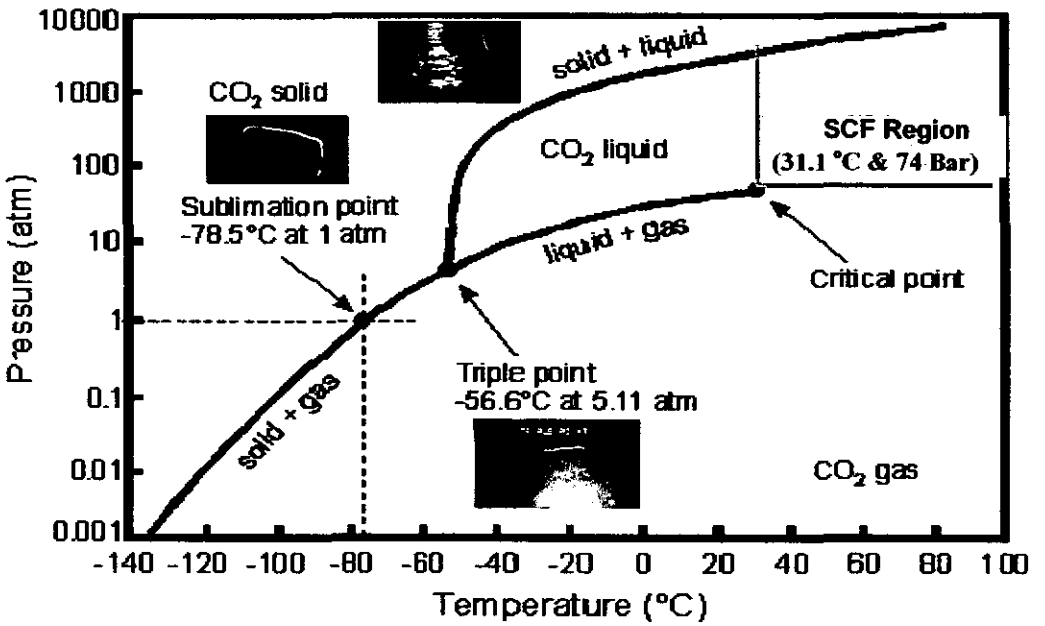

Figure 2 - 1: Phase diagram for CO_2 [Taylor 1996].

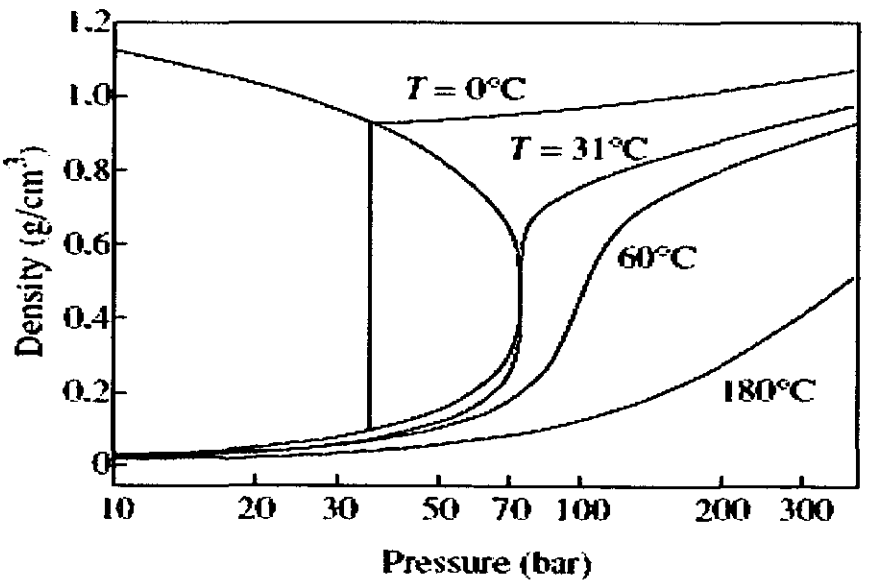

Figure 2 - 2: Variation of density with pressure and temperature [Kazarian 2000].

Carbon dioxide does not exist in the liquid form at atmospheric pressure at any temperature. The pressure-temperature phase diagram of CO_2 shows that carbon dioxide at 20 °C requires a pressure of at least 30 atmospheres in order to exist in the liquid state (see Figure 2 - 1).

A useful feature of supercritical fluids is that they possess the solvating powers of liquids but the transport properties of gases. The following table (Table 2 - 2) shows typical values of several physical properties of CO_2 as a gas, as a liquid, and as a SCF. It is the high density of supercritical CO_2, similar to the density of many liquid organic solvents that contributes to the surprising solvent power of a supercritical fluid. At the same time as showing a liquid-like density, supercritical CO_2 has a diffusivity approximately 100 times greater than a liquid, allowing rapid transport properties [Rothman et al 2002].

Table 2 - 2: Physical properties of CO_2 [Rothman et al 2002].

Properties	Liquid	Gas	Critical Point	Sc-CO_2
Density (kg/m^3)	1000	~ 1.0	500	300 – 700
Diffusivity (m^2/s)	$< 10^{-9}$	$\sim 10^{-5}$	$\sim 10^{-7}$	$10^{-6} - 10^{-9}$
Viscosity (Pa.s)	$\sim 10^{-3}$	$\sim 10^{-7}$	$\sim 10^{-3}$	$10^{-4} - 10^{-7}$

2.1.2 Advantages and Uses of Supercritical CO_2

Supercritical fluids (SCFs) in theory offer many advantages since they have intermediate properties between liquids and gases, and can be used as alternatives to traditional industrial solvents with their excellent diffusion rates and solvent power. SCF-based processes usually consume much less energy than those using organic solvents, because they avoid high temperatures and expensive distillation and condensation processes. In addition, supercritical CO_2 is attractive for cleaning because no rinsing with water or drying is needed since supercritical CO_2 evaporates completely upon depressurization to atmosphere [Tomasko et al 2003]. Most other organic solvents, furthermore, constitute both occupational and environmental hazards, because many of them are volatile, highly inflammable, and toxic, in contrast to CO_2.

2.2 Polymers

2.2.1 Definition of a Polymer

Polymers are a large class of materials consisting of many small molecules (called monomers) that are linked together to form long chains. The word polymer comes from the Greek word "poly", which means "many", and the word "mer", which means "part". A typical polymer may include tens of thousands of monomers and, is thus a macromolecule. There are two main types of polymers: thermoplastic (linear and branched), and thermoset (cross-linked). The following diagram presents these types (see Figure 2-3):

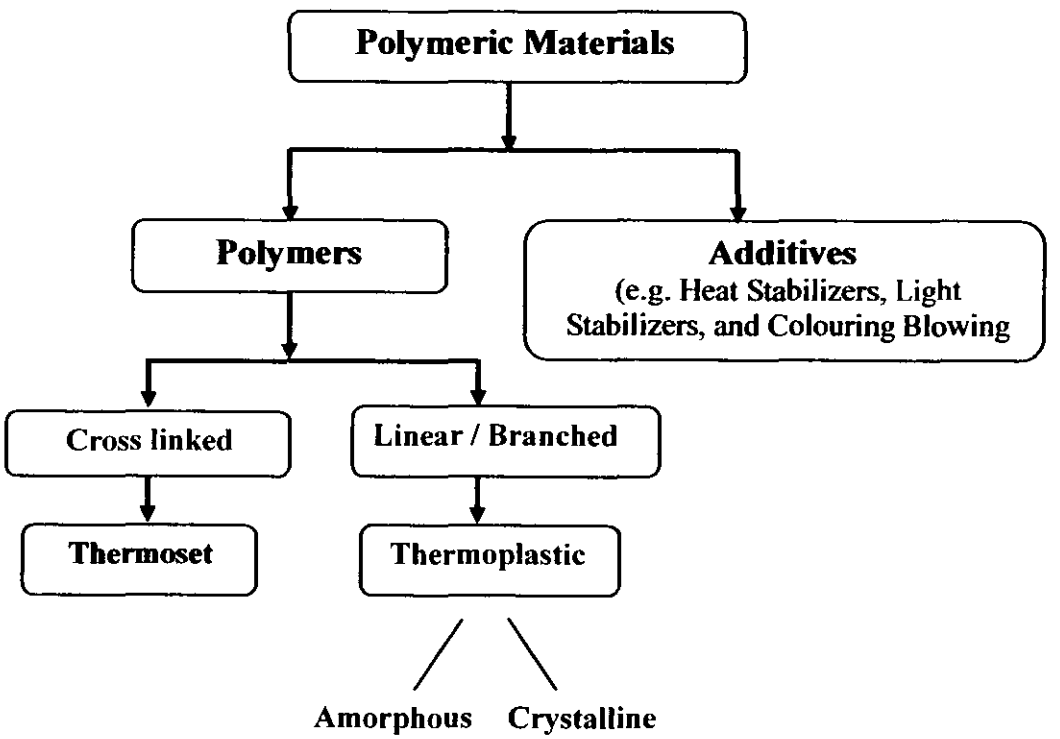

Figure 2 - 3: Polymer types [Gilbert 2005].

These types are now described in more detail.

2.2.2 Types of Polymers

2.2.2.1 Thermoplastics

Thermoplastics are a class of polymer that can be softened on heating (i.e. exhibit a glass transition, see section 2.3). Many thermoplastics can be heated up to its melting point and be reshaped by molding before cooling. This is how plastic objects such as soda bottles and other plastic containers are formed. The molecular chains of thermoplastic polymers are not cross-linked. The chains are held together with weak secondary bonds. These weak bonds are what allow the melting and reshaping of thermoplastics. Commonly used thermoplastics are polyethylene, polystyrene, polypropylene, and poly (vinyl chloride). This research project will be examining the behaviour of this class of polymer [Kokturk and Howdle 2002].

2.2.2.2 Thermosets

Thermosets are a class of polymer that cannot be softened on heating (do not exhibit a glass transition temperature). This means that it cannot be melted or easily reformed. In thermosetting polymers, a process of cross-linking polymer chains by covalent bonds occurs. Since thermosets chains are cross-linked, they have a very high molecular weight. This high molecular weight makes these polymers insoluble. Thermosets are usually supplied as partially polymerised or as monomer-polymer mixtures. Important thermosets include polyesters, silicones and rubbers.

2.2.3 Uses of Polymers

Polymers are finding increasing use as engineering materials not only as the major constituents of familiar plastics, resins, and rubbers but also in more specialised applications such as catalyst supports, chemical reagents, conducting and semi-conducting devices, drug release systems, and membranes.

2.3 The Glass Transition Temperature

2.3.1 Introduction

The glass transition is where polymers (and some other materials) change from a glassy to a rubbery state over a small temperature range as the molecules become mobile. The glass transition is associated with the amorphous regions in a material and therefore occurs in amorphous polymers, and amorphous regions in semi crystalline polymers. Each polymer has a different glass transition temperature (T_g), although the glass transition is not a single event but occurs in stages over a temperature range as different parts of the polymer become more mobile [Tomasko et al 2003]. Different techniques are sensitive to different stages and thus produce slightly different values of T_g. A number of physical properties change around the glass transition temperature due to the increase in molecular mobility. These include elastic modulus (severe decrease), volumetric thermal expansivity (small increase), specific heat capacity (small increase), and dielectric constant (increase).

2.3.2 Methods of Measuring the Glass Transition Temperature

There are several methods available to measure the glass transition temperature. The methods can be categorised according to the property which they are measuring.

1. Mechanical methods (elastic modulus)
2. Volumetric methods
3. Dielectric constant methods
4. Heat capacity methods
5. Spectroscopic methods (molecular mobility)

Since the value of the glass transition temperature depends on the strain rate and cooling or heating rate, there cannot be a single exact value for T_g. These methods are now described in more detail.

2.3.2.1 Mechanical Methods

It is possible to calculate a value for the glass transition temperature by measuring the elastic modulus of the polymer as a function of the temperature, for example by using a torsion pendulum. Around T_g there is a large fall in the value of the modulus. (see Figure 2 - 4).

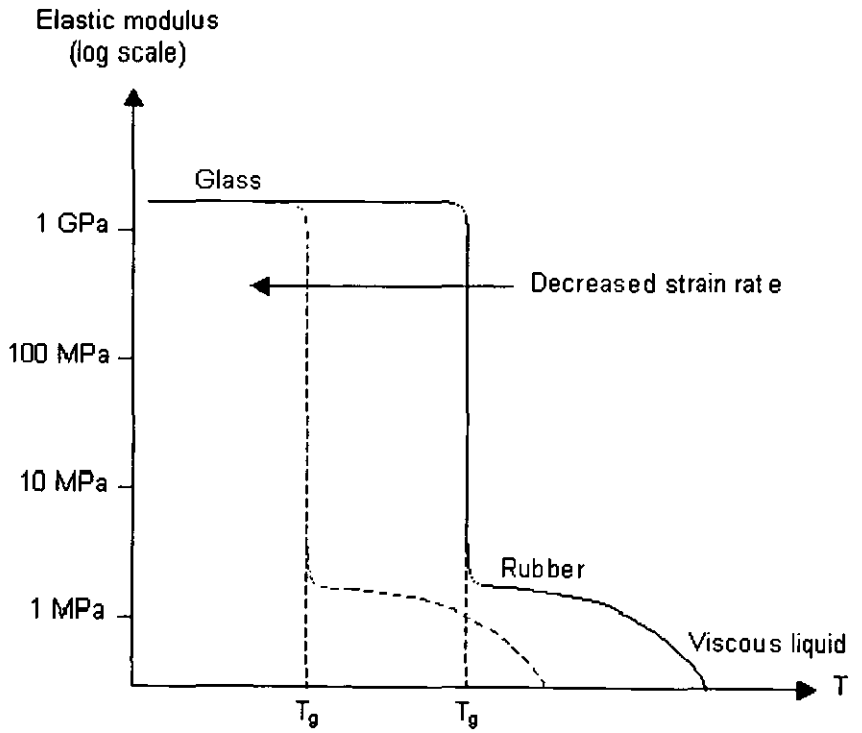

Figure 2 - 4: Elastic modulus versus temperature [Haines 2002].

Mechanical methods comprise Thermo-Mechanical Analysis (TMA) and Dynamic Mechanical Thermal Analysis (DMTA). These are now described in more detail.

2.3.2.1.1 Thermo-mechanical Analysis (TMA)

Thermo-mechanical Analysis (TMA) is a thermal analysis technique used to measure changes in the physical dimensions (length or volume) of a sample as a function of temperature and/or time, and can also be used to measure stiffness. TMA is commonly used to determine thermal expansion coefficients a change in which occurs around the glass transition temperature. In this technique (TMA), dimensional changes in a sample are the primary measurement, while the sample is heated, cooled, or studied at a fixed temperature. A schematic of a typical TMA instrument is shown below:

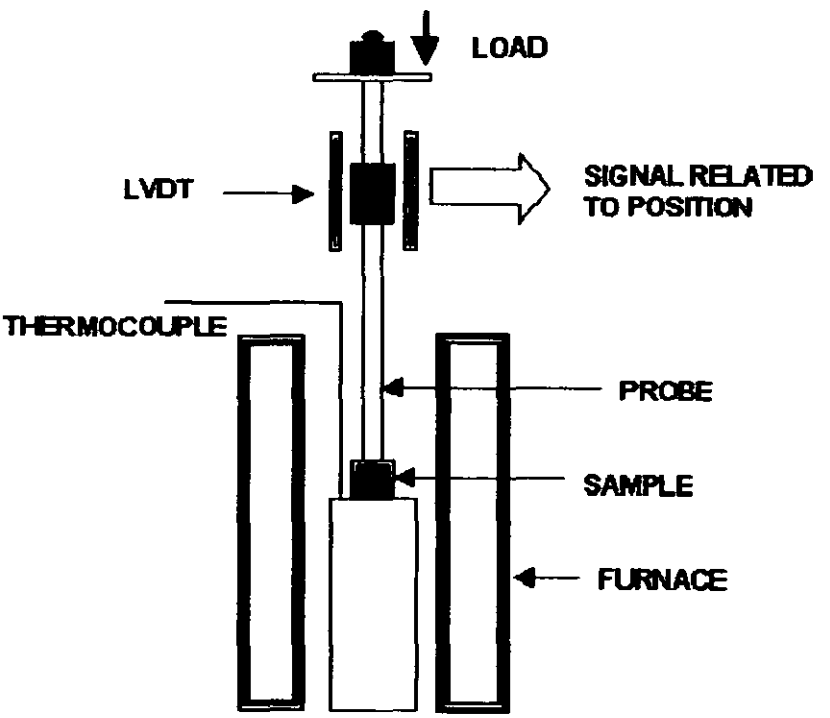

Figure 2 - 5: TMA instrument.

A short explanation of the TMA technique may be described as follows. A specimen is placed onto the base of a quartz sample holder and a suspended quartz probe is lowered down and positioned so that it just touches the top surface of the sample. Different probe types of varying tip geometry may be used and, typically, the probe is loaded with some finite weight. The TMA sample holder assembly is then placed into a furnace unit and the vertical movement of the quartz probe is continuously monitored. Typically, TMA tests are run in a heating mode at a controlled heating rate.

The materials studied are usually rigid or nearly rigid solids, as implied by most of the experimental arrangements. The major application areas of TMA are in the polymer field. TMA is better suited to comparative measurements on a range of materials, and for measurements of transition temperatures and expansion coefficients on relatively small samples, in a conveniently short time.

2.3.2.1.2 Dynamic Mechanical Thermal Analysis (DMTA)

A more common method is dynamic mechanical thermal analysis (DMTA) or dynamic mechanical analysis (DMA), which measures the stress and strain of a specimen in response to an oscillatory stress or strain which is imposed on the sample. The glass transition can be observed by scanning the temperature during the experiment and measuring the peak amplitude of the stress (σ_{max}), and strain (ε_{max}) and the phase difference (δ) by using the following equations, as shown in the following figure (Figure 2-6 and Figure 2 -7).

$$E' = \frac{\sigma_{max}}{\varepsilon_{max}} \cos\delta \qquad \textbf{Eg. 2 - 1}$$

$$E'' = \frac{\sigma_{max}}{\varepsilon_{max}} \sin\delta \qquad \textbf{Eg. 2 - 2}$$

$$\frac{E''}{E'} = \tan\delta \qquad \textbf{Eg. 2 - 3}$$

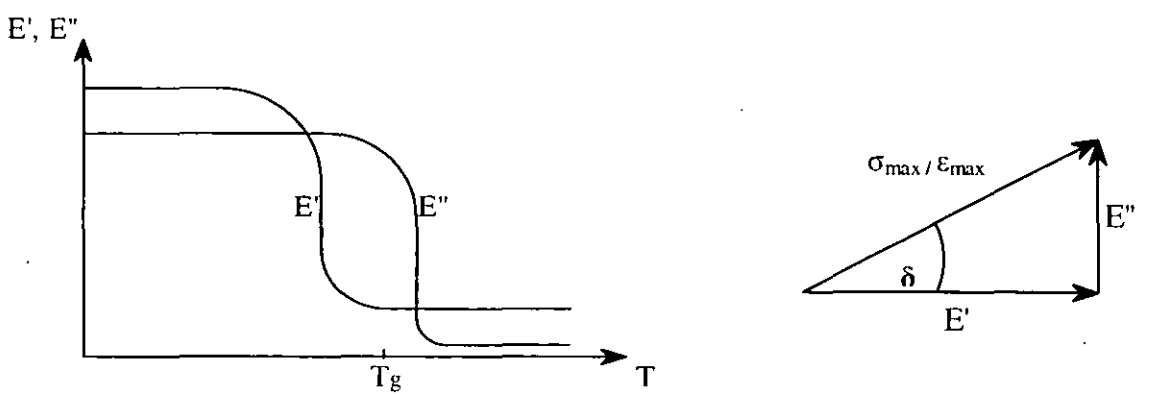

Figure 2 - 6: Scanning the temperature during the experiment and measuring the peak amplitude of the stress (σ_{max}), and strain (ε_{max}) and the phase difference (δ).

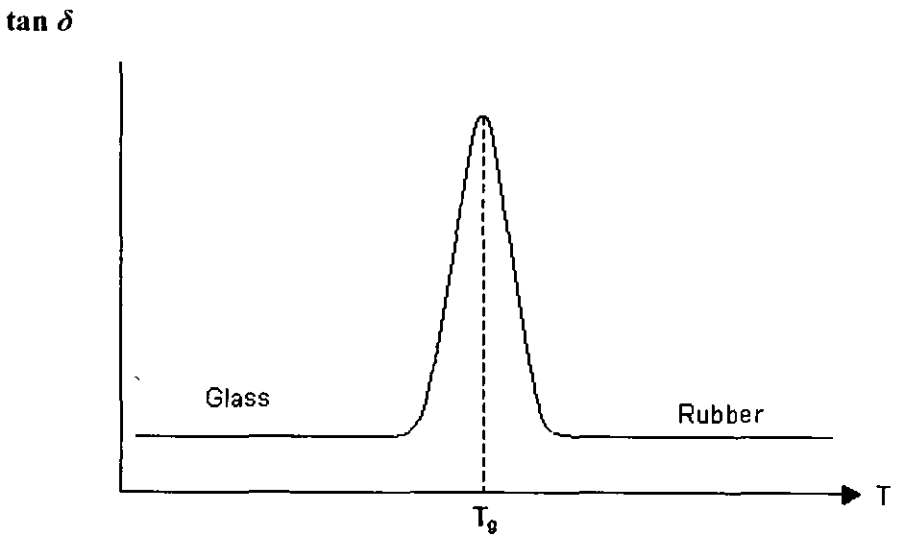

Figure 2 - 7: Measurement of T_g using DMTA.

Tan δ represents the energy loss (loss angle δ) of the sample and $\tan\delta = E''/E'$ where; E' in phase (storage modulus), E'' out of phase (loss modulus).

In addition; polymers can show other transitions, e.g. the side chain motion of $COOCH_3$ in PMMA - β transition at 60°C whereas the T_g for PMMA is 100 °C. Therefore; the first sign of softening is the side group softening T_g and its called β sign. A plot of tan δ versus temperature shows these temperature transitions. The following Figure represents these relations (see Figure 2-8).

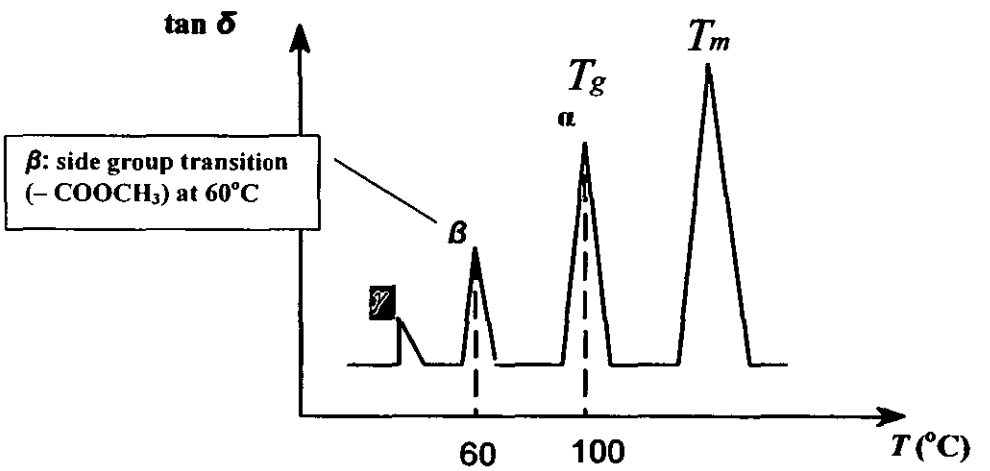

Figure 2 - 8: β and T_g for PMMA [Gilbert 2005].

where: γ is the transition is observed if CH_3 replaced by C_3H_7 – poly(propyl methacrylate). β is the transition of the side chain motion (-$COOCH_3$), α is the glass transition temperature (T_g) and T_m is the melting temperature of the polymer [Gilbert 2005].

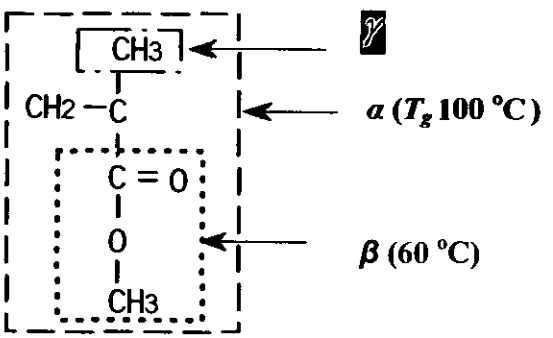

Poly(methyl methacrylate), PMMA

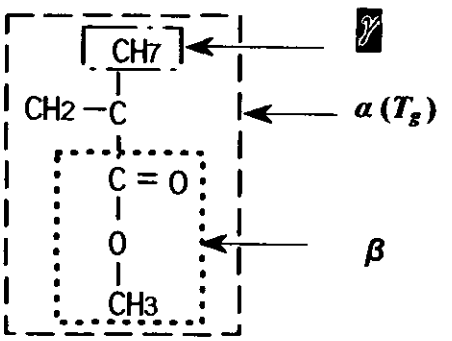

Poly(propyl methacrylate), (PPMA)

2.3.2.2 Volume Method

The changes in conformation that occur above T_g require more volume, so plotting a graph of specific volume or thermal expansion coefficient against temperature can give a value for T_g. The actual volume of the molecules stays the same through T_g, but the *free volume* (the volume through which they can move) increases. Thermo-mechanical Analysis (TMA) which can also be used to measure T_g by stiffness (see section 2.3.2.1.1) can be used to measure changes in volume versus temperature.

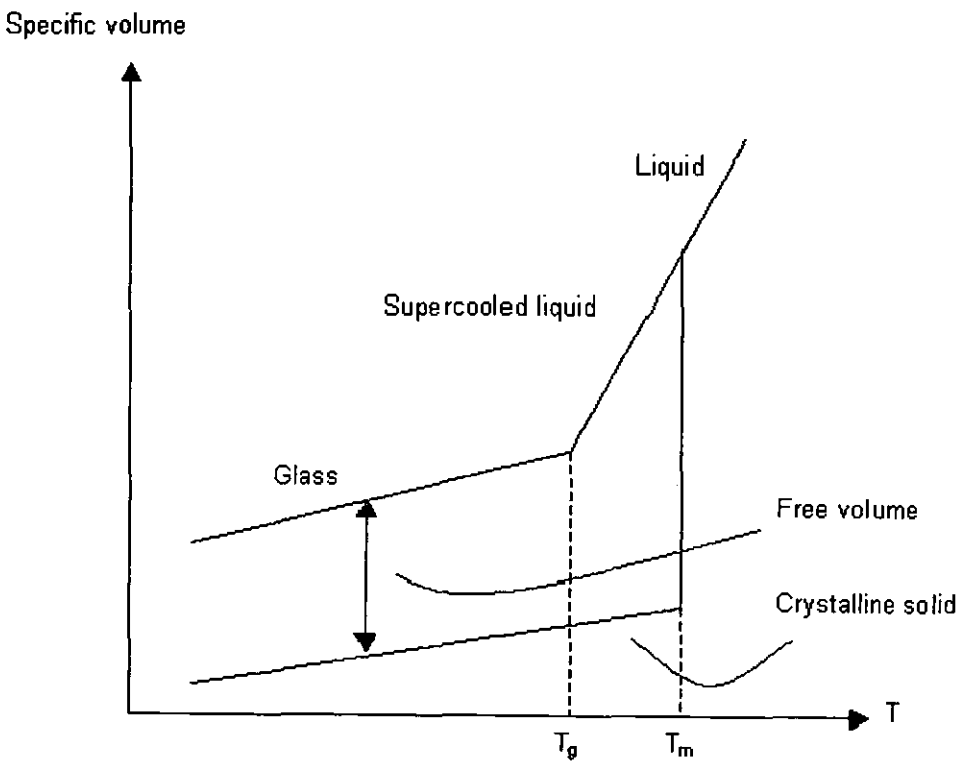

Figure 2 - 9: Specific volume versus temperature for a typical polymer [Haines 2002].

2.3.2.3 Dielectric Constant

If a varying electric field is applied to a polymeric material, any polar groups will align with the field. Below T_g rotation of the bonds is not possible, so the permittivity will be low, but there is a large increase around T_g (see Figure 2-10). At higher temperatures the increased thermal vibrations cause the permittivity to drop again. If the frequency of the field is increased, the polar groups have less time to align, so the glass transition is observed at a higher temperature.

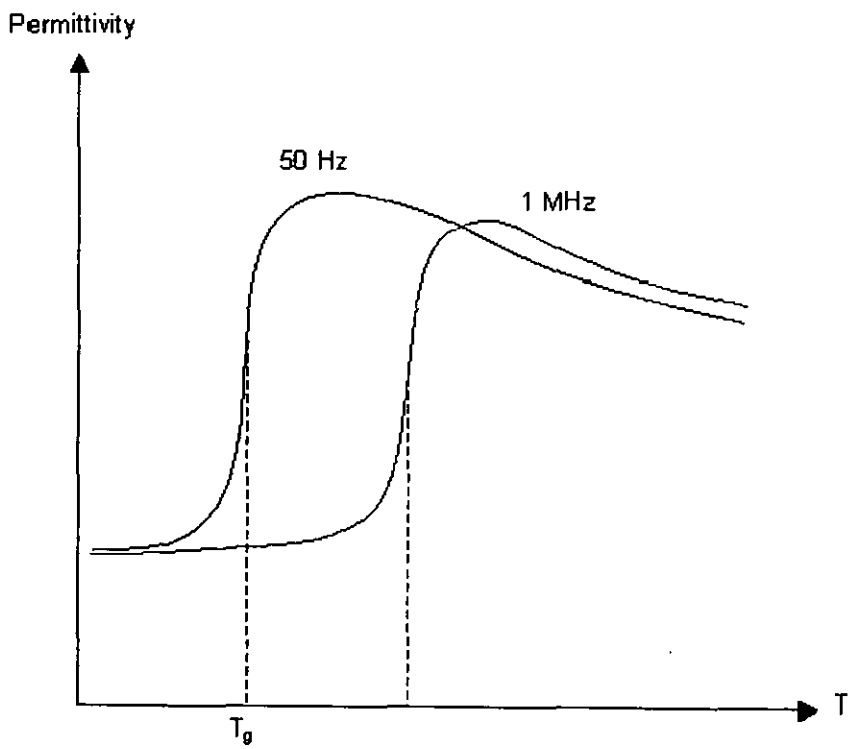

Figure 2 - 10: Dielectric method [Haines 2002].

2.3.2.4 Heat Capacity

The specific heat capacity, C_p, can be measured using calorimetry, e.g. differential scanning calorimetry (DSC) and differential thermal analysis (DTA). The enthalpy of a polymer increases as the temperature increases, but with a change in slope in the graph at T_g. Taking the derivative of this graph with respect to temperature, the specific heat capacity can be plotted, as shown below (see Figure 2 - 11):

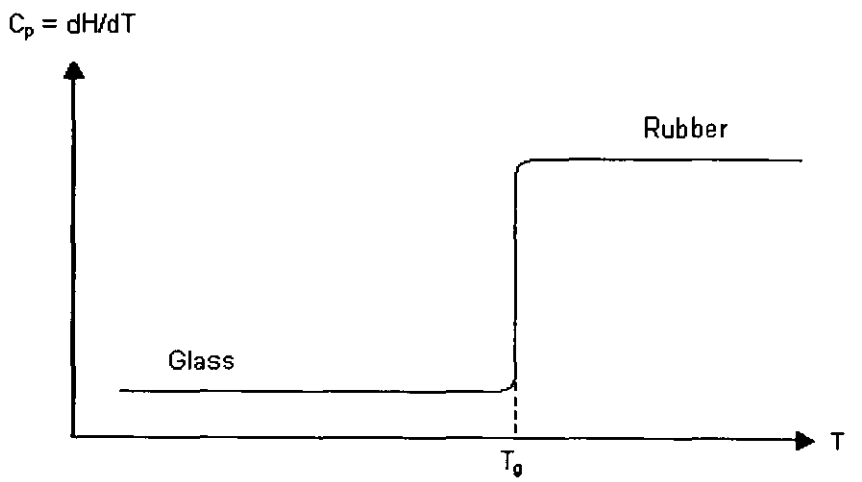

Figure 2 - 11: Measurement of T_g depending in C_p using DSC method.

The DTA and DSC methods are now described in more detail:

2.3.2.4.1 Differential Thermal Analysis (DTA)

Differential Thermal Analysis (DTA), also known as heat flux Differential Scanning Calorimetry (DSC), is the simplest and one of the most widely used thermal analysis techniques. The difference in temperature, ΔT, between the sample and the reference material is recorded while both are subjected to the same heating conditions. The sample and reference, in similar holders (usually flat pans) are placed on individual thermally conducting bases (see Figure 2 - 12). The thermocouple junctions are attached to these bases and are thus not directly in the sample or reference material. This configuration (compared to DSC) has the advantage that the output signal is less dependent upon the thermal properties of the sample, but the response is slower.

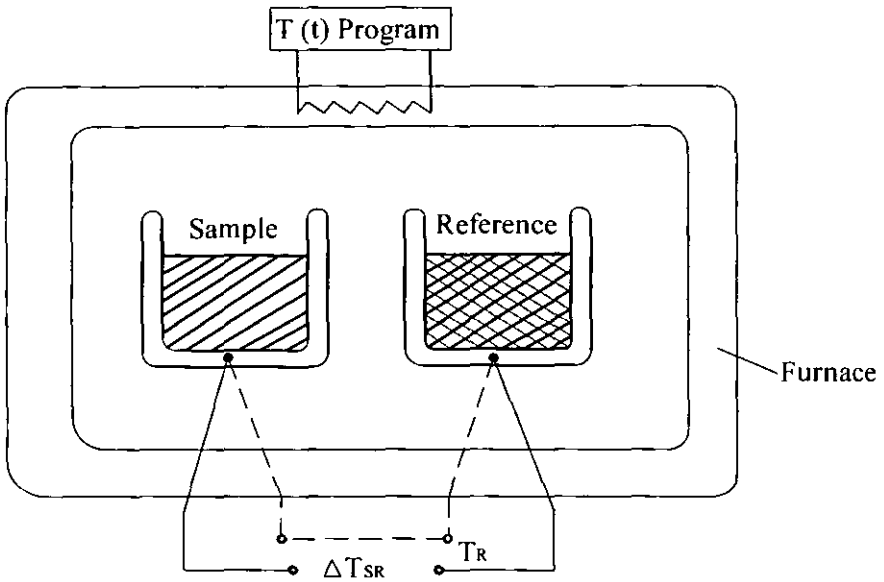

Figure 2 - 12: Schematic illustration of DTA system [Brown et al 1998].

2.3.2.4.2 Differential Scanning Calorimetry (DSC)

There are many similarities between DSC and DTA, including the superficial appearance of the thermal analysis curves obtained, but the principle of power-compensated DSC is distinctly different to that of heat-flux DSC. In power compensated DSC, the pans are individually heated such that they rise in temperature at the same rate (K/min) and the power difference is measured, see Figure 2 - 13.

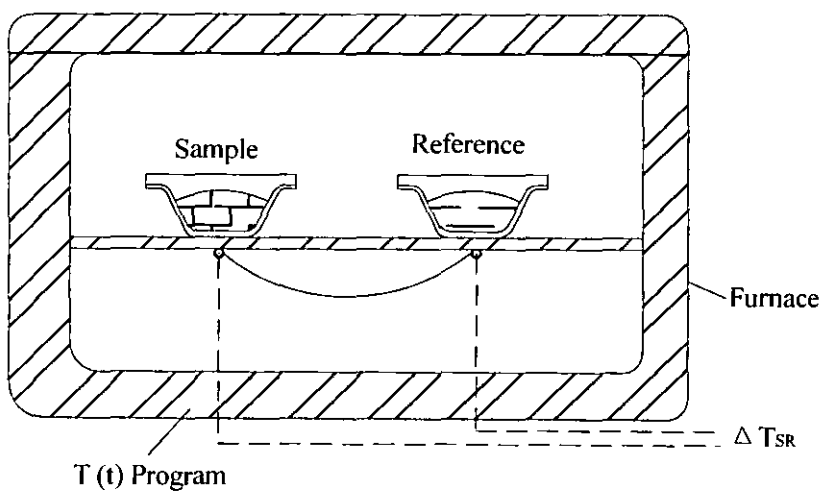

Figure 2 - 13: Disk type DSC [Brown et al 1998].

2.3.2.5 Molecular Mobility

A very common method to measure molecular mobility is Fourier Transform Infrared Spectroscopy. FTIR spectroscopy is a powerful tool for identifying types of chemical bonds in a molecule by producing an infrared absorption spectrum that is like a molecular "fingerprint". In addition, FTIR spectroscopy can also study polymeric materials subjected to high-pressure or supercritical CO_2. *In situ* monitoring using FTIR spectroscopy helps us to understand and optimize high-pressure supercritical fluid processes. FTIR spectroscopy probes interactions between CO_2 and polymers at a molecular level and provides a fundamental understanding of the origin of many effects of $scCO_2$ on polymeric materials (such as plasticisation, swelling) [Kazarian 2000].

This technique measures the absorption of various infrared light wavelengths by the material of interest. These infrared absorption bands identify specific molecular components and structures. The technique can be utilized to analyse components of an unknown mixture, and can be applied to the analysis of solids (polymer) see Figure 2-14, liquids, and gases.

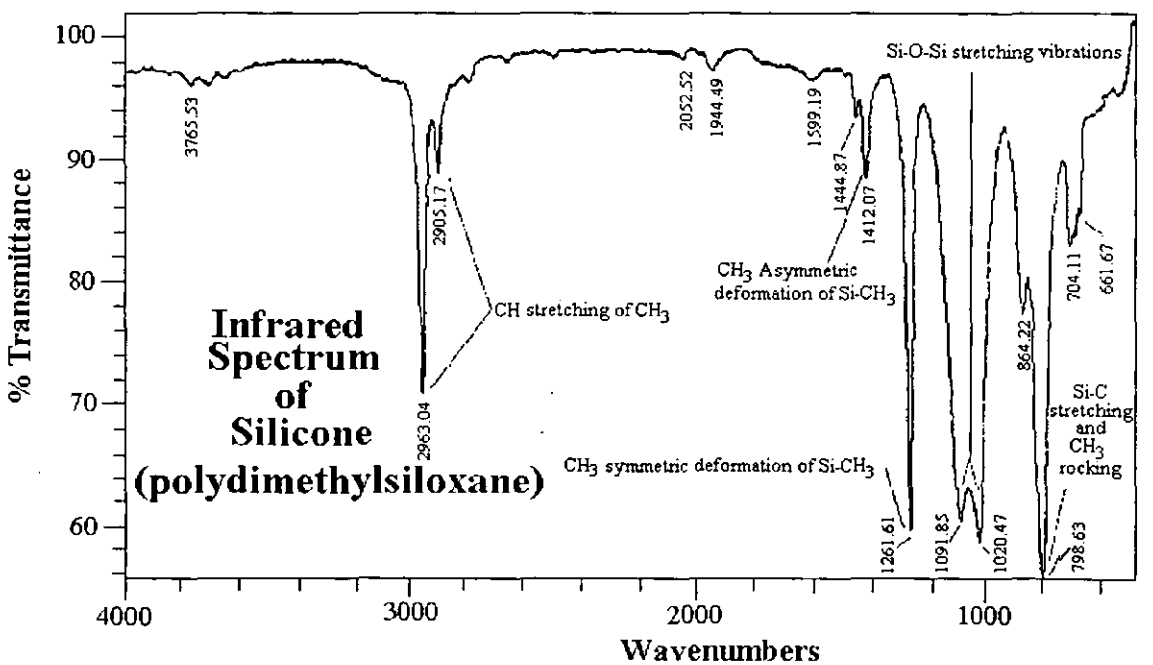

Figure 2 - 14: FTIR spectroscopy analysis of Silicone (polydimethylsiloxane) [WACS 2006].

2.4 Interaction of CO_2 with Polymers

The use of supercritical fluids (SCF) has recently received much attention in polymer science. $ScCO_2$ is the most frequently used of these because of the advantages mentioned earlier. Other fluids, such as supercritical propane and supercritical water, are also used. In Figure 2 - 15 the interactions between polymers and supercritical fluids in general as well as possible applications are outlined:

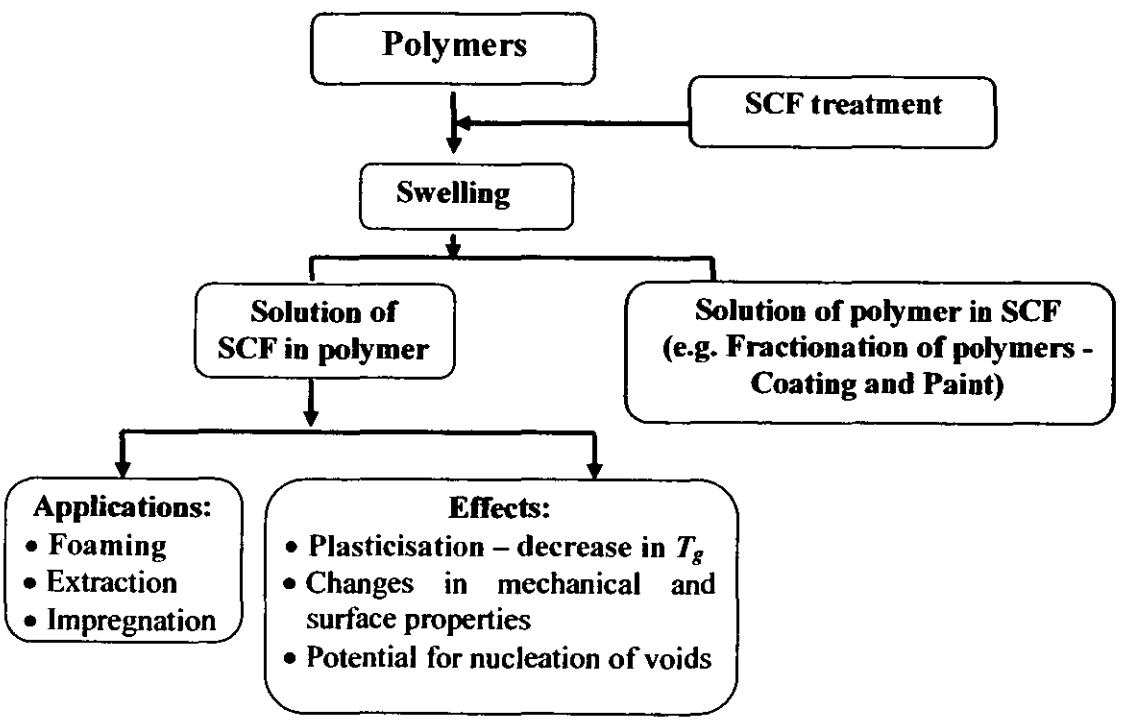

Figure 2 - 15: Diagram of the interaction of SCFs with polymers [DeGooijer 2002].

The plasticising effect of carbon dioxide is the result of the ability of CO_2 molecules to interact with the basic sites in polymer molecules and is not simply a pressure effect. It has been shown experimentally that interactions between CO_2 and polymer groups reduce chain-chain interactions and increase the mobility of polymer segments there being direct FTIR spectroscopic evidence for the interaction between CO_2 and polymers [see Kazarian et al 1997]. Evidence of CO_2 induced motion of phenyl rings in polystyrene has also been observed using ^{13}C nuclear magnetic resonance spectroscopy (NMR) [Miyoshi et al 1997].

2.4.1 Solubility of CO_2 in Polymers

The solubility and the diffusivity of CO_2 in polymers are important transport properties for processes involving CO_2 and polymers. When CO_2 dissolves into a polymer, the polymer swells and the density of the polymer/CO_2 system reduces. The sorption of carbon dioxide results in a strong plasticisation effect for a number of polymers and has been investigated using a variety of techniques such as FTIR spectroscopy, DSC and gas sorption/gas permeation techniques [Kazarian 2000]. Sorption is a generalised term used to describe the diffusion of penetrates molecules in a polymeric matrix to form a mixture. The swelling kinetics of all polymer samples exhibit two distinct regimes: an initial region of large swelling accompanied by diffusion of CO_2 into the polymer and a subsequent region of small volume increase which progresses asymptotically to an equilibrium swelling value.

Two main methods are used to study sorption: (i) pressure decay method, (ii) quartz spring method. The pressure decay method uses two chambers connected by a valve; one of the chambers contains a polymer sample. The test starts by charging the empty chamber with carbon dioxide to a measured pressure, and the chamber is then isolated. The next step is to open the value in between the two chambers for short time. The pressure in both chambers is measured over time. Knowing the volume of the two chambers it is possible to calculate the gas absorbed into the polymer sample from the variation of pressure in the two chambers. Pressure decay method is as sensitive as the time available for the test and is simple and requires relatively simple equipment [Pantoula and Panayiotou 2006].

The extent of swelling increases with both pressure and molecular weight but exhibits different trends with temperature depending on the system pressure. For pressures below 15 MPa, the extent of swelling decreases monotonically with temperature. However, for pressures above this threshold, a maximum in swelling is observed as the temperature is increased [Royer et al 1999]. There are a number of sorption studies of the CO_2/PS systems in the literature. Morel and Paul (1982) measured sorption on PS at 35°C and at low pressures, up to 40.5 bar, using the pressure decay method. Vogt et al. (2003) used the same method (pressure decay) to investigate the sorption of CO_2/ PS between 60 and 100°C and at pressures up to 120 bar.

The quartz spring balance is used to study the sorption by suspending the sample from the quartz spring in the view cell, which was then placed in the constant temperature bath and evacuated for 3-6 h. After the initial spring extension was measured, CO_2 was added to the cell, and the spring extension was measured periodically until the pressure stabilized and the spring extension reached a constant value. Wissinger and Paulaitis (1987 and 1991) studied sorption with a quartz spring balance on PS at 32–65°C and pressures up to 100 bar. Shim et al. (1997) used a similar method to measure sorption on PS at much higher pressures, up to 300 bar. Sato et al. (1996) went on to higher temperatures and evaluated sorption of CO_2 on PS up to 180°C and up to 200 bar by the pressure decay method.

Another technique was presented for measuring the swelling and solubility of $scCO_2$ in polymer melts [see Royer et al 1999] based on optically monitoring polymer swelling in real time. This provides information on the swelling kinetics, swelling equilibrium, and rates of CO_2 diffusion. Arora et al. (1998) measured the solubility of CO_2 on PS in their study of microcellular polystyrene foams, in order to estimate the sorption of CO_2 in PS at 80°C and 243.3 bar (3530 psi). The following figure presents a compilation of the above mentioned data:

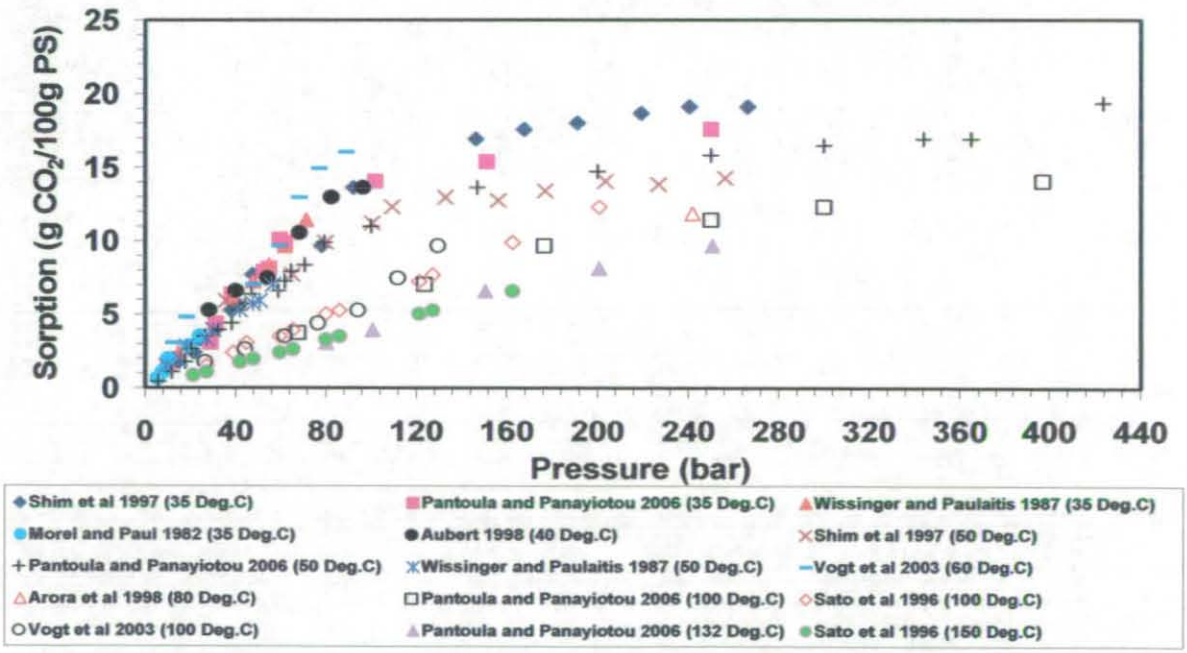

Figure 2 - 16: Solubility of PS / CO_2 by other researchers (from 0 to 440 bar at 35 to 150 °C).

As shown in the previous figure (Figure 2-16), the sorption data from different researchers and techniques generally agree with each other, especially at lower pressures. However, at high pressure, there are large deviations in the data of Shim et al (1997), which are probably due to the buoyancy effect and the swelling estimation. They used a quartz spring balance method, "a gravimetric method whose results need correction for the buoyancy" (as they report) [Pantoula and Panayiotou 2006]. Pantoula and Panayiotou (2006) measured the solubility by two different methods: quartz crystal microbalance (isotherms at 35 and 51 °C) and mass-loss analysis (at 35, 51, 81, 100 and 132 °C). All the sorption data at 35, 40, 50, and 60 °C give a linear curve up to a pressure of (~100 bar). At higher temperatures of 80, 100, 132, and 150 °C, the linearity is maintained up to ~ 200 bar.

The following values of Henry's constant (K_H) are determined from the sorption data by using Henry's law ($P = K_H c_{PS/CO_2}$), see following figure (Figure 2-17) and table (Table 2-3). It should be noted, however that at low temperatures (< 50 °C) the curves become non linear at high pressure (> ~ 100 bar).

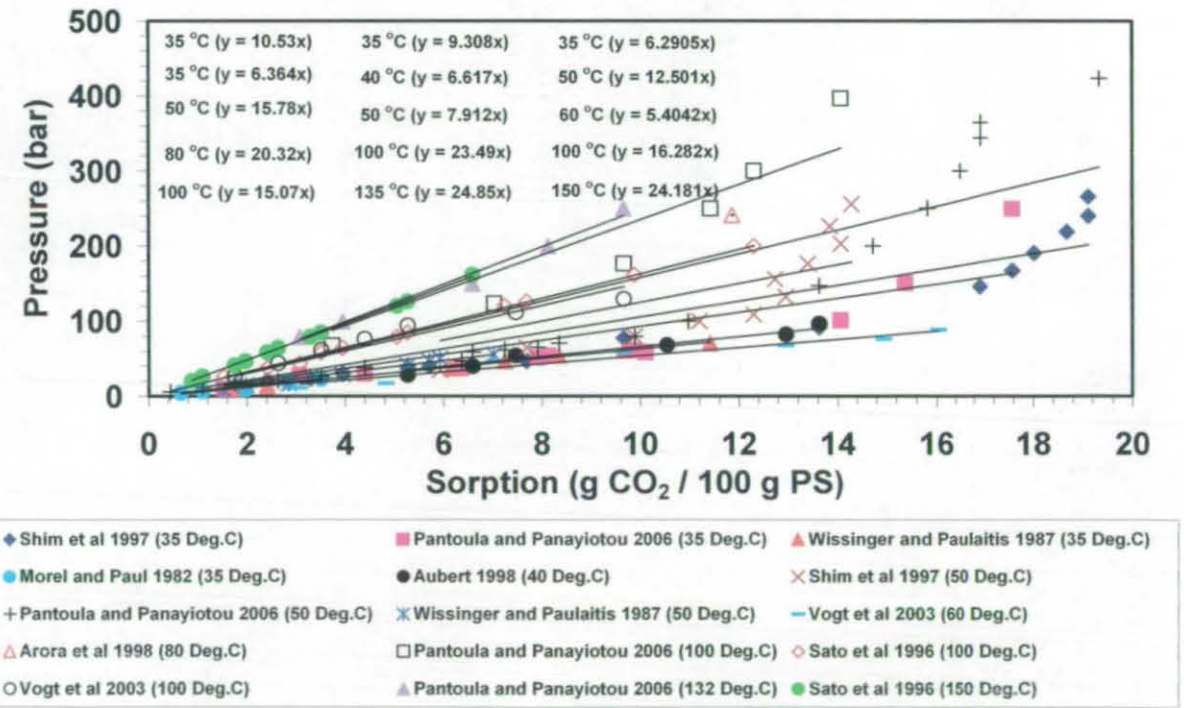

Figure 2 - 17: Pressure versus concentration to find Henry's constant.

Table 2 - 3: Henry's constant literature values.

Temperature (°C)	Pressure range (bar)	Henry's constant (bar)	Reference
35	7 – 266	1053.0	Shim et al 1997
35	10 – 250	930.8	Pantoula and Panayiotou 2006
35	10 – 70	629.1	Wissinger and Paulaitis 1987
35	5 – 24	636.4	Morel and Paul 1982
40	28 – 96	661.7	Aubert 1998
50	35 – 255	1250.0	Shim et al 1997
50	6 – 424	1578.0	Pantoula and Panayiotou 2006
50	9 – 56	791.2	Wissinger and Paulaitis 1987
60	11 – 88	540.4	Vogt et al 2003
80	241	2032.0	Arora et al 1998
100	68 – 397	2349.0	Pantoula and Panayiotou 2006
100	26 – 200	1628.2	Sato et al 1996
100	26 – 130	1507.0	Vogt et al 2003
132	80 – 250	2485.0	Pantoula and Panayiotou 2006
150	20 – 162	2418.0	Sato et al 1996

2.4.2 Diffusion Coefficients of CO_2 in Polymers

Diffusion coefficients of CO_2 in polymers have been obtained by a number of workers from high pressure sorption experiments by using mass-loss analysis [Tang et al 2004], magnetic suspension balance [Sato et al 2001], gravimetric method [Berens et al 1992, Nikitin et al 2003], and timed absorption [Webb & Teja 1999]. These have been obtained by fitting diffusion based equations for the uptake of CO_2 with time. Published values are shown for each polymer for various combinations of temperature and pressure.

Table 2 - 4: Published values of diffusion coefficients of CO_2 in PC, PS and PMMA.

Polymer	Pressure (bar)	Temperature (°C)	Diffusivity (10^{-10} m^2 s^{-1})	Methods and Reference
PC	200	40	0.122	Mass-loss analysis (MLA)
	200	50	0.168	[Tang et al 2004]
	200	60	0.336	
PS	24	100	0.81	Magnetic suspension
	44	100	1.14	balance (MSB)
	63	100	1.46	[Sato et al 2001]
	83	100	1.67	
	83	150	5.33	
	84	200	9.9	
PS	90	50	0.87	Gravimetric method
	90	65	1.57	[Nikitin et al 2003]
	125	50	1.27	
	125	65	2.98	
PMMA	105	40	1.04	Timed absorption
				[Webb & Teja 1999].
PMMA	33	25	0.01	Gravimetric method
	65	25	0.1 – 0.25	[Berens et al 1992]

This table (Table 2-4) shows that diffusivity varies significantly with both temperature and pressure and it also is clear that the published diffusion coefficients of CO_2 in PMMA are lower than with PC and PS.

2.4.3 Plasticisation of Polymers by CO_2

As mentioned earlier CO_2 is able to plasticise polymers (i.e. lower the glass transition temperature) to a significant degree at high pressure. The study of the CO_2 plasticisation of polymers is made more difficult than those for other plasticise by the need to perform experiments under conditions of high pressure. This limits the techniques that can be used. The following figures (Figure 2 - 18 to Figure 2 - 20) summarise the glass transition temperature (T_g) values for PC, PS, and PMMA that are reported in the literature, which will be of use for later in this thesis.

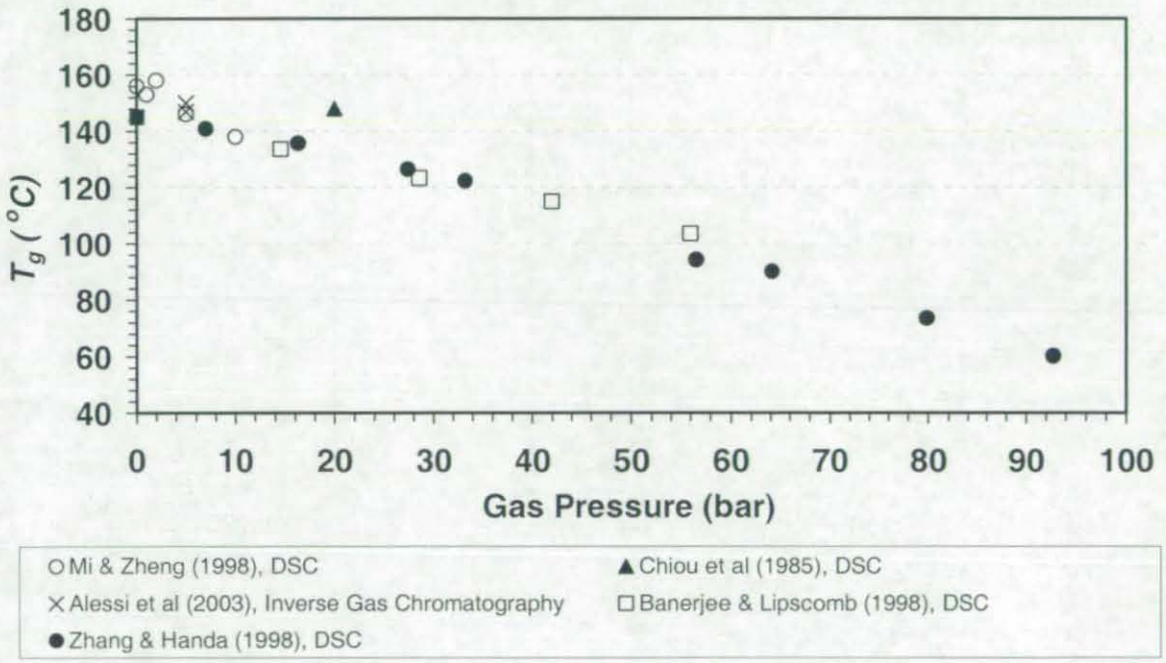

Figure 2 - 18: Glass transition temperatures for PC reported in the literature.

2.4.3 Plasticisation of Polymers by CO_2

As mentioned earlier CO_2 is able to plasticise polymers (i.e. lower the glass transition temperature) to a significant degree at high pressure. The study of the CO_2 plasticisation of polymers is made more difficult than those for other plasticise by the need to perform experiments under conditions of high pressure. This limits the techniques that can be used. The following figures (Figure 2 - 18 to Figure 2 - 20) summarise the glass transition temperature (T_g) values for PC, PS, and PMMA that are reported in the literature, which will be of use for later in this thesis.

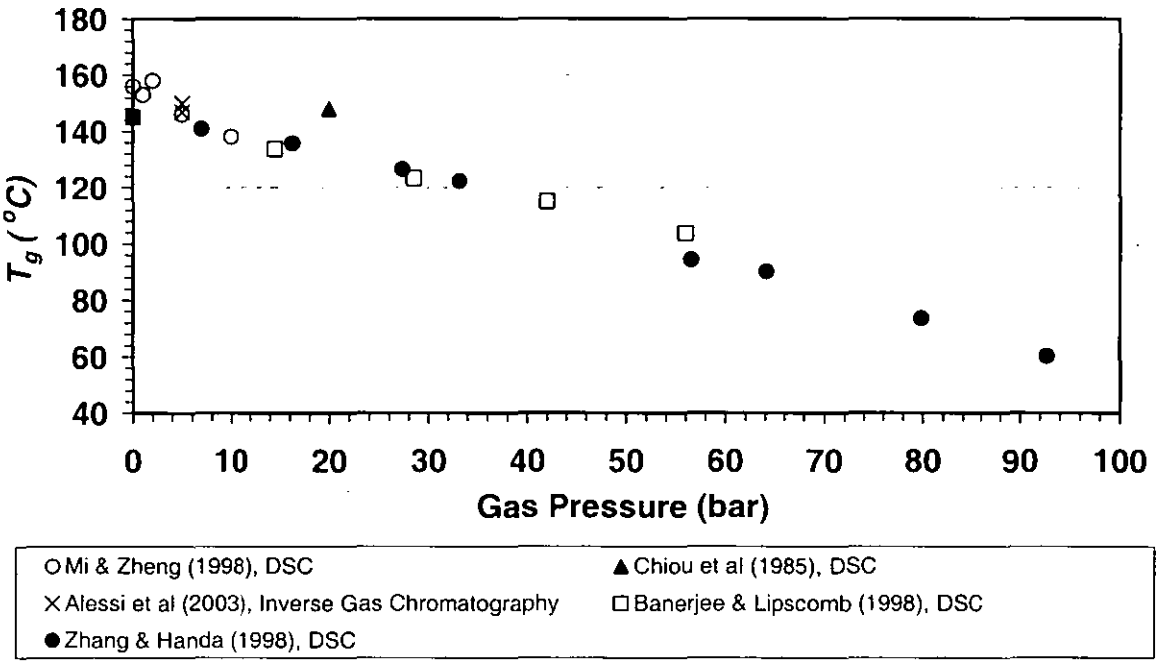

Figure 2 - 18: Glass transition temperatures for PC reported in the literature.

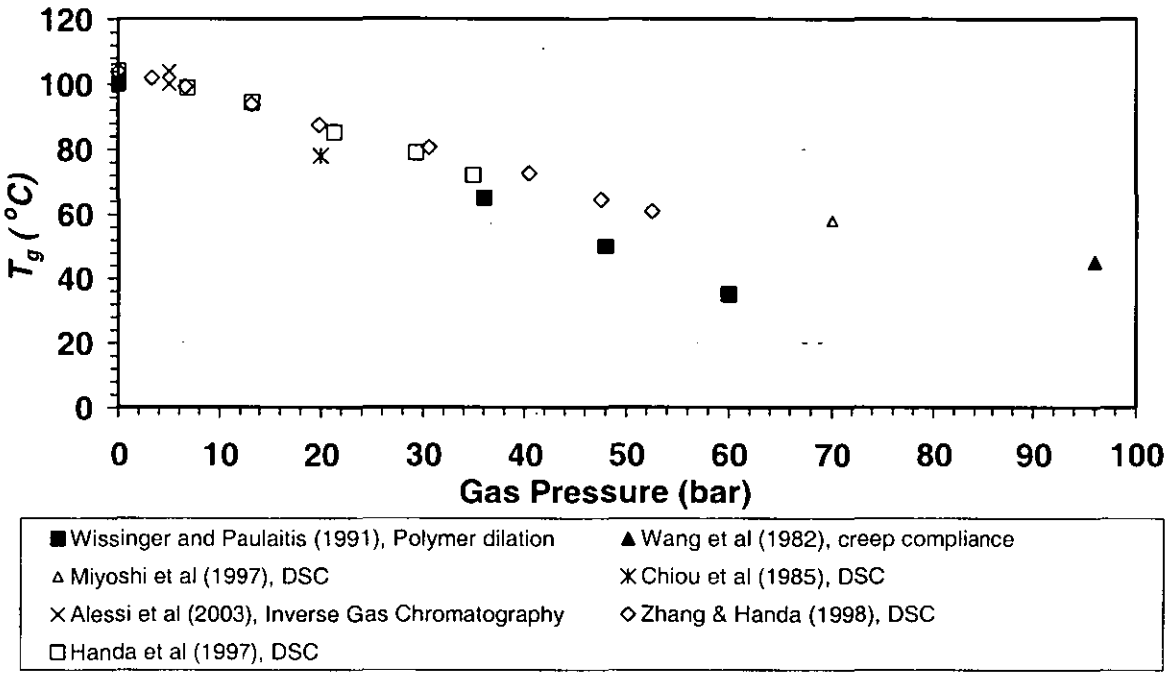

Figure 2 - 19: Glass transition temperatures for PS reported in the literature.

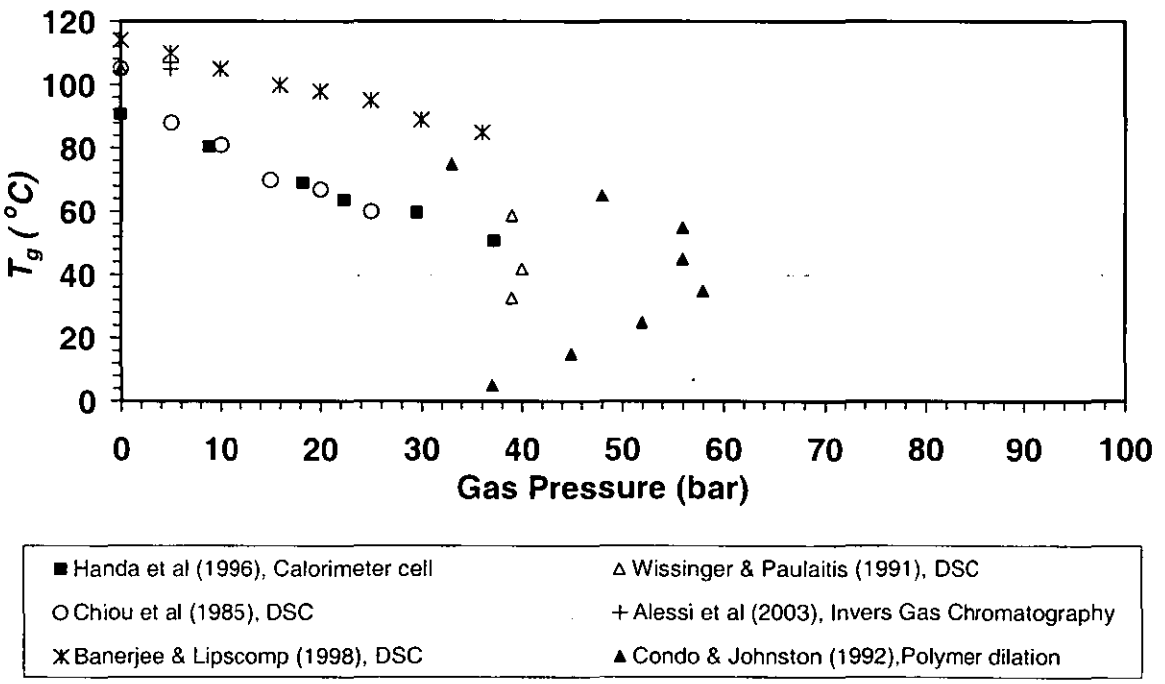

Figure 2 - 20: Glass transition temperatures for PMMA reported in the literature.

The general trend of the curves is a linear decrease of T_g with increasing pressure of approximately 1 K/bar. The literature data only cover a limited range of pressure up to 60 bar for PMMA and up to 90 bar for PC and PS. Measurements of the softening temperature for the same polymer can differ significantly between researchers, probably due to the different techniques, samples, and experimental procedures used.

2.4.4 Mechanical Properties of Polymers Exposed to High Pressure CO_2

Mechanical properties are, however, of prime importance when plasticisation is used to aid extrusion or other shape forming processes, and so a direct test would be of most benefit in such situations. Relatively few studies have directly examined the effect of CO_2 on the mechanical properties of polymers. However, only a few of the studies exceeded 60 bar of CO_2 pressure. These have encompassed a range of methods including measurements of:

(i) The hardness of PMMA by an indentation test [Flichy et al 2001].

(ii) The high frequency elastic modulus of PS from its response to ultrasonic waves [Wang et al 1982].

(iii) The creep compliance of PS measured using a linear variable displacement transducer (LVDT) [Wang et al 1982], and also for PS and PMMA [Wissinger and Paulaitis 1991].

(iv) The linear dilation of PVF; also by LVDT [Shenoy et al 2003]

(v) The temperature at which the central deflections of PETG and PMMA strips exceed a threshold point [Yoon and Cha 2001]. This was indicated when a magnet placed on the sample inside a high pressure cell was detected by a magnetic switch placed outside the cell.

(vi) Dynamic mechanical analysis (DMTA) of samples after exposing to high pressure carbon dioxide, quenching the high pressure cell in liquid nitrogen to cool the samples to trap the absorbed CO_2 and analysing the samples by DMTA as they are slowly warmed [Fried et al 1989].

Because of the similarity of the Yoo and Cha (2001) method to the one used in this thesis this method is discussed in more detail. Yoon and Cha (2001) designed a device that measures the glass transition temperature at high pressure (see Figure 2 - 21). The change of the glass transition temperature was measured in pressure chamber. The change was measured by magnetic circuit. A circuit that includes a lead switch equipped outside the chamber to detect any changes in the magnetic field. The lead switch closes the circuit when the strength of the magnetic field goes over the threshold value and opens the circuit below the threshold value, when the chamber temperature reaches the glass transition the specimen sag down.

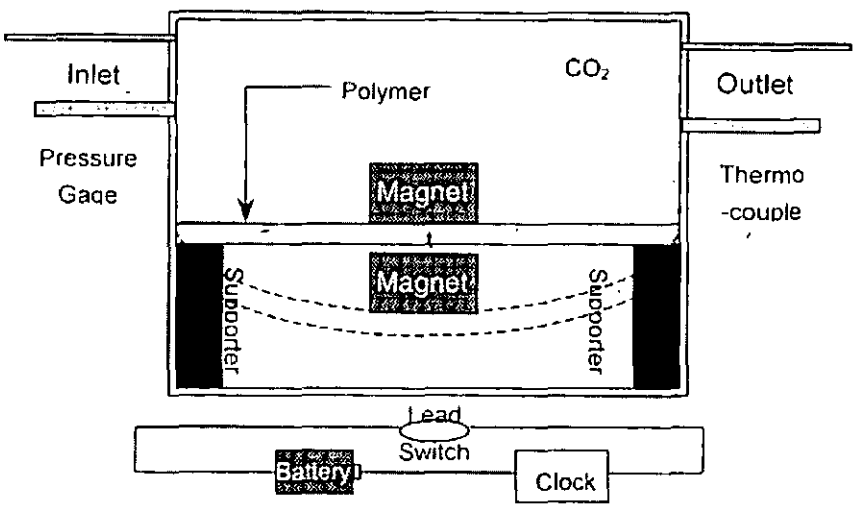

Figure 2 - 21: A schematic diagram of a newly devised glass transition temperature detecting machine [Yoo and Cha 2001].

2.4.5 Viscosity of CO_2 / Polymer Systems

Viscosity is a very important characteristic for polymers when being processed. In general, the viscosity is observed to decrease as the dissolved CO_2 concentration increases into various polymer melts (see review by Tomasko et al 2003). The viscosity reduction is greatly eases the processing of high molecular weight polymers where high viscosity can be the major difficulty. It also assists the processing of temperature sensitive polymers at lower temperatures, preventing thermal degradation and saving energy. It is found that the viscosities of the CO_2/polymer solution are reduced by increasing the temperature or increasing the pressure. For example the shear viscosity of PS/CO_2 is decreases from ~ 2000 to ~ 200 (Pa.s) as the shear rate is increased from 10 – 1000 (1/ sec) at 175 °C, see the following figure [Tomasko et al 2003].

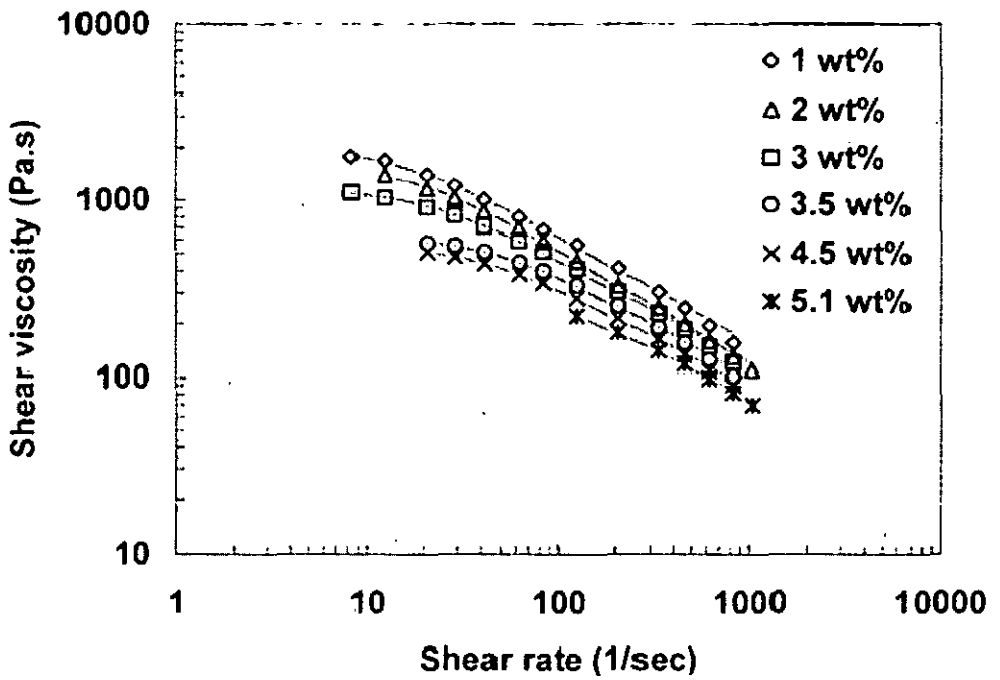

Figure 2 - 22: Viscosity reduction of PS/CO_2 with different CO_2 content at 175 °C [Tomasko et al 2003].

2.5 Polymer Foaming

2.5.1 Introduction

The use of polymeric foams in today's technology continues to grow at a rapid pace throughout the world. Numerous reasons for this growth include the light weight, excellent strength/weight ratio, superior insulating abilities, energy absorbing performance, and comfort features of polymeric foams. The main applications include furniture, transportation, carpet underlay, packaging, toys and sports. Foams can be prepared from virtually any polymer. The selection of a polymer suitable for an industrial foam application depends upon its properties.

The first step in producing foam is the formation of gas bubbles in liquid system. If the bubbles are formed in an initially truly homogenous liquid the process is called *self-nucleation*. If a second phase is initially present, especially if it is in the form of finely divided solids, the bubbles will usually form more easily at the liquid-solid interface. In this case the bubbles are said to form by *a heterogeneous nucleation process*, and the solid particles are called *a nucleating agent* [Klempner and Frisch 1991].

The foaming of polymer has been studied by many authors, theoretically [Amon and Denson 1984, Feng and Bertelo 2004, Tuladhar and Mackley 2005] and experimentally [Han and Yoo 1981, Amon and Denson 1984, Goel and Beckman 1994, Royer et al 1999, Liang and Wang 2000, Tuladhar and Mackley 2005]. Polymer foams can be produced by a wide variety of processes including injection moulding and extrusion. When the polymer exits from an extrusion die, sudden pressure and temperature changes occur resulting in nucleation and growth of bubbles, producing a foamed structure. The bubble growth data are important for understanding the foam growth.

2.5.2 Properties of Foams

Foams are usually classified as flexible, semi-flexible (semi-rigid), or rigid and can be fabricated to any desired degree of hardness. Foams may be flexible or rigid, depending upon whether their glass transition temperature is below or above room temperature, which in turn depends upon their chemical composition, the degree of crystallinity and the degree of cross-linking. Polymeric foams comprise a wide selection of materials, with densities ranging from as low as 1.6 kg/m^3 to 960 kg/m^3 [Klempner and Frisch 1991], depending on processing method. At low densities, these materials have thermal insulation properties which compare favourably with well-known insulators such as glass fibre. At higher densities, they offer substantial material and weight savings in structural applications where rigidity is required [Amon and Denson 1984].

Bubbles are small spherical gas objects in a denser medium (i.e. polymer). Bubbles tend to rise owing to the buoyancy force and may react with the polymer both physically and chemically. The behaviour of very small bubbles is also influenced by surface tension. A decrease in pressure or an increase in temperature causes the growth of the bubble volume [Nemec and Klouzek 2003]. In many materials the liquid phase actually contains many micro-bubbles of air and they serve as sites for bubble nucleation [Klempner and Frisch 1991]. Bubbles in polymers are frequently multicomponent in nature as some components come from the impurities of the gas (i.e. CO_2) in a closed system and from atmosphere components in an open system such as nitrogen, oxygen, and argon [Nemec and Klouzek 2003].

2.5.3 Manufacturing Methods of Foams

Foams can be manufactured by a variety of processes, depending upon the application. Typical processing methods include molding, spraying and lamination [Klempner and Frisch 1991]. In general, the foaming results from a sudden reduction in pressure [see Everitt et al 2006] or change in the temperature [see Nemec and Klouzek 2003].

Foams can be produced from several major types of polymer [Klempner and Frisch 1991]:

- Thermoplastic polymers; which are formed first as solid, melted to provide the fluid phase foamed, and finally cooled to solidify and thus stabilize the foam.
- Thermoset foam system, in which the reactants are formed while only partially reacted and are still fluid, followed by curing to the thermoset state to stabilize the foam.
- A latex that is formed and then stabilized by phase inversion, achieved by lowering the pH, freezing, or both, frequently with additional curing in the formed state.

The gases that may be used for foaming may be derived form any of number of sources [Klempner and Frisch 1991;

- Air may be whipped into the liquid as in the frothing of latexes.
- Carbon dioxide may be dissolved in the liquid or solid (like polymer), often under pressure and may be brought out of solution for forming by reducing the pressure or by heating the solution (Liang and Wang, 2000). With increases in initial pressure, the density decreases as more gas is absorbed in the polymer. The rate of decrease of mixture density is relatively high, as the pressure regime where CO_2 density is rapidly increasing and thus the amount of CO_2 sorbed also increases rapidly [Goel and Beckman 1994].
- A low boiling liquid such as pentane or a fluorocarbon may be dissolved in the polymer and then converted to a gas by heating or reducing the pressure.

- Gas generated by a chemical reaction, such as the reaction of an Isocyanate (Isocyanate is the functional group of atoms –N=C=O) with water or the decomposition of Azodicarbonamide. Azodicarbonamide is an organic chemical ($C_2H_4O_2N_4$) a light red crystalline powder, which is used in the food industry as a food additive. Polyurethane foams (polymers consisting of a chain of organic units joined by urethane (or Carbamates) links -NH(CO)O) are made by this method.

2.5.4 Optical Observations of Bubble Formation and Growth

Blowing bubbles in plastics first began around 1970. In 1973 Stong succeeded in blowing plastic bubbles and developed the project as a hobby. He made a bubble solution by dissolving the polymer in acetone then he tried number of variations before settling on a combination of poly(vinyl acetate) and acetone at 20 °C [Stong 1973], see Figure 2 - 23. After this novel finding by Stong (1973), polymer foaming has received growing interest by academic and industrial researchers (see review by Tomasko et al 2003).

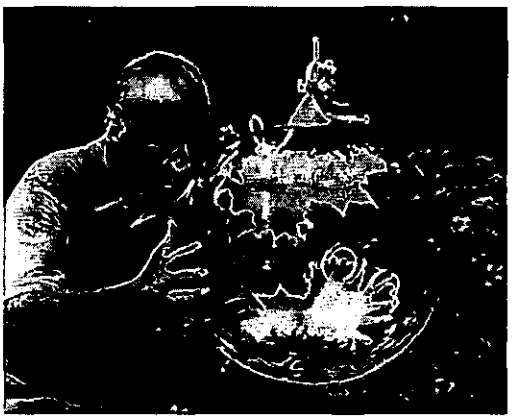

Figure 2 - 23: Plastic bubbles of poly(vinyl acetate) and acetone at 20°C [Stong 1973].

Most researchers have used optical observations to study the swelling behaviour and bubble nucleation and growth [e.g. Han and Yoo 1981, Goel and Beckman 1994, Liang and Wang 2000, Royer et al 1999, Martinache et al 2001, Tuladhar and Mackley 2005]. These studies were conducted to obtain the diffusion coefficient of different polymers under high pressure with a CCD camera. The method advantages are high pressure view cells which limit the diffusion of CO_2 and polymer swelling to one dimension.

Most experimental investigations have been done after the molten point has stabilised around 200 °C during mold filling and injected a pressure of 20.6 bar [Han and Yoo 1981], see Figure 2-24. Han and Yoo (1981) used a rectangular mold cavity with glass windows on both sides to observe the growth of gas bubbles during mold filling. The smallest bubbles they observed were 0.03 mm in size and the shape of these bubbles was spherical. Han and Yoo (1981) experimentally recorded the growth of bubble during injection molding of PS foam with CO_2 as blowing agent, and this work provides the most detailed description of the experimental conditions and results [Chen and Feng 2006].

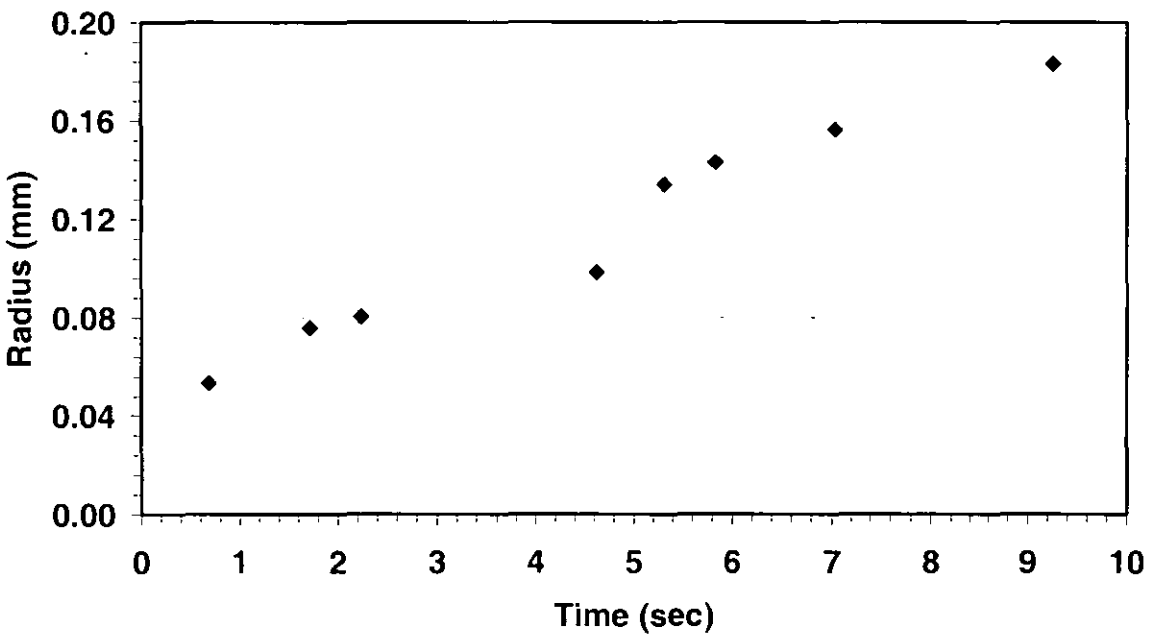

Figure 2 - 24: Bubble radius of PS/CO_2 at 200 °C and 20. 6 bar [Han and Yoo 1981].

After Han and Yoo (1981) no experimental work has been found for PS/CO_2 except that by Tuladhar and Mackley (2005). Their study was on the foaming of PS using an in house developed Multipass Rheometer (MPR) as a variable pressure device to follow foaming at 140 °C and pressure of 92 bar. The micro bubbles were followed during the foaming of molten PS that was supersaturated with CO_2. Figure 2 – 25 expresses Tuladhar and Mackley (2005) findings:

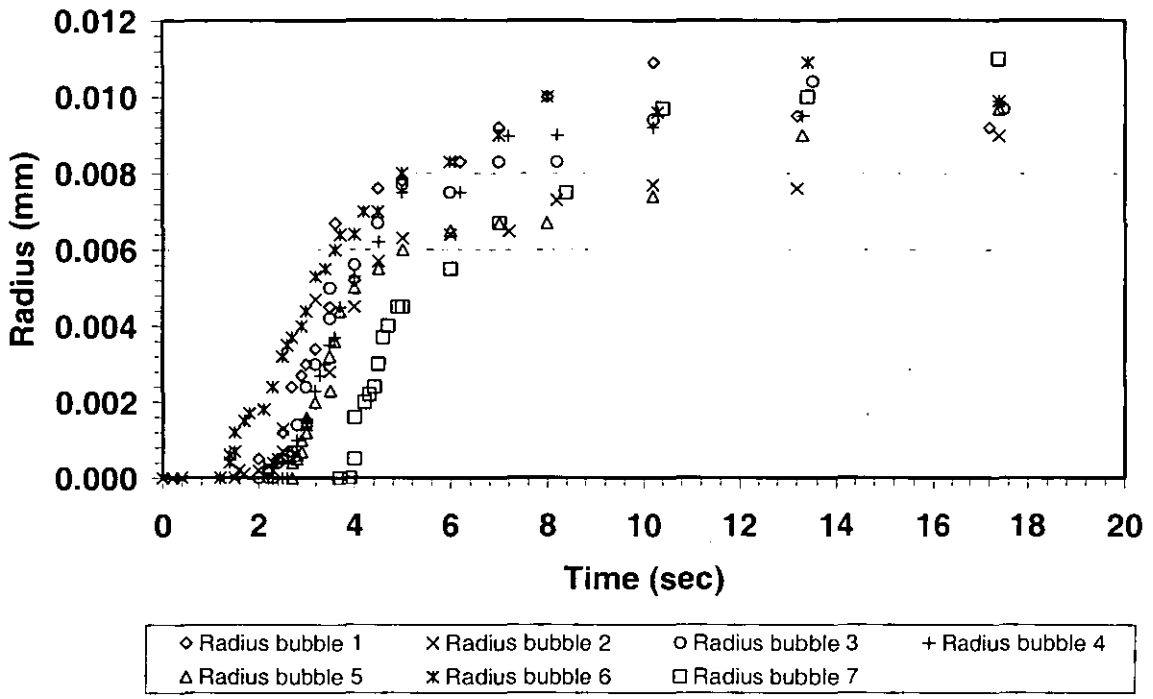

Figure 2 - 25: Bubble radius of PS/CO_2 at 140 °C and 92 bar [Tuladhar and Mackley 2005].

By comparing the previous figures (Figure 2-24 and 2-25) it can be seen that the Han Yoo (1981) bubbles grow faster than those observed by Tuladhar and Mackley (2005). This is because Han and Yoo (1981) used higher temperatures and they reduced the pressure more suddenly which made the foaming happen more quickly. In addition, this may be due to the fact that, as the temperature is increased, the viscosity is decreased, which in turn favours both bubble formation and growth.

To explain the foaming behaviour will discuses Goel and Beckman (1994) studied, as they used a microcellular high pressure view cell and it is different from what the others used. This study was done in amorphous polymer sample as the swelling was increased by a supercritical fluid (CO_2) over a sufficiently long period of time to ensure that an equilibrium amount of fluid is absorbed by the polymer. Nucleation is induced by supersaturation caused by a sudden pressure drop from the equilibrium solution state, and the nuclei grow until the polymer vitrifies at a lower pressure. The following scheme illustrates the general nucleation and growth mechanism (see Figure 2 - 26).

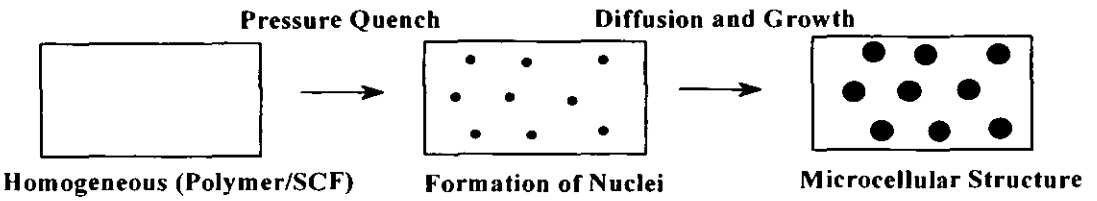

Figure 2 - 26: Schematic of nucleation and growth mechanism [Goel and Beckman 1994].

Royer et al 1999, used a novel experimental setup to investigate *in situ* the swelling behaviour of a polymer melt in contact with a high-pressure fluid. This approach, based on optically monitoring polymer swelling in real time, was used to determine the swelling kinetics, swelling equilibrium, and rates of CO_2 diffusion into poly-(dimethylsiloxane) (PDMS) melts of three different molecular weights. The equilibrium swelling of PDMS were unaffected by molecular weight within the range of molecular weights studied. However, increased pressure enhanced the extent of swelling whereas a maximum was observed with increasing temperature, at pressure above 15 MPa. Below 15 MPa, a monotonic decrease in the equilibrium swelling ratio is observed with increasing temperature.

In 2000 Liang and Wang provided an alternative technique to foam poly(ethylene terephthalate) (PET) and polycarbonate (PC) by rapid depressurisation of CO_2-saturated molten resin. They used a saturation tank with an internal volume of 150 ml equipped with a heating jacket and a temperature controller. The pressure was adjusted through a back pressure regulator and the microstructure of the foams was inspected by scanning electron microscopy (SEM). The foams prepared by slow depressurization were inspected using an optical microscope. It is found that the foamable temperatures and pressures for PET and PC were nearly identical. The temperature influences nucleation via two effects, a viscosity effect and a solubility effect which compete. As temperature rises the viscosity falls which aids nucleation, but also the solubility decrease which hinders nucleation. However, the effect of saturation pressure on the nucleation is more straightforward. Higher initial pressures lead to greater subsequent supersaturation and lower viscosity during depressurisation which both aid nucleation.

2.5.5 Bubble Growth Modelling Background

Foam modelling can by divided into three stages; bubble nucleation, bubble growth, and possibly coarsening. Bubble growth is the most thoroughly studied of the three [Chen et al 2006]. Many models have been proposed for radial growth of a single bubble in an infinite expanse of melt, and most of the models are similar.

Viscosity, diffusivity and surface tension are potentially significant to foaming. All three factors directly affect the growth of gas bubbles, and therefore will have an impact on the bubble-size and ultimate properties of the foamed product [Chen et al 2006]. These properties are likely to vary with concentration as follows:

i. Viscosity. This will fall when the blowing agent is dissolved (a polymer melt typically experiences a drastic reduction in viscosity). Conversely as the concentration of blowing agent drops during foaming the viscosity will be restored to near its original value.
ii. Gas diffusivity. The dissolved gas will modify the molecular environment for its diffusion through the polymer during foaming, typically raising the gas diffusivity. The gas diffusivity varies approximately inversely with the viscosity.
iii. Gas-polymer interfacial tension. The interfacial tension reflects the interaction between the two species of molecule, which will be influenced by the presence of the blowing agent molecules in the melt.

Amon and Denson (1984) is the one of the earliest workers to develop a mathematical analysis of bubble growth in expanding foams and subsequent workers have used a very similar framework [Arefmanesh and Advani 1991, Ramesh et al 1991, Shafi et al 1997, Joshi et al 1998, Venerus and Yala 1997, Venerus et al 1998, and Feng and Bertelo 2004]. Amon and Denson's analysis is based on a cell model whereby the foam is divided into spherical microscopic unit cell of equal and constant mass, each consisting of a liquid envelope (or shell) and a concentric spherical gas bubble. The gas bubble initially has a radius (R_0), internal pressure (P_{g0}), and the polymer cell has an outer radius (S), see Figure 2

- 27. The expansion occurs by diffusion of a dissolved gas from the supersaturated polymer envelope into the bubble.

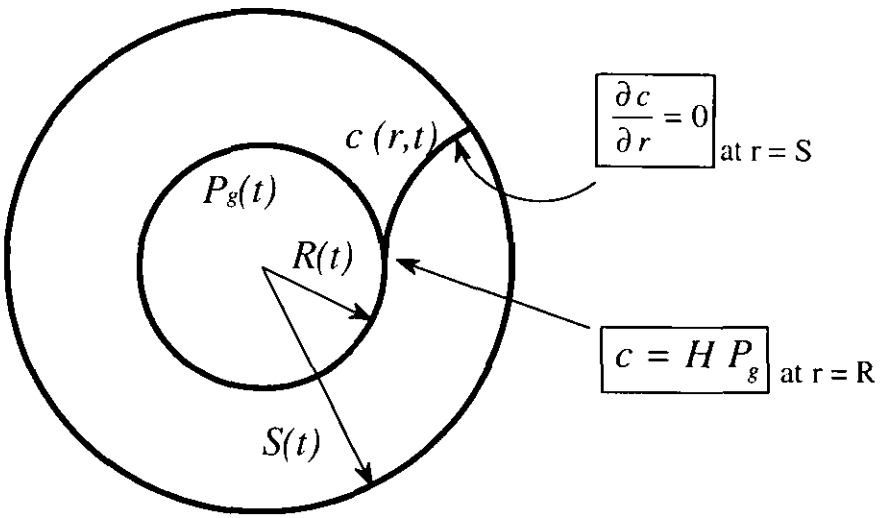

Figure 2 - 27: Schematic diagram of a unit cell [Amon and Denson 1984].

The bubble growth equation is represented by three equations based on combined equation of momentum and continuity of the melt surrounding the bubble in radial component (r) of spherical coordinates (Eq.1-1), mass balance of the gas at the bubble surface (Eq.1-2) and diffusion of gas in the melt (Eq.1-3):

$$P_G = P_L + \frac{2\gamma}{R} - 4\eta\frac{dR}{dt}\left(\frac{1}{R} - \frac{R^2}{S^3}\right) \qquad \textbf{Eq. 1 - 1}$$

$$\frac{d}{dt}\left(\frac{4\pi R^3}{3}\frac{P_G M}{\Re T}\right) = 4\pi R^2 D\rho\left(\frac{\partial c}{\partial r}\right)_{r=R} \qquad \textbf{Eq. 1 - 2}$$

$$\frac{\partial c}{dt} + \frac{R^* R^2}{r^2}\frac{\partial c}{\partial r} = \frac{D}{r^2}\frac{\partial c}{\partial r}\left(r^2\frac{\partial c}{\partial r}\right) \qquad r \geq R \qquad \textbf{Eq. 1 - 3}$$

where P_L is the ambient pressure, P_G is the pressure of gas in the bubble, c is the dissolved gas concentration in the melt, D is the diffusion coefficient, ρ is the melt density, T is the temperature, M is the molecular weight of the gas, η is the viscosity of the polymer, γ is the surface tension and $\Re$ is the gas constant.

The goal of the mathematical analysis is to determine the bubble radius as a function of time, by deriving and solving the governing equations with some assumptions, as summarised below:

1. The gas inside the bubble is an ideal gas.
2. Thermodynamic equilibrium is maintained at all times at the gas-liquid interface according to Henry's law.
3. The mass of dissolved and free gas is negligible in comparison with the mass of polymer.
4. The polymer is an incompressible, Newtonian liquid.
5. No gas loss to the surroundings.
6. Negligible latent heat of solution of the gas in the liquid and negligible temperature change of the free gas upon expansion.
7. The shear viscosity is 1/6 of the extensional viscosity.

Amon and Denson (1984) noted that the polymer undergoes extensional rather than shear deformation, a fact that was not appreciated by some later workers who assumed shear thinning behaviour for the viscosity rather than tension thickening.

Tuladhar and Mackley (2004), used the same main equations of developing a bubble growth model using PS / Pentane to provide theoretical predictions of the bubble growth during foaming. The growth model was developed to describe the process. After the onset of nucleation the pressure of the gas in the bubble (P_G) provides the driving force to expand while the viscosity (η) of the polymer and surface tension (σ) of the bubble wall provide resistance to bubble growth. Each bubble is assumed to be spherical with nucleation radius (R_0 = 1 μm), and is surrounded by a finite volume of melt with an initial radius (S_0 = 0.15 mm).

Further work were done by Feng and Bertelo in the same year (2004), developed a nucleation model based on the concept of heterogeneous nucleation originating from pre-existing micro-voids on solid particles. The model is included many concepts used by Ramesh et al 1994a. Theses concepts are summarized below:

1. An existence of microvoids on rubber particles added to PS as nucleation agents, the microvoids were measured by electron microscopy.
2. Each particle produced one bubble from its largest microvoid.
3. The size of the nucleation bubbles scales with the size of the particle.
4. There is a minimum size for the bubbles to be viable, larger ones grow further but smaller ones disappear.

Recently, Chen et al 2006 studied the radial growth of a single bubble in an infinite expanse of melt, using parameter values based on experiments on the polystyrene-CO_2 system. Their results show that the increase of blowing-agent diffusivity due to plasticization can greatly increase the rate of bubble growth, even at relatively low gas concentration and the reduction in melt viscosity and surface tension has little effect on bubble growth. The interfacial tension between PS and CO_2 was predicted by the density gradient theory to be 27.7 dyn/cm at atmospheric pressure and 200 °C and it is close to the Han Yoo (1981) result (28 dyn/cm).

2.6 Conclusion

Carbon dioxide is a small but important constituent of air. Carbon dioxide is a multipurpose material and has common uses in a vapour, liquid, solid or supercritical fluid. Carbon dioxide does not exist in liquid form at atmospheric pressure at any temperature. One of the important states of the carbon dioxide is the supercritical state which occurs above a temperature of 31.1 °C and above a pressure of 74 bar. Supercritical CO_2 has diffusivity approximately 100 times greater than a liquid, allowing rapid transport properties. This is because the viscosity of the supercritical fluids is closer to that of a gas. In addition, supercritical CO_2 is an attractive for solvent because no rinsing with water or drying is needed since supercritical CO_2 evaporates completely upon depressurisation to atmosphere.

Polymer are a large class of materials consisting of many small molecules that are linked together to form long chains. There are two main types of polymers, thermoplastics and thermoset. Thermoplastics can be softened on heating and its exhibit a glass transition temperature, commonly used are polyethylene, polystyrene, and polypropylene. This research project will examine this type of polymer. Thermosets cannot be softened by heating and do not exhibit a glass transition temperature.

Glass transition temperature where polymers change from a glassy to a rubbery state over a small temperature range as molecules become mobile. Each polymer has a different glass transition temperature (T_g) and its not a single event but occurs in stages over a temperature range as different parts of the polymer become more mobile. A number of physical properties change around the glass transition temperature due to the increase in molecular mobility. These include elastic modulus (severe decrease), specific heat capacity (small increase), and dielectric constant (increase).

There are several methods available to measure the glass transition temperature, mechanical methods, volumetric methods, dielectric constant methods, heat capacity methods, and spectroscopic methods. Differential scanning calorimetry (DSC) is one of the most popular techniques for measuring T_g as it is fast and accurate. However, it is not a simple task to do so at high pressure as the high pressure cells have a typical pressure limitation about 6.9 MPa (1000 psi) [Tomasko et al 2003].

Also note that measured T_g values for the same polymer differ between researchers, perhaps due to different techniques and experimental procedures. Many factors affect the T_g of a polymer. Some factors are due to the chemistry of the polymer:

- Chain length
- Chain flexibility
- Side group
- Branching
- Presence of plasticisers (e.g CO_2)

Other factors are to do with the method of measuring T_g:

- Strain rate
- "Cooling" or "heating" rate
- Property that is probed

It has been known for many years that the compressed gasses change the physical properties of the solid materials (as polymers) and the dissolution of CO_2 can dramatically lower the T_g of polymers. Relatively few studies have directly examined the effect of CO_2 on the mechanical properties of polymers. Only several researchers measured the glass transition experimentally and few of these studies have exceeded 60 bar of CO_2 pressure. Yoo and Cha (2001) measured the glass transition in the pressure chamber, by detecting using a magnetic switch when the polymer had sagged by a certain amount. This technique, however, is very close to our novel technique measures the deflection (sag) from inside the cell, as the LVDT sensor is touches the specimen surface to measure and monitor the softening processes.

Bubble growth has been theoretically addressed by number of researchers and most of the models are similar. The gas bubble initially has a radius (R_0), internal pressure (P_{g0}), and cell outer radius (S), the expansion occurs by diffusion of a dissolved gas from the supersaturated polymer envelope into the bubble. Foam modeling can by divided into bubble nucleation and bubble growth. Many theories have been proposed for nucleation radial growth of a single bubble in an infinite expanse of melt. The main parameters that play the potentially significant in bubble foaming are viscosity, diffusivity and surface tension. All this three factors (μ, D, and σ) directly affect the growth of gas bubbles, and therefore will have an impact on the bubble-size and ultimate properties of the foam product

Optical observation is a powerful technique to study polymer foaming. Only a few researchers have used these observations to study the swelling behaviour, bubbles nucleation and bubble growth. Most experimental investigations have been performed above the melting point (around 140 to 200 °C).

From this literature reviews the following information will be directly use in this work:

- Published values of the glass transition temperature of carbon dioxide with various polymers and at various pressures.
- Published values of solubility and diffusion coefficient of carbon dioxide with various polymers.
- Published values of Henry's constant and surface tension.
- Bubble growth model techniques.
- Published data for bubble growth in CO_2/PS systems.

Chapter 3 Experimental Apparatus, Methods & Materials

3 Introduction

This chapter presents two specially constructed types of experimental cell working under high pressure (up to 200 bar) and high temperature (up 200 °C). The aim of this research is study the mechanical response of polymers to carbon dioxide. Firstly the polymers softening temperature was determined as a function of applied CO_2 pressure using a novel mechanical measurement. A linear variable displacement transducer (LVDT) was used to continuously monitor the deflection of a polymer strip undergoing a 3-point bending test, the main purpose is to measure how the deflection varies as the temperature is slowly increased for various pressures of CO_2.

Secondly to study bubble nucleation and polymer foaming on depressurisation, using a high pressure cylindrical view cell with 2 optical widows, connected to a digital still camera with a high magnification lens (60 mm) to monitor and record the bubbles growing. These two high pressure cells have been designed and manufactured at a Loughborough University workshop.

3.1 Common Apparatus

3.1.1 Introduction

Some common instruments have been used in the polymer softening experimental setup as well as the polymer foaming experimental setup. Both experimental setups are equipped with a platinum resistance temperature (PRT) probe located close to the sample in the cell to measure the specimen temperature, a pressure transducer to measure the cells pressure, and a computer using Pico Log software was used to collect the experimental data. These instruments are now described in details:

3.1.2 PRT Probe

The sample temperature was measured by a PR-13 platinum resistance thermometer (Omega Eng. Limited). This operates on the principle of the change in electrical resistance in the wire as a function of temperature. Standard PRT probe assemblies are rated for use in temperatures up to 600 °C. The PRT probe was positioned with the tip close to the surface of the polymers sample.

3.1.3 Pressure Control

The pressure control in the cells was achieved as follows:

- CO_2 cylinder which enables pressure up to 54 bar to be achieved directly.
- Pump which enables high pressure to be achieved (up to 120 bar) – not needed below 54 bar.
- Back pressure regulator – used to control the pressure.
- Pressure relief valve – used as a safety device.
- Heat exchanger – using ice bath to cool CO_2 (pump is acting on liquid CO_2).

The desired pressure for each experiment was set by the use of a backpressure regulator. Pressures of 0, 20, 40, 54, 70, 85, 100 and 120 bar were employed in separate experiments.

3.1.4 Pressure Transducer

The pressure transducer sensor (type PMP 1400, Druck) (see Figure 3 - 1) was chosen to monitor the cell pressure. The stainless steel isolation diaphragm and fully welded stainless steel pressure module ensures excellent media compatibility. The pressure range of the transducer used is 0 - 250 bar and the operation temperature is –20 to 80 °C. The manufacturer's calibration data were used to convert the voltage output signal to a pressure value.

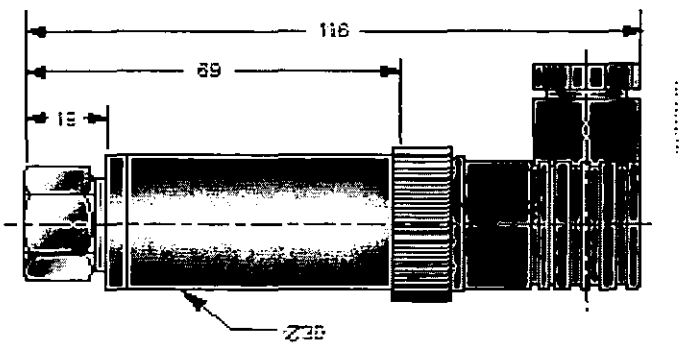

Figure 3 - 1: Pressure Transducer (type PMP 1400, Druck).

3.1.5 Pico Log software

Data acquisition was performed using a Pico ADC-16 which is a self-contained high accuracy data logger for use with PCs. It was connected to a RS 232 port (data lines); this port was connected to the following instruments to collect the data.

A. Pressure transducer; cell pressure (bar).
B. PRT probe; specimen temperature (°C).
C. LVDT; central deflection of the polymers strip (mm), this is described in section 3.2.2 (only used with polymer softening cell).

The input signals to the Pico logger are in volts. The ADC-16 generates readings, which are in ADC counts.

3.1.6 Temperature Controller

A Eurotherm programmable temperature controller (Type 812) was used to control the cell's temperature (initially an oil bath (deep fryer) was used and later electric heaters). Both isothermal and liner ramps of the set-point temperature can be programmed into the controller. The Eurotherm controller has a front control panel to make adjustments for temperature hold (ranged 0 to 50 °C), ramp rate (± 0.5 %), dwell time (± 1sec.), loop counter, proportional band, integral and derivative time constant, output power limit and cycle time, and alarm setting. In addition, the front panel displays power output, alarm, temperature hold, program end, ramp and dwell segments.

3.2 Polymer Softening - High Pressure Cell

3.2.1 Introduction

Polymer softening experiments were carried out in a cylindrical stainless steel cell. The cell houses a linear variable displacement transducer (LVDT) which was suspended from the top of the cell, and measures the central deflection of a polymer strip (of dimensions 80 mm length x 20 mm width) placed horizontally at the base of the cell in a 3-point bending configuration. The cell is externally heated by a temperature controlled bath (deep fat fryer) containing vegetable oil, which can be heated from ambient temperature to 200 °C, see Figure 3 - 2. The nominal glass transition temperature was recorded as the onset temperature where the central deflection suddenly begins to increase.

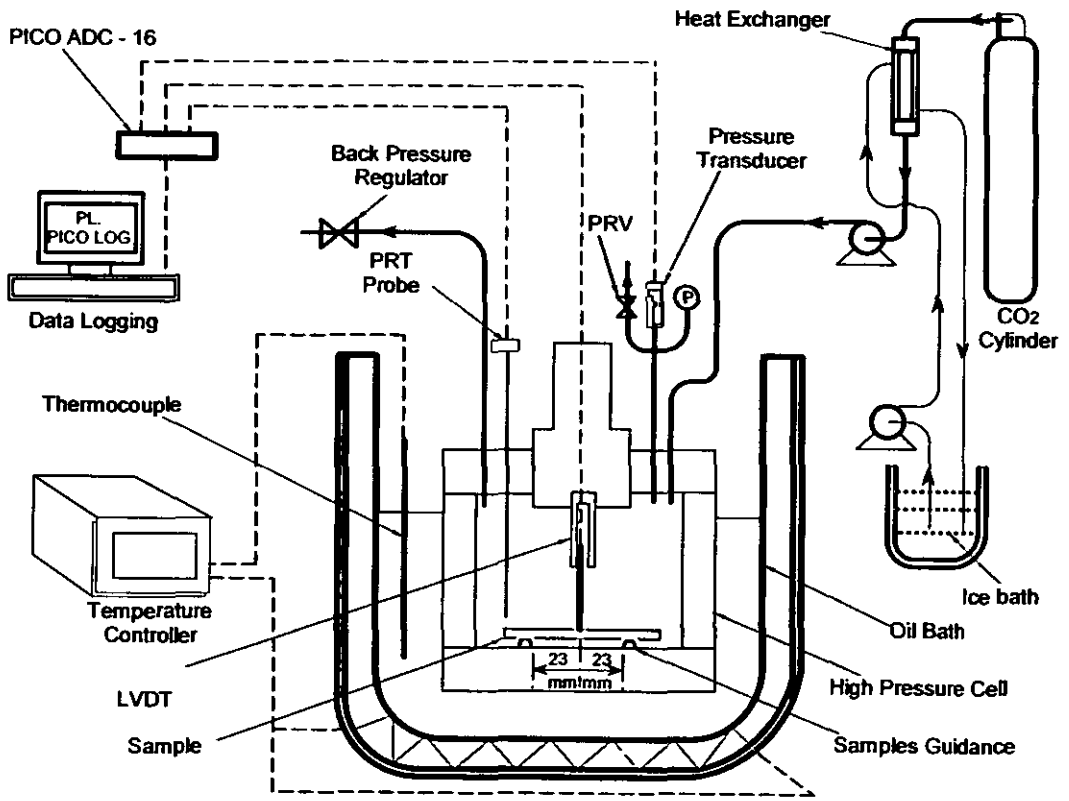

Figure 3 - 2: Experimental set-up showing connections to the high-pressure cell.

The high-pressure cell is made of stainless steel with dimensions of 115 mm (high) x 130 mm (diameter). This type of cell is specially designed to work with high pressure (200 bar) and high temperature (up to around 200 °C). The cell has three parts and can be opened from the top or the bottom (see Figure 3 - 3a and 3 – 3b). The top part contains the LVDT sensor and the arm of displacement transducer, the arm of the transducer touches the surface of the sample to measure the central bending. The bottom of cell is opened for fitting or taking out the sample (polymer specimen) and had a holder that the sample fits into. From this following figure, we can see the sample position in relation to the LVDT.

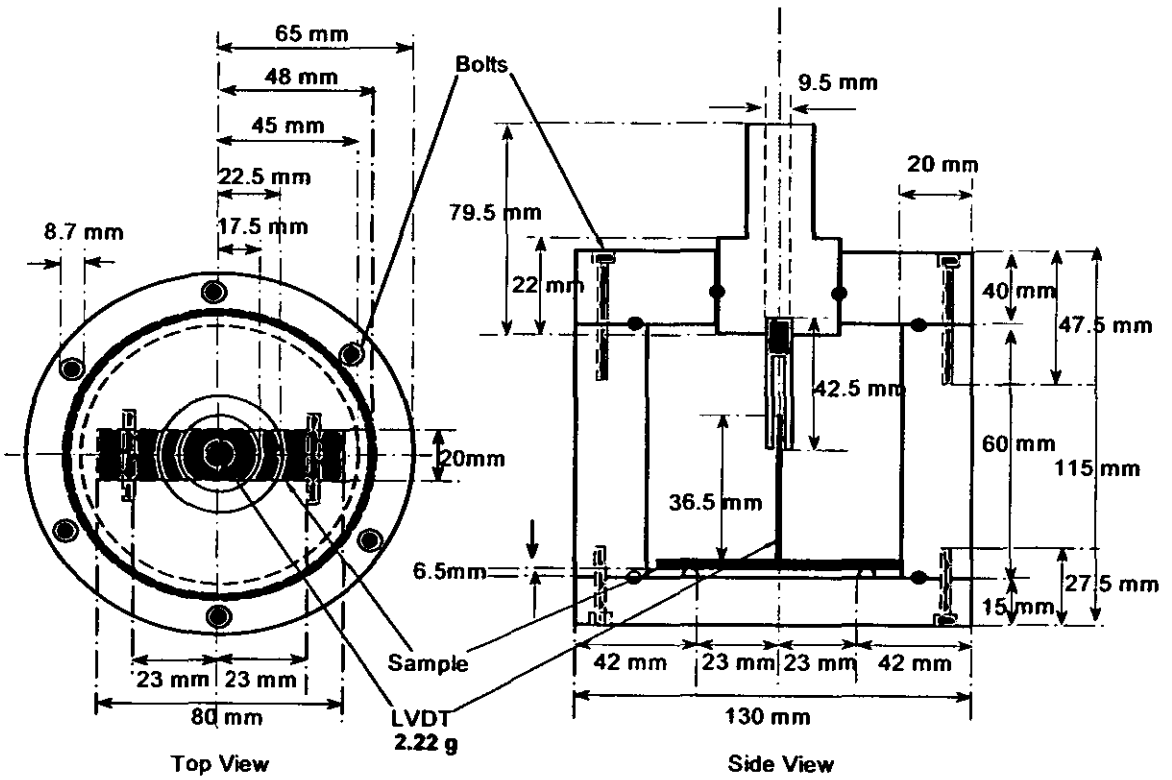

Figure 3 – 3a: Drawing of High – Pressure cell.

Figure 3 - 3b: Photograph of high-pressure cell.

As presented in the experimental setup, the cell has an oil bath (controlled by temperature controller), LVDT, and sealing gland. Now these additional items will described in more details:

3.2.2 LVDT

Linear variable displacement transducers (LVDT) are widely used for making measurements of relatively small displacement, they comprise a primary and two secondary windings variable coupled by a magnetic core. In this study the LVDT with flat tip (type sm3, RS Components, UK) was used to measure the central bending (deflection) of the polymer strip.

An LVDT is an accurate sensing device that converts linear position or motion to a proportional electrical output. The basic LVDT design, as shown in Figure 3 - 4 consists of three elements:

1. One primary winding
2. Two identical secondary windings
3. A movable magnetic armature or "core" (2.22g)

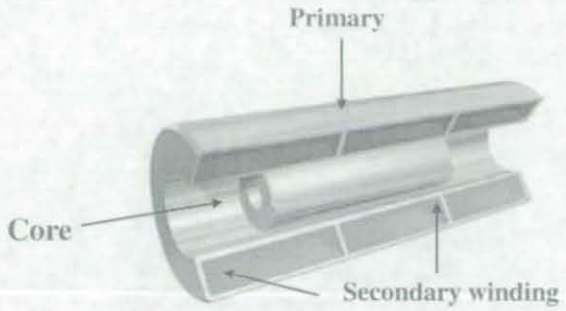

Figure 3 - 4: LVDT – Manufactures Catalogue.

The primary winding is excited with an AC supply generating a magnetic field which, when the core is placed in the central position, induces an equal voltage in both of the secondary windings. The secondary windings are wired in opposition so that their combined output represents the difference in the voltage induced in them, which in this case is zero. As the core is moved relative to the windings, the difference in induced voltages produces an output that is linearly proportional in magnitude to the displacement of the core. LVDTs are virtually frictionless, as there is no necessary contact between the core and the internal bore of the coils, and can offer excellent resolution with outstanding repeatability. LVDTs are excited with AC voltages with frequencies as high as 10 kHz and have low mass cores, they are ideal for use in dynamic motion measurement situations.

The calibrations were done manually by measuring the movable magnetic armature (core) by the transducer indicator (mV) (Figure 3 - 5) and measuring the length of the displacement arm by a digital calliper (mm). Figure 3 - 6 shows the LVDT calibration.

Figure 3 - 5: Transducer indicator.

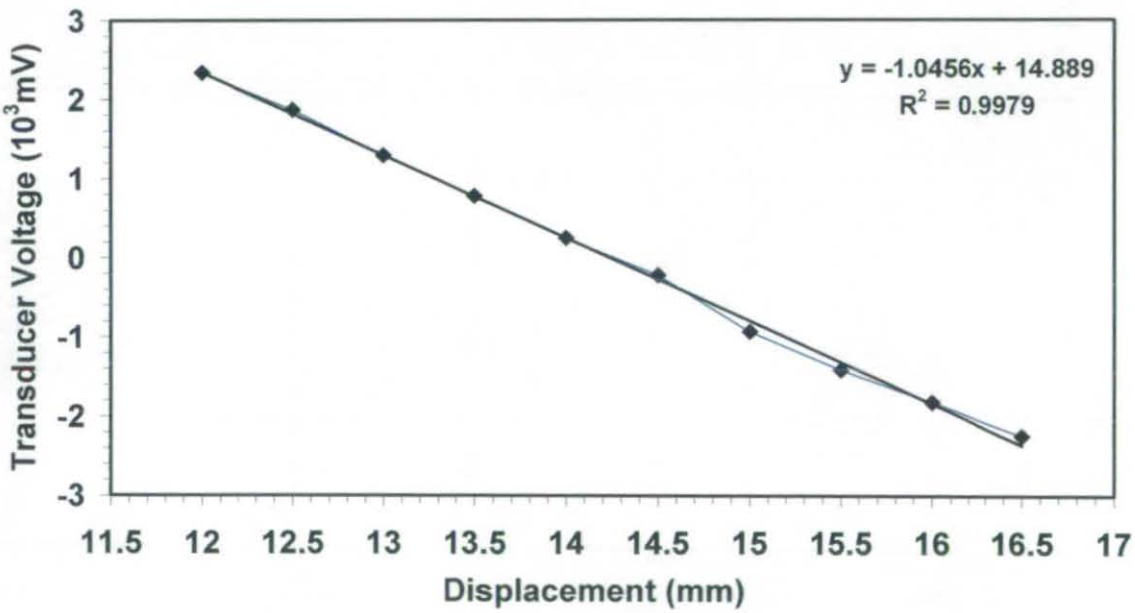

Figure 3 - 6: LVDT calibration.

3.2.2.1 LVDT Core Net Weight

Because the core is sitting free on the sample with 2.2 g weight, and in the 3 point techniques force is applied by gravity (sample weight), therefore the core net weight is important to see if the weight of the core is significant or not. The following sketch shows the force direction, core weight, and core dimension. Figure 3 - 7 illustrate the core dimensions (2.4 mm radius x 36.5 mm high) and position.

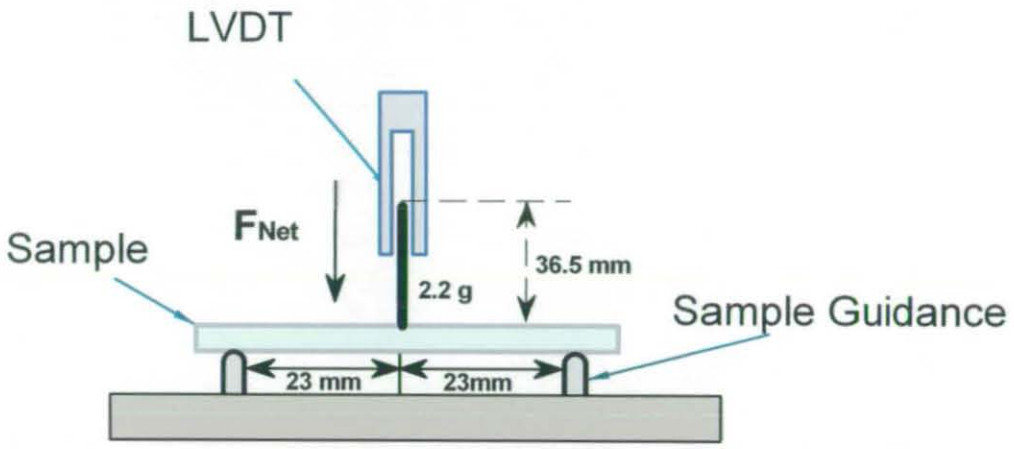

Figure 3 - 7: LVDT core position.

The following equations have been used to calculate the force net weight of the rod:

$$\Sigma Fy = 0 \qquad \textbf{Eq. 3 - 1}$$

$$F_{Net} = m.g - F_{buoyancy} \qquad \textbf{Eq. 3 - 2}$$

$$F_{Buoyancy} = V_{Rod}.Mw_{CO_2}.\rho_{CO_2}.g \qquad \textbf{Eq. 3 - 3}$$

$$V_{Rod} = \pi r^2 L \qquad \textbf{Eq. 3 - 4}$$

$$(F_{Net} = kg.\frac{N}{kg} - m^3\frac{mol}{m^3}\frac{kg}{mol}\frac{N}{kg} = N)$$

where: F_{Net} is the rod net force on the sample, $F_{buoyancy}$ is the rod buoyancy, m is the weight of the rod, g is the standard gravitational intensity, V_{Rod} is the rod volume, Mw_{CO_2} is the carbon dioxide molecular weight, and ρ_{CO_2} is the carbon dioxide density.

The force (F_{Net}) applied to the sample by the rod was calculated at the following pressures 0, 20, 40, 54, 70, 85, 100, 120 bar which were used in this study. The density values of CO_2 were calculated using the Soave Redlich Kwong (SRK) equation (equation of the state) for all the pressures used in this study [Wang and Gmehling 1999].

$$P = \frac{\Re T}{V-b} - \frac{a(T)}{V(V+b)} \qquad \textbf{Eq. 3 - 5}$$

where: P is the pressure, T is the absolute temperature, $\Re$ is the gas constant, and V is the molar volume. The values of a and b is show below [Wang and Gmehling 1999]:

$$a = 0.42748 \frac{\Re T_c}{P_c} \qquad \textbf{Eq. 3 - 6}$$

$$b = 0.08664 \frac{\Re T_c}{P_c} \qquad \textbf{Eq. 3 - 7}$$

where: P_c is the critical pressure (73 bar), T_c is the critical temperature (304.2 K), and $\Re$ (8.314 J/ mol K) is the gas constant. Figure 3 - 8 shows a plot of CO_2 molar density versus temperature for all the pressures used in this study:

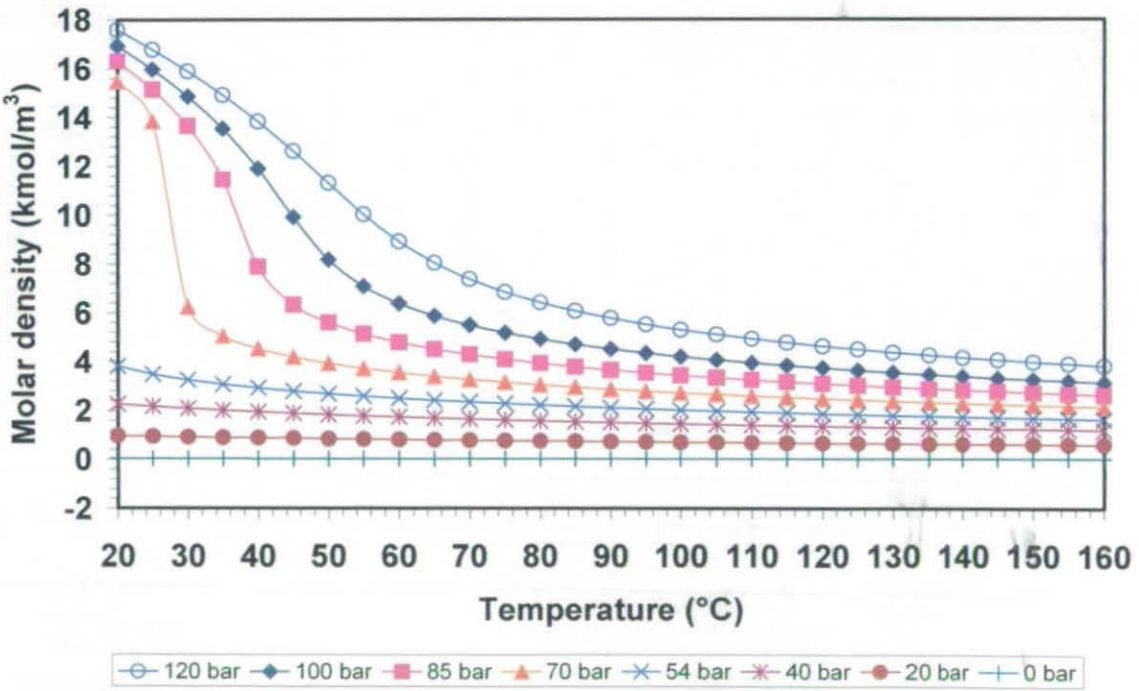

Figure 3 - 8: CO_2 molar density vs. temperature at the versus pressure used in this study.

From this figure we can get the density values of CO_2 at 20 °C and at other temperatures and pressures ranges which will help our study further on. The density values for 0, 20, 40, 54, 70, 85, 100, and 120 bar at 20 °C were found to be 0.0412 kmol/m^3, 0.978 kmol/m^3, 2.279 kmol/m^3, 3.828 kmol/m^3, 15.485 kmol/m^3, 16.311 kmol/m^3, 16.935k mol/m^3, 17.598 kmol/m^3 respectively. The following figure demonstrates the net force of the rod over the applied pressure range.

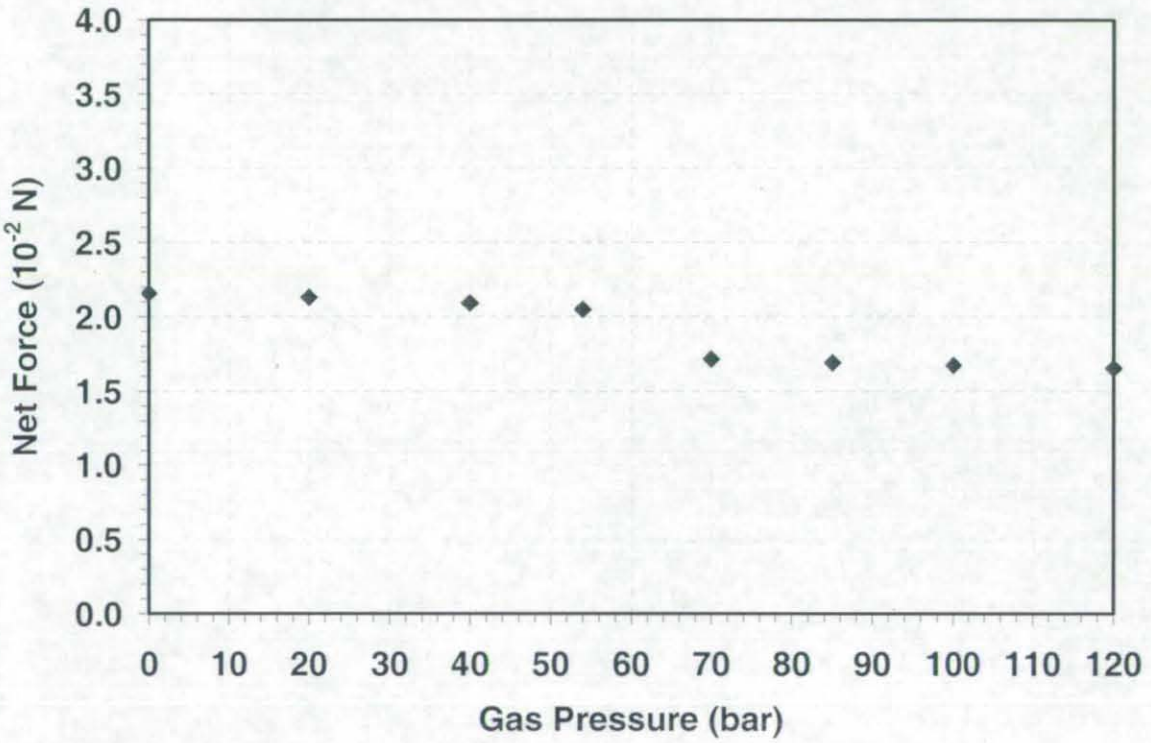

Figure 3 - 9: Core net force.

It is very obvious from this figure that the core net force change is insignificant and the maximum change is 0.00502 N during the ranges of pressure applied, therefore the sample is deflected by weight of the sample and gas diffusion into the sample.

3.2.2.2 High Pressure Sealing Gland

A sealing gland was used to feed the LVDT wires through the wall of the pressure vessel to enable them to connect to the data acquisition card. This type of seal has a high-pressure capability (vacuum to 960 bar), and temperature range (-185 to 870 °C). With this type of gland we can make sure that there is no leak between the cell and LVDT connections (because of the wires) and it can easily screw in to the cell. Figure 3 - 10 illustrate the high-pressure sealing gland.

Figure 3 - 10: High pressure sealing gland.

3.2.3 Oil Bath Temperature Controller

The oil bath (deep fryer) was controlled by a Eurotherm programmable temperature controller (see section 3.1.6). The temperature range was measured by comparing the inside temperature (sample temperature) and the outside temperature (cell temperature), as shown in following figure, there is about 20 °C interval between the inside and the outside temperature. The equilibrium time occurs at around 2000 sec, see Figure 3 - 11.

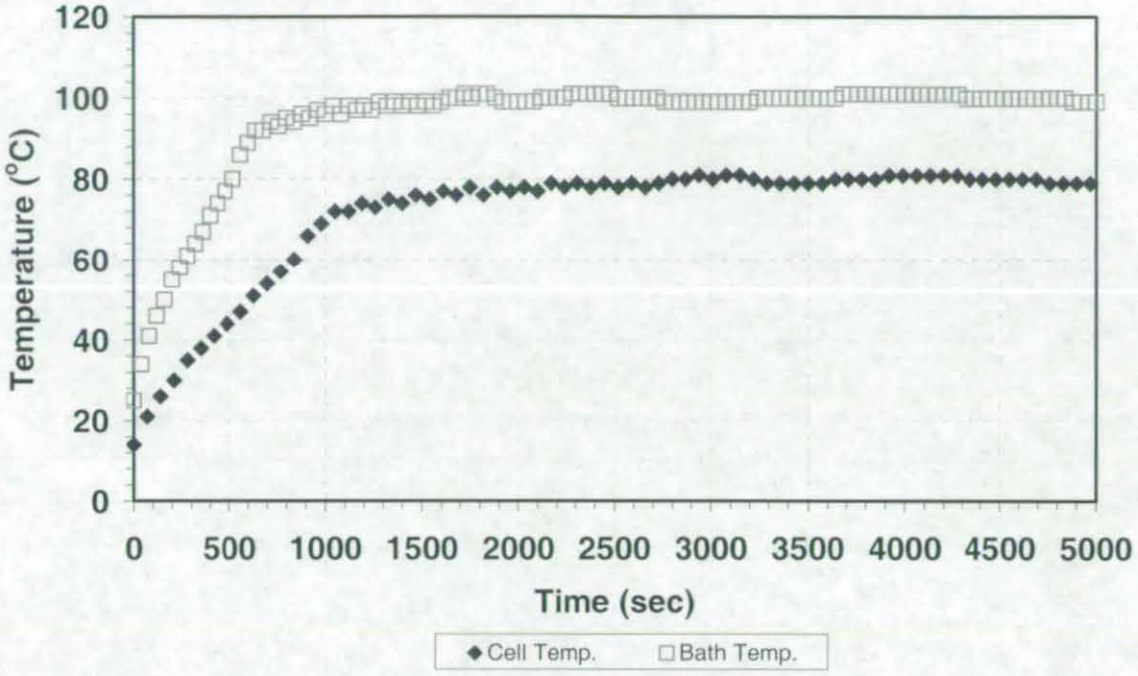

Figure 3 - 11: Oil bath temperature rate of the inside and outside.

3.2.4 Sample Loading

In order to load and unload the cell with the polymer strip the cell was placed on its side as shown in Figure 3-12, the polymers strip was loosely held in place by a number of screws. The cell was sealed and placed in the oil bath at ambient temperature and the various piping and electrical connections made.

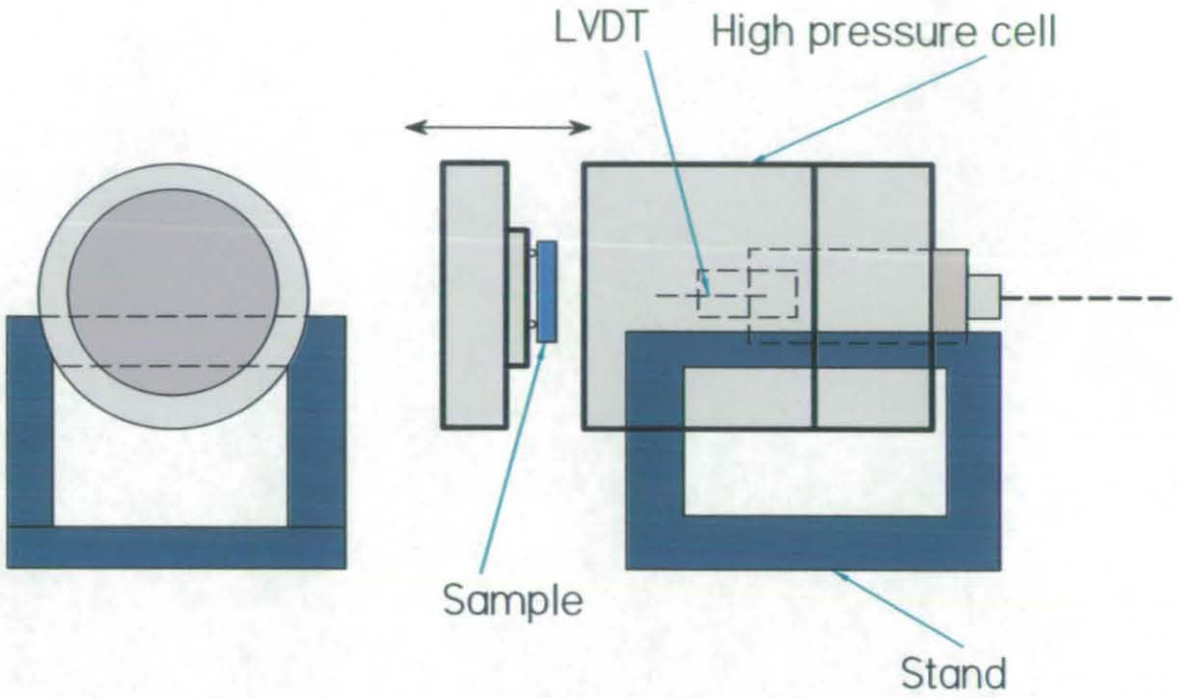

Figure 3-12 a: Sampling procedure.

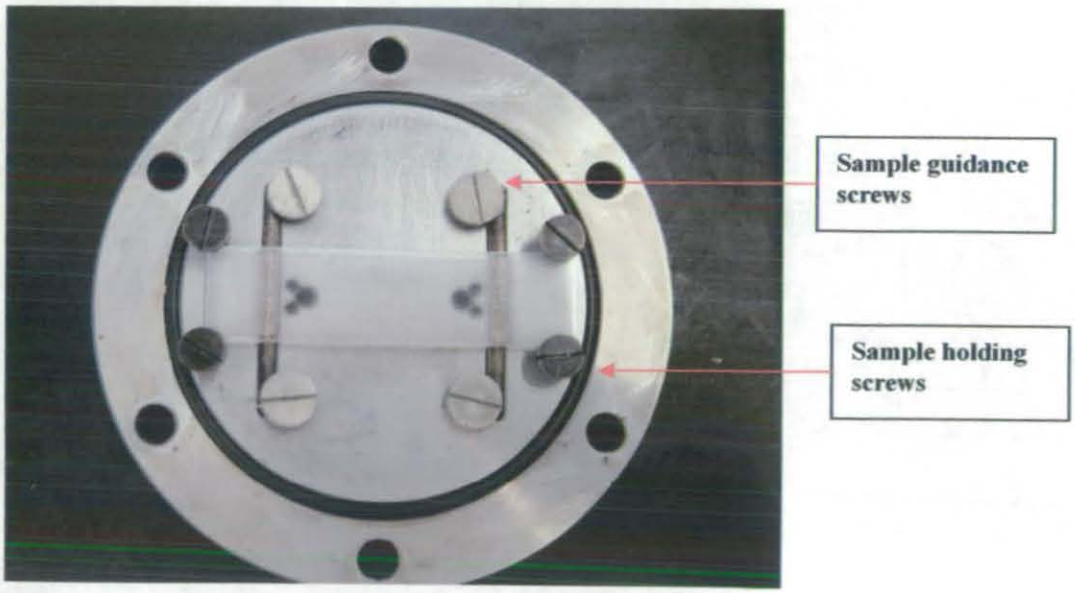

Figure 3 - 12 b: Polymers strip was loosely held in place by a number of screws.

3.2.5 Experimental Procedure

The experimental procedure was performed according to the following method:

1. The polymer sample was placed in the cell in contact with the LVDT, and the cell sealed and placed in the oil bath at ambient temperature.
2. Carbon dioxide was introduced into the cell from a supply cylinder, using a pump where necessary to reach the desired pressure. The desired pressure for each experiment was set by the use of a backpressure regulator. Pressures of 0, 20, 40, 54, 70, 85, 100 and 120 bar were employed in separate experiments.
3. The oil bath was then heated at a heating rate of 1°C/minute, up to 160 °C for PC and 140°C for PS, PMMA and PETG.
4. Heating was then stopped and the cell de-pressurised over the course of 3 minutes.
5. After the cell had completely cooled (after 1 hour) the samples were extracted.
6. Softening points were extracted from the LVDT data using two alternative methods:
   - Method A - The softening value T_A is taken from the point where the increase in displacement first exceeded 0.01 mm over a 10K temperature interval (lower temperature value quoted). This was intended to provide an initial indication of softening whilst filtering out noise in the data.
   - Method B - The softening temperature T_B is taken as the point where the deflection reached 0.5 mm. This was intended to provide an indication of the temperature where gross deformation of the sample was occurring.

3.3 Polymer Softening - High Pressure Cell (Modified)

3.3.1 Introduction

When using the same cell described in the previous section (section 3.2), we faced difficulties with noise of the LVDT output signal and close temperature control of the cell values because of experimental error (See chapter 5). Therefore, improvements have been made to the existing high pressure cell to achieve better results by reducing experimental errors.

The experimental setup was improved by changing the LVDT and the heating system (electric heater cartridges), see Figure 3 - 13. The rest of the system was unchanged; these changes are now described in detail:

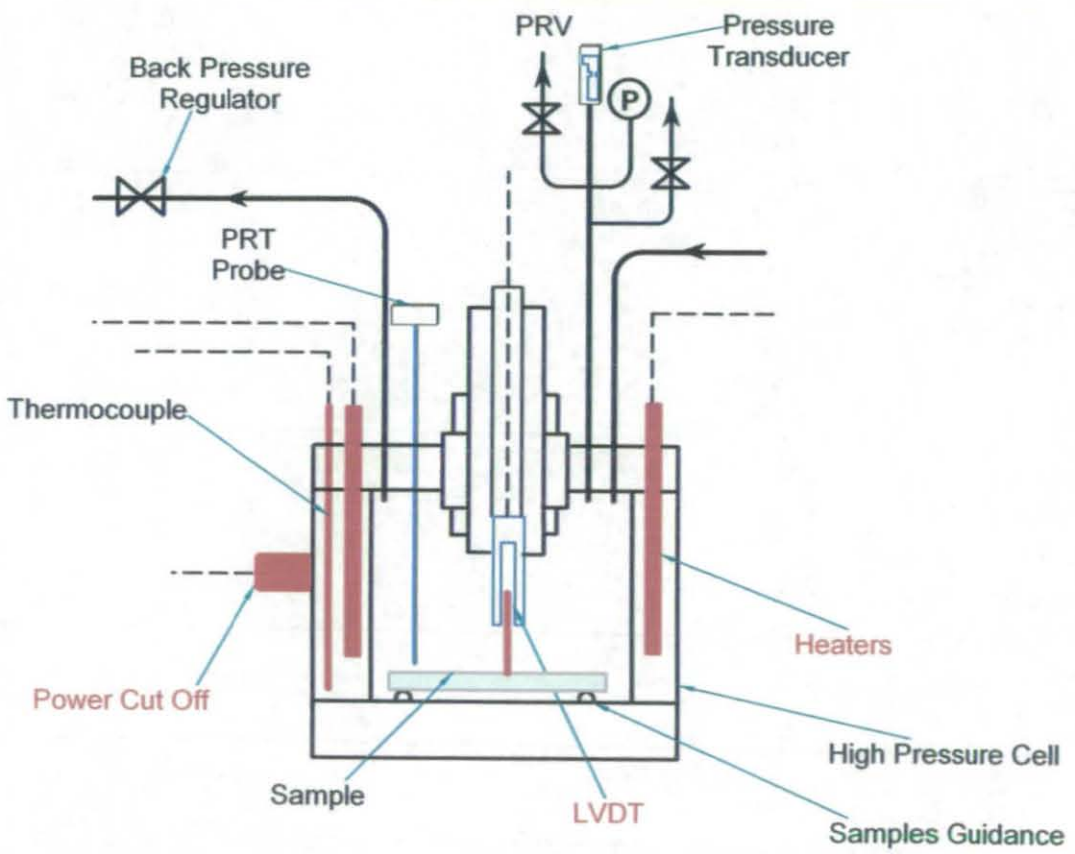

Figure 3 - 13: Cut away view of cell (3-point bend test rig) after modifications showing LVDT, and heater cartridge.

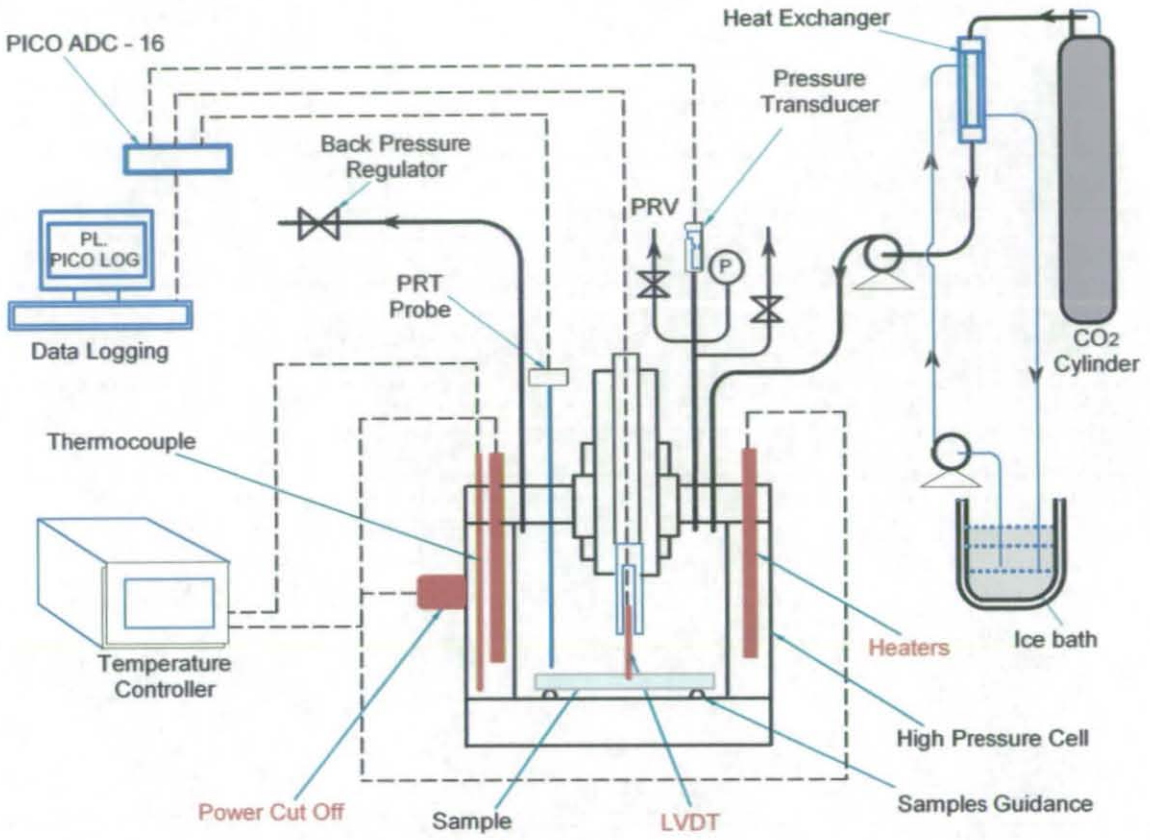

Figure 3 - 14: Experimental set-up showing connections to the high-pressure cell.

3.3.2 LVDT (New Type)

The first experiments (section 3.2) used a LVDT with a flat tip (type sm3, RS Components, UK) that is designed to work at a temperature range of - 40 to 85 °C as stated in the specification sheet. However the experiments were over a range of 25 to 160°C. Therefore, the cell was redesigned to work with special type of LVDT (type mach 1, Solartron Metrology) which is capable to measuring the displacement changing under wider operating conditions of up to 200 °C and 200 bar.

The calibrations were done manually by measuring the position of the movable magnetic armature (core) and the transducer output (mV), measuring the length of the portending core using a digital calliper (mm). The calibration is shown in Figure 3 - 15.

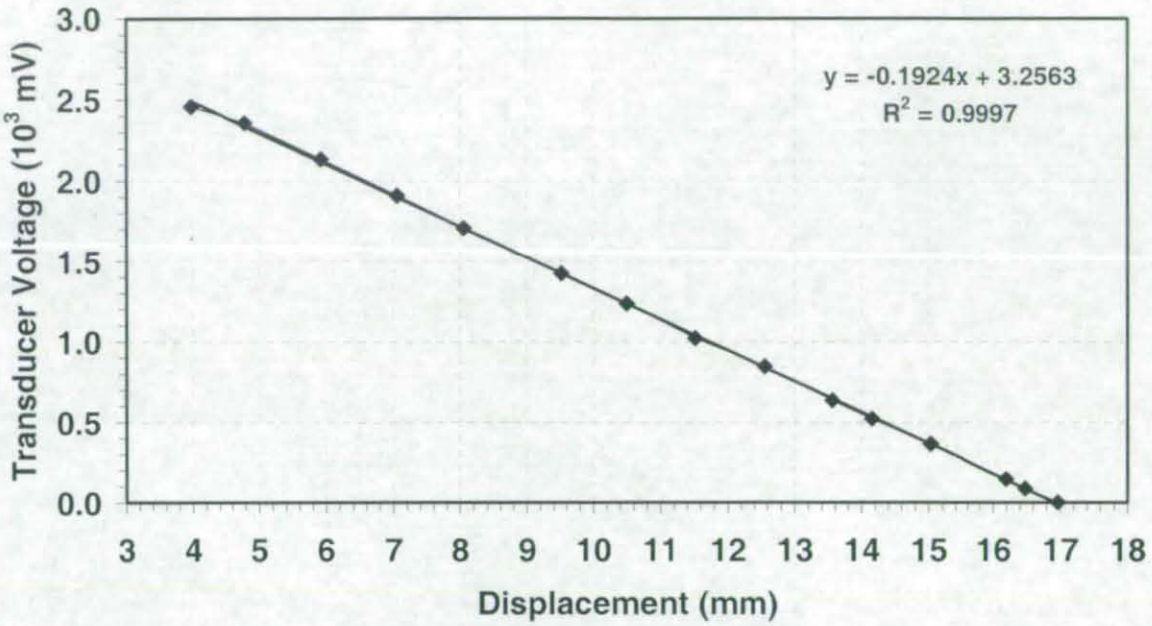

Figure 3 - 15: LVDT calibration.

3.3.3 LVDT Observations

3.3.3.1 Flat tip

First experimental setup (series one) was carried out with stainless steel LVDT with a flat tip, this type of LVDT is less sensitive to the surface softening because of the flat tip but it's very good for studying the bending only. The stainless steel LVDT is however not a suitable material, because the metal tip can heat up quickly, and this can result in a fast softening and melting of the polymer material because the tip is hotter than the polymer.

3.3.3.2 Pointed tip

With the second experimental setup (series two), the system was improved by using a pointed tip and nonconductive materials (ceramic tip), which will not heat the polymer surface and therefore will be better for identifying T_g of sample (if scanning). See the following photo (Figure 3-16). Better data were obtained by using a sharper probe, rather than the flat tip.

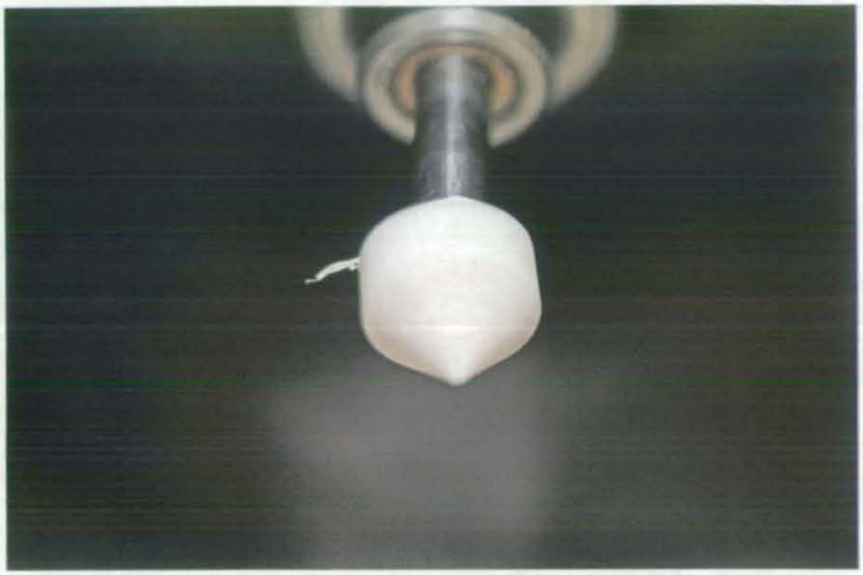

Figure 3 - 16: LVDT with ceramic pointed tip.

3.3.4 Temperature Controller

The same temperature controller as described in section 3.1.6 was used to control the new heating system (electric heater cartridge) which controls the cell temperature. This new system has been applied because of the big difference between the inside and outside temperatures (about 20 °C). Therefore we introduced a new heating system, by using a heater cartridge and also changing the sensing thermocouple position from the oil bath container ("outside") to "inside" the wall of the cell close to one of the heaters. In addition; a thermostatic cut-off switch, was used as a safety cut-off to prevent overheating (electrical circuits as required, in response to the temperature change (see Figure 3 - 17). The thermostatic safety cut-off switch sensor device prevents the temperature going above 200 °C. This switch is fixed on the cell wall close to the heaters.

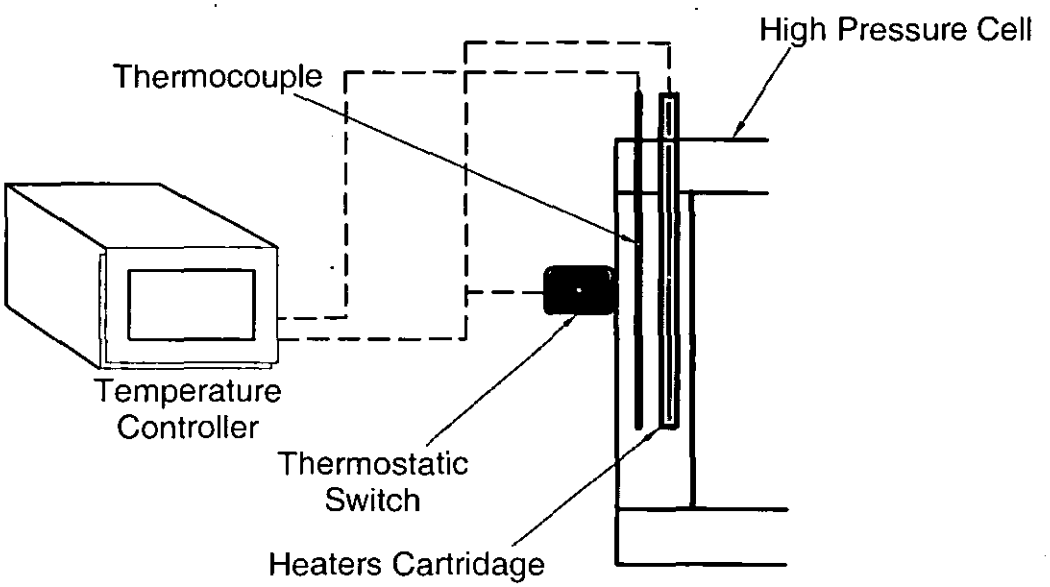

Figure 3 - 17: Heating control systems.

Because of the polymer sensitivity to temperatures change and the surrounding atmosphere, the "inside" temperature (polymer specimen temperature) was measured and compared with the "outside" temperature (cell temperature). As is shown in the following Figure 3 - 18, the equilibrium time occurs around 1000 sec and is half that of the old heating system (oil bath, around 2000 sec), and it was found that the new design reduced the temperature difference from 20 to 2 °C.

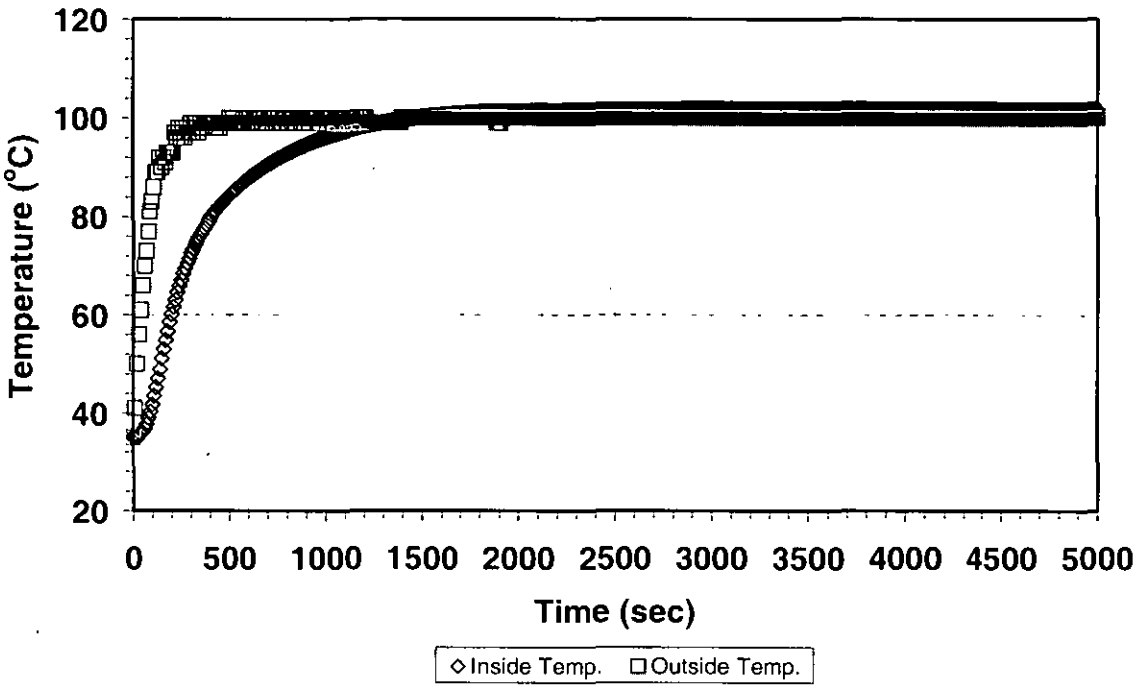

Figure 3 - 18: "Inside and Outside" temperature controller.

3.3.4.1 Heaters Cartridge

The rig was modified to accommodate a heating system (six heaters - RS Company Ltd.). This was achieved by making six holes in the side wall of the pressure vessel. Heater cartridges are cylindrical heating elements with broad range of application and are controlled by the temperature controller. The element can be used as radiation heater or conductive heater. The diameter was 10 mm with 100 mm length, the temperature range up to 600 °C, and the power rating are 200 watt for each heater, see Figure 3 - 19.

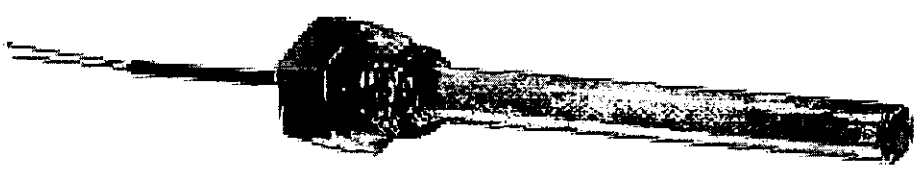

Figure 3 - 19: Heater cartridge.

3.3.5 Sample Loading

A different stand was used to hold the high pressure cell which allowed the sample to be lifted into the cell from below. The stand equipped with protection mesh and earth wires connected to the stand as earthing to comply with Loughborough University safety regulations. With this type of the stand we can do the sampling without taking off the fittings pipes or any of the electric connections, it just opened from the base (bottom) part of the cell and the sample put on the base which was then bolted to the cell, as shown in Figure 3 - 20.

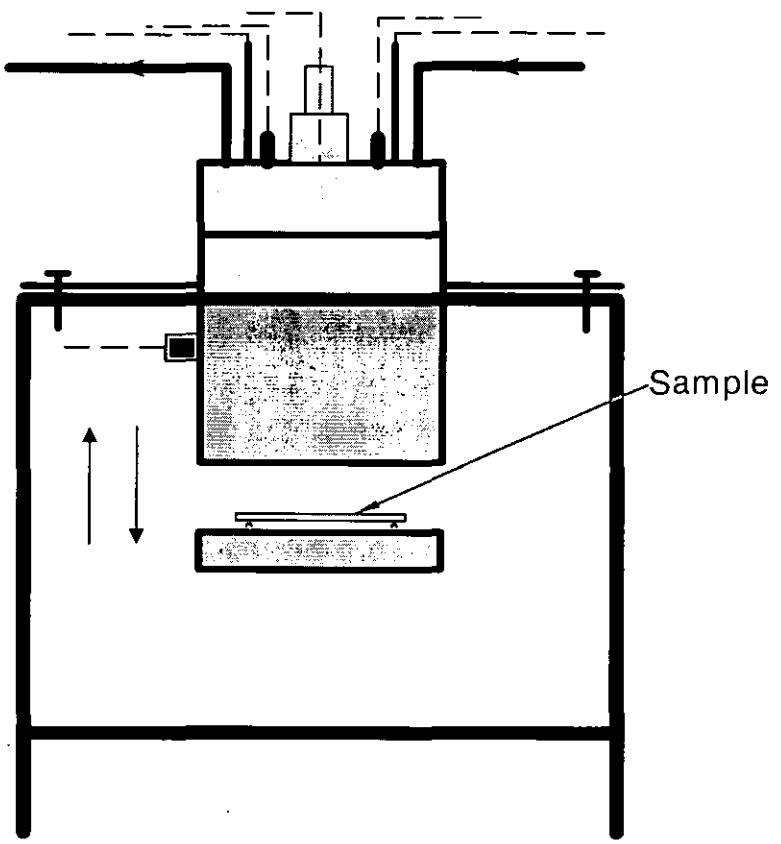

Figure 3 - 20: Sampling procedure.

In addition; this system is able to cool down much faster than the previous experimental setup (oil bath heated assembly). This setup was further improved by employing a cooling fan to cool the cell after completion of an experiment.

3.3.6 Experimental Procedure

The same experimental procedure as was explained before (see section 3.2.5) was used with some changes. These changes are now described in detail:

1. Isothermal tests are performed at constant temperature and pressure.
2. Scanning temperature rate (0.1, 0.2, 0.5, 1 °C/min)
3. Heating then stopped.
4. After the cell had completely cooled (after around 1 hour) the samples were extracted.
5. Softening points were extracted from the LVDT data using two alternative methods:
    - Method A - The softening value T_A is taken from the point where the increase in displacement first exceeded 0.01 mm. This was intended to provide an initial indication of softening whilst filtering out noise in the data.
    - Method B - The softening temperature T_B is taken as the point where the deflection reached 0.5 mm. This was intended to provide an indication of the temperature where gross deformation of the sample was occurring.

3.4 Polymer Foaming - High Pressure View Cell

3.4.1 Introduction

This type of cell is specially designed to investigate polymer foaming and bubble growth. The experimental set up (view cell) is an extended study of polymer softening but has concentrated on sample appearance, bubble nucleation and bubble radius. The cylindrical cell was constructed from 316 stainless steel with two window (type Pyrex) ports incorporated so that the sample can be continuously viewed through one window whilst using the second window for illumination (see Figure 3 - 21). The cell has high-pressure connections to work as inlet and outlet ports for CO_2 transfer. Each window has two o-rings (silicon ring can work up 200 °C), one in the face and one for radial sealing. The cell was made in two sections and can be opened from the centre. Around the sample there are three heating cartridges and a thermocouple fitted in the wall of the cell.

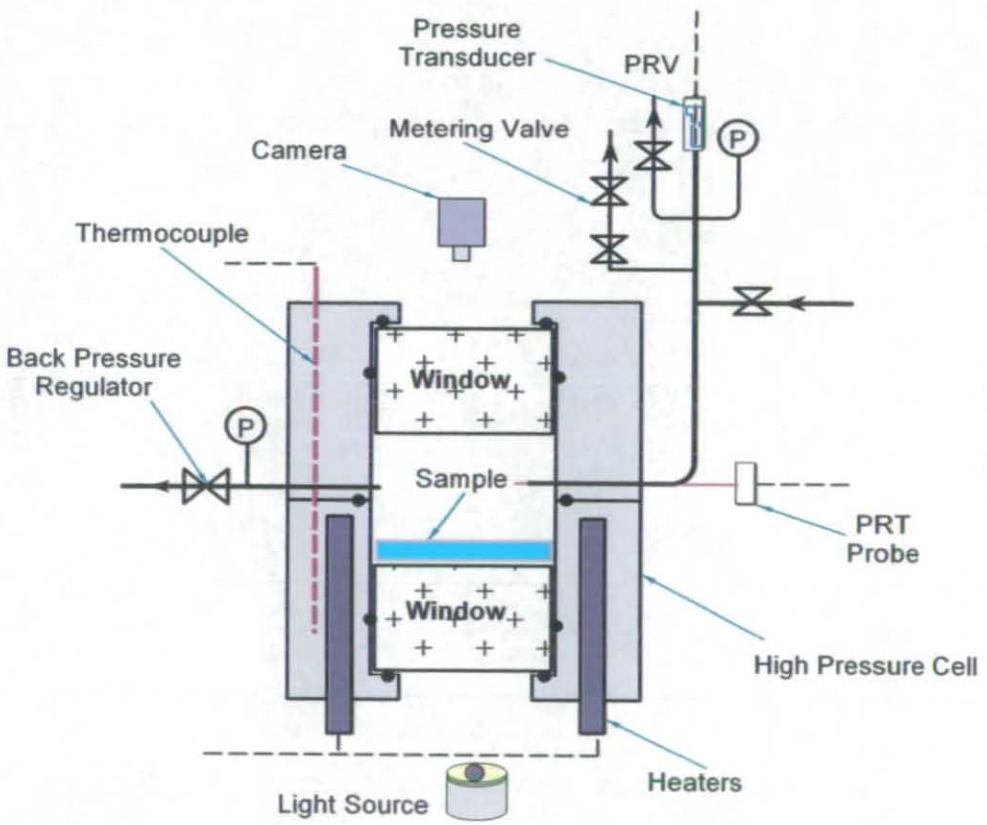

Figure 3 - 21. Cut away view of the view cell, showing polymer strip and PRT probe.

The cell is design to reuse equipment such as the temperature controller, the pressure control system and Pico log software. In addition, some new equipment was used such as a light source, a metering valve and a digital camera see Figure 3 - 22.

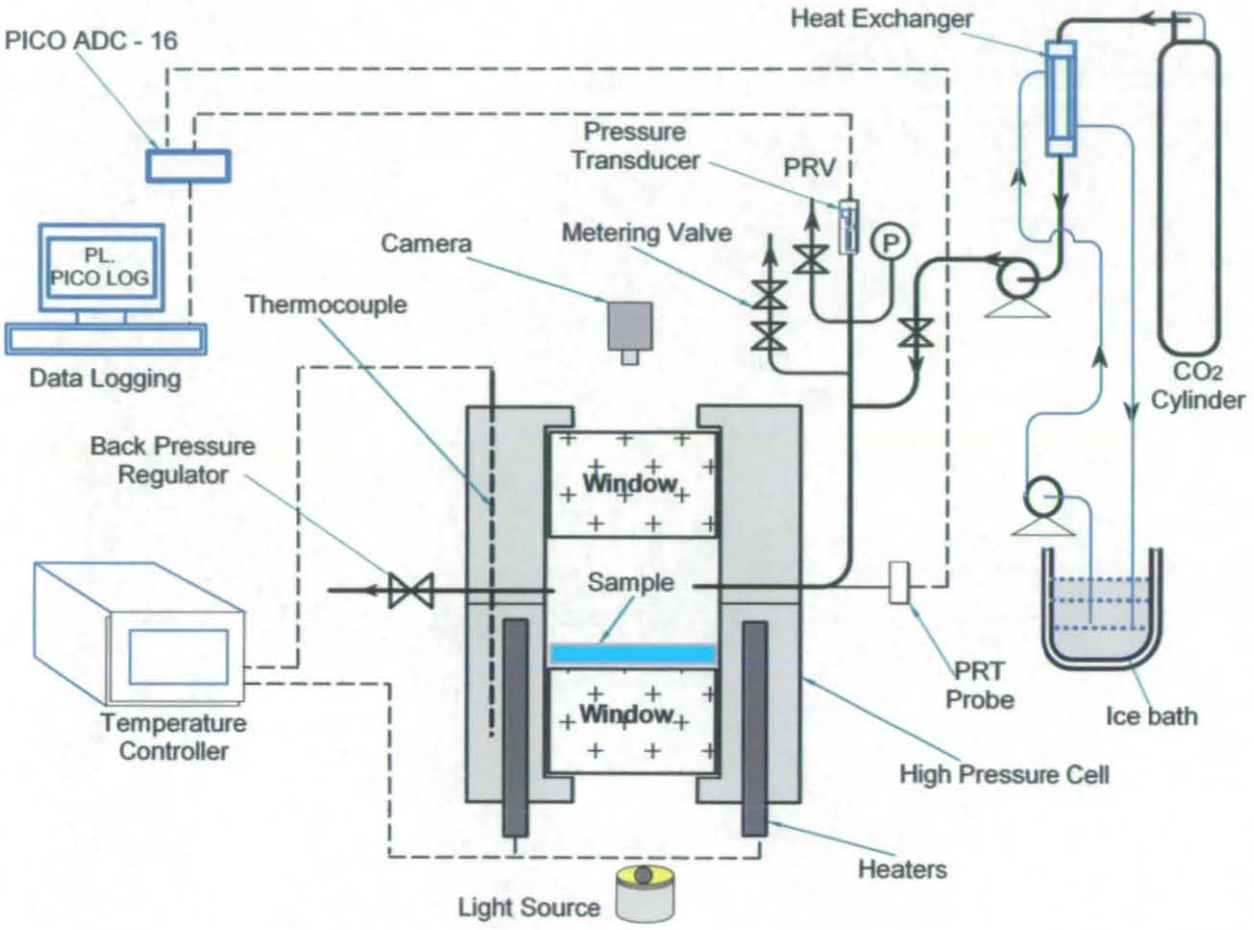

Figure 3 - 22: Experimental set-up showing connections to the viewing cell.

The high-pressure view cell is made of stainless steel with dimensions of 95 mm (high) x 65 mm (diameter), see Figure 3 - 23. With this cell it is also possible to control and record all pressure and temperature data during an experiment and at the same time obtain digital pictures of the experiments progress. The heaters are rated up to a temperature of 600 °C and the power rating is 300 watt for each heater.

Figure 3 - 23: High pressure view cell.

3.4.2 De-pressurisation Techniques (Metering Valve)

Controlling the depressurising time is a very important parameter. We improved the system with new and better depressurising technique. The technique used a "Metering valve", the control was achieved by "decreasing" or "increasing" the opening percentage of the valve. For example, for high pressure depressurisation the valve was opened to about 20 % and for low pressure depressurisation it was opened about 15 %, therefore, with this control we can control the time of the pressure drop from 3 -5 minutes (see Figure 3 - 24).

Figure 3 - 24: Metering valve.

3.4.3 Digital Camera

The digital camera (Canon EOS 20D (8.2 Mega Pixel)) was used to obtain digital pictures of the experiments progress and this is important as it allows us to monitor the process of bubble nucleation growth and the foam structure. The frame rate was adjusted to be 1 frame / 3 sec, and this was set by an external timer remote controller (TC-80N3). In addition, a special macro leans with 60 mm focal length has been used to track the micro bubble radius. The camera was vertically positioned using a separate stand close to the cell

3.4.4 Calibration of Frame Distance

This picture (Figure 3-25) has been taken by the digital camera using the high pressure viewing cell to calibrate the image distance and convert the image from pixels to millimetre. As we can see the scale is 2.5 cm and this equivalent to 3504 pixels (width), therefore 1mm is equivalent to 140.2 pixels.

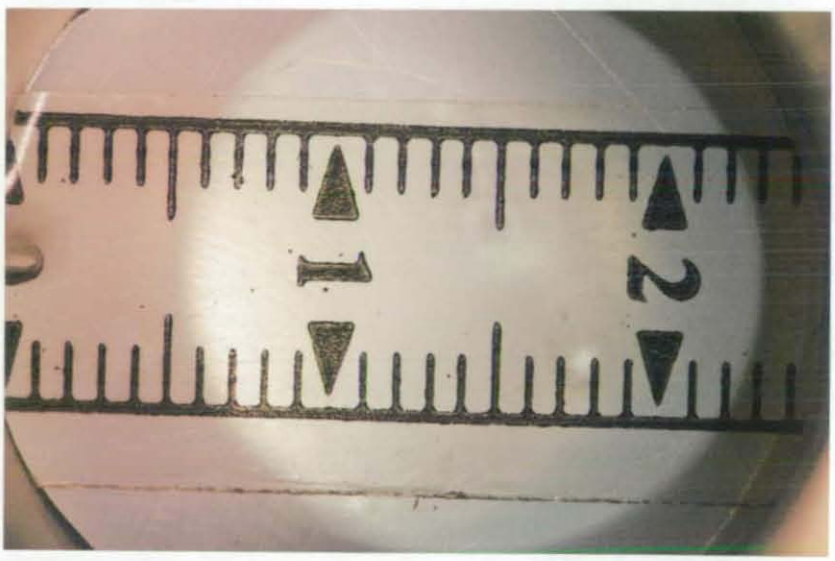

Figure 3 - 25: Calibration of frame distance, (scale of images is 6 x 6 mm).

3.4.5 Image-J Analysis Software

Image J (Image-J 1.38p) is a powerful image analysis program that was created by the National Institutes of Health. Image J is a Java image processing program. It can display and read many image formats including, edit, analyze, process 8-bit, 16-bit and 32-bit images. It can calculate area, distances and angles. It supports standard image processing functions such as contrast manipulation, sharpening, smoothing, edge detection and median filtering. Image can be zoomed up to 32:1. The Image J software has various buttons on the tool bar to allow function such as measure, draw, label, and fill. A window will appear on the desktop as shown below:

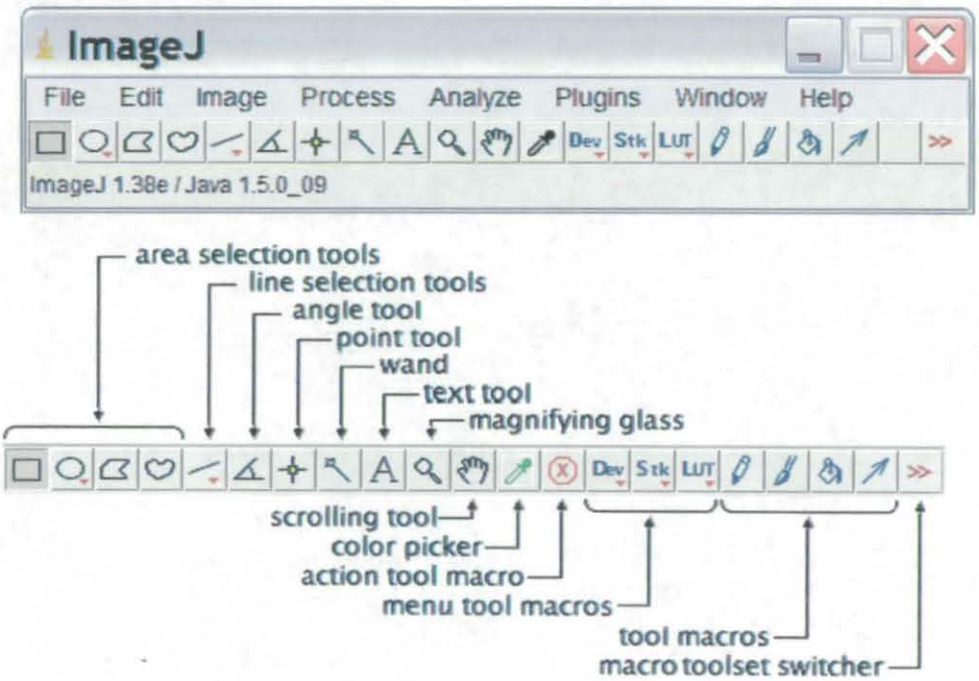

Figure 3 - 26: Image J (Image-J 1. 38 p) tool bar.

To measure an area, this can be done with an area selection tool by surrounding an area with a tool bar perimeter. For particle counting, convert the image to 8-bit grayscale and then "threshold" the image ("Analyze Particles" function), within a given size range (defined by the user). As shown in Figure 3-27 (from photo A to D), the software can filter and convert the image to 8-bit grayscale (see photo B), then threshold the image (see photo C) to give a black and white image, a typically threshold value was 120. Each counted particle will be outlined and numbered in a new widow (see photo D).

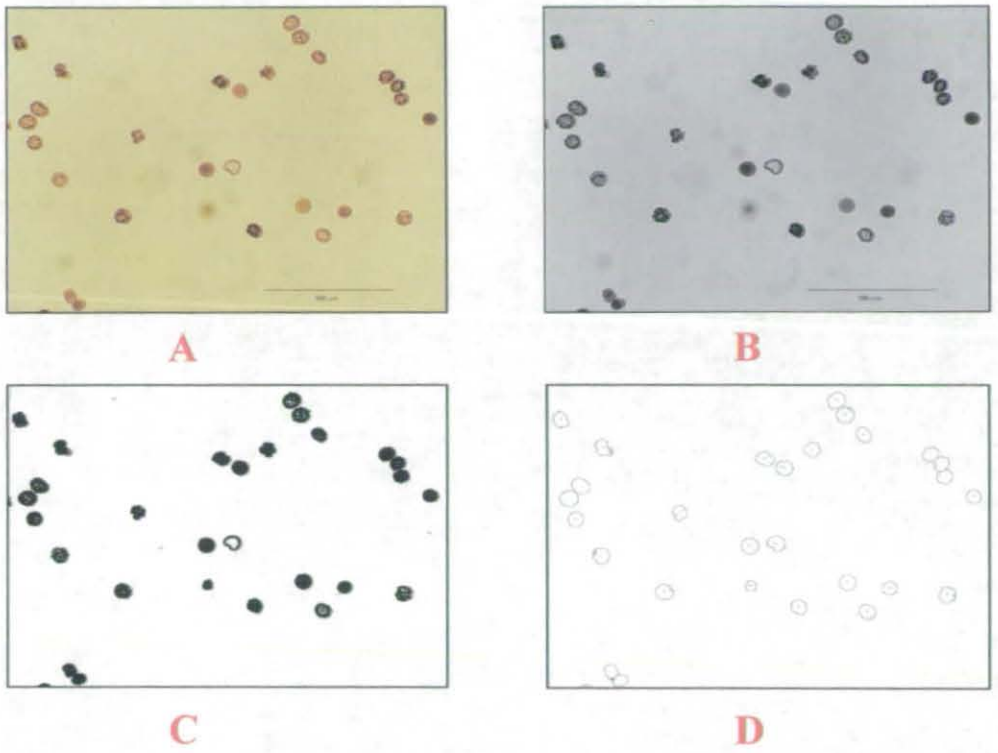

Figure 3 - 27: Area and particles counting by using Image J analysis software.

3.4.6 Experimental Procedure

The experimental procedure was performed according to the following method:

1. The polymer sample was placed in the cell then the cell sealed.
2. Carbon dioxide was introduced into the cell from a supply cylinder, using a pump where necessary to reach the desired pressure.
3. Isothermal tests were performed at 100 °C with different pressure range (20, 40, 54, 70, 85, 100, 120 bar) for 2 hours, each test was done in a separate experiment.
4. Heating was then stopped and the cell depressurised over the course of 3 minutes.
5. Recording the bubble nucleation and growth by the digital camera (1 frame / 3 sec).
6. After the cell had completely cooled the samples were extracted.
7. The bubble radius then was analysed by image analysis software (Image - J).

3.5 Materials

Four polymer materials were tested, that had suitable properties for the test conditions used in the current work. Polycarbonate (PC), Polystyrene (PS), Glycol modified Poly(ethylene-terephthalate) (PETG) and Poly(methyl-methacrylate) (PMMA) were chosen from Thermoplastic types. All of these polymers have a glass transition temperature at the acceptable range (0 – 200 °C). These materials were supplied by Polybron Plastics Ltd, Shepshed, UK. The polymer strips were cut from sheets of different thicknesses: PC strips were 3 mm thick and PS, PETG, and PMMA strips were 2 mm thick.

3.5.1 Polycarbonate: (PC)

Polycarbonate , also known as Lexan, is approximately 250 times stronger than plate glass and 30 times stronger than acrylic of equal thickness. Polycarbonate sheet provides permanent protection against damage and burglary, as well as against natural incidents, such as high winds, snow loads, and hailstorms.

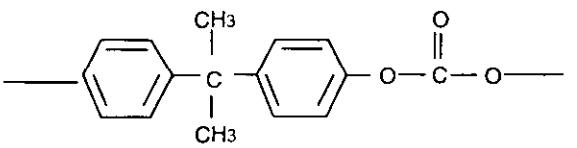

Figure 3 - 28: Structure of PC, Thermoplastic [Calvert and Farrar 1999].

3.5.2 Polystyrene: (PS)

Probably the best known use of polystyrene is the colourful computer casings for the popular IMac computers. Some of the other uses are drinking cups, model cars, lighting panels and lenses.

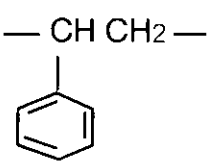

Figure 3 - 29: Structure of PS, Thermoplastic [Calvert and Farrar 1999].

3.5.3 Glycol modified poly(ethylene-terephthalate): (PETG)

PETG is one of the most widely used polymers in industry today; it is used to make most plastic bottles and containers.

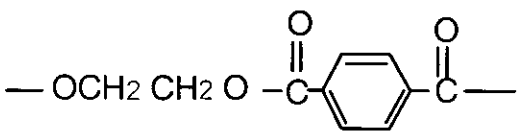

Figure 3 - 30: Structure of PETG, Thermoplastic [Calvert and Farrar 1999].

3.5.4 Poly (methyl-methacrylate): (PMMA)

Poly (methyl methacrylate) PMMA (Syndiotactic) is a clear plastic, used as a shatterproof replacement for glass. Some chemical companies make windows out of it and call it Plexiglas. When it comes to making windows, PMMA has another advantage over glass. PMMA is more transparent than glass. In fact, the largest single window in the world, an observation window at California's (USA) Monterrey Bay Aquarium, is made of one big piece of PMMA which is 16.6 m long, 5.5 m high, and 33 cm thick.

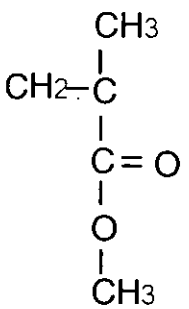

Figure 3 - 31: Structure of PMMA, Thermoplastic [Calvert and Farrar 1999].

3.5.5 In House Moulded Materials

The first experimental work was carried out using the four purchased polymers with different thicknesses (PC 3 mm, PETG 2 mm, PS 2 mm, PMMA 2 mm), the different thickness will affect the results. Work was then focused on one polymer (PS) but with different thicknesses. One major problem was the thickness range (1-5mm), because we couldn't find this range of thickness from one supplier. If we had to get these polymers from different supplier and we were concerned because each supplier use different raw materials and different manufactured methods. As we have polymer labs at Loughborough we could use their equipment to make our polymer specimens and they have the raw material of the required polymer (PS). We succeeded in making our polymer samples using the same raw materials and with the required range of thickness (1-5 mm). The preparations processes are described in details:

1. A frame was made to make the specimen sheet. The specimen sheet was cut into two sizes a disk (20 mm diameter) for the viewing cell and a rectangle (80 mm x 20 mm) for the 3-bend test rig.
2. Fill the frame with the polymer pellets, then close it by the two solid plates (sandwich wise) (see Figure 3 - 32).

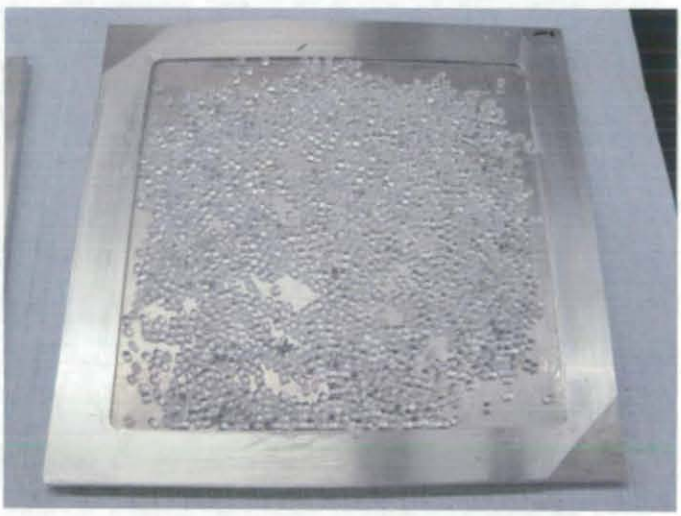

Figure 3 - 32: Polymers specimens preparations.

3. Heat up the press number 1 to 200 °C, and then place the sample case in the hot press position (see Figure 3 - 33).

Figure 3 - 33: Specimens press (Press1 &2).

4. Press it gradually until you reach 15 ton then keep it for 4 - 6 minutes.
5. Remove the sample case then place it into press 2 (cold press), this press has a water circulator to cool it down to room temperature at the same pressure as will as before (15 ton) and keep it for 2 - 5 minutes.
6. After it has cooled down to room temperature, take out the specimens and clean the frames and redo the process again with different frame thickness (see Figure 3 - 34).

Figure 3 - 34: Polymers specimens.

3.5.6 Materials Characterisation

3.5.6.1 Molecular weight (*Mw*)

Polymers molecular weights were determined by the solution viscosity method using a capillary viscometer (C type - capillary diameter). Pump the liquid to the start point then record the time for it to fall from the start point to the end point as shown in the figure below.

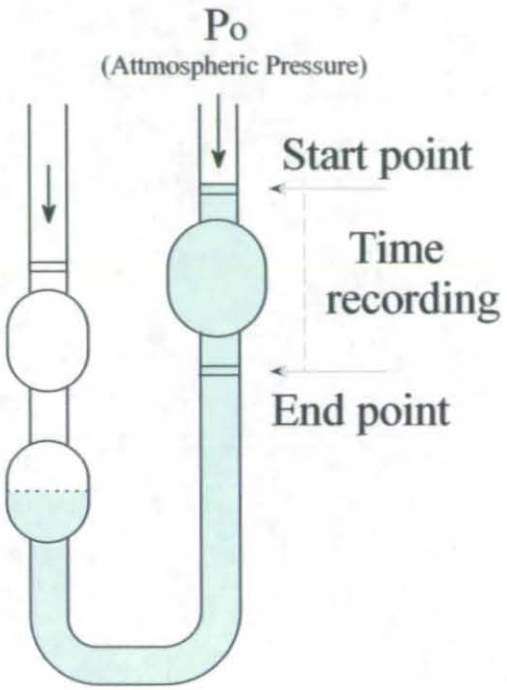

Figure 3 - 35: Capillary viscometer (C type- capillary diameter).

The method is applied by measuring the time for the solvent (t_o) of known viscosity (η_o), then measuring the time (t) for the solvent containing dissolved polymer. The polymer /solvent viscosity (η_{sp}) is calculated from specific equations below [Glasstone and Lewis 1960]:

$$\frac{\eta}{\eta_0} = \frac{t}{t_0} \qquad \text{Eq. 3 - 8}$$

$$\eta_{sp} = (\frac{\eta}{\eta_0}) - 1 \qquad \text{Eq. 3 - 9}$$

From equation 3-8 and 3-9 we can calculate the polymer viscosity, and the specific viscosity. Finally, use equations 3-10 to determine the molecular weights of the polymers.

$$\frac{\left(\frac{\eta}{\eta_0}\right)-1}{c} = KMw^{\alpha} \quad , \quad \frac{\eta_{sp}}{c} = KMw^{\alpha} \quad , \quad Mw = \left(\frac{\eta_{sp}}{cK}\right)^{\frac{1}{\alpha}} \qquad \textbf{Eq. 3 - 10}$$

where: c is the polymer concentration (g / 100ml), K and α are the polymer/solvent constant, and Mw is the molecular weight of the polymer.

Each measurement was repeated three times. The following figure illustrates the specific viscosity / concentration versus different concentration of the PC, PS, PETG and PMMA (0.3g/100ml, 0.5g/100ml, 0.7g/100ml, and 1g/100ml). The limiting value at c extrapolated to zero of the η_{sp}/c is the value used to calculate the polymer molecular weight.

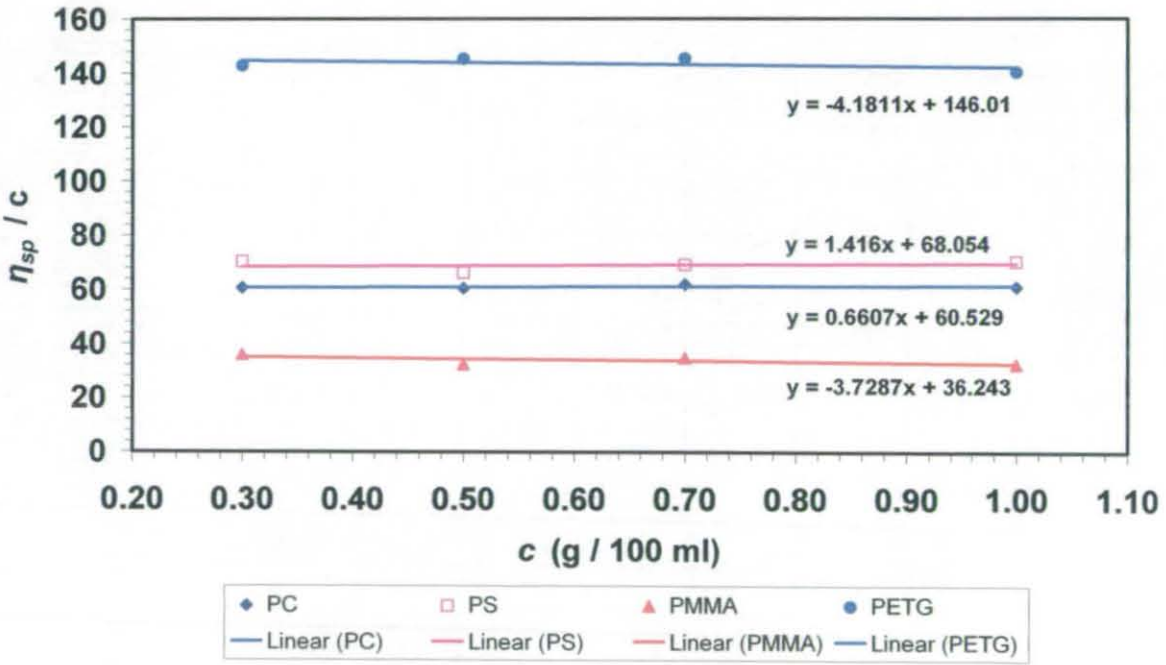

Figure 3 - 36: Specific viscosity / polymers vs. concentration of the polymer.

The following table summarise the values of the Mw and all the used values of the solvent viscosity and the polymer/solvent constant [Bandrup J. 1999]:

Table 3 - 1: Solvent viscosity and the polymer/solvent constant and molecular weight of the polymers.

Polymers	Solvent	η_0 (Pa.s)	K (L / kg)	α	Mw
PC	Dichloromethane	0.44	0.0299	0.74	29400
PS	Toluene	0.55	0.037	0.62	184000
PETG	Dichloroacetic Acid	0.83	0.4	0.5	128000
PMMA	Acetone	0.31	0.053	0.73	179000

3.5.6.2 Glass Transition Temperature (T_g)

Glass transition temperature (T_g) were measured by Differential Scanning Calorimetry (DSC) (Q10, TA Instruments, New Castle, DE) see Figure 3 - 37. The T_g was determined from the midpoint of the heat capacity change observed at a heating rate of 5 °C/min. An empty pan was used in the reference holder. This measurement has been done in Loughborough University labs.

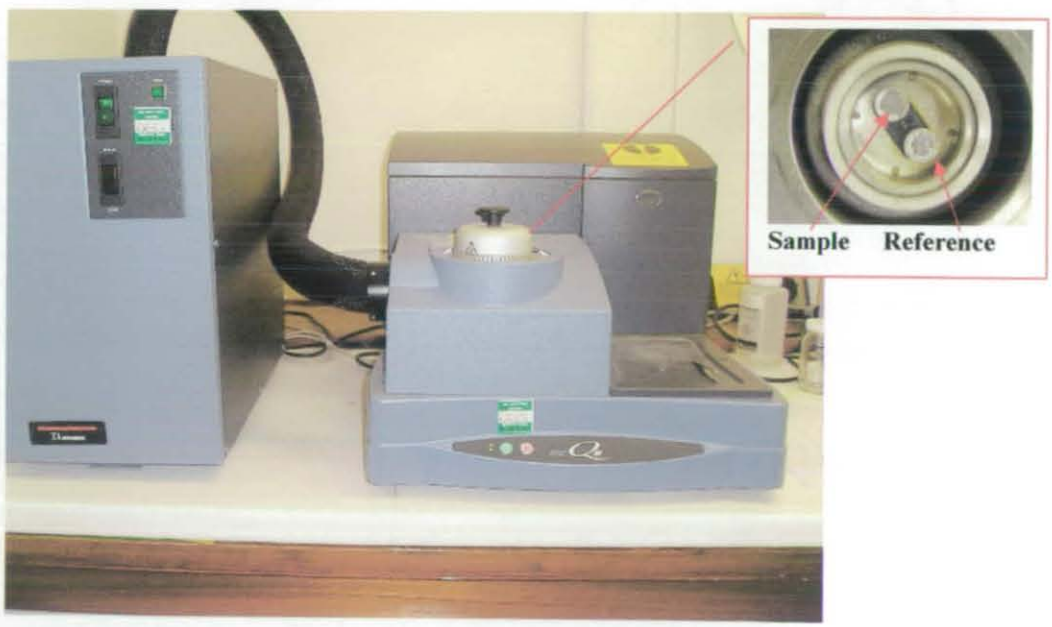

Figure 3 - 37: DSC Instrument (Loughborough University).

The following figures (Figures 3-38 to 3-41) illustrate the T_g values of the PC, PS, PMMA, and PETG and it is determined from the mean value between the two point of inflection on the heat flow / over a range of temperatures.

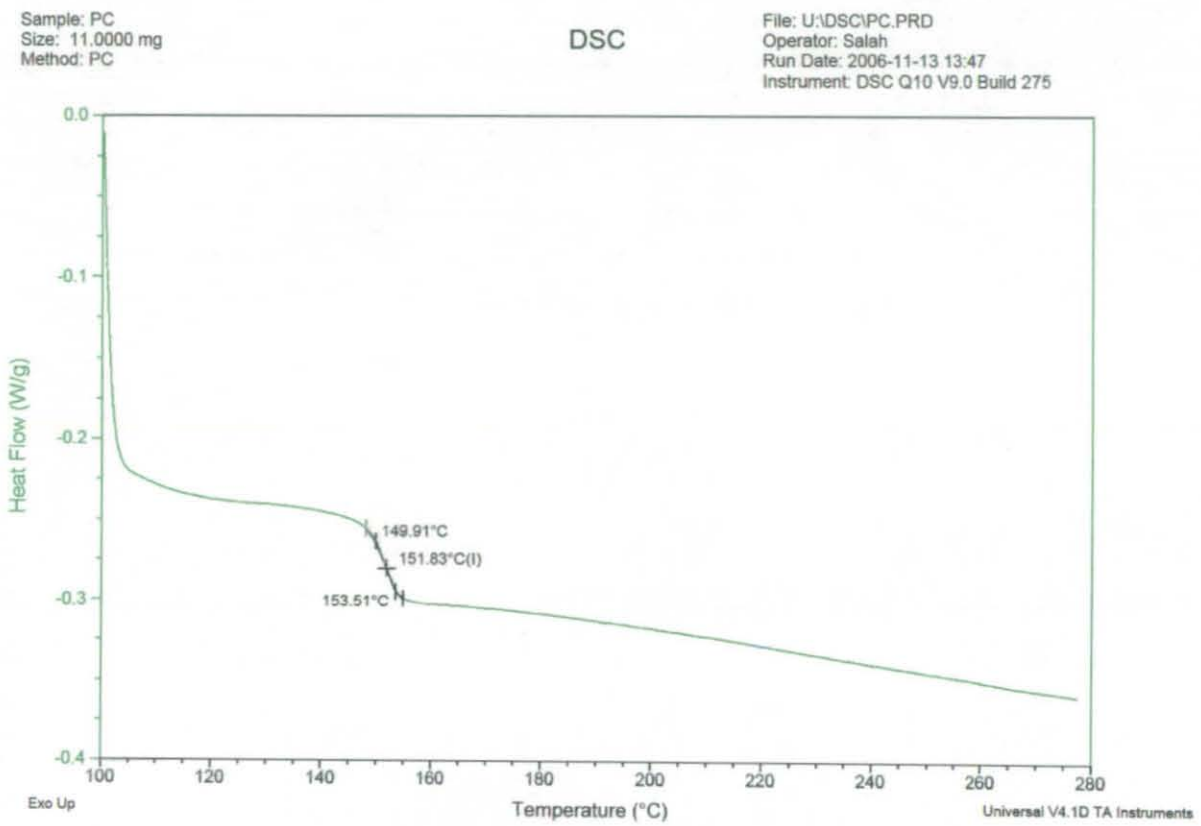

Figure 3 - 38: T_g of PC measured by DSC (Mw 29 400).

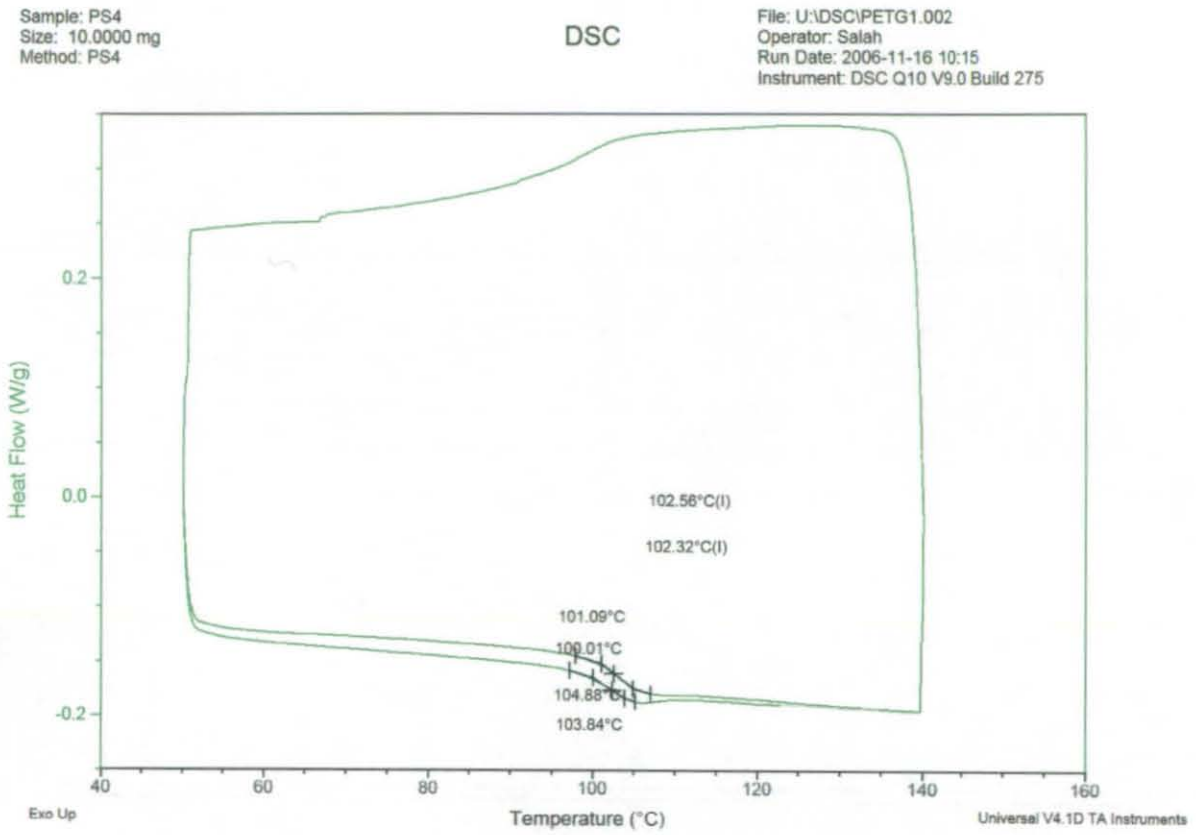

Figure 3 - 39: T_g of PS measured by DSC (Mw 184 000).

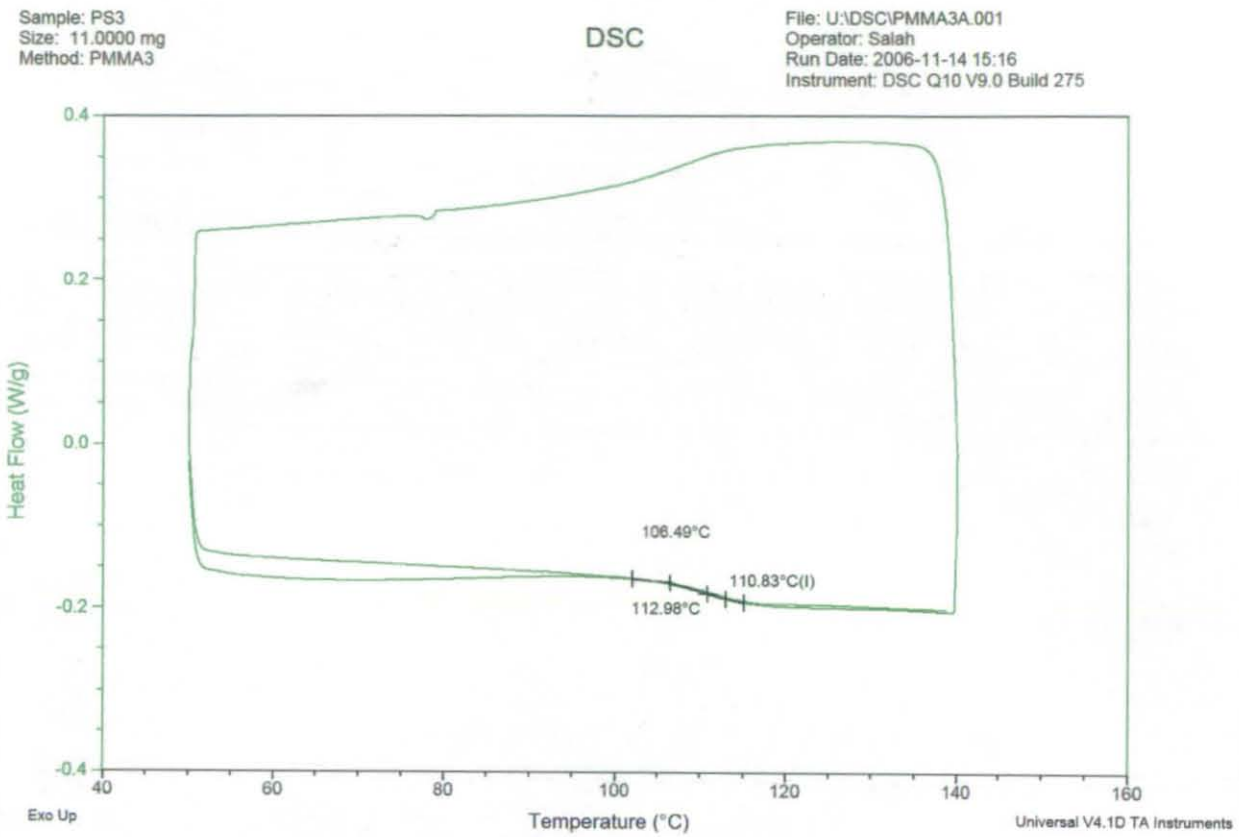

Figure 3 - 40: T_g of PMMA measured by DSC (Mw 179 000).

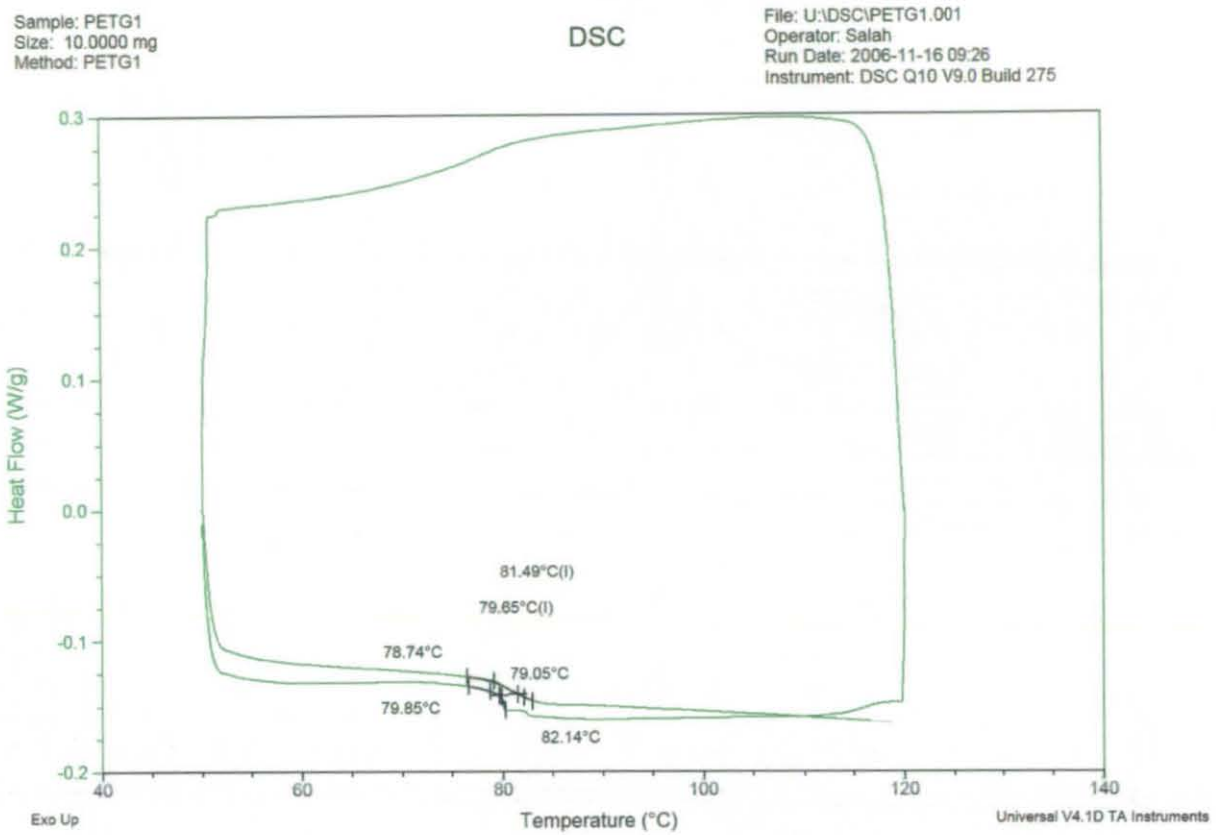

Figure 3 - 41: T_g of PETG measured by DSC (Mw 128 000).

The following table summarises the values of the polymer T_g for all the polymers tested.

Table 3 - 2: Summary of the polymer T_g measured by DSC.

Polymers	T_g (°C)
Polycarbonate (PC)	151
Polystyrene (PS)	102
Poly(methyl-methacrylate) (PMMA)	110
Glycol modified poly(ethylene-terephthalate) (PETG)	81

3.5.6.3 Sample Densities

Densities were determined using a Micromeritics 9200 Helium Pycnometer. This instrument is designed to measure the skeletal volume of a sample in order to determine the absolute solid density. Averages of 5 measurements were taken for each sample. Table 3 - 3 present the pure polymer (2 – 3 mm thick x 20 mm width x 80 mm long) density values at room temperature:

Table 3 - 3: Polymer weight, volume and densities values.

Polymer	Weight (g)	Volume (cc)	Density (g/cc)
Polycarbonate	5.3	4.46	1.18
Polystyrene	3.1	3.19	0.97
Poly(methyl-methacrylate)	4.4	3.67	1.19
Glycol modified poly(ethylene-terephthalate)	3.7	3.32	1.11

3.5.7 Specimen Preparation and Location in Cell

The sample preparation was done according to the cell size and the sample position (Mechanical measurement of polymer softening cell). The polymer strips were cut from sheets by a saw machine to give dimension of 20 mm width x 80 mm long x 2-3mm thick. See Figure 3 - 42.

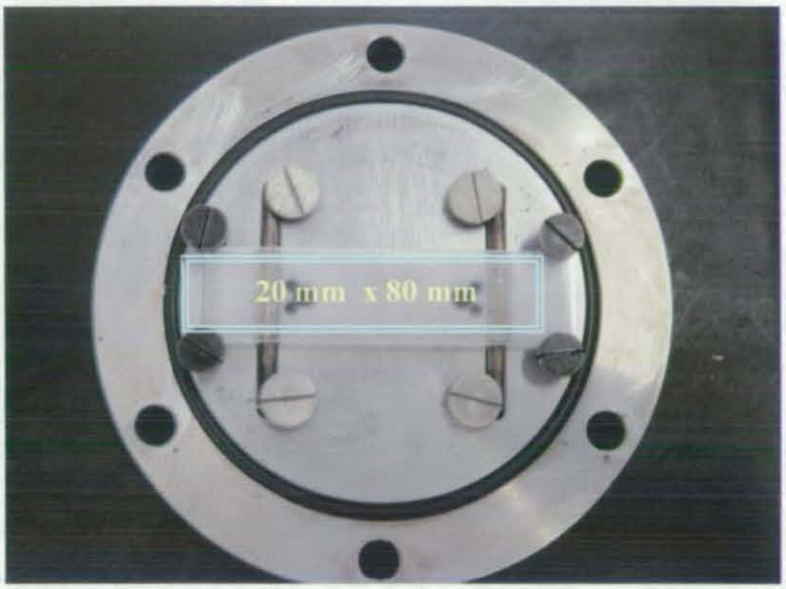

Figure 3 - 42: Polymer specimen for the mechanical measurement of polymer softening cell.

The second part of the study is bubble nucleation (Optical measurement of polymer foaming cell) and the specimen dimension is a 20 mm diameter (disk) x 1mm thick.

Figure 3 - 43: Polymer specimen for the optical measurement of polymer foaming cell (view cell).

3.6 Conclusion

This chapter presents two specially constructed experimental cells; these two sets of experimental arrangements have been made to conduct tests up to 200 bar and high temperature up 200 °C. The procedures described in this chapter have the objective of studying the effect of carbon dioxide on the polymers. The first experimental setup investigated the polymer softening by using a linear variable displacement transducer (LVDT) to continuously monitor the deflection of a polymer strip undergoing 3-point bending test. The second experimental setup was used to study the polymer foaming and bubble formation during depressurisation using a special cylindrical view cell with 2 optical widows.

The mechanical measurement of polymer softening was developed during the project. The first high pressure cell system used oil bath heating; the second system used the same high pressure cell but with significant modification. These improvements were made to give easy operation and provide better temperature and depressurising controls.

First experimental setup was carried out with a stainless steel LVDT with a flat tip, this type of LVDT is less sensitive to the surface softening because of the flat tip but it is good for a study of only the bending. In addition, the stainless steel LVDT is not the best material, because the metal tip can heat up quickly, and this can result in a fast softening and melting of the polymer material. But with the second experimental setup we used a pointed tip and nonconductive material (ceramic), which will not heat the polymer surface and therefore be better for identifying T_g of sample if scanning is used.

Four polymer materials were selected based on the range of conditions that could be achieved with the equipment: Polycarbonate (*Mw* 29 400, T_g 151.8 °C), Polystyrene (*Mw* 184 000, T_g 102.6 °C), Glycol modified poly(ethylene-terephthalate) (*Mw* 128 000, T_g 81 °C), and Poly(methyl-methacrylate) (*Mw* 179 000, T_g 110.8 °C), were chosen from Thermoplastic types. Molecular weights were determined by the solution viscosity method, and T_g values by DSC. The polymers were supplied in sheets of different thickness: PC

strips were 3 mm thick whereas PS (25 mm disk sample for the foaming experimental), PTEG and PMMA strips were 2 mm thick for the softening experiments.

Chapter 4 Derivations of the Mathematical Models Used

4 Introduction

In this chapter mathematical models are derived to help interpret the experimental data for gas diffusion in polymer strips and polymer deflection (chapter 5) and bubble growth (chapter 6).

4.1 Estimation the Diffusivity of CO_2 in Polymer Strips

The local concentration of CO_2 determines the mechanical behaviour of the polymer as it affects whether the polymer is in the glassy or rubbery region. At a given temperature one can define a "glass transition concentration" (c_g). Concentrations above c_g correspond to the rubbery state and concentrations below c_g correspond to the glassy state.

When the polymer strip is exposed to CO_2 the outer region will experience high values of c and will more likely to be rubbery whereas the inner reigns will have a low value of c and will more likely to be glassy. One can envisage that a front dividing the glassy and rubbery regions will exist where $c = c_g$. This front will more into the polymer as time proceeds, see Figure 4-1.

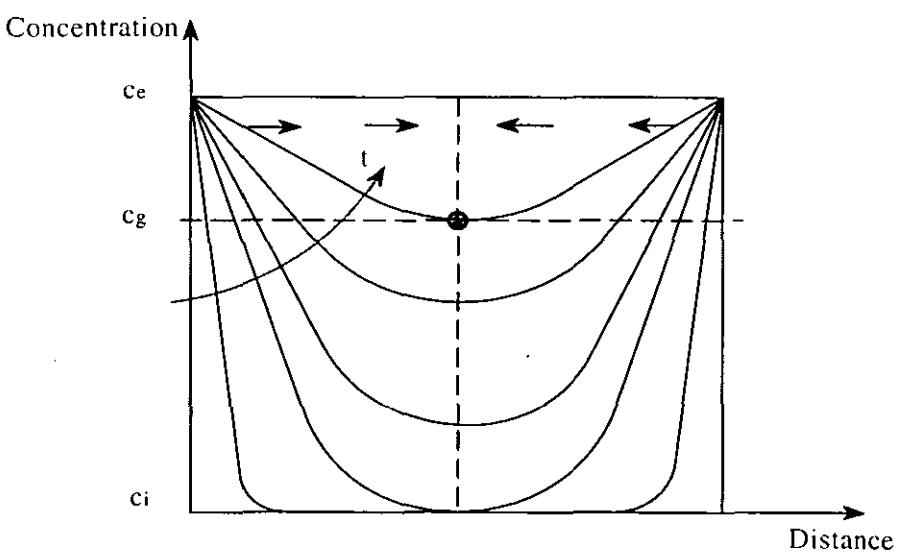

Figure 4 - 1: General diffusion description.

To test the hypothesis that T_B (see chapter 3 section 3.2.5) values are influenced by the time taken to diffuse CO_2 into the sample, a calculation to gain an order of magnitude estimate of the average diffusion coefficient of the carbon dioxide in the polymer samples based on values of T_A and T_B was made as follows:

The diffusion of CO_2 in to the polymers can be modelled assuming Fick's second law [Tang et al 2004]. The standard solution for diffusion into both faces of a slab of thickness d is [Crank 1975]:

$$\frac{c-c_e}{c_i-c_e}=\frac{4}{\pi}\sum_{n=0}^{\infty}\frac{(-1)^n}{(2n+1)}\sin\left(\frac{(2n+1)\pi y}{d}\right)\exp\left(-\frac{(2n+1)^2\pi^2}{d^2}Dt\right) \qquad \textbf{Eq. 4 - 1}$$

where: c – concentration of CO_2 (at time t and distance x into the slab)

c_i – initial concentration of CO_2 in slab

c_e – equilibrium concentration in slab (corresponding to infinite time)

d – thickness of slab

D – diffusion coefficient

t – time

y – distance from surface

The centreline concentration, c_c, (at $y = d/2$ i.e. $\sin (2n+1)\,\pi/2 = 1$), is thus:

$$\frac{c_c-c_e}{c_i-c_e}=\frac{4}{\pi}\sum_{n=0}^{\infty}\frac{(-1)^n}{(2n+1)}\exp\left(-\frac{(2n+1)^2\pi^2}{d^2}Dt\right) \qquad \textbf{Eq. 4 - 2}$$

Noting that the initial concentration c_i is zero yields:

$$\frac{c_c}{c_e}=1-\frac{4}{\pi}\sum_{n=0}^{\infty}\frac{(-1)^n}{(2n+1)}\exp\left(-\frac{(2n+1)^2\pi^2}{d^2}Dt\right) \qquad \textbf{Eq. 4 - 3}$$

Now, the glass transition temperature can be expressed as a linearly decreasing function of CO_2 concentration [Wissinger & Paulaitis (1991), Condo & Johnston (1992)], i.e.:

$$T_g = T_{g0} - \beta c \qquad \textbf{Eq. 4 - 4}$$

The first (onset) softening point (T_A) corresponds to the softening of the surface regions where $c = c_e$. Therefore:

$$T_A = T_{g0} - \beta c_e \Rightarrow c_e = \frac{T_{g0} - T_A}{\beta} \qquad \textbf{Eq. 4 - 5}$$

We now assume that the second softening point (T_B) occurs when the centre of the sample has also reached the glass transition, that is:

$$T_B = T_{g0} - \beta c_c \Rightarrow c_c = \frac{T_{g0} - T_B}{\beta} \qquad \textbf{Eq. 4 - 6}$$

This is shown schematically in Figure 4-2.

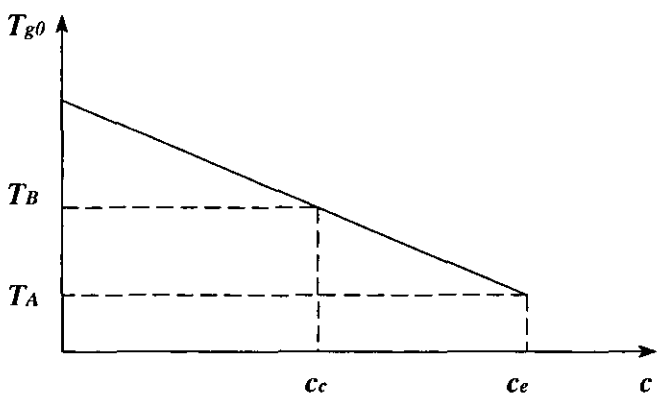

Figure 4 - 2: Variation of T_g with concentration (c) assumed in the model.

Substituting c_e and c_c from equations 4-5 and 4-6 into equation 4-3:

$$\frac{c_c}{c_e} = \frac{T_{g0} - T_B}{T_{g0} - T_A} = 1 - \frac{4}{\pi} \sum_{n=0}^{\infty} \frac{(-1)^n}{(2n+1)} \exp\left(-\frac{(2n+1)^2 \pi^2}{d^2} Dt \right) \qquad \textbf{Eq. 4 - 7}$$

Thus an estimate of the diffusivity can be made by comparing the ratio of the decrease in the softening point by method T_B compared to that by method T_A. The equation can be further simplified by noting that at the long times used in this analysis only the first term ($n = 0$) is significant.

$$\Rightarrow \frac{T_{g0} - T_B}{T_{g0} - T_A} = 1 - \frac{4}{\pi} \left(\frac{1}{2(0)+1} \right) \exp\left(-\frac{(2(0)+1)^2 \pi^2}{d^2} Dt \right)$$

$$\Rightarrow \frac{T_{g0} - T_B}{T_{g0} - T_A} = 1 - \frac{4}{\pi} \exp\left(-\frac{\pi^2}{d^2} Dt \right)$$

This can be plotted, or individual values of D estimated for individual experiments.

$$D = -Ln\left(\frac{\pi}{4} \left(1 - \frac{T_{g0} - T_B}{T_{g0} - T_A} \right) \right) \left(\frac{d^2}{\pi^2 t} \right) \qquad \textbf{Eq. 4 - 8}$$

It is also assumed that the thickness (d) is constant and the time (t) corresponds to the time from when the polymer is initially exposed to the carbon dioxide to when the second softening occurred.

This equation is used to calculate CO_2 diffusivities in polymers strips in sections 5.1.3 (for PC, PS, PETG and PMMA) and 5.2.4 (for PS only).

4.2 Deflection Model

This model attempts to describe in more detail how the central deflection of a thin polymer strip supported at its ends varies with time as CO_2 diffuses in and the polymer softens. If one postulates that only the glassy regions provide any significant mechanical strength then one can use the position of the front (which can itself be modelled as a function of time) to estimate the bending of the polymer. This model will be used to generate an equation for central deflection versus time which can be fitted to the experimental data (Isothermal experiments of PS/CO_2) gained in section 5.4. The following diagrams (Figure 4 - 3 and 4-4) express this estimation:

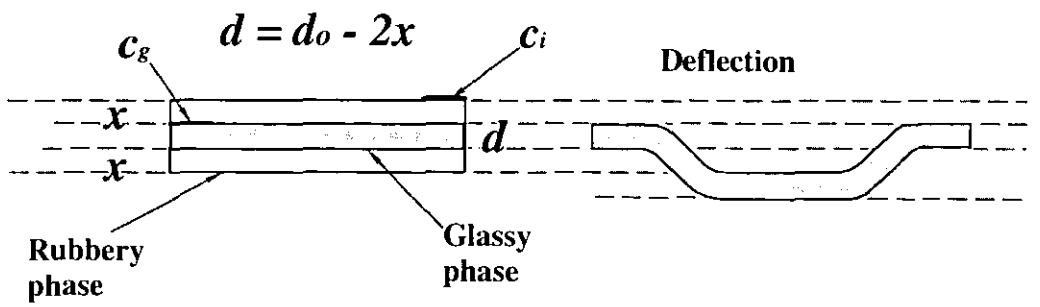

Figure 4 - 3: Generalized deflection diagram.

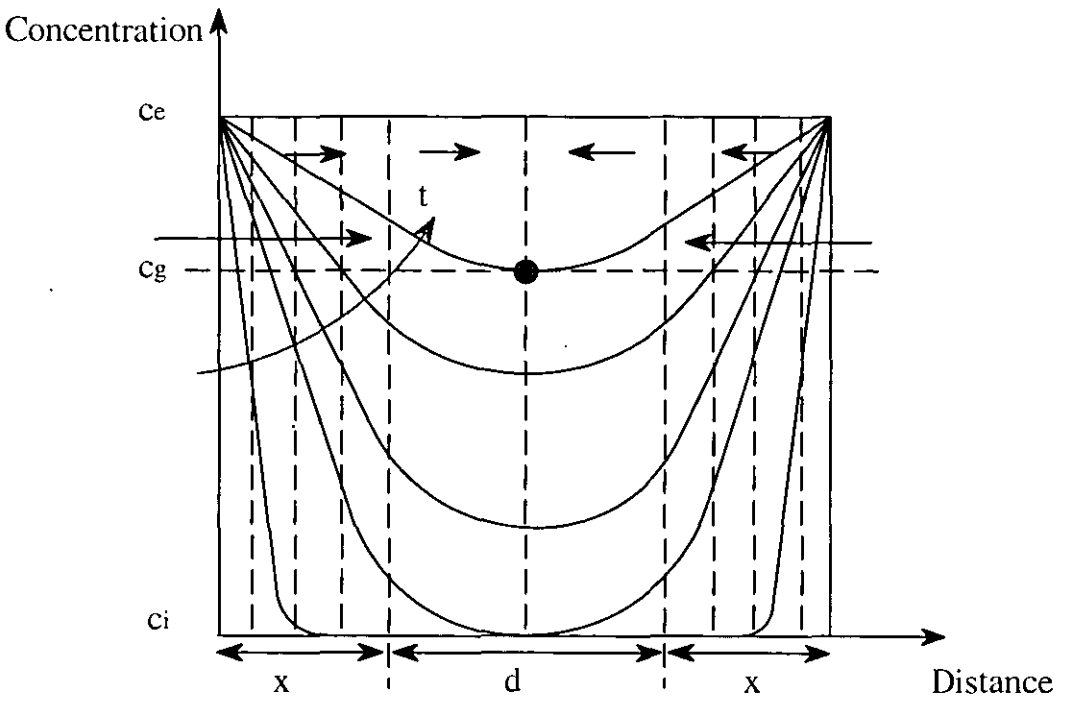

Figure 4 - 4: General diffusion description.

The depth of the front can be estimated from the solution for diffusion into a semi-infinite solid which is: [Calvert & Farrar 1999]

$$\frac{c_g - c_i}{c_e - c_i} = 1 - erf\left(\frac{x}{2\sqrt{Dt}}\right) = 1 - erf(z) \qquad \textbf{Eq. 4 - 9}$$

For values of $z < 0.7$ the following approximation can be made

$$erf\left(\frac{x}{2\sqrt{Dt}}\right) \approx \frac{x}{2\sqrt{Dt}}$$

$$\Rightarrow \frac{x}{2\sqrt{Dt}} = 1 - \frac{c_g - c_i}{c_e - c_i} = \frac{c_e - c_i - (c_g - c_i)}{c_e - c_i}$$

$$\Rightarrow \frac{x}{2\sqrt{Dt}} = \frac{c_e - c_g}{c_e - c_i}$$

Noting that c_i is zero, therefore:

$$\frac{c_g - c_e}{-c_e} = \frac{x}{2\sqrt{Dt}} \qquad \textbf{Eq. 4 - 10}$$

$$x = 2\sqrt{Dt}\left(\frac{c_g - c_e}{-c_e}\right) \qquad \textbf{Eq. 4 - 11}$$

The deflection of a slab (by its own weight see chapter 3 section 3.2.2.1) of effective thickness d is: [Calvert & Farrar 1999]

$$\text{Deflection} = \frac{5WL^3}{384EI} \quad , \qquad \left(\frac{Nm^3}{(N/m^2).m^4} \rightarrow m\right) \qquad \textbf{Eq. 4 - 12}$$

where:

$$\text{Moment of inertia, } I = \frac{bd^3}{12} \quad , (m^4) \qquad \textbf{Eq. 4 - 13}$$

and,

L : overall length (m)

W: point load (N)

I : moment of inertia (m^4)

E : modulus of elasticity (N/m^2)

b: width of the sample strips (m)

d: thickness of the strip (m)

Substituting I from equation 4-13 into equation 4–12:

$$\text{Deflection} = \frac{5WL^3}{384E}\frac{12}{bd^3} \qquad \textbf{Eq. 4 - 14}$$

If the effective thickness d is given by:

$$d = d_0 - 2x \qquad \textbf{Eq. 4 - 15}$$

where d_o is the thickness of the strip and x is the depth of the front then:

$$\text{Deflection} = \frac{5WL^3}{384E}\frac{12}{b}\frac{}{(d_0 - 2x)^3} \qquad \textbf{Eq. 4 - 16}$$

Substituting x from equation 4 - 11 into equation 4 – 16:

$$\text{Deflection} = \frac{5WL^3}{384E}\frac{12}{b}\frac{}{(d_0 - 4\sqrt{Dt}.(\frac{c_g - c_e}{-c_e}))^3}$$

$$\text{Deflection} = \frac{5}{32}\frac{WL^3}{Eb}\frac{}{(d_0 - 4\sqrt{Dt}.(\frac{c_g - c_e}{-c_e}))^3} \qquad \textbf{Eq. 4 - 17}$$

This model gives a description of how the central deflection of a thin polymer strip supported at its ends varies with time as the polymer softens. These calculations will be discussed in more detail in chapter 5, where they will be applied to isothermal bending data.

4.3 Bubble Growth Model

4.3.1 Model Framework

This model is to be used to fit to experimental data of bubble growth. The general model framework uses a finite difference technique as illustrated by the following diagram (see Figure 4 - 5). The bubble, assumed to contain pure CO_2, is surrounded by a polymer sphere which is divided into 20 concentric shells of equal volume.

The polymer density is assumed to be constant, and hence the volumes associated with each shell remain constant. Therefore, knowledge of the current bubble radius at any time allows all the nodal radii to be evaluated.

$$\frac{4}{3}\pi r_a^3 + fV_{polymer} = \frac{4}{3}\pi r^3 \qquad \textbf{Eq. 4 - 18}$$

where $V_{polymer}$ is the volume of polymer, f is the fraction of polymer volume inside the nodal radius, and r is the radius at the node.

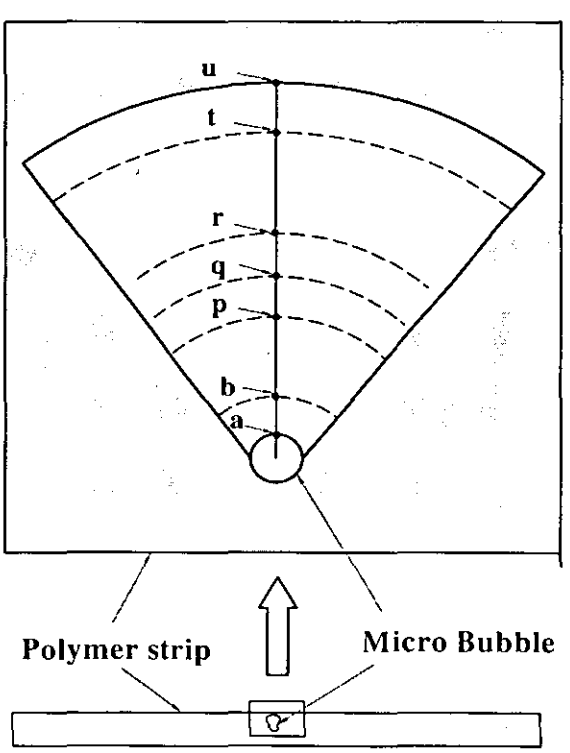

Figure 4 - 5: General bubble growth model sketch.

4.3.2 Diffusion Equations

Different equations are required to model concentrations at the bubble interface (node " a"), exterior (node "u"), and within the polymer (nodes "b" to "t").

Main body (nodes "b" to "t":

Here node "q" is used as an example node for explanatory purposes with adjacent nodes "r" (outside) and "p" (inside). Equations for other nodes are essentially identical.

The volume associated with node "q" is a shell with outer radius $\frac{1}{2}(r_q + r_r)$ and inner radius $\frac{1}{2}(r_q + r_p)$.

$$Flux\ In = D_{qr}\frac{(c_r - c_q)}{(r_r - r_q)} \qquad Area = 4\pi(\frac{r_q + r_r}{2})^2 \qquad \textbf{Eq. 4 - 19}$$

(From node "r") of "q, r" boundary

$$Flux\ Out = D_{qp}\frac{(c_q - c_p)}{(r_q - r_p)} \qquad Area = 4\pi(\frac{r_q + r_p}{2})^2 \qquad \textbf{Eq. 4 - 20}$$

(to node "p") of "q, p" boundary

$$Accumulation = \frac{dc_q}{dt}\ \text{x}\ Volume \qquad \textbf{Eq. 4 - 21}$$

$$Volume = \frac{4}{3}\pi(\frac{r_q + r_r}{2})^3 - \frac{4}{3}\pi(\frac{r_q + r_p}{2})^3 \qquad \textbf{Eq. 4 - 22}$$

$Accumulation = Flux\ in$ x $Area - Flux\ out$ x $Area$

$$\frac{dc_q}{dt}\frac{4}{3}\pi\left[(\frac{r_q + r_r}{2})^3 - (\frac{r_q + r_p}{2})^3\right] = 4\pi(\frac{r_q + r_r}{2})^2 D_{qr}\frac{(c_r - c_q)}{(r_r - r_q)} - 4\pi(\frac{r_q + r_p}{2})^2 D_{qp}\frac{(c_q - c_p)}{(r_q - r_p)}$$

Cancelling π:

$$\frac{dc_q}{dt}\frac{1}{6}\left[(r_q + r_r)^3 - (r_q + r_p)^3\right] = (r_q + r_r)^2 D_{qr}(\frac{c_r - c_q}{r_r - r_q}) - (r_q + r_p)^2 D_{qp}(\frac{c_q - c_p}{r_q - r_p}) \qquad \textbf{Eq. 4 - 23}$$

Exterior boundary – no flux – node "u":

$$Flux\ Out = D_{tu}\frac{(c_u - c_t)}{(r_u - r_t)} \qquad Area = 4\pi(\frac{r_t + r_u}{2})^2 \qquad \textbf{Eq. 4 - 24}$$

(to node "*t*") of "*q, r*" boundary

$$Accumulation = \frac{dc_u}{dt}\ \text{x}\ Volume \qquad \textbf{Eq. 4 - 25}$$

$$Volume = \frac{4}{3}\pi(r_u)^3 - \frac{4}{3}\pi(\frac{r_t + r_u}{2})^3 \qquad \textbf{Eq. 4 - 26}$$

$$Accumulation = -\ Flux\ Out\ \text{x}\ Area$$

$$\frac{dc_u}{dt}\left[\frac{4}{3}\pi(r_u)^3 - \frac{4}{3}\pi(\frac{r_t + r_u}{2})^3\right] = -D_{tu}\frac{(c_u - c_t)}{(r_u - r_t)}4\pi(\frac{r_t + r_u}{2})^2$$

Cancelling π:

$$\frac{dc_u}{dt}\frac{1}{6}\left[(2r_u)^3 - (r_t + r_u)^3\right] = -D_{tu}\frac{(c_u - c_t)}{(r_u - r_t)}(r_t + r_u)^2 \qquad \textbf{Eq. 4 - 27}$$

Bubble Surface (node "*a*") – equilibrium corresponding to bubble pressure

The bubble pressure is in equilibrium with the concentration of CO_2 in the polymer at the bubble surface (represented by the concentration at node "*a*").

$$P = Hc_A \qquad \textbf{Eq. 4 - 28}$$

$$P = \rho\Re T \qquad \Rightarrow \qquad Hc_A = \rho\Re T$$

As P and c_A are linked, the mass balance relating to node "*a*" should also include the CO_2 in the bubble as well as that in node "*a*"

The amount (moles, M) of CO_2 associated with node "*a*" and the bubble is:

$$M = V_{node(a)} \text{ x } c_A + V_{bubble} \text{ x } \rho \qquad \textbf{Eq. 4 - 29}$$

Hence the accumulation term for the rate of change of M is;

$$\frac{dM}{dt} = V_{node(a)} \frac{dc_A}{dt} + \rho \frac{dV_{bubble}}{dt} + V_{bubble} \frac{d\rho}{dt} \qquad \textbf{Eq. 4 - 30}$$

This is equal to the rate at which CO_2 is transported cross the boundary between nodes "a" and "b".

$$Flux \text{ x } Area = \frac{dM}{dt}$$

where:

$$Flux\ Into\ Bubble = D_{ab} \frac{(c_b - c_a)}{(r_b - r_a)} \qquad Area = 4\pi(\frac{r_a + r_b}{2})^2 \qquad \textbf{Eq. 4 - 31}$$

$$\frac{dM}{dt} = D_{ab} \frac{(c_b - c_a)}{(r_b - r_a)} \ 4\pi\left(\frac{r_a + r_b}{2}\right)^2 \qquad \textbf{Eq. 4 - 32}$$

The molar density of CO_2 in the bubble is given by an Equation of State. At low pressure one can use the Ideal Gas Law $\rho = \frac{P}{\Re T}$, but in general we will use the Soave Redlich Kwong (SRK) Equation of State

$$P = \frac{\Re T}{V - b} - \frac{a}{V(V + b)} \qquad \textbf{Eq. 4 - 33}$$

For CO_2 , $a = 270485.7$, $b = 0.029683$, $\Re$ = 8314 J / kmol K], [P (Pa), T (K), v (m^3/kmol) [Calvert & Farrar 1999].

An iterative equation for calculating the molar volume for given values of pressure and temperature can be defined in Visual Basic

$$V = b + \frac{\Re T}{P + \frac{a}{V(V + b)}} \qquad \textbf{Eq. 4 - 34}$$

The value of molar volume can then be converted into a molar density value.

4.3.3 Model A - Diffusion Limited (Infinitely Low Viscosity)

The simplest model (Model A) assumes that bubble growth is only limited by diffusion of gas into the bubble and is not limited by the viscosity of the polymer. The pressure of CO_2 inside the bubble is assumed to be the same as the exterior pressure.

If the exterior (and bubble) pressure varies with time then equation 4-30 is used i.e.:

$$D_{ab}\frac{(c_b-c_a)}{(r_b-r_a)}4\pi(\frac{r_a+r_b}{2})^2=[\frac{4}{3}\pi(\frac{r_a+r_b}{2})^3-\frac{4}{3}\pi r_a^3]\frac{dc_a}{dt}+\rho 4\pi r_a^2\frac{dr_a}{dt}+\frac{4}{3}\pi r_a^3\frac{d\rho}{dt}$$

$$\Rightarrow dr_a=\frac{1}{\rho r_a^2}[D_{ab}\frac{(c_b-c_a)}{(r_b-r_a)}(\frac{r_a+r_b}{2})^2dt-(\frac{1}{3}(\frac{r_a+r_b}{2})^3-\frac{r_a^3}{3})dc_a-\frac{1}{3}r_a d\rho] \qquad \textbf{Eq. 4 - 35}$$

4.3.4 Model B - Constant Diffusivity and Viscosity

This model now assumes that the polymer viscosity has an effect on the bubble growth. Diffusion of gas into the bubble now leads to an increase of gas pressure in the bubble, the pressure difference between the inside and outside of bubble then leads to the inflation of the bubble.

This model will first consider the case of constant diffusivity and constant viscosity. First of all, an expression relating the rate of bubble growth to the pressure difference is derived. A surface tension term is also included to model the pressure drop at the gas/polymer interface due to surface tension.

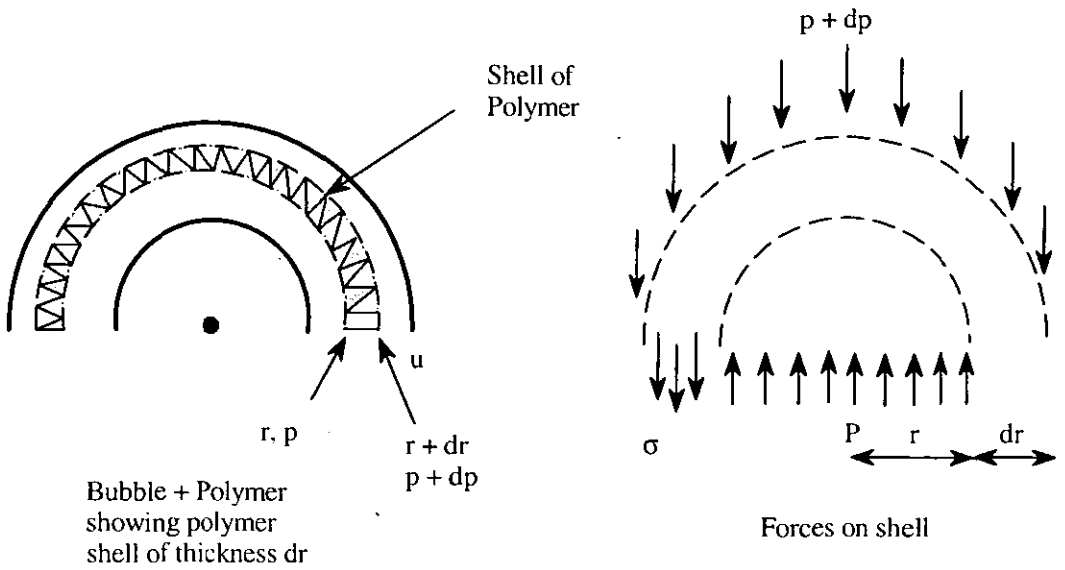

Figure 4 - 6: Force balance diagram.

Force balance on a spherical shell element of thickness *dr* (see Figure 4-6).

Inside pressure force = extensional force in polymer element + outside pressure force

$$P\pi r^2 = \sigma 2\pi r dr + (p+dp)\pi(r+dr)^2$$

$$Pr^2 = \sigma 2rdr + (p+dp)(r+dr)^2$$

$$Pr^2 = \sigma 2rdr + (p+dp)(r^2 + 2rdr + dr^2)$$

$$Pr^2 = 2\sigma rdr + pr^2 + 2prdr + r^2dp + 2rdrdp$$

If regard p << σ then $2prdr$ is a negligible term:

$$2\sigma rdr = -r^2dp \qquad \Rightarrow 2\sigma dr = -rdp \qquad \textbf{Eq. 4 - 36}$$

Extensional stress σ related to extensional strain rate ε̇ by:

$$\sigma = \mu_{ext}\dot{\varepsilon} \quad , \quad (\dot{\varepsilon} = \frac{\dot{r}}{r}) \qquad \textbf{Eq. 4 - 37}$$

where μ_{ext} is the extensional viscosity.

therefore:

$$2\mu_{ext}\frac{\dot{r}}{r}dr = -rdp \qquad \textbf{Eq. 4 - 38}$$

However $\dot{r}$ varies with r. Consider a bubble of radius R growing at $\dot{R}$ and a point at radius r moving at $\dot{r}$. The volume between r and R remains constant.

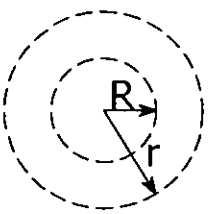

$$\frac{4}{3}\pi r^3 = \frac{4}{3}\pi R^3 + c$$

Differentiate with respect to t

$$4\pi r^2\frac{dr}{dt} = 4\pi R^2\frac{dR}{dt} + 0$$

$$\Rightarrow \dot{r} = \frac{R^2}{r^2}\dot{R} \qquad \textbf{Eq. 4 - 39}$$

Insert Eq. 4–39 into Eq. 4-38:

$$2\mu_{ext}\frac{R^2}{r^2}\dot{R}\frac{1}{r}dr = -rdp$$

$$2\mu_{ext}\frac{R^2\dot{R}}{r^4}dr = -dp \qquad \textbf{Eq. 4 - 40}$$

If μ_{ext} is a constant we can integrate

$$2\mu_{ext}R^2\dot{R}\int_R^{R_{ext}}\frac{1}{r^4}dr = \int_{p_b}^{p_{ext}} -dp$$

where R_{ext} is the external radius of the polymer sphere

$$2\mu_{ext}R^2\dot{R}\left[-\frac{1}{3}r^{-3}\right]_R^{R_{ext}} = \frac{2\mu_{ext}R^2\dot{R}}{3}\left[\frac{1}{R^3}-\frac{1}{R_{ext}^3}\right] = p_b - p_{ext}$$

Now $\mu_{ext} = 6\mu$, where μ shear viscosity [Amon and Denson 1984]

$$4\mu R^2\dot{R}\left[\frac{1}{R^3}-\frac{1}{R_{ext}^3}\right] = p_b - p_{ext} \qquad \textbf{Eq. 4 - 41}$$

If surface tension fores are significant then an extra term can be added to reflect this:

$$p_b - p_{ext} = 4\mu R^2\dot{R}\left[\frac{1}{R^3}-\frac{1}{R_{ext}^3}\right]+\frac{2\gamma}{R} \qquad \textbf{Eq. 4 - 42}$$

where; γ is the surface tension [see e.g. Tuladhar and Mackley 2004]

This final equation can be used to calculate the bubble growth rate $\dot{R}$, based on the pressure difference inside the bubble and outside the polymer.

$$\dot{R} = \frac{p_b - p_{ext} - \left(\frac{2\gamma}{R}\right)}{4\mu R^2\left[\frac{1}{R^3}-\frac{1}{R_{ext}^3}\right]} \qquad \textbf{Eq. 4 - 43}$$

N.B. in some studies R_{ext} is considered large compared to R and thus the $\frac{1}{R_{ext}^3}$ term is regarded as negligible.

The bubble pressure is calculated based on the current size of the bubble and the number of nodes in the bubble and node *a*.

$$4\pi D_{AB}\frac{(c_b - c_a)}{(r_b - r_a)}\left(\frac{r_a + r_b}{2}\right)^2 = \frac{dM}{dt} \qquad (M = c_a V_a + \rho V_{bub}) \qquad \textbf{Eq. 4 - 44}$$

where: V_{bub} = volume of the bubble

Then based on current values for V_{bub} (or R) and M, one can calculate ρ and c_A and p_B from

$$M = c_a V_a + \rho V_{bub} = \frac{V_a p}{H} + \frac{V_{bub}}{v}$$

where

$$p_B = \left(\frac{\Re T}{V - b} - \frac{a}{V(V+b)} \right) \quad \text{(Equation of State)}$$

and v is the mole volume and p_B is the pressure of the bubble.

i.e.

$$M = \frac{V_a}{H}\left(\frac{\Re T}{V - b} - \frac{a}{V(V+b)} \right) + \frac{V_{bub}}{V} \qquad \textbf{Eq. 4 - 45}$$

Therefore the correct value for v can be found numerically from ρ and c_a.

4.3.5 Model C – Diffusivity and Viscosity Variable

The same general equation for bubble growth can be used as before (Eq. 4.40).

$$2\mu_{ext} \frac{R^2 \dot{R}}{r^4} dr = -dp$$

However we now consider the case that viscosity is not a constant.

$$-\int_{p_b}^{p_{ext}} dp = 2R^2 \dot{R} \int_{R}^{R_{ext}} \frac{\mu_{ext}}{r^4} dr = 12R^2 \dot{R} \int_{R}^{R_{ext}} \frac{\mu}{r^4} dr$$

In our analysis we will consider viscosity and diffusivity to vary according to the Williams–Landel–Ferry (WLF) equation, where the local concentration will affect the local glass transition temperature. A similar approach was adopted by Goel and Bechman (1995) for modelling viscosity (but not diffusivity), and by Chen et al (2006) who varied both the viscosity and diffusion according to the WLF equation.

The WLF equation is [Williams et al 1955]:

$$\log \frac{\mu}{\mu_o} = \frac{-c_1\left(T - T_g\right)}{c_2 + \left(T - T_g\right)}$$

Eq. 4 - 46

$$\frac{\mu}{\mu_o} = 10^{\frac{-c_1\left(T-T_g\right)}{c_2+\left(T-T_g\right)}} = F$$

where $c_1 = 17.44$, $c_2 = 51.6$ k [Williams et al 1955], and F is a scaling factor arising from the WLF equation.

As $D \sim \frac{1}{\mu}$ [Bird et al 1960]

$$\frac{D}{D_o} = 10^{\left(\frac{c_1\left(T-T_g\right)}{c_2+\left(T-T_g\right)}\right)} = \frac{1}{F}$$

Eq. 4 - 47

Now we can say $T_g = T_{g0} - \beta c$ [Condo & Johnston (1992)]

The value of β is determined from the slope of the plot of T_g versus pressure and the Henry's law constant:

$$(T_g = T_{g0} - mp\,, \qquad p = Hc \qquad \Rightarrow \beta = mH\,)$$

For each concentration one can calculate:

$$F = 10^{\left(\frac{-c_1(T-T_{g0}+\beta c)}{c_2+(T-T_{g0}+\beta c)}\right)}$$

Eq. 4 - 48

$$D = \frac{D_0}{F}$$

Eq. 4 - 49

$$\mu = \mu_0 F$$

Eq. 4 - 50

For the bubble growth relationship

$$-\int_{p_b}^{p_{ext}} dp = 2R^2\dot{R}\int_{R}^{R_{ext}} \frac{\mu_{ext}}{r^4}dr = 12R^2\dot{R}\int_{R}^{R_{ext}} \frac{\mu}{r^4}dr$$

as $\frac{1}{r^4}$ varies so dramatically with r it is better to change the variable for integration as per Tuladhar and Mackley (2004) paper $z = \frac{1}{r^3}$ (m^{-3}).

$$p_b - p_{ext} = 4R^2\dot{R}\int_{z_R}^{z_{ext}} \mu dz = 4R^2\dot{R}\int_{z_R}^{z_{ext}} F dz \text{ , integrated numerically by trapezium rule}$$

$$\dot{R} = \frac{p_b - p_{ext} - \left(\frac{2\gamma}{R}\right)}{4R^2\mu_0\int_{z_R}^{z_{ext}} F dz} \qquad \textbf{Eq. 4 - 51}$$

4.4 Conclusion

These mathematical models will be used in the following ways to interpret the data measured in this work:

(i) Diffusion coefficient can be estimated from temperature measured of onset of softening (T_A) and complete softening (T_B) in non-isothermal experiments.

(ii) Polymer deflection is predicted as a function of time assuming it is a diffusion controlled process (used for isothermal experiments).

(iii) Bubble growth in a polymer is predicted as a function of time based on three different assumptions. These are:

  (a) Diffusion control (Model A)

  (b) Constant diffusivity and viscosity (Model B)

  (c) Diffusivity and viscosity varying in accordance with the Williams–Landel–Ferry (WLF) equation (Model C).

Chapter 5 Mechanical Measurement of Polymer Softening

5 Introduction

This chapter presents three sets of experiments. A first set of experiments (see chapter 3 section 3.2) were performed to measure the softening temperature of polymers as a function of applied CO_2 pressure using a linear variable displacement transducer (LVDT). This used a flat tip to measure the central deflection of 2-3 mm thick samples of 4 different polymers undergoing 3-point bending whilst exposed to CO_2 at pressures of up to 120 bar. Difficulties occurred assessing the data because of noise of the LVDT output signal and a large temperature lag between the heating medium and the cell. Therefore modifications were made to the existing high pressure cell to achieve better results. This included direct heating of the cell body using cartridge heaters, replacement of the LVDT to one with lower noise and modification of the LVDT tip to a pointed tip.

This lead to a second set of experiments (see chapter 3 section 3.3). These experiments were partly a repeat of the previous work which monitored how the deflection varied as the temperature was slowly increased for various pressures of CO_2, of 2 mm thick samples of only two polymers (PS and PMMA) undergoing 3-point bending whilst exposed to CO_2 at pressures of up to 120 bar. Further experiments were also performed on PS only using different scanning rates (0.2 and 0.5°C/min). In the third set of experiments isothermal tests (PC/CO_2) were also carried out to test the deflection versus time model (see chapter 4 section 4.2).

In the first two sets of experiments the nominal glass transition temperature was recorded as the onset temperature where the central deflection suddenly begins to increase. All the results and the measurements are discussed and compared with published data. Finally the experimental data are compared with a two models. "Onset" (T_A) and "full softening" (T_B) temperatures extracted from non-isothermal (constant heating rate) experiments were used to estimate CO_2 diffusivities using the model discussed in section 4.1. Isothermal experimental data are fitted to a model describing how the central deflection varies with time (section 4.2).

5.1 First Experimental Setup

5.1.1 Effect of CO_2 Pressure on Polymer Softening

The displacement (deflection) versus temperature curves for all four polymers are presented in Figure 5 - 1 to Figure 5 - 4. In all cases the deflection curve was initially relatively flat but then underwent a dramatic increase as the temperature was raised over a 20K interval. It can be assumed that this is due to softening occurring in the sample. The temperatures were the increase occurred varied with both the polymer and the pressure used. Increasing the pressure, in general, caused the curves to shift to lower temperatures, by typically 40 K (20 K for PMMA). The variation is generally monotonic, although with some exceptions, which may be due to experimental error (which is addressed later in this chapter). PC showed the highest temperatures required to soften the sample (~120 °C to ~160 °C), whereas lower temperatures were sufficient for the other polymers (~60°C to ~100 °C for PS; ~70 °C to ~110 °C for PETG; ~80 °C to ~100 °C for PMMA).

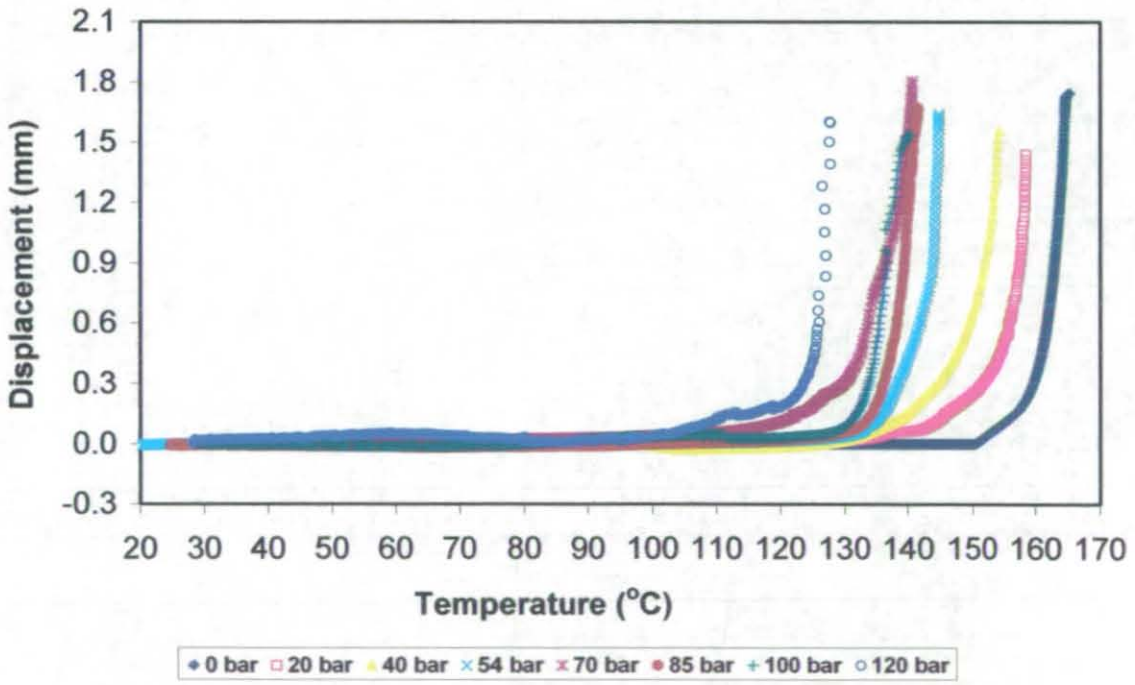

Figure 5 - 1: Central deflection versus temperature of PC strips heated at 1 °C/minute in CO_2 at various pressures.

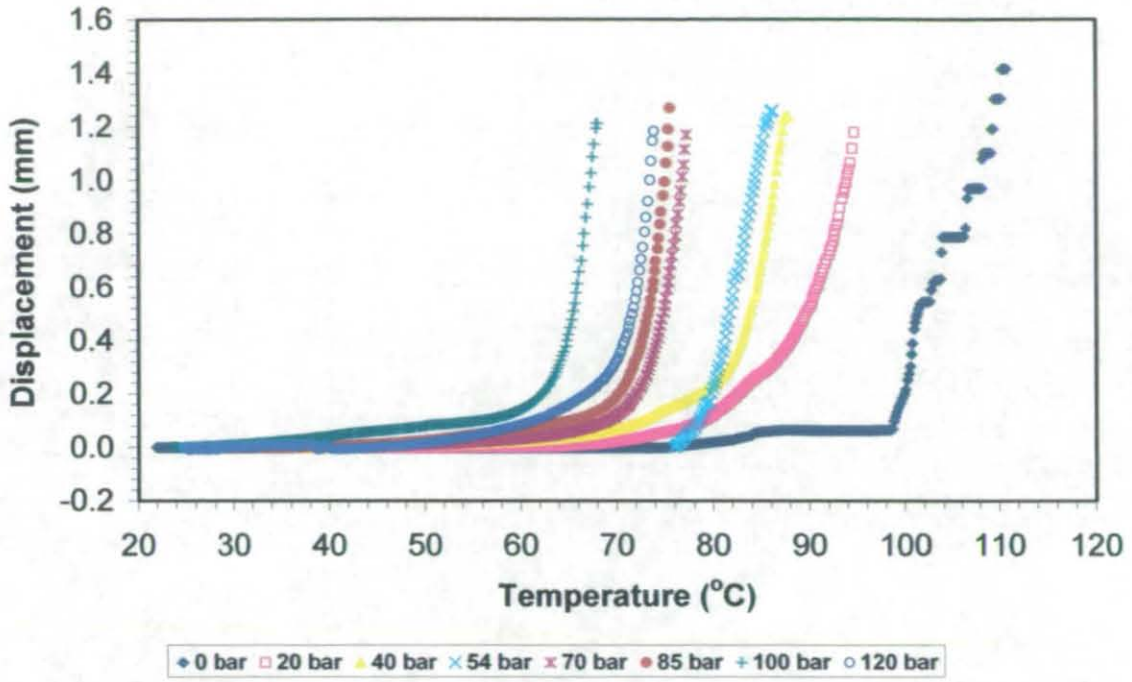

Figure 5 - 2. Central deflection versus temperature of PS strips heated at 1 °C/minute in CO_2 at various pressures.

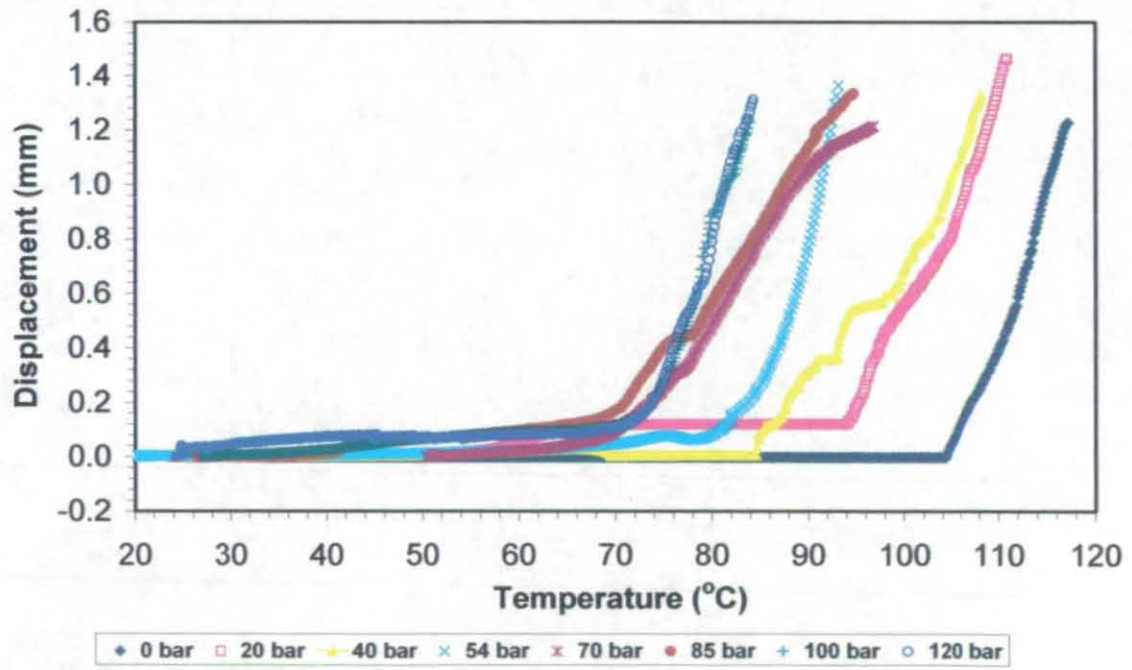

Figure 5 - 3: Central deflection versus temperature of PETG strips heated at 1 °C/minute in CO_2 at various pressures.

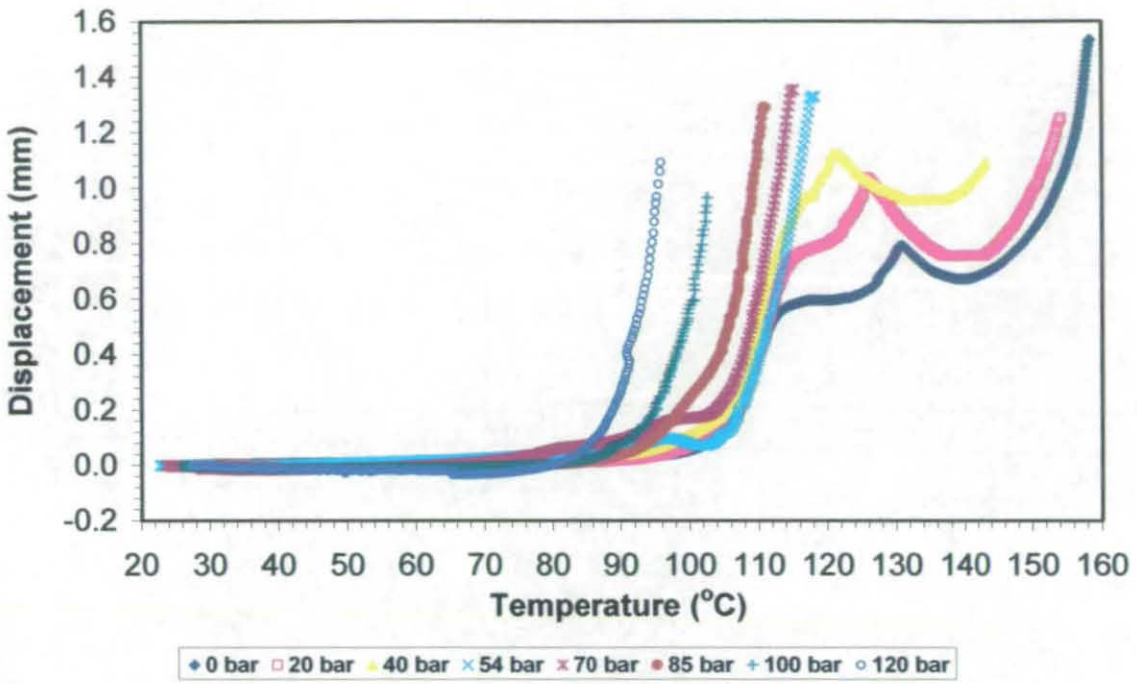

Figure 5 - 4: Central deflection versus temperature of PMMA strips heated at 1 °C/minute in CO_2 at various pressures.

The most important finding of this research work is that the onset softening temperature is clearly lowered by increasing the applied pressure of CO_2. Unusual behaviour was observed for PMMA at low pressures (0 bar, 20 bar and 40 bar) as the variation of deflection with temperature was not monotonic, but this was a reproducible effect. The reasons for this are unclear, but could be due to pre-stressing of the samples when they were originally formed.

The above observations are borne out by the variation of the extracted softening temperatures T_A and T_B (see chapter 3 section 3.2.5). A much smoother variation is seen with the values for T_B than T_A, which is due to the much greater difficulty in detecting the initial onset of the increase in deflection (T_A) than the temperature associated with the gross deflection (T_B) where the slopes of the curves are much greater, see Figure 5 - 5.

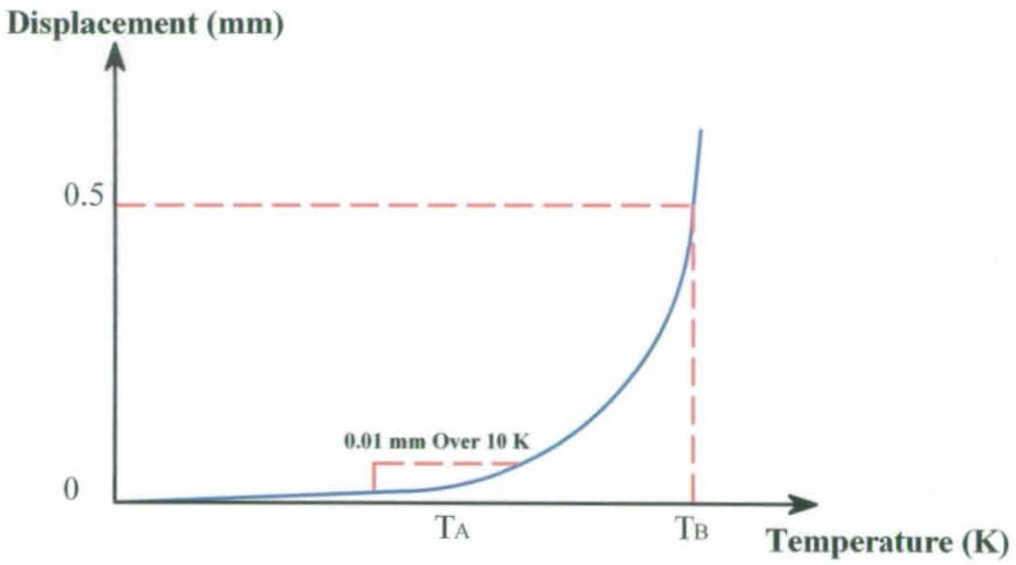

Figure 5 - 5: Softening temperature of PC showing method T_A & T_B.

It should also be remarked that the forms of the curves observed in Figure 5 - 1 to Figure 5 - 4 also varied with pressure. At zero bar the deflection curves displayed a noticeable kink at the onset of softening. At intermediate pressures a more gradual onset of softening is observed. At high pressures (100 bar and 120 bar) a small but significant deflection is apparent even at low temperatures.

5.1.2 Comparison of T_A and T_B with Literature Values

The extracted values of T_A and T_B (using the method presented in section 3.2.5) are compared with literature values for PC in Figure 5 - 6, PS in Figure 5 - 7 and PMMA in Figure 5 - 8. Insufficient data were found in the literature for PETG to merit a comparison. The literature data range is up to 60 bar for PMMA and for PC and PS up to about 90 bar.

The data from different workers are generally consistent with one another, with a linear decrease of T_g below the normal (un-plasticised) T_g with increasing pressure of approximately 1K/bar. Two exceptions are the data of Wissinger & Paulaitis 1991 and Condo & Johnston 1992 for PMMA which both show a large departure from linearity at around 40-50 bar. These provided the first evidence in the literature for the retrograde vitrification phenomenon, which appears to be a very strong effect for PMMA.

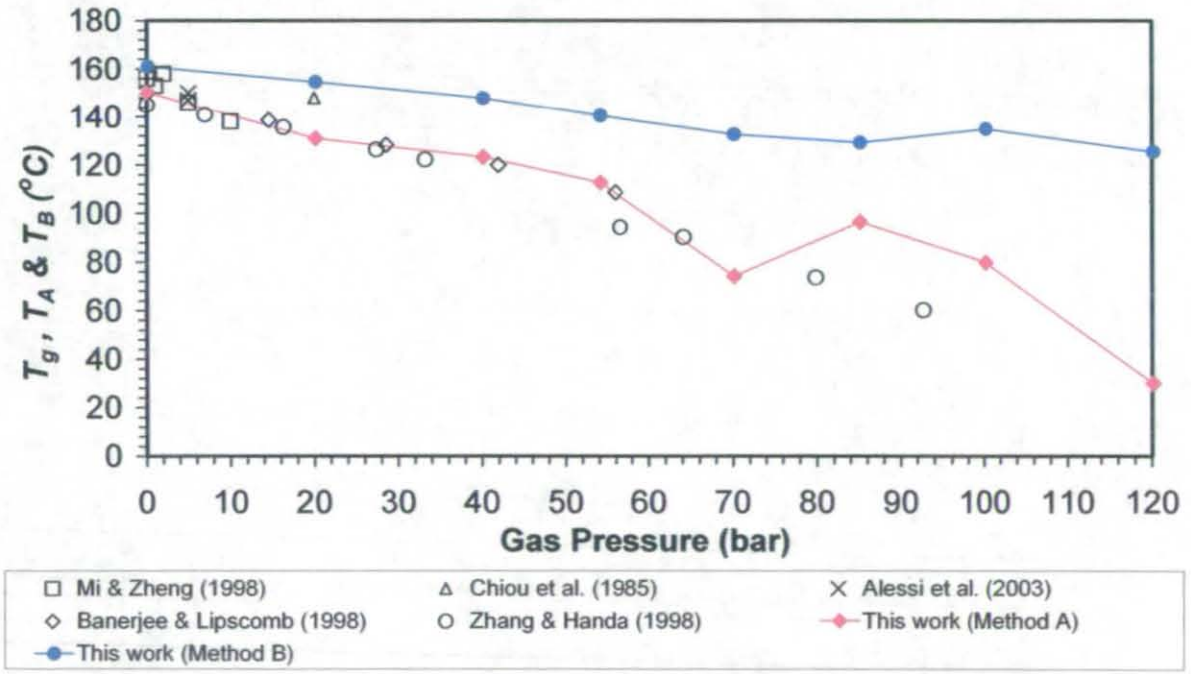

Figure 5 - 6: Softening temperature of PC versus applied CO_2 pressure as measured by LVDT using methods A (T_A) and B (T_B), compared to T_g reported in the literature for PC.

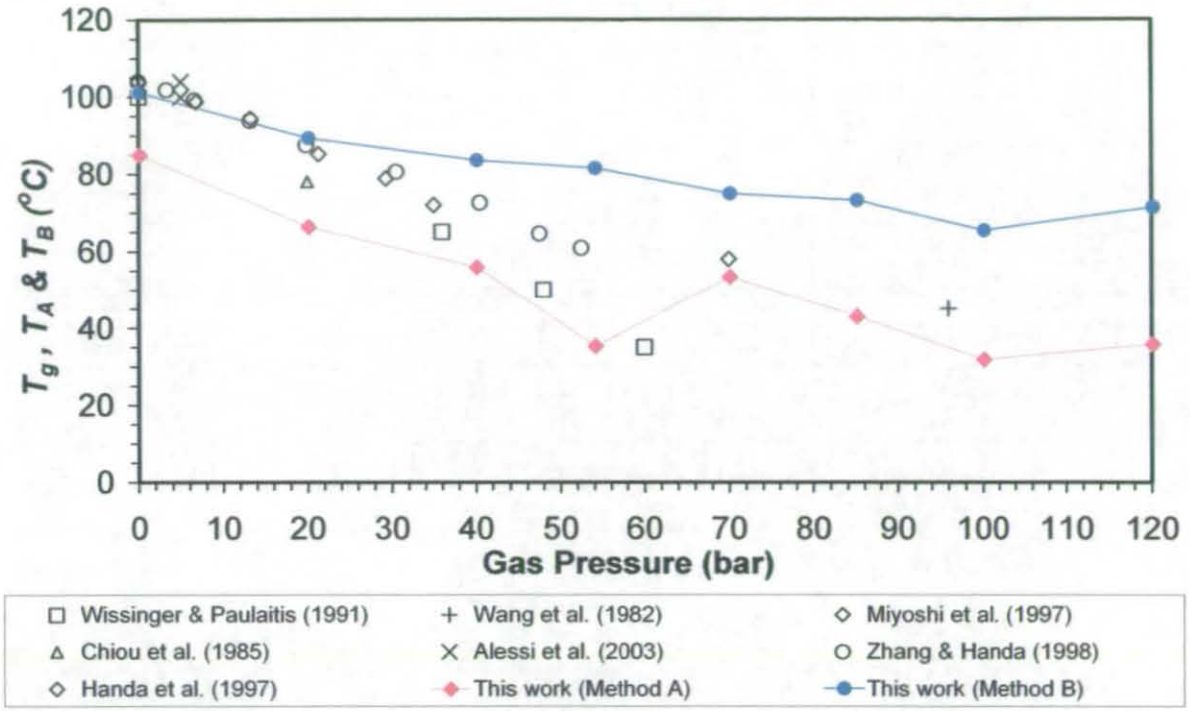

Figure 5 - 7: Softening temperature of PS versus applied CO_2 pressure as measured by LVDT using methods A (T_A) and B (T_B), compared to T_g reported in the literature for PS.

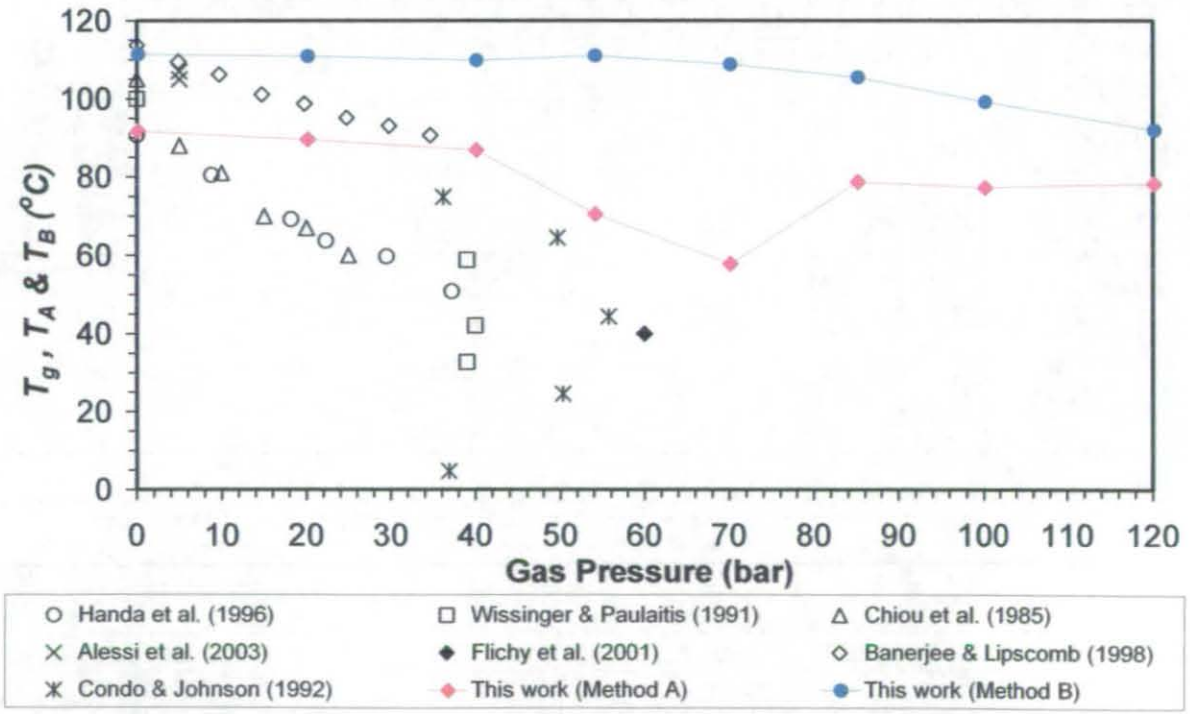

Figure 5 - 8: Softening temperature of PMMA versus applied CO_2 pressure as measured by LVDT using methods A (T_A) and B (T_B), compared to T_g reported in the literature for PMMA.

Also shown in Figure 5 - 6, Figure 5 - 7, and Figure 5 - 8 are the softening points extracted from our LVDT data by methods T_A and T_B. It can be seen that T_A values for PC (Figure 5 - 6) lie reasonably close to the literature data for T_g. The same is almost true for PS, with the only anomaly being at zero bar. However, inspection of the LVDT curves in Figure 5 - 2, shows a minor blip in the curve at around 80°C which has lead to this T_A value being used in Figure 5 - 7, where as the more obvious sudden increase of deflection at 98°C corresponds quite closely to the literature data for T_g. The T_A values for PMMA, however generally lie well above the literature data.

The T_B values for all the samples, on the other hand, lie well above the literature values in all cases with a modest decrease of T_B with increasing pressure. The T_B and T_A curves converge at low pressure, which suggests that at high pressure the degree of softening required for large deformations is subject to a time lag. It is likely that this is caused by the time necessary for CO_2 to diffuse into the centre of the polymer strips to cause plasticization and softening at the centre of the sample.

5.1.3 Estimation the Diffusivities of CO_2 in Polymer Strips

The model shown in chapter 4, section 4.1, which estimates values of diffusion coefficients based on input values of T_A, T_B and diffusion time was applied to the experimental data. Values of T_A however were taken from literature correlations of T_g with applied CO_2 pressure. The figure 5 -9 shows the resulting diffusivity values of CO_2 in polymer strip versus the applied pressure (0-120 bar).

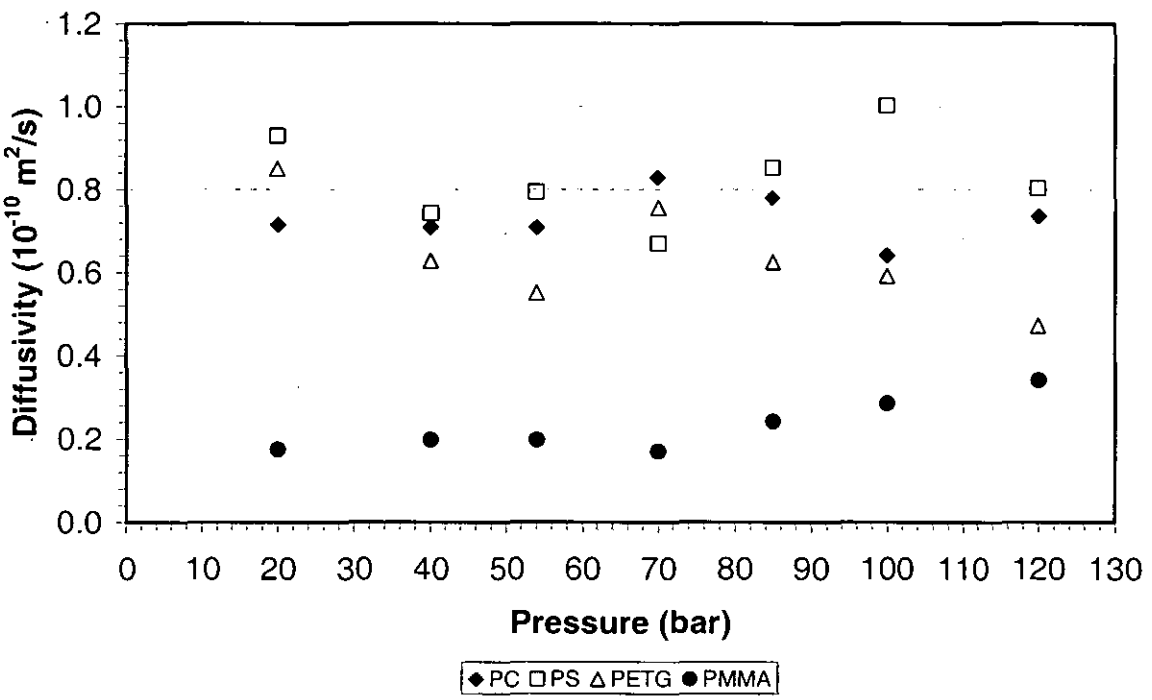

Figure 5 - 9: Diffusion of CO_2 in polymer strip versus the applied pressure (25 to 160 °C).

The average values and standard deviations for CO_2 diffusivity in PC, PS and PMMA using the estimation model are presented in table 5-1.

Table 5 - 1: Diffusivity (10^{-10} m^2/s) of CO_2 in polymers strips.

Polymer	This work	Literature values (see Table 2.4)
PC	0.73 ± 0.6	0.12 – 0.33
PS	0.82 ± 1.2	0.30 - 2.98
PETG	0.67 ± 0.5	-
PMMA	0.23 ± 0.6	0.01 – 1.04

Table 5-1 shows distinctly smaller diffusivity values for CO_2 in PMMA compared to in other polymers. This may also explain the higher than expected values of T_A that we recorded for PMMA. Diffusion coefficients of CO_2 in polymers have been obtained by a number of workers from high pressure sorption experiments [e.g. Tang et al 2004, Sato et al 2001, Berens et al 1992, Nikitin et al 2003, and Webb & Teja 1999]. Published values are shown for each polymer in Table 5-1 for various combinations of temperature and pressure.

The table shows that diffusivity varies considerably with both temperature and pressure and as such the constant diffusivity model that we employed will lack accuracy. However, it is clear that the published diffusion coefficients are generally of a similar order of magnitude to those extracted from our experimental data, and confirms the lower diffusivity of CO_2 in PMMA compared to PC and PS. This strongly suggests that the full softening of the samples is indeed limited by diffusion of carbon dioxide into the sample.

The slow rate of diffusion of CO_2 into the samples would also explain the difference between the very sharp onsets for the LVDT curves at zero bar compared to the smoother onsets at higher pressures. At zero bar the softening is not diffusion limited as there is no CO_2 to diffuse, and so the softening is quite sudden, and only limited by the effects of viscosity and the heat transfer, which must be present as zero bar data does not show an immediate change in deflection. However, at higher pressures the overall stiffness of the polymer strips is only gradually reduced as the CO_2 gradually plasticises the sample to greater depths as time proceeds.

5.2 Second Experimental Setup

In the previous section 5.1, difficulties were faced extracting onset softening values because of the noise of the LVDT output signal and time lags in the temperature control of the cell. Therefore improvements were made to the existing high pressure cell to achieve better results as described in chapter 3 section 3.3. The modifications are mainly to give easier operation, provide better temperature control and use a better quality LVDT.

This section will present the second set of experiments measuring polymer softening. This set of experiments was partly a repeat of the previous work which monitored how the deflection varies as the temperature slowly increased for various pressures of CO_2, and applies new conditions such as different scanning rates (0.1, 0.2, and 0.5 °C/min) and isothermal tests to develop the deflection model (see chapter 4 section 4.2). Two polymers were tested (PS & PMMA) using the modified cell.

5.2.1 Effect of CO_2 Pressure on Polymer (PS & PMMA) Softening

Displacement versus temperature results for PS and PMMA at different pressures are shown in Figures 5-10 and 5-11. As observed previously in section 5.1 the deflection curves are initially relatively flat and then undergo a dramatic increase as the temperature is raised over 5 – 10 K interval, due to softening occurring in the sample. Increasing the pressure, in general, caused the curves to shift to lower temperatures, by about 45 K, over the pressure range of 0 – 120 bar.

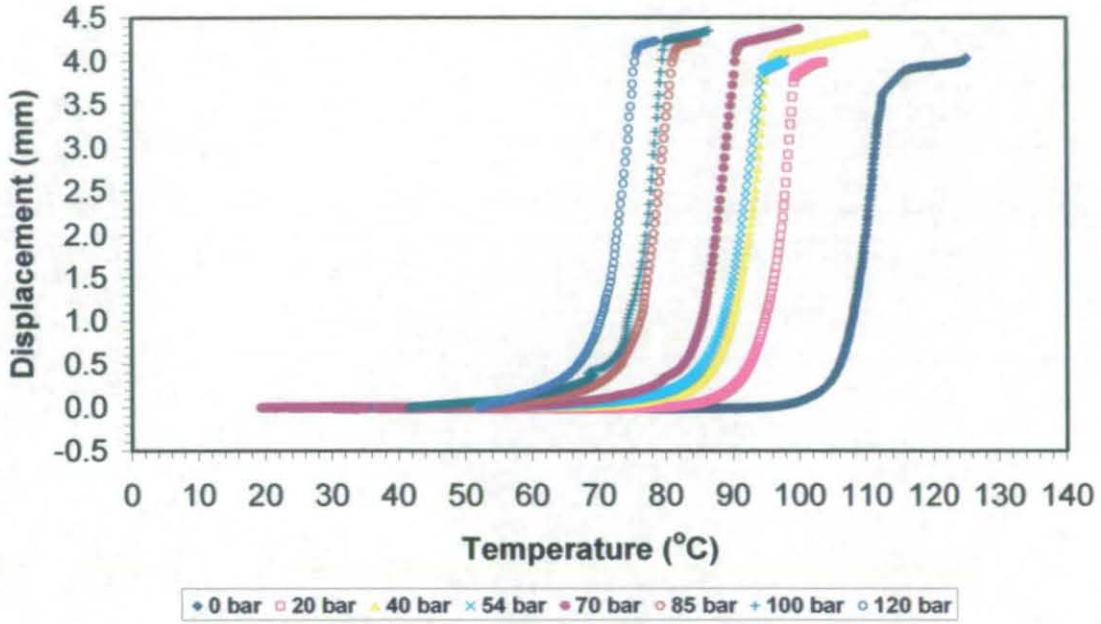

Figure 5 - 10: Central deflection versus temperature of polystyrene (PS) strips heated at 1°C/minute in carbon dioxide at various pressures.

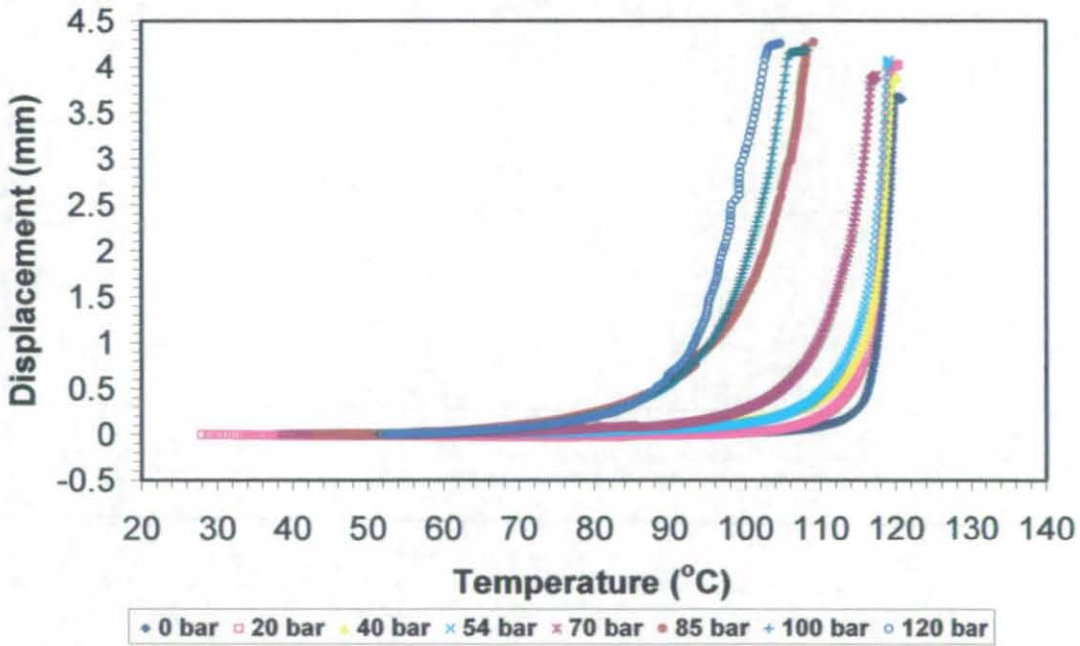

Figure 5 - 11: Central deflection versus temperature of PMMA strips heated at 1°C/minute in carbon dioxide at various pressures.

Again the onset softening temperature is clearly lowered by increasing the applied pressure of CO_2. The displacement of a polymer increases with the increase of the applied pressure. In content which the data presented in section 5.1 the curves are smooth and do not have a noisy LVDT output signal.

Therefore, a new measuring technique was applied to extract T_A and T_B values (as described, see chapter 3 section 3.3.6. Figure 5-12 shows how the initial softening point (T_A), and final softening point (T_B) are determined.

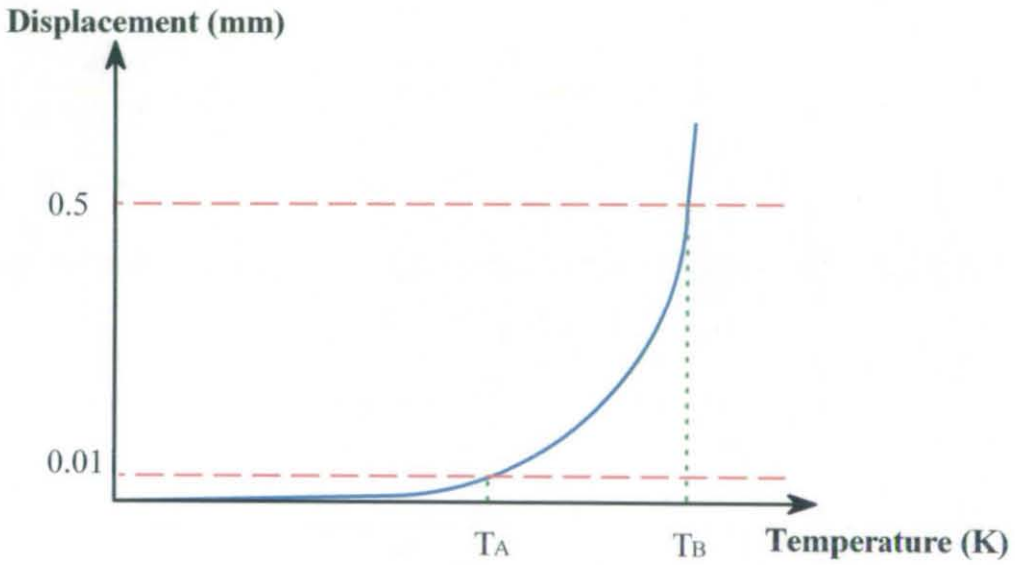

Figure 5 - 12: Reading the softening temperature points by using method A & B.

5.2.2 Comparison of T_A and T_B with Literature Values

The extracted values of T_A and T_B (from Figure 5-12) are compared with literature values for PS in Figure 5-13 and PMMA in Figure 5-14. The literature data ranges up to 95 bar for PS, and 60 bar for PMMA, it can be seen that the T_A values for this work lie reasonably close to the literature data for T_g. The exceptions are the Wissinger and Paulatitis (1991) and Condo and Johnston (1992) values, who used a dilation method, and this techniques gives lower values of T_g at high pressure (40 – 60 bar) compared with all other authors. At lower pressures this method gives similar results. The discrepancy at higher pressure may be due to the use of different techniques.

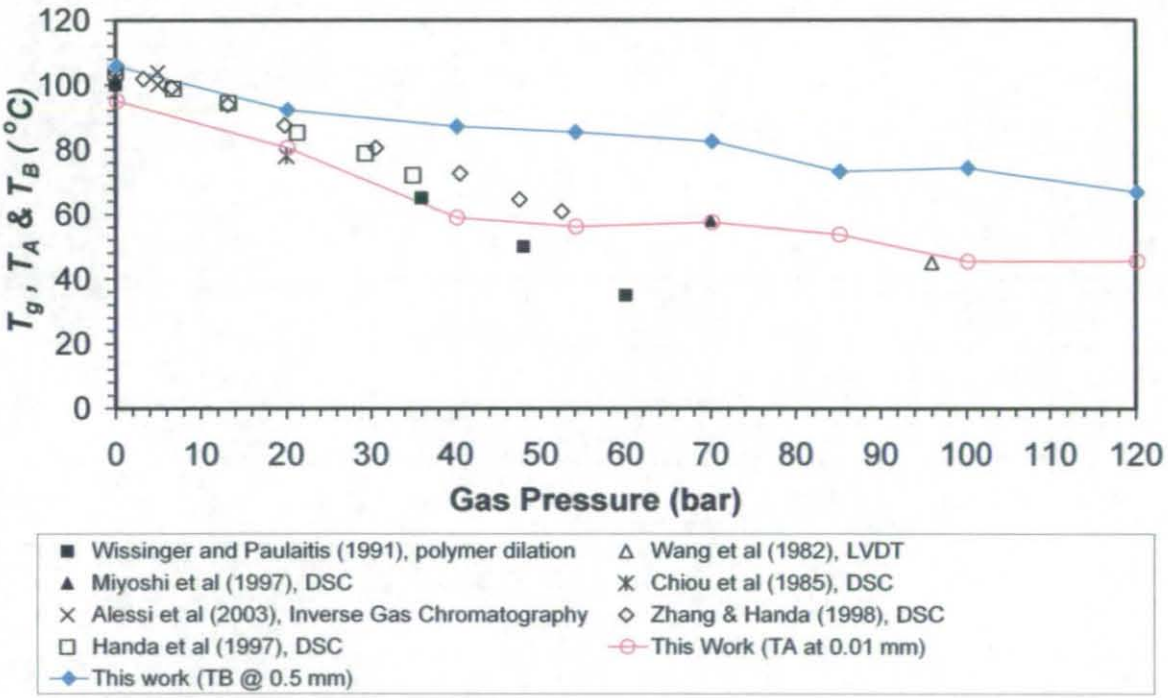

Figure 5 - 13: Softening temperature of PS versus applied CO_2 pressure as measured by LVDT using methods A and B, compared to glass transition temperatures reported in the literature for PS (After modification).

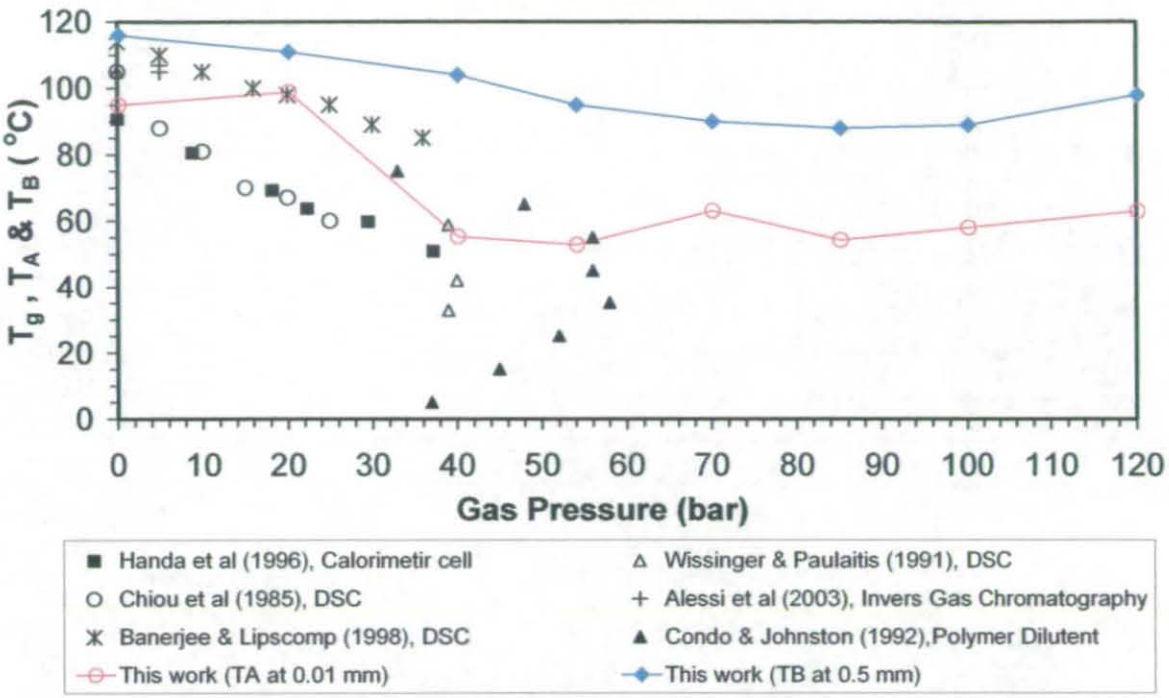

Figure 5 - 14: Softening temperature of PMMA versus applied CO_2 pressure as measured by LVDT using methods A and B, compared to glass transition temperatures reported in the literature for PMMA (After modification).

Also shown on Figure 5-13 and 5-14, the softening points extracted from our LVDT data lie reasonably close to the literature data for T_g, with the only 5 – 10 °C higher around 70 bar and above for PS and 10 – 40 °C around 54 bar for PMMA. This is because this technique measures the softening temperature of the interior polymer specimen, which suggests that at high pressure the degree of softening required for large deformations is subject to a time lag. As found in the earlier experiments the T_B values were significantly higher than the T_A values.

5.2.3 Influence of Scanning Rate for the PS/CO_2 System

All our previous work was done at relatively fast scanning rates (1 °C/min). As we believe that the softening profiles are influenced by the time taken for the CO_2 to diffuse into the samples we wished to test the response using different scan rates. Therefore different scanning rates of 0.2 and 0.5°C/min were applied (over the applied pressure ranges 20 – 70 bar), which gives the gas more time to diffuse in the polymer, and give the gas more chance to plasticise and bend the polymer than with a faster scanning range (1 °C/min).

The following figures (Figure 5 - 15 to 5 – 18) present the central deflection of PS strips versus temperature heated at different scanning time (0.2, 0.5, and 1 °C/min). One pressure (54 bar) was tested with an even slower rate (0.1°C/min), and this shows the same trend:

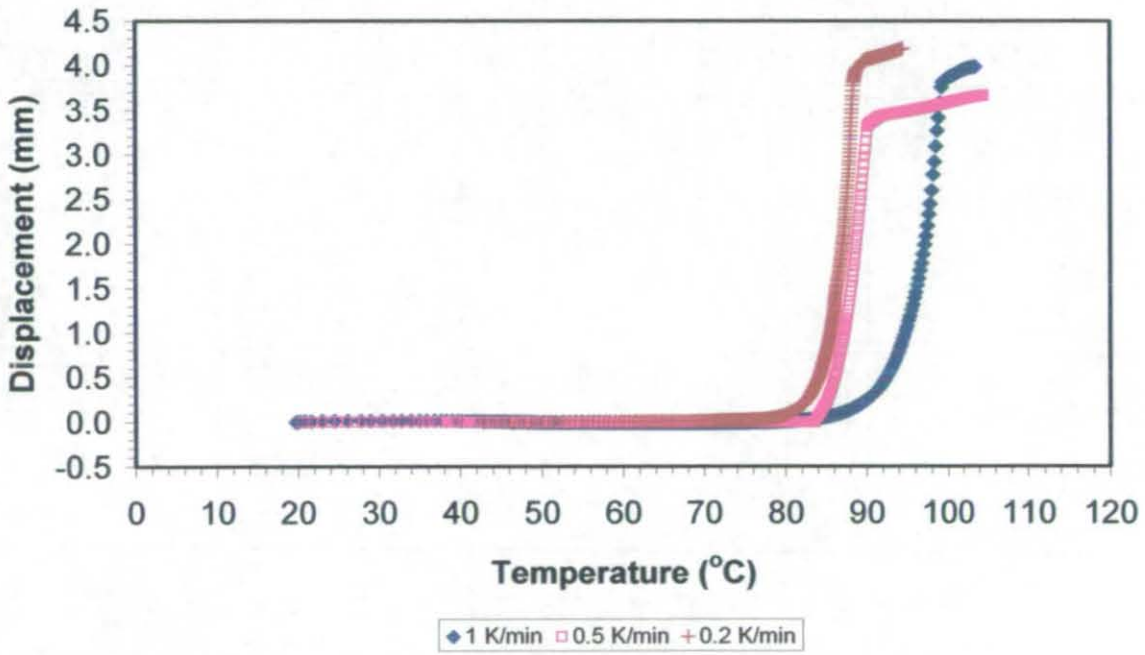

Figure 5 - 15: Central deflection versus temperature of PS strips heated at 0. 2, 0. 5 , and 1 °C/minute in carbon dioxide at 20 bar.

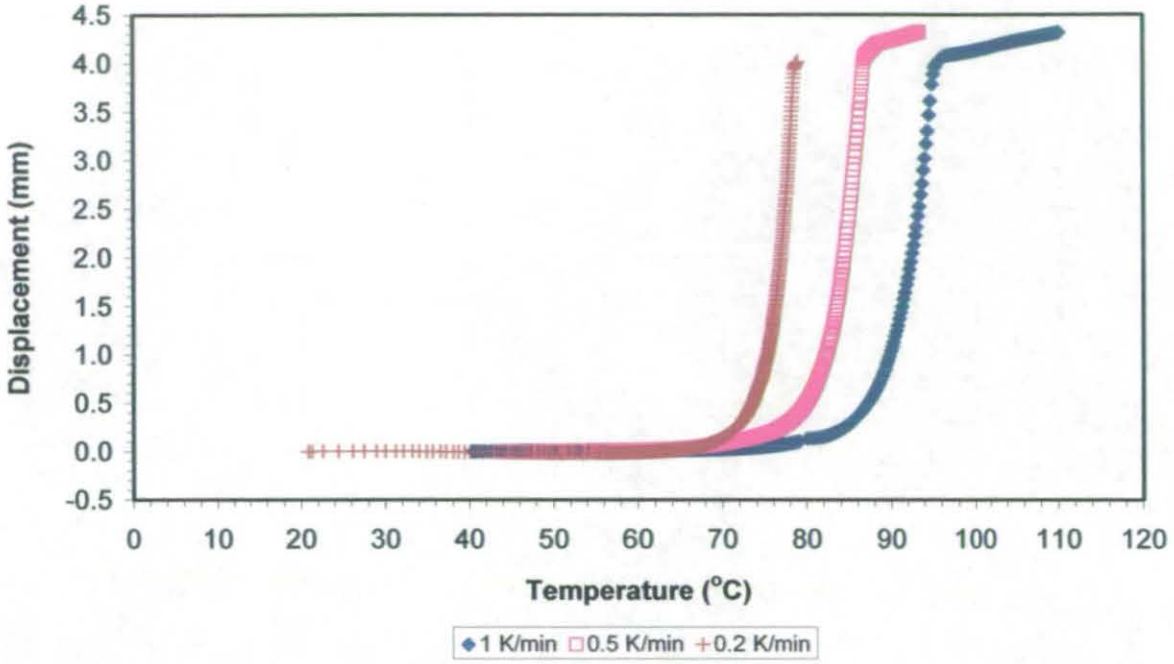

Figure 5 - 16: Central deflection versus temperature of PS strips heated at 0. 2, 0. 5, and 1 °C/minute in carbon dioxide at 40 bar.

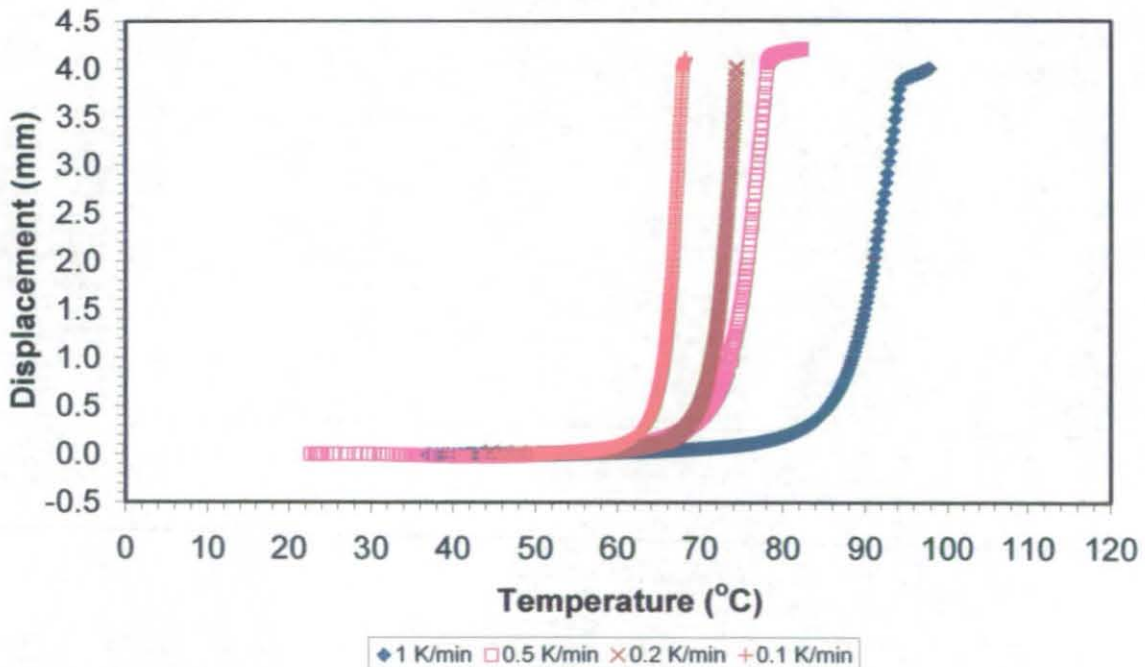

Figure 5 - 17: Central deflection versus temperature of PS strips heated at 0. 1 to 1 °C/minute in carbon dioxide at 54 bar.

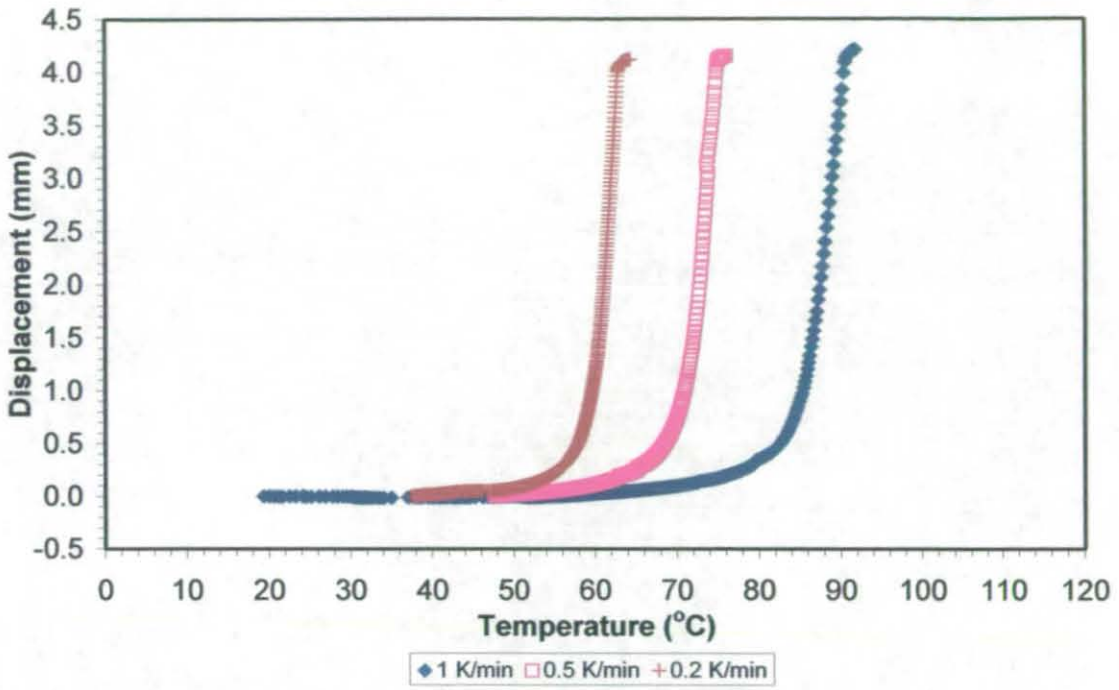

Figure 5 - 18: Central deflection versus temperature of PS strips heated at 0. 2, 0. 5, and 1°C/minute in carbon dioxide at 70 bar.

In all cases, as shown in the previous figures, slower scanning rates have sharper deflection curves. The difference in temperature whereby large scale deflection occurs varies by up to 30 K according to scanning rate. This again supports the view that large scale deflections are limited by diffusion. With slower scanning rate the polymer has more time to be exposed to the gas for diffuse into the polymer.

Figure 5 – 19 presents the T_A and Figure 5 – 20 presents T_B values of central deflection versus different scanning time (0.1, 0.2, 0.5, and 1°C/min) over the applied pressure ranges (20 – 70 bar). The data were also linearly extrapolated to a scanning rate of 0 °C/min, and are compared with literature values of T_g in Figure 5 – 21.

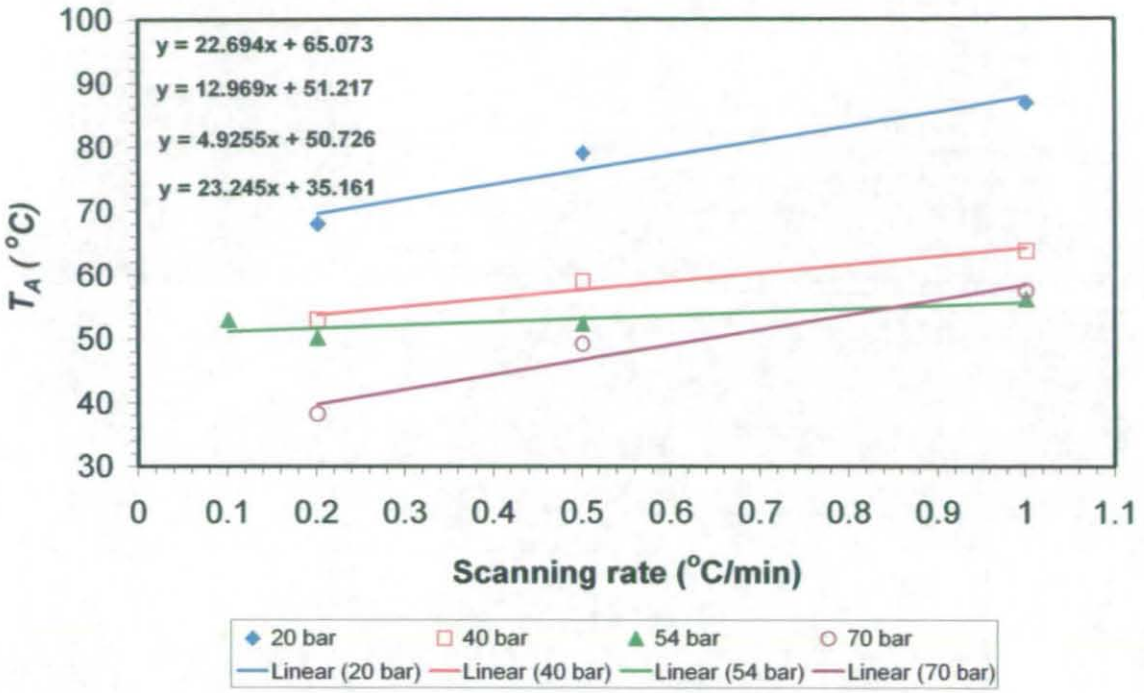

Figure 5 - 19: T_A values of PS strips heated in carbon dioxide at various pressures plotted versus scanning rate.

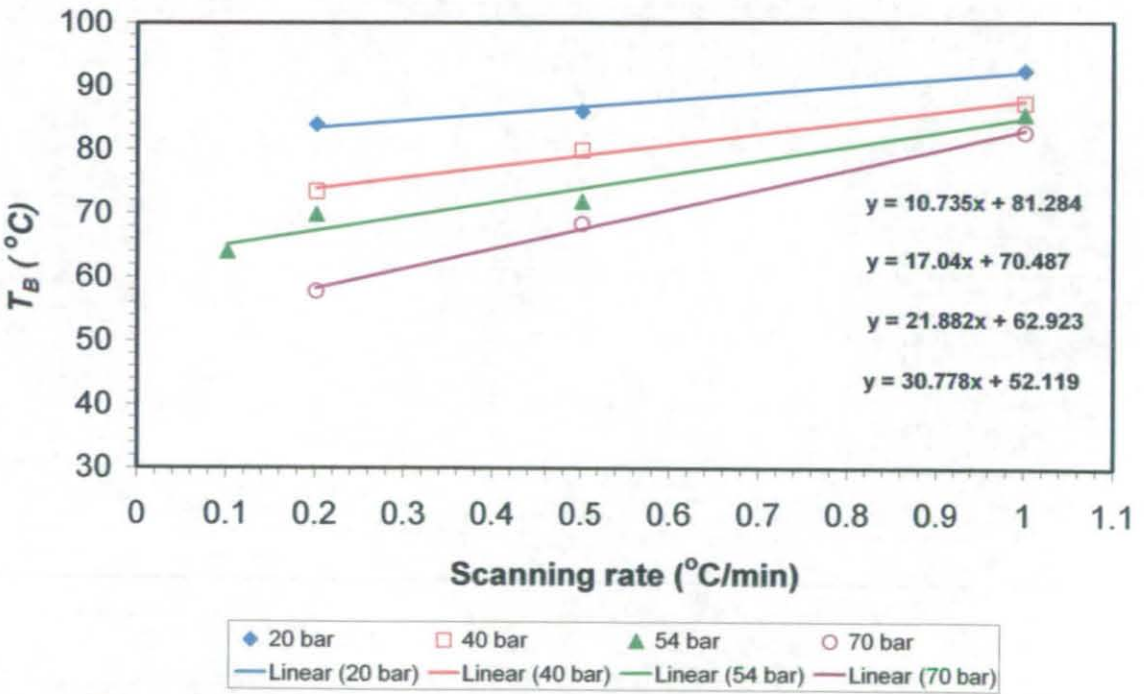

Figure 5 - 20: T_B values of PS strips heated in carbon dioxide at various pressures plotted versus scanning rate.

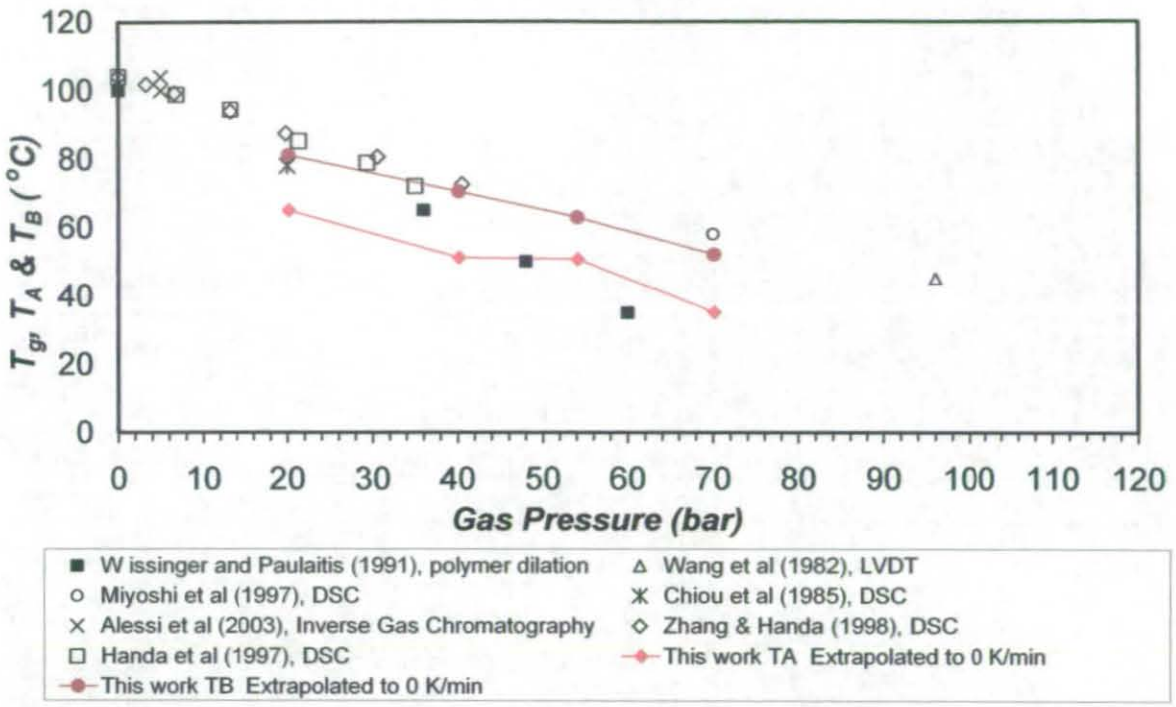

Figure 5 - 21: Softening temperature of PS versus applied CO_2 pressure as measured by LVDT using TA and TB extrapolated to 0 °C/min of different scan times, compared to T_g reported in the literature for PS.

From this figure (Figure 5- 21) it is obvious that the smaller scanning rates gives better agreement with the published T_g values of PS. We can also see that the T_B values give better agreement with literature values of T_g than T_A.

5.2.4 Estimation the Diffusivity of CO_2 in PS Strips

This section will present the diffusion coefficient estimation results from the different scanning rates (0.2 to 1K/min). A comparison of the diffusion coefficient values of CO_2 in PS strips from our work at the same temperature scanning rate (1 °C/min) using the two different experimental setups ("old" and "new" modifications) with all pressure ranges (20, 40, 54, 70, 85, 100, and 120 bar) is shown in figure 5 - 22.

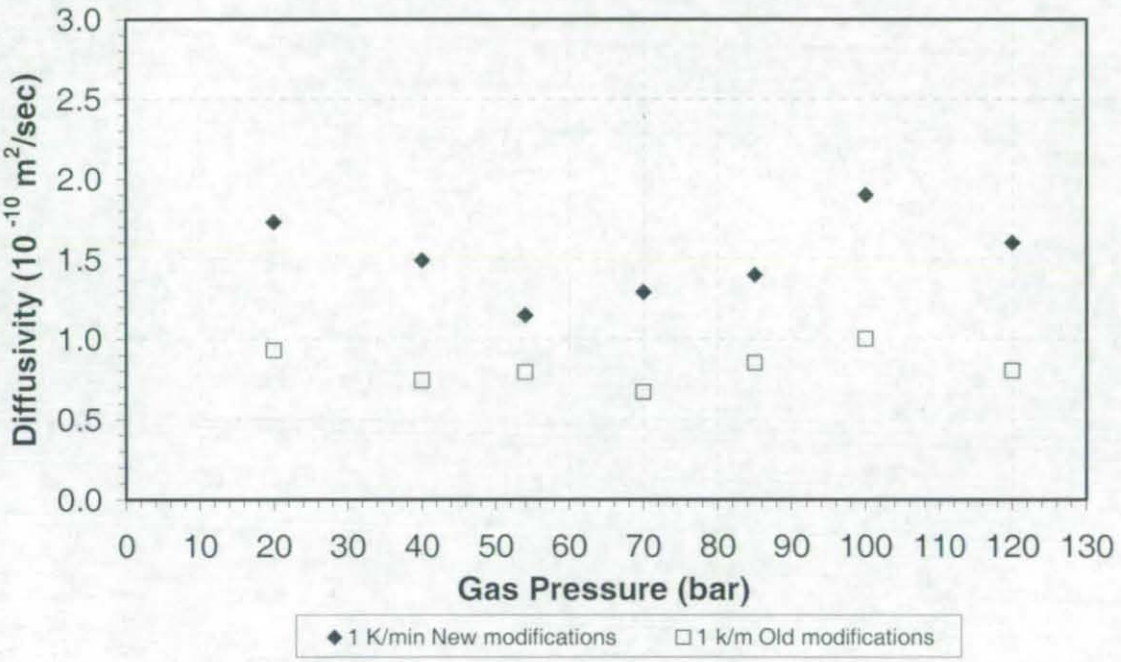

Figure 5 - 22: Diffusivity values of CO_2 in PS at 1 °C/min.

The comparison shows differences between the two setups. The higher diffusivities found with the new set up are possibly most influenced by the method of determining T_A.

Figure 5 – 23 present a comparison of diffusivity values found with scan rates of the 0.2, 0.5, and 1 °C/min with literature values (see previous table 2-4).

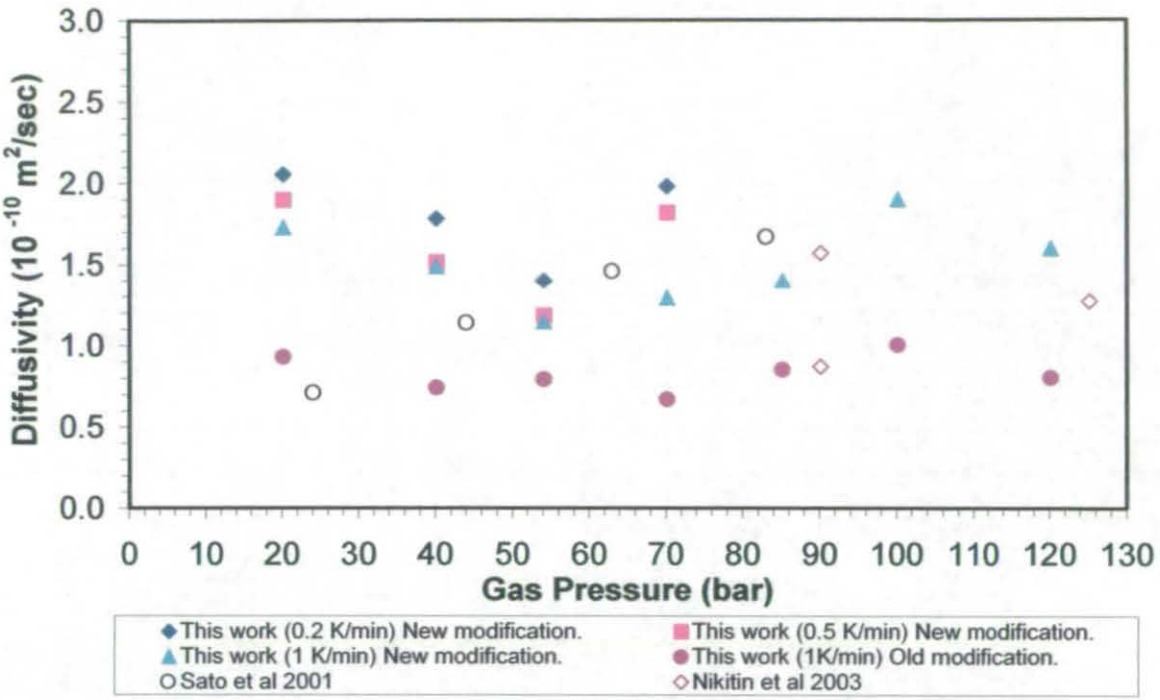

Figure 5 - 23: Diffusivity values of CO_2 in PS at 0.2, 0.5, and 1 °C/min for 20 to 120 bar.

As we can see from the Figure 5 - 23, all the diffusivity values from this work and others have the similar order in magnitude. Our values are bigger than the literature value and this is because of the thickness of our sample (sheet 2 mm) compared with the literature sample (film) and the time taken to achieve the full softening point (T_B). Nikitin et al (2003) have different value of diffusivity at the same pressure (at 90 bar), this is because of the different temperature values used (as showed in table 2-4). The diffusivity values of Sato et al (2001) at 100 °C only.

5.3 Isothermal Experiments (PS/CO_2)

This section reports the results of isothermal deflection experiments with PS, and the fitting of the data to the model developed in section 4.2. Three temperatures were selected (50, 70, and 90 °C). The pressures were selected to always be above the glass transition of the PS, as shown before in chapter 2. That is for a temperature of 50 °C one needs around 70 bar and above to plasticise, at 70 °C ones need above 54 bar to plasticise, and at 90 °C one needs around 20 bar and above to plasticise. The results are shown in the following figures.

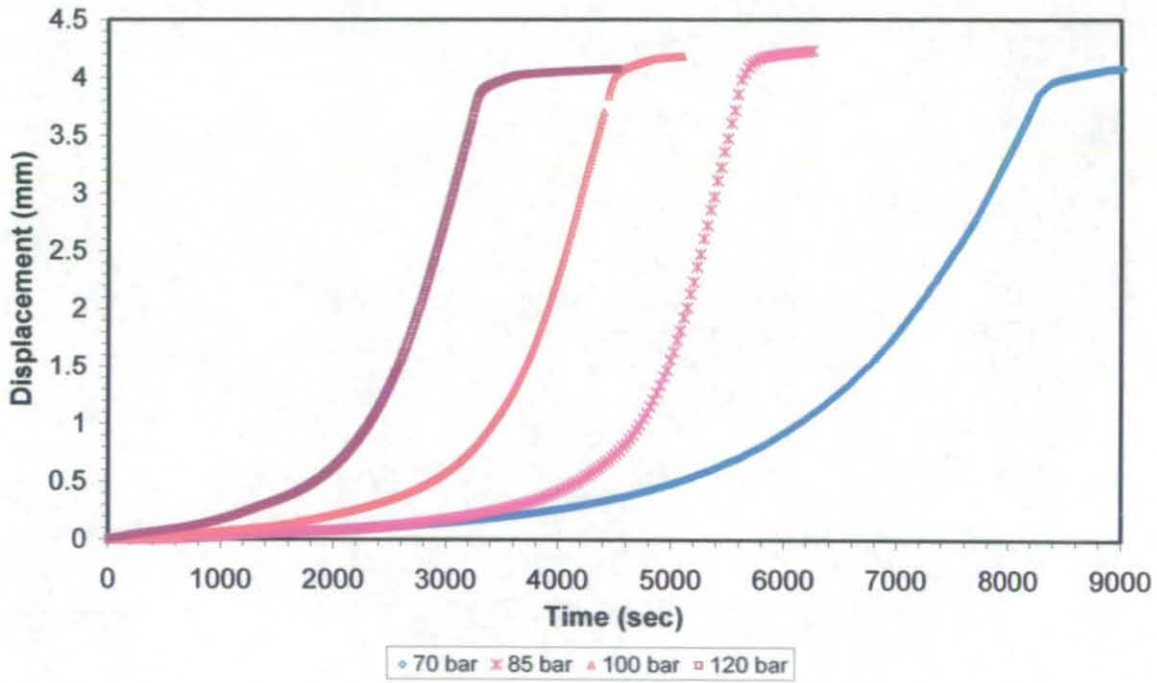

Figure 5 - 24: Isothermal test at 50 °C and 70 to 120 bar.

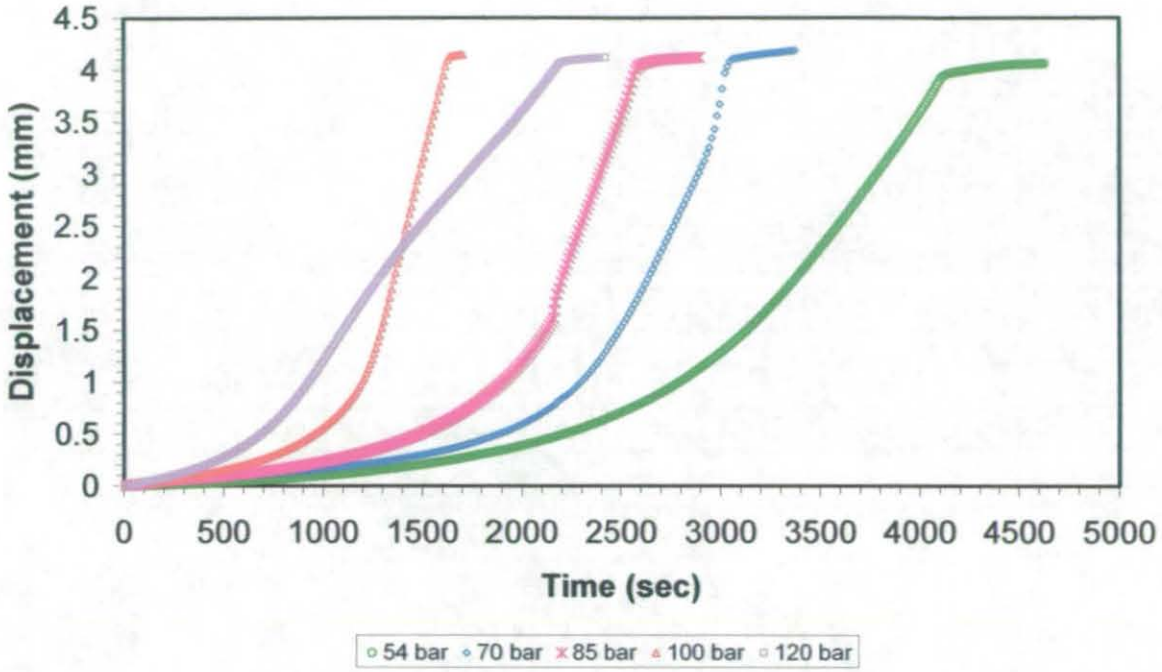

Figure 5 - 25: Isothermal test at 70 °C and 54 to 120 bar.

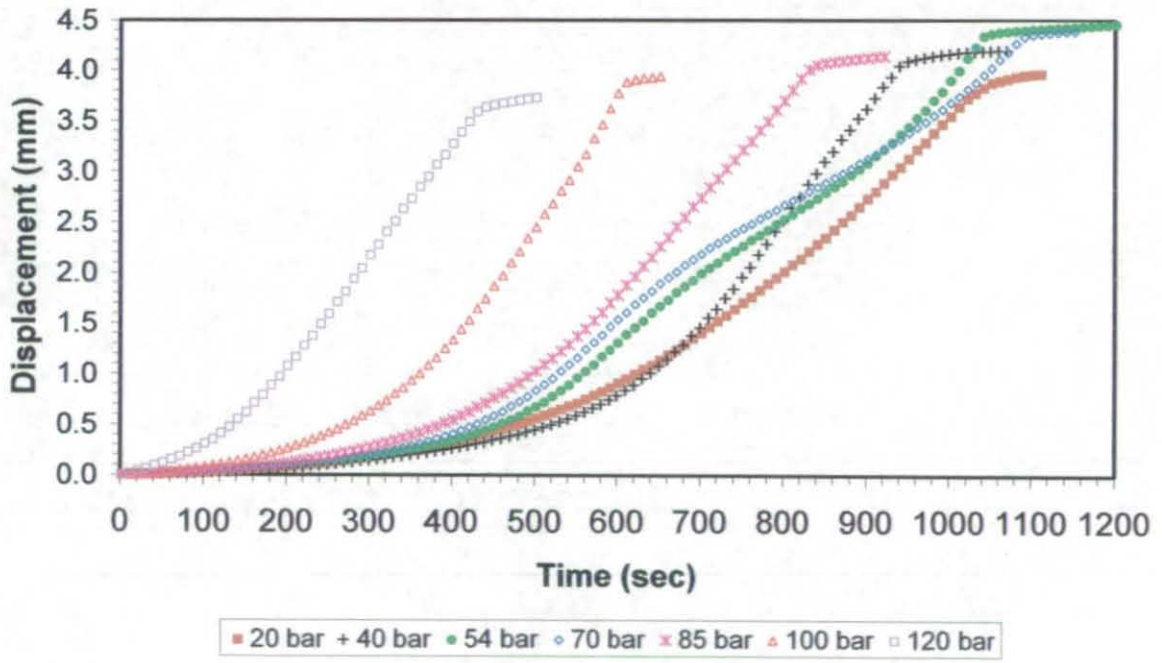

Figure 5 - 26: Isothermal test at 90 °C and 20 to 120 bar.

The figures show that the low temperature runs need more time for the sample to plasticise, however the high temperature need shorter time to plasticise (see Figure 5 – 26). For example at 70 bar we can see that the 50 °C run takes 8000 sec compared to 1000 sec at 90 °C.

There are two factors influencing this:

(i) The diffusivity of CO_2 is likely to be an increasing function of temperature.

(ii) The concentration of CO_2 required to plasticise the polymer is lower at the higher temperatures, thus requiring less diffusion of CO_2 to have occurred.

5.4 Deflection Model of PS/CO_2

In this section the experimental isothermal deflection data are fitted to the deflection model outlined in chapter 4 section 4.2 Eq. 4-17. The fit equation is:

$$\text{Deflection} = \frac{5}{32}\frac{WL^3}{Eb}\frac{}{(d_0 - 4\sqrt{Dt}\,(\frac{c_g - c_e}{-c_e}))^3}$$

or $$\text{Deflection} = A\,(\frac{1}{d_o - B\sqrt{t}})^3$$

where: $$A = \frac{5}{32}\frac{WL^3}{Eb} \qquad \textbf{Eq. 5 - 1}$$

$$B = 4\sqrt{D}(\frac{c_g - c_e}{-c_e}) \qquad \textbf{Eq. 5 - 2}$$

The above equation (Eq. 4-17) predicts an initial deflection of $\frac{A}{0.002^3}$

As experimental deflection values are quoted relative to the initial deflection, the model equation requires an adjustment so that it also represents the change in deflection

relative to t = 0. Therefore the modified equation used to fit the experimental data is:

$$\text{Deflection} = A*\left(\frac{1}{(0.002 - B\sqrt{t})^3} - \frac{1}{(0.002)^3}\right) \qquad \textbf{Eq. 5 - 3}$$

A least squares fit is applied to the data to extract the fit constant A and B.

From the first constant (A) we can calculate the Young's modulus (E), but for the second constant (B) we need to estimate the concentration ratio ($\frac{c_g - c_e}{-c_e}$), before estimating the diffusivity (D). For this purpose literature data for the solubility of CO_2 in PS was used as mentioned earlier in chapter 2 (see Figure 2- 17), the following graphs present these data, concentrating on the pressure range up to 120 bar.

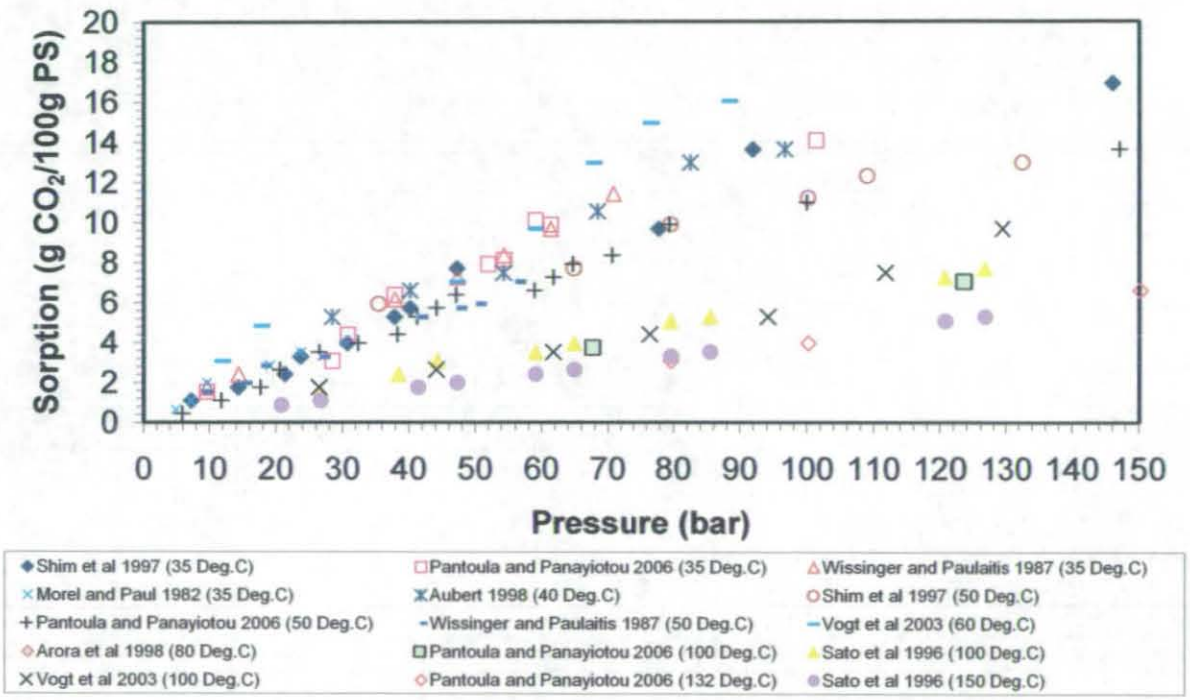

Figure 5 - 27: Solubility of PS / CO_2.

From this graph the equilibrium concentrations (c_e) at the various combinations of pressure and temperature, corresponding to the glass transition can be found. These concentration values are plotted against temperature (the glass transition temperature) in the following figure.

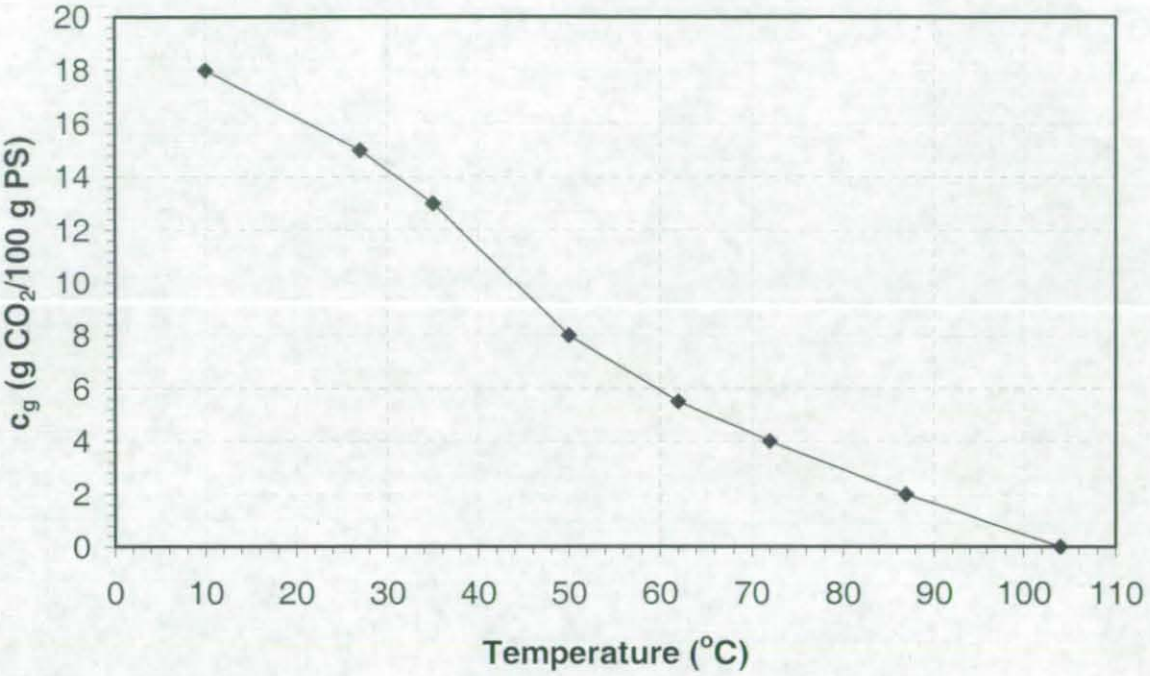

Figure 5 - 28: Concentration of CO_2 / PS required for glass transition (c_g) versus temperature.

It is recalled from section 4.2 that in the description of equation 4-9 the assumption $z \approx \text{erf}(z)$ was made where $z = \frac{x}{2\sqrt{Dt}}$. This requires values of z of less than 0.7 [Calvert and Farrar 1999]. This was tested by noting that z can be evaluated from concentration data.

$$z = -\left(\frac{c_g - c_e}{c_e}\right)$$

Values of z are plotted in Figure 5-29. It can be seen that the high the assumption is valid, with the exception of the high pressure at 90 °C. However this is only a small transgression.

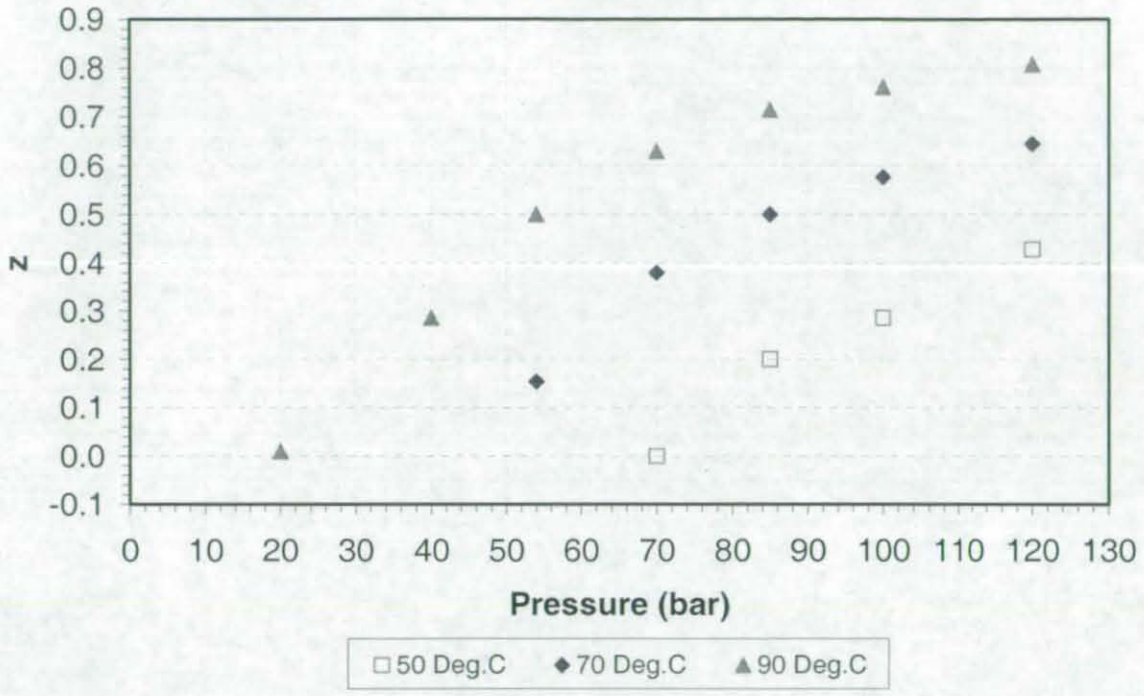

Figure 5 - 29: z values.

The following table represents the values of concentration values, Diffusivity and the Young modulus for these operating conditions:

Table 5 - 2: Calculating values of Diffusivity and Young's modulus of isothermal tests calculate from equations 5-1 and 5-2.

Temperature (°C)	Pressure (bar)	c_e (g/100 g)	c_g (g/100 g)	Diffusivity (10^{-10} m^2/s)	Young's modulus (10^5 N/m^2)
50	70	8.0	8.0	15.1	2.8
	85	10.0		8.6	13.4
	100	11.2		4.6	4.1
	120	14.0		2.4	2.1
70	54	5.2	4.4	17.1	2.9
	70	7.1		3.9	4.5
	85	8.8		2.5	3.2
	100	10.4		3.2	4.1
	120	12.4		1.6	0.72
90	20	1.0	1.8	19.1	1.1
	40	2.8		13.1	2.2
	54	4.0		3.7	0.66
	70	5.4		3.4	1.1
	85	7.0		2.9	1.1
	100	8.4		3.3	0.98
	120	10.4		3.5	0.52

The experimental data along with the curve fits are shown in the following figures:

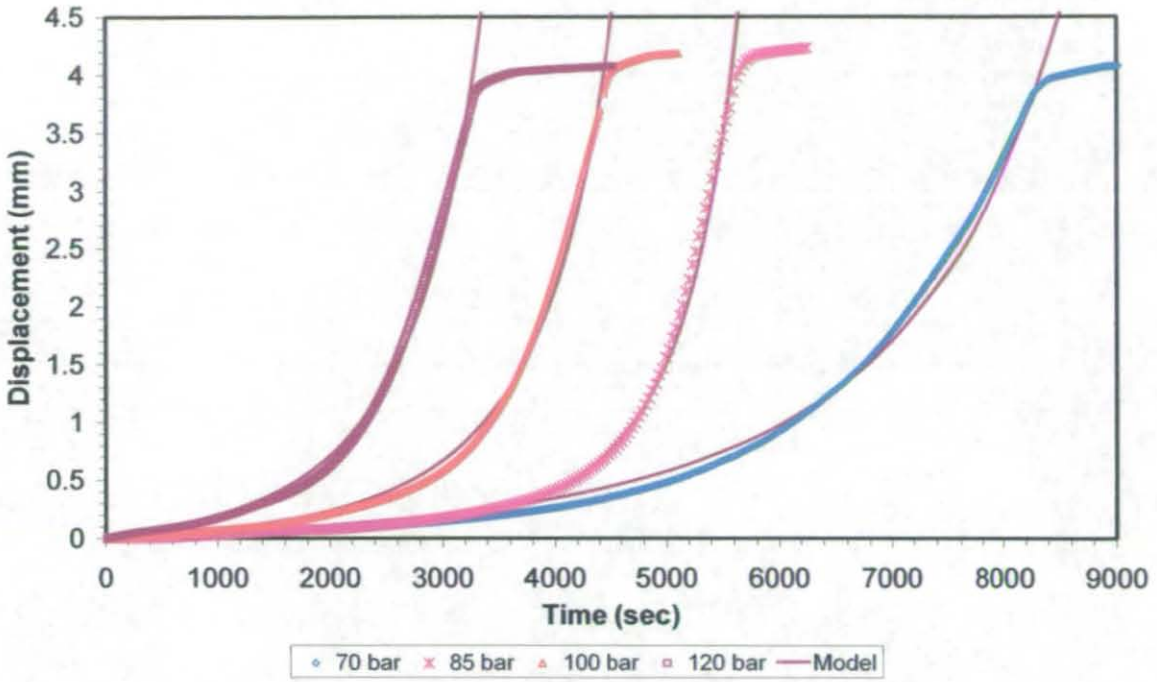

Figure 5 - 30: Experimental versus Deflection Model of 70 – 120 bar at 50 °C.

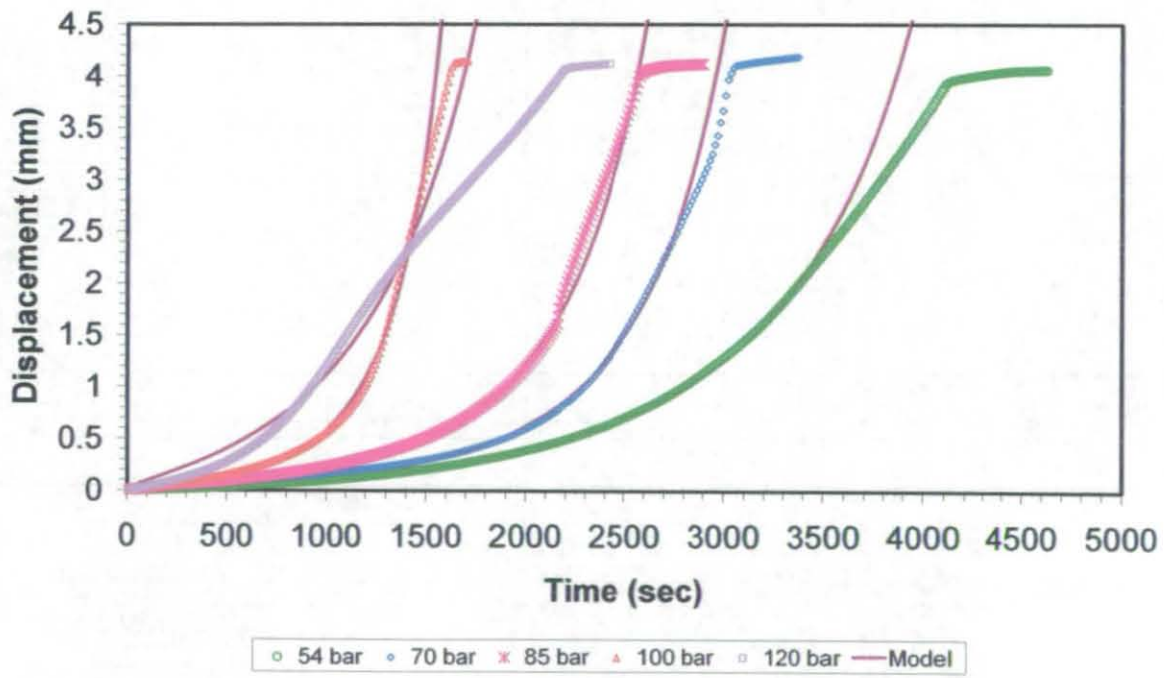

Figure 5 - 31: Experimental versus Deflection Model of 54 – 120 bar at 70 °C.

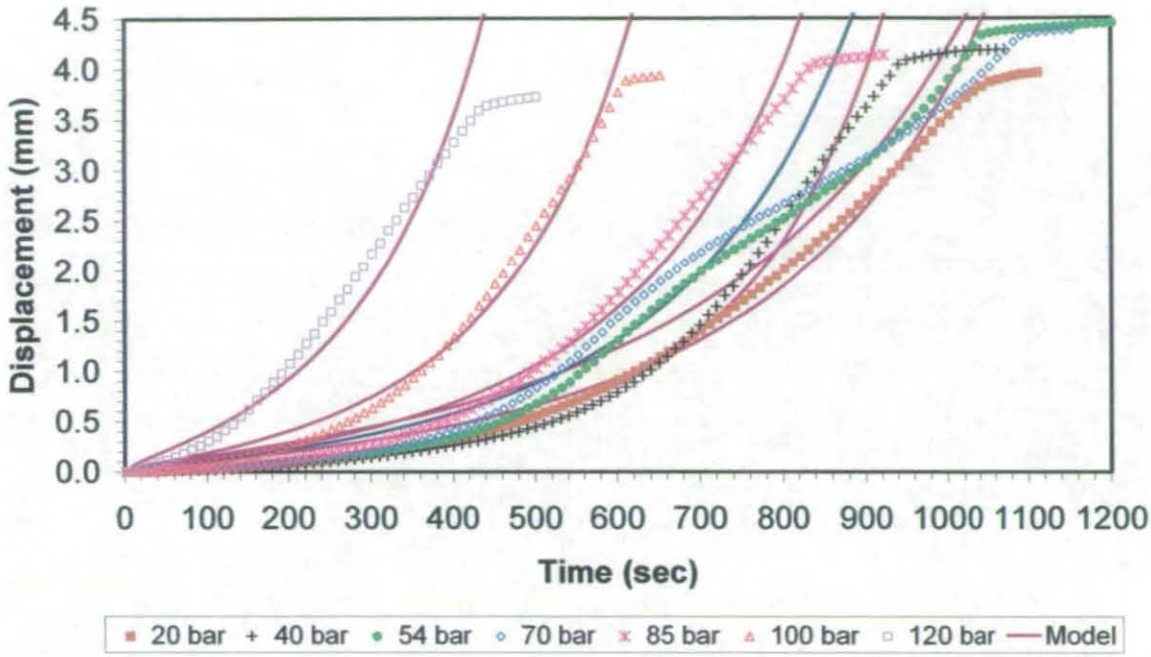

Figure 5 - 32: Experimental versus Deflection Model of 20 – 70 bar at 90 °C.

As shown in the previous figures (Figure 5-30 to 5-32), this model provides good fits to the experimental data. However, with some exceptions; this model can work very well with longer time as shown in figure 5-30, but with shorter time the model has small intervals (see figure 5-31 and 5-32). And this probably because of the viscosity flow, which with long times the viscosity is insignificant but with shorter time the viscosity is holding the deflection rate. In all cases the model provided good fits with experimental data until 1 mm and it faraway from the starting softening point (T_A), which still can express the deflection rates. In general this basic model is good and can express our experimental data.

5.5 Conclusion

Three sets of experiments were carried out:

(i) Non-isothermal before rig modification.

(ii) Non-isothermal after rig modification to improve the quality of the data produced.

(iii) Isothermal after rig modification.

The two sets of non-isothermal runs showed significant reductions in the bending onset temperature for the polymers tested of typically 50 – 100 K over the range of pressures applied. The onset values (assumed to be surface softening) were similar to glass transition temperature reported in the literature. Results were closest with modified cell which used a pointed tip on the LVDT sensor. The results suggested that full softening was limited by the diffusion of CO_2 into the sample.

This hypothesis was tested using a model to extract diffusion coefficient of CO_2 from onset and full softening data. The resulting diffusion coefficient values were similar to those reported in the literature, and confirm the hypothesis (although viscous flow also influences the data). In non-isothermal experiments diffusion coefficients were estimated by comparing the ratio of the decrease in the softening point by method T_B (gross softening) compared to that by method T_A (surface softening). The diffusivity average values of PC, PS, PETG and PMMA were found to be 0.73 x 10^{-10} m^2 /s, 0.82 x 10^{-10} m^2 /s, 0.68 x 10^{-10} m^2 /s, and 0.23 x 10^{-10} m^2/s respectively. The average values of different scanning rate (0.2, 0.5, 1 °C/min) of PS were found to be 2.03 x 10^{-10} m^2 /s, 1.9 x 10^{-10} m^2 /s, and 1.9 x 10^{-10} m^2 /s respectively.

Further experiments were also performed to monitor the central deflection of the polymer strips with time at isothermal condition. The diffusivity average values of isothermal experiments for 50, 70 and 90 °C were found to be 7.6 x 10^{-10} m^2 /s, 5.6 x 10^{-10} m^2 /s and 7.0 x 10^{-10} m^2 /s respectively.

The deflection model was successfully used to fit our experimental data. The model worked very well with longer time, but not full agreed with the shorter time. This disagreement was far away from the starting softening point (T_A).

Diffusion models for both non-isothermal and isothermal data provide realistic estimates of diffusion coefficients which suggest that diffusion is major influence aspect of the softening of these polymer strips. However the variations of D formed suggest that the models are not complete description and that the viscous resistance of the polymers to sagging may also be an important factor.

Interesting effects were also observed to take place during subsequent depressurisation, as the carbon dioxide gas can expand within the material to create a foamed structure. Moreover, the new constructed cell (Polymer Foaming High Pressure (Viewing) Cell) will investigate this finding.

Chapter 6 Optical Measurement of Polymer Foaming

6 Introduction

When removing the polymer samples at the end of the LVDT experiments (chapter 5) it was noticed that bubbles had formed within the samples. The size and number of bubbles was variable and some samples could be described as foamed structures. Bubble formation and foaming is caused by CO_2, previously dissolved in the polymer under pressure, to be released upon depressurisation. This has been well reported in the literature (see chapter 2 section 2.5) and a number of models for bubble growth have been presented. However, relatively few experimental studies have been performed, and these have not considered the possible effect of the glass transition on bubble formation and growth. It was therefore decided to study this topic further, beginning with observations of the samples removed from the LVDT experiments and then continuing by observing bubble formation *in situ* using a specially constructed high pressure view cell (see chapter 3 section 3.4 for details).

This chapter is divided into three sections; the first section investigates the appearance of samples of PC, PS, PETG and PMMA after the LVDT experiments. The second section presents experimental data for polymer foaming of PS/CO_2 using the high pressure view cell. The experimental data are analysed by measuring bubble radii at different times during depressurisation using image analysis software (see chapter 3, section 3.4.5). Ultimately, the third section aims to interpret the experimental data of bubble growth using various bubble growth models (see chapter 4, section 4.3).

6.1 Preliminary Findings on Foamed Samples from LVDT Experiments

6.1.1 Appearance of Samples After Depressurisation

Photographs of the polymer samples of PC, PS, PETG, and PMMA after the depressurisation stage (section 5.1) are shown in Figure 6-1a and 6-1b. Each photograph shows the results after different earlier holding pressures (shown) and temperatures ranging up to160 °C for PC, and 140 °C for PS, PETG and PMMA. These show the presence of bubbles, the volume of which increases if the pressure at the start of depressurisation is increased. The higher pressure samples have expanded into a recognisably foamed structure.

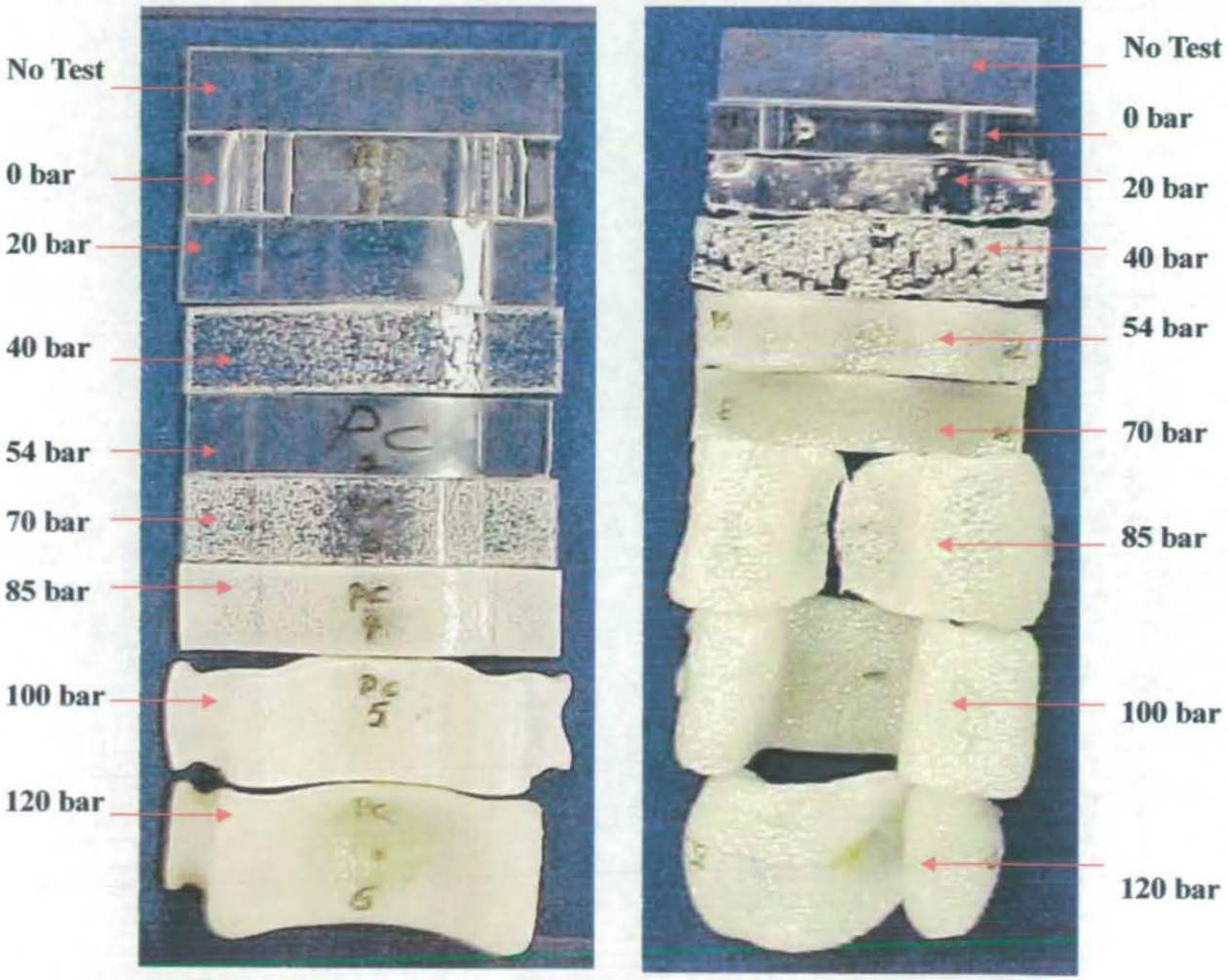

(a) PC (b) PS

Figure 6 - 1a: Photographs of polymer strips after depressurisation from various pressures after having passed through the softening point, (a) PC, (b) PS (depressurisation time 300 sec).

(a) PETG **(b) PMMA**

Figure 6 - 2: Photographs of polymer strips after depressurisation from various pressures after having passed through the softening point, (a) PETG, (b) PMMA (depressurisation time 300 sec).

In all cases the original sample was transparent with a smooth surface whereas the final sample became translucent (off-white colour) because of the formation of bubbles. Foaming is a well-known phenomenon with CO_2/polymers systems [Liang and Wang 2000, Goel and Beckman 1995, and Siripurapu et al 2002], and is caused by there being insufficient time for the CO_2 to diffuse out of the sample during depressurisation. At higher initial pressures, more CO_2 is absorbed into the sample and thus the volume of bubbles produced is liable to be greater.

The densities of these polymer samples were measured by a Micromeritics 9200 Helium Pycnometer. To compare the results between pressures, it is convenient to define a parameter for the percent of swelling after the release of the pressure as seen in Eq.6-1 and 6-2 (e.g. Martinache et al (2001) in situ swelling):

$$S = \frac{V_f - V_i}{V_i} \qquad \textbf{Eq. 6 - 1}$$

$$\rho = \frac{m}{V_f} \qquad \textbf{Eq. 6 - 2}$$

where: S is the swelling ratio, V_f is the volume of the swollen sample, V_i is the initial volume of the polymeric sample before CO_2 pressurization, m is the mass of the specimen and ρ is the final polymer density. See Figure 6-2 to 6-5.

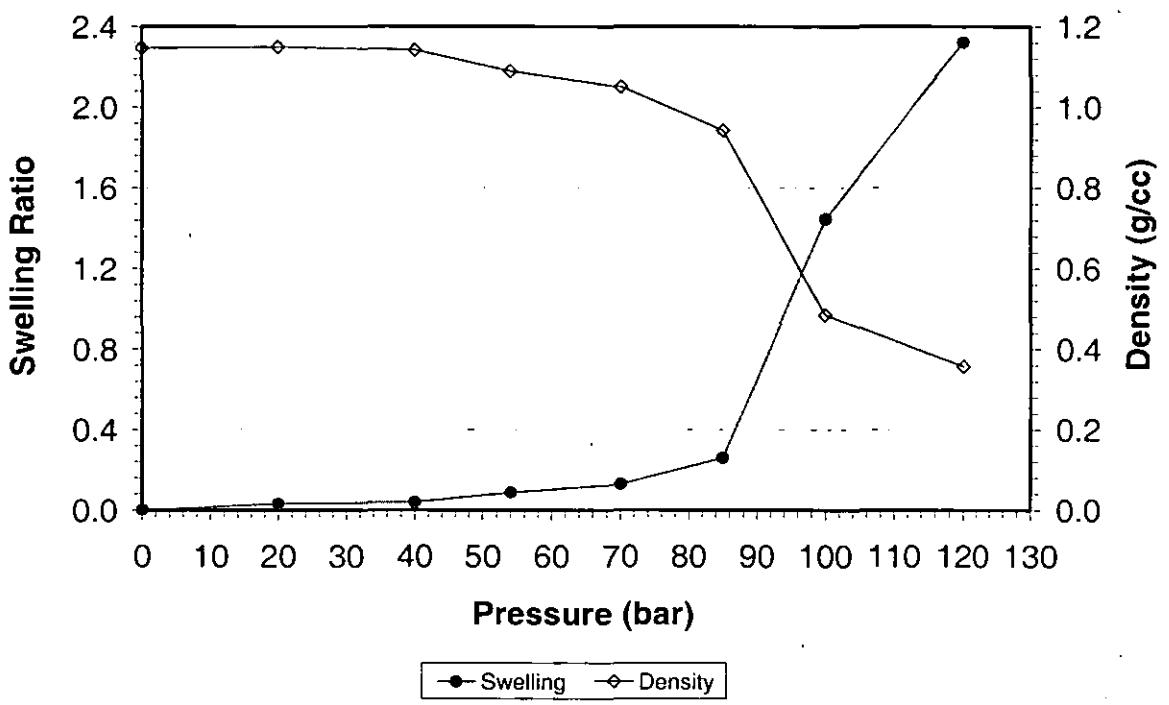

Figure 6 - 3: Final sample density and swelling ratio for PC (after depressurisation) versus experimental holding pressure.

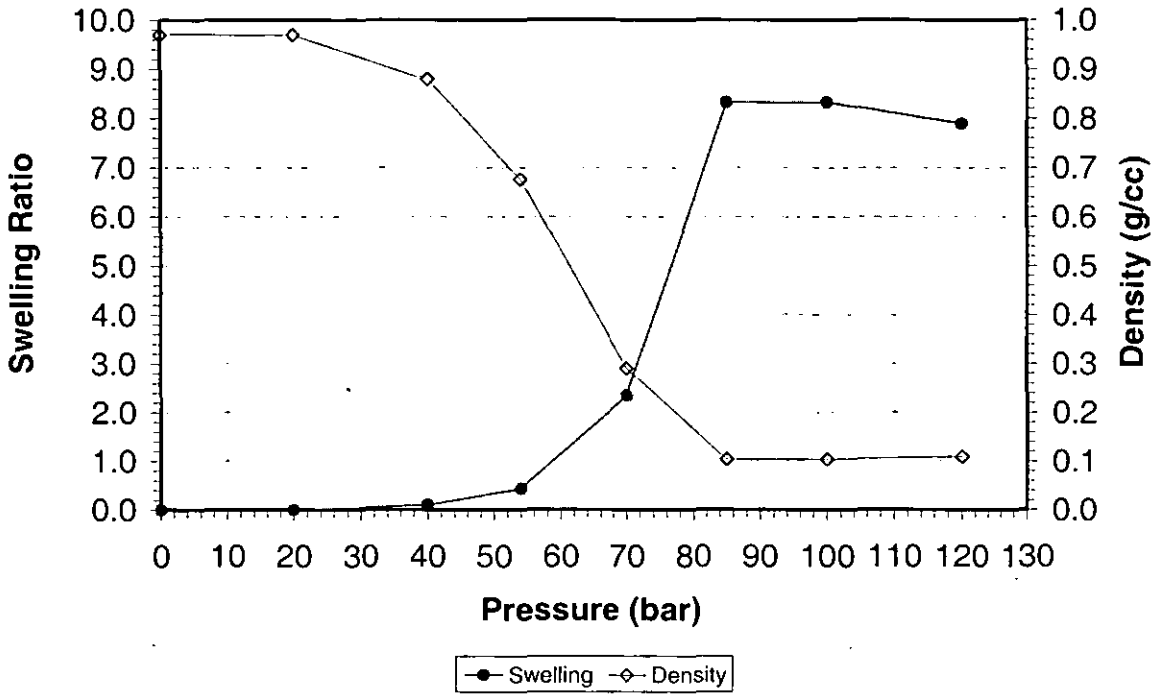

Figure 6 - 4: Final sample density and swelling ratio for PS (after depressurisation) versus experimental holding pressure.

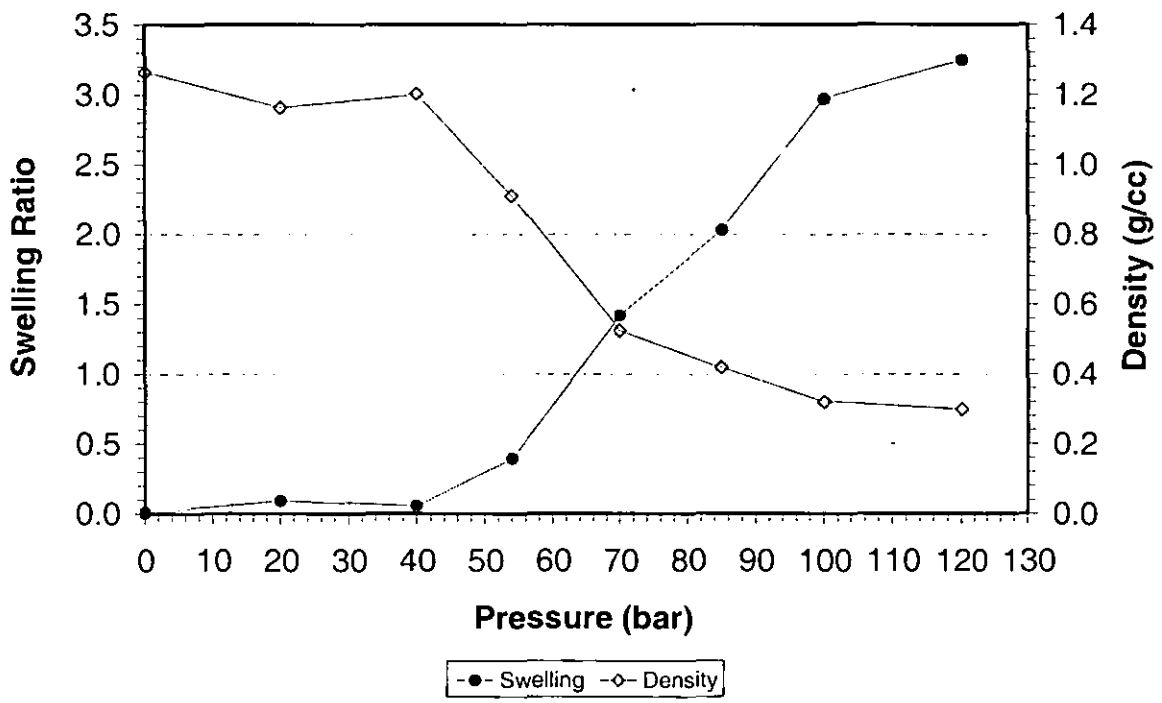

Figure 6 - 5: Final sample density and swelling ratio for PETG (after depressurisation) versus experimental holding pressure.

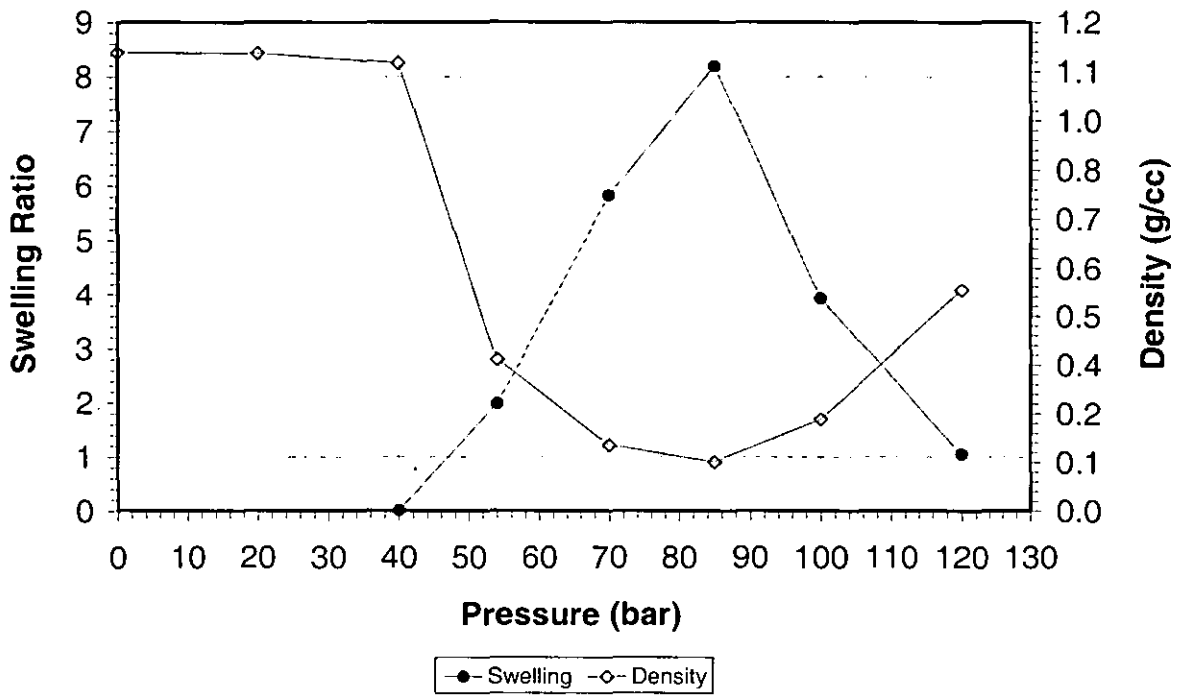

Figure 6 - 6: Final sample density and swelling ratio for PMMA (after depressurisation) versus experimental holding pressure.

Our observations showed that a significant reduction in density was generally obtained after the polymer had been subjected to pressures above 40 bar. The maximum swelling ratio and the pressure at which this occurs differed from one sample to another. The reasons for this are uncertain but may be influenced by the temperature of the sample in relation to its glass transition temperature during the depressurisation process. It can be postulated that as the pressure falls the gas in the sample desorbs and expands until the glass transition temperature corresponding to the amount of CO_2 still remaining in the sample rises above the sample temperature, at which point the sample hardens into a temporarily formed structure. Consequently PC samples could have a greater final density as they reach the glass transition earlier than other samples (as the underlying T_g is higher) and thus have less opportunity to expand. The PMMA shows anomalous behaviour at high pressure, the reason for which is not clear.

6.1.2 Bubble Measurements

6.1.2.1 Radius

The following photos of the extracted specimens of PC, PS, PETG, and PMMA were taken through a microscope. Average bubble diameters were calculated from the images shown in Figure 6-6 to 6-9, based on all identifiable bubbles for which a diameter could be measured in each image. In some images this was difficult (e.g. Figure 6-7, 85 bar), but a best estimate was made in such cases. The final average bubble diameter ranges between 0.08 to 0.6 mm for PC, 0.03 to 2.1 mm for PS, 0.18 to 1.2 mm for PETG and 0.03 to 1.26 mm for PMMA.

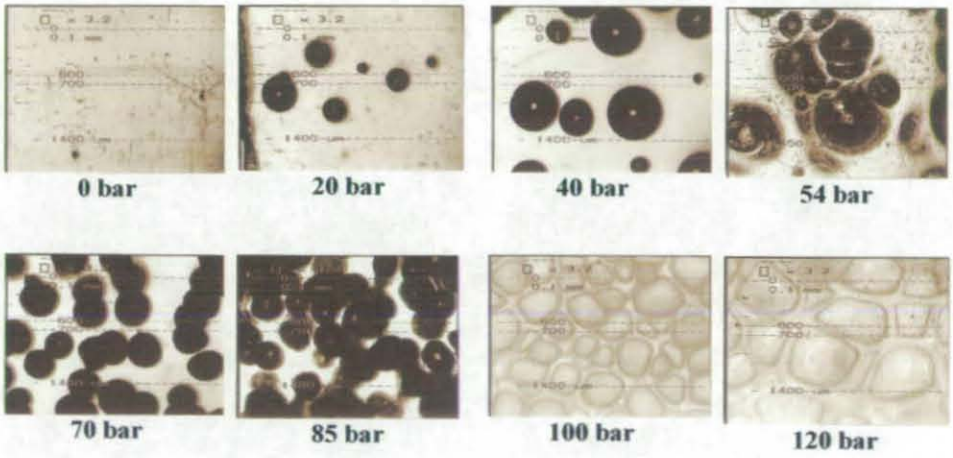

Figure 6 - 7: Microscope images of PC specimens (scale of images is 95 x 70 mm)

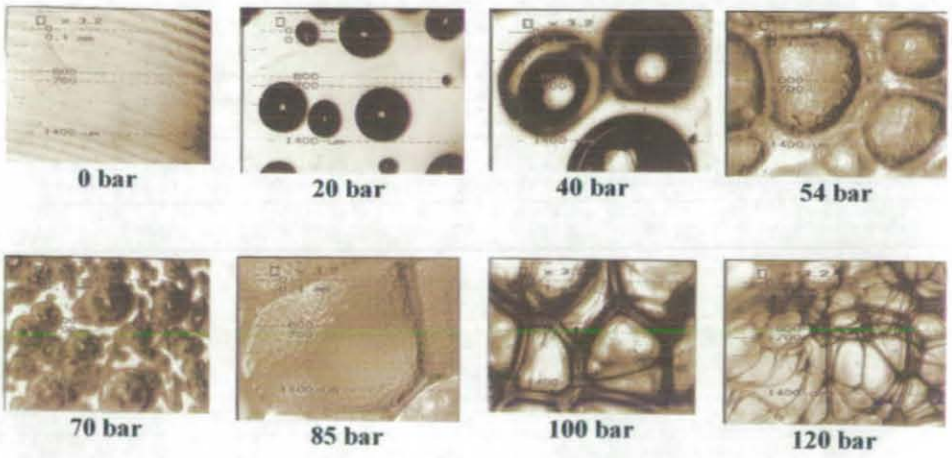

Figure 6 - 8: Microscope images of PS specimens (scale of images is 95 x 70 mm).

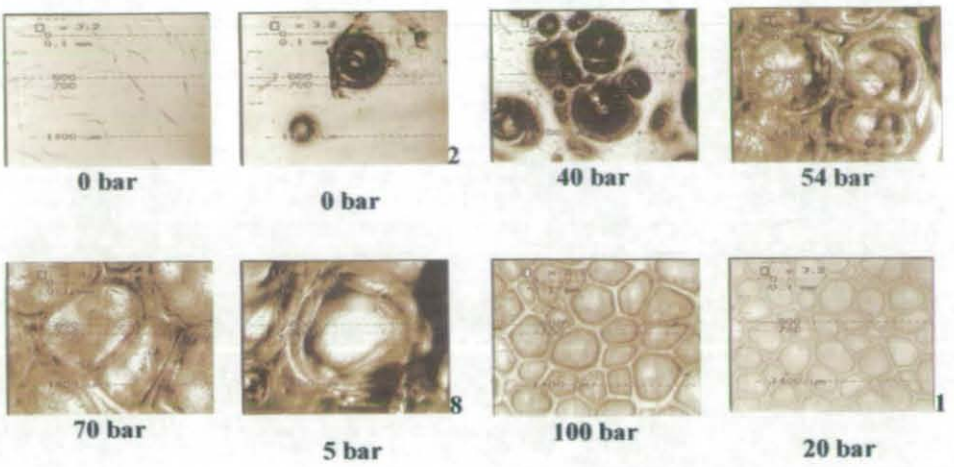

Figure 6 - 9: Microscope images of PETG specimens (scale of images is 95 x 70 mm)

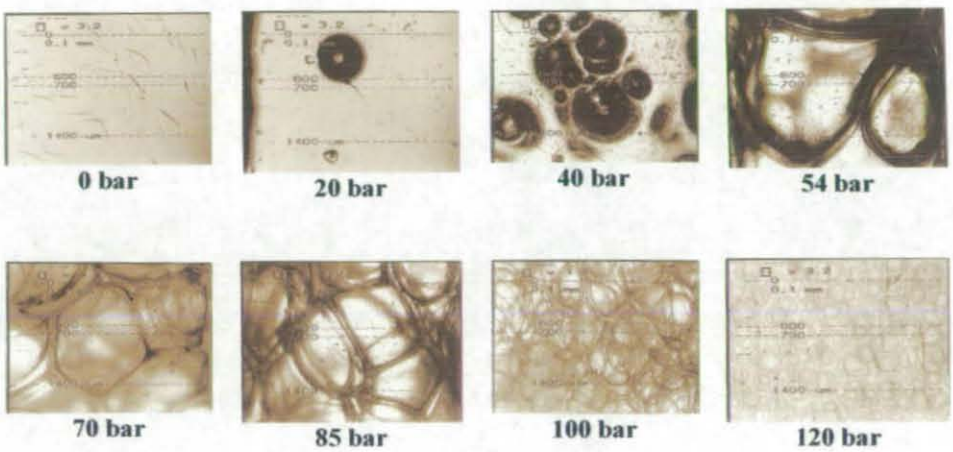

Figure 6 - 10: Microscope images of PMMA specimens (scale of images is 95 x 70 mm).

These figures show large variations in bubble size and appearance. At low pressures the bubbles are small and well separated, but as the pressure is increased they become larger and begin to impinge upon one another (typically above 54 bar except for PC). However as the pressure is further increased above 100 bar the bubbles are smaller. This coincides with the density measurements (section 6.1.1). It is possible that the bubbles first expand and then collapse for the experiments at higher initial pressures.

6.1.2.2 Estimation of Bubble Number

The following equations can be used to estimate the number of bubbles in a sample [Calvert & Farrar (1999)]:

$$N_B = \frac{\Delta V}{V_{Sphere}} \qquad \text{Eq. 6 - 3}$$

$$V_{Sphere} = \frac{4}{3}\pi r^3 \qquad \text{Eq. 6 - 4}$$

$$\Delta V = V_f - V_i \qquad \text{Eq. 6 - 5}$$

where:

r : Radius of a representative bubble (m^3)

N_B : Number of bubbles

V_{Sphere} : Volume of a representative bubble (m^3).

V_i: Volume of the specimen before foaming (m^3).

V_f: Volume of the specimen after foaming (m^3).

From the previous photos (Figure 6-6 to 6-9) we have the representative bubble radius for each sample, therefore we can calculate the corresponding bubble volume (V_{Sphere}) by equation 6-3. The volumes (V_i & V_f) of the specimen were measured as previously in section 6.1.1.

The following figures (Figures 6-10 to 6-13) present the average bubble radius (as taken from the previous Figures 6-6 to 6-9) and the estimated number of bubbles for PC, PS, PETG and PMMA. From these figures (Figures 6-10 to 6-13), we can see that all the polymer samples show the same general trend, showing large increases in the bubble numbers with increasing initial gas pressure. However, with both PC and PS the trend was not always monotonic.

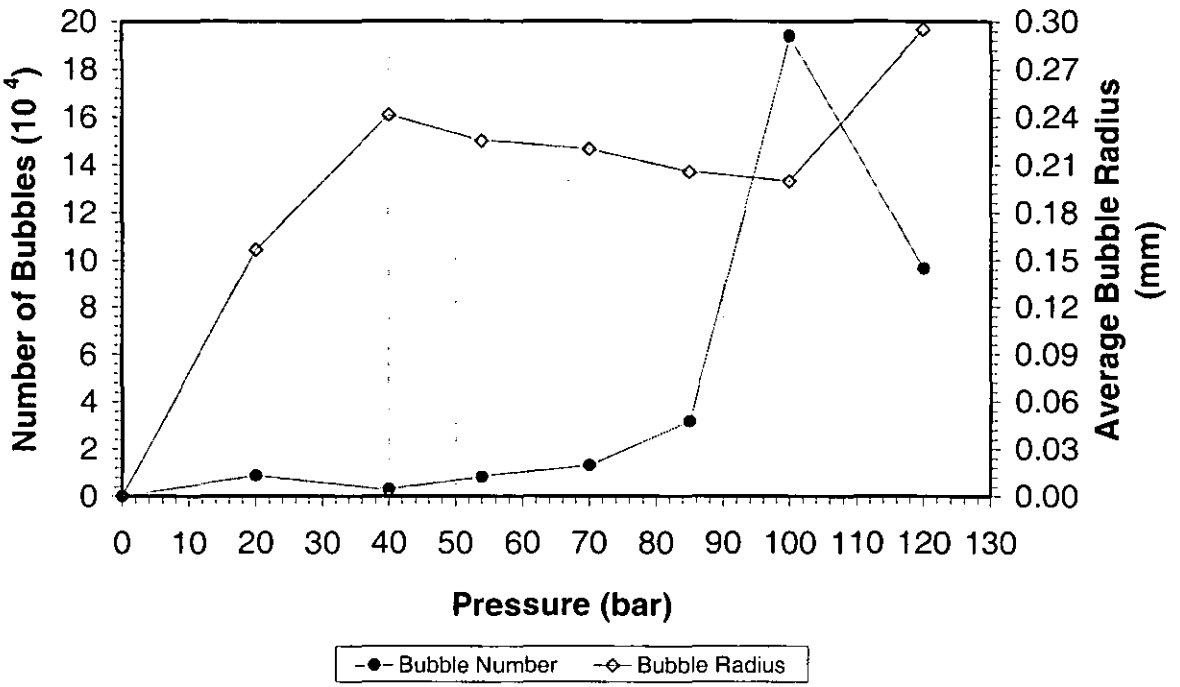

Figure 6 - 11: Bubble number and bubble average radius for PC samples.

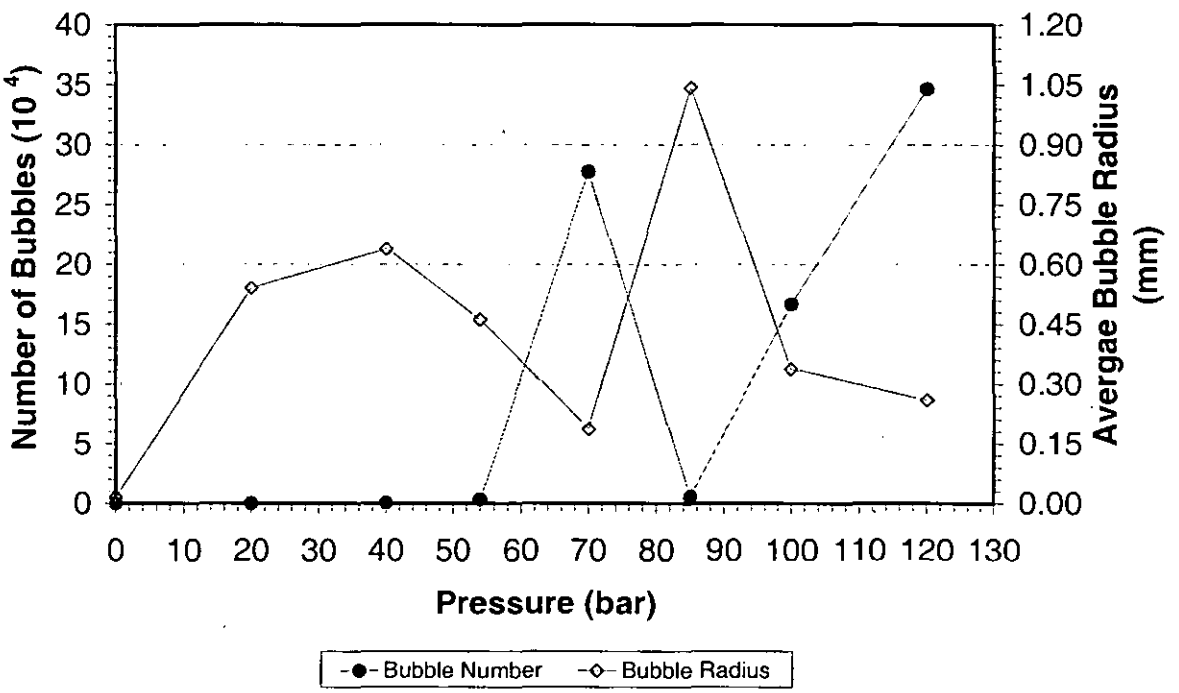

Figure 6 - 12: Bubble number and bubble average radius for PS samples.

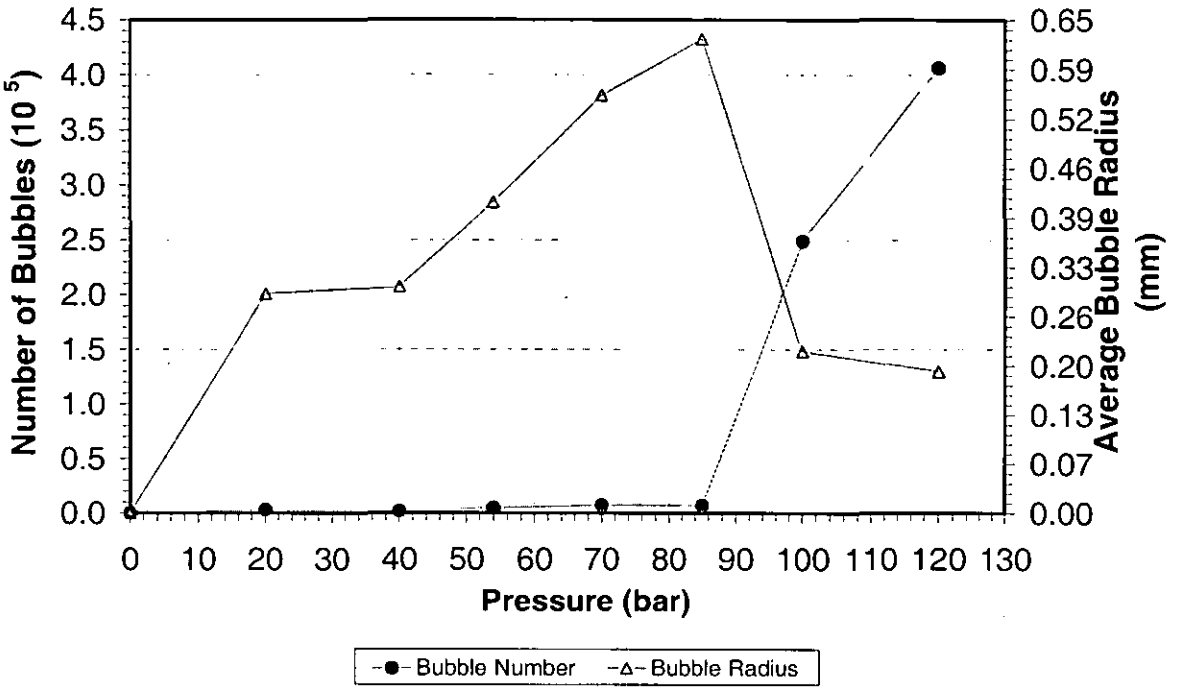

Figure 6 - 13: Bubble number and bubble average radius for PETG samples.

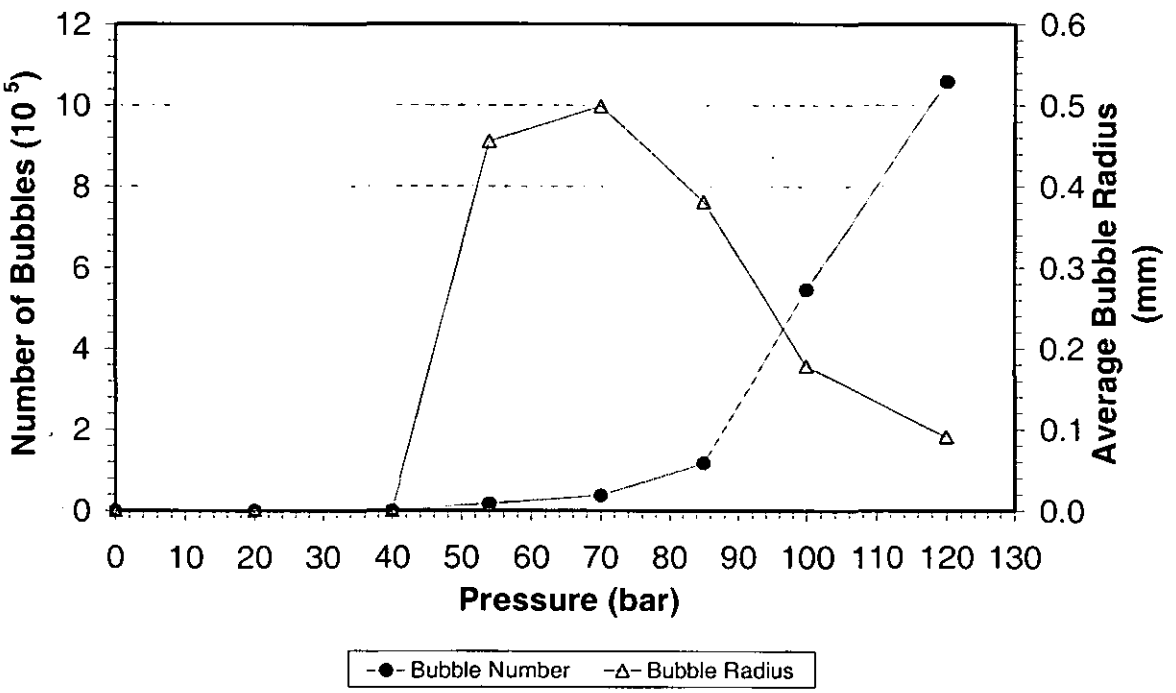

Figure 6 - 14: Bubble number and bubble average radius for PMMA samples.

6.1.3 Conclusion

If the polymer is subjected to high-pressure gas, and the pressure is suddenly decreased or the temperature is rapidly increased, the gas will try to escape from the polymer. The supersaturation of gas causes the nucleation and growth of bubbles within the polymer.

The bubble size, number and density do not vary monotonically with the previous holding pressure. This suggests that foaming is not a simple process and only a limited understanding can be achieved by the examination of samples after depressurisation. The following section (section 6.2) presents an *in situ* polymer foaming investigation using a high pressure view cell with two optical windows under isothermal conditions. This should enable a better understanding to be gained.

6.2 Polymer Foaming (PS/CO_2)

6.2.1 Introduction

In order to develop a more complete understanding of bubble foaming and growth experiments were performed in which these processes could be observed as they occur. These experiments were carried out in the view cell described in chapter 3 section 3.4. Photographs of specimens during different stages of the experiment were analysed using image analysis software to provide data for bubble radius versus time. In these sets of experiments only one polymer (PS) was tested to enable a more extensive study of the effect of process variables to be made. Initial experiments were carried out in order to establish the best operating conditions, for thickness of sample (1 – 5 mm) and conditioning time (30 to 180 minutes).

6.2.2 Effect of Thickness

Experiments were first performed with samples prepared in-house (see section 3.5.2) with different thicknesses to asses the optimum sample thickness for the rest of study. Different thicknesses (1 – 5 mm) of PS sample were held under experimental conditions (isothermal) of 100°C and 54 bar for 30 minutes before depressurisation. It was noted (see Figure 6-14) that with the thinnest (1mm) specimen it was easiest to observe individual bubbles.

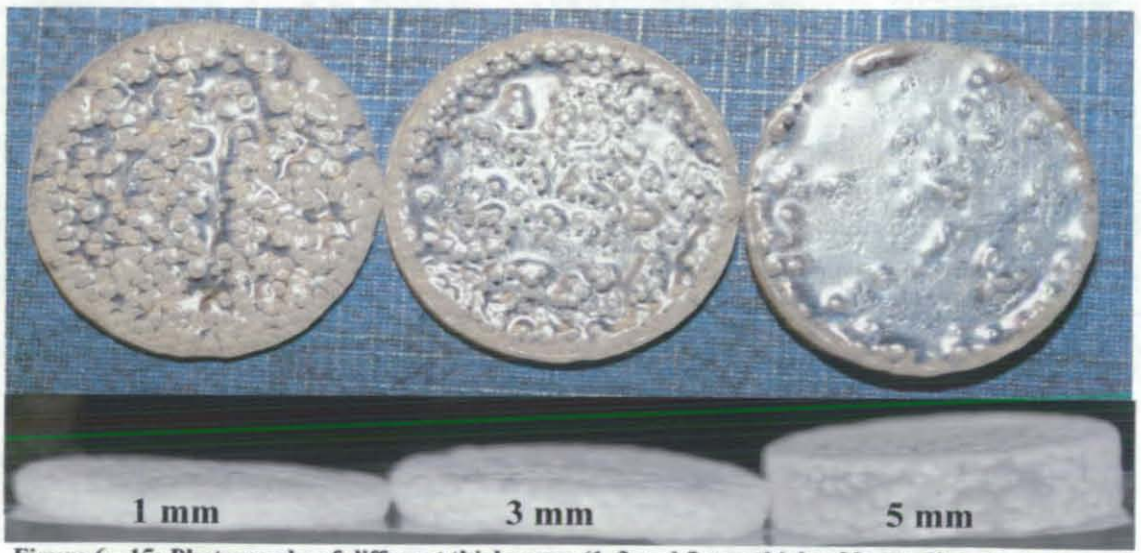

Figure 6 - 15: Photographs of different thicknesses (1, 3 and 5 mm thick x 20 mm diameter) of samples of PS after holding at 100 °C and 54 bar in CO_2 for 30 minutes and then depressurisation.

6.2.3 Effect of Conditioning Time

Experiments were performed with different conditioning times of 30, 60, 120, 160 and 180 minutes with the same pressure (54 bar), temperature (100 °C), thickness (1 mm) and disk diameter (20 mm). This was in order to assess the time required for CO_2 to satisfactorily equilibrate in the sample prior to depressurisation.

Figure 6 - 16 : Photographs of samples of PS depressurised after holding for different times (30 to 120 min) at 100 °C and 54 bar (1 mm thick x 20 mm diameter).

As the conditioning time is increased up to 120 minutes it can be seen that the radius of the foamed sample increases and there is less interstitial space between the bubbles. Both indicate a greater bubble volume as the conditioning time is increased. This must be caused by more CO_2 diffusing into the sample at the longer conditioning times indicating that the 30 minute and 60 minute times are insufficient to allow equilibration of CO_2 in the sample to occur.

It can be seen that although the 180 minute sample grew to the largest size this was only slightly larger than the 120 minute sample. Therefore it was decided that the 120 minute conditioning time was sufficient for our experiments.

6.2.4 Heterogeneity on the Surface

Figure 6-16 shows photos from different times during the depressurisation of "in-house" prepared samples where the majority of the surface was rough but a small amount (at the bottom) was smooth. It can be seen that bubble formation occurred preferentially where the surface was rough. This may be due to a greater number of nucleation sites (e.g. small pre-existing gas bubble) or faster diffusion into the rougher region. Where the polymer surface is not smooth bubbles form in about 6 sec, whereas bubbles do not appear in the smooth surface until after 30 sec.

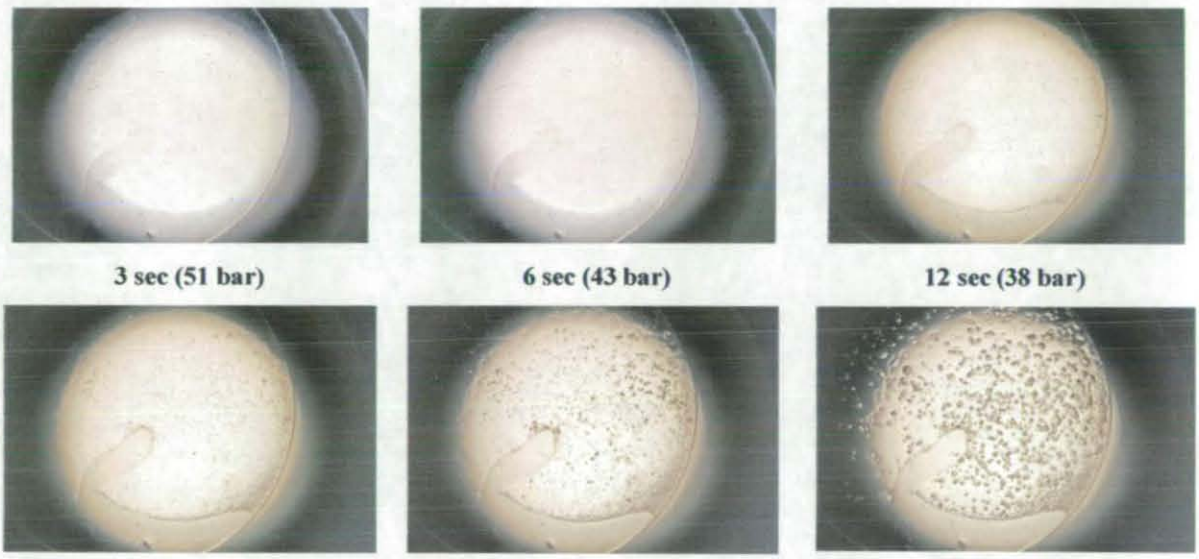

3 sec (51 bar) **6 sec (43 bar)** **12 sec (38 bar)**

18 sec (31 bar) **24 sec (24 bar)** **30 sec (18 bar)**

Figure 6 - 17: Photographs of sample of PS (1 mm thick x 20 mm diameter) during depressurisation after holding at 54 bar and 100 °C (scale of images is 25 x 25 mm).

As such sample heterogeneity is undesired in a systematic study it was decided to perform future experiments using commercially bought samples (PS) of 1 mm thickness.

6.2.5 Effect of a Scratch on the Polymer Surface

In many bubble growth systems, such as carbonated drinks, bubbles often form at cracks or holes in a solid surface. To further examine the roughness effect seen in section 6.2.4 an artificial scratch was made on a sample. However, as can be seen in Figure 6-17 this appeared to have little influence on bubble formation.

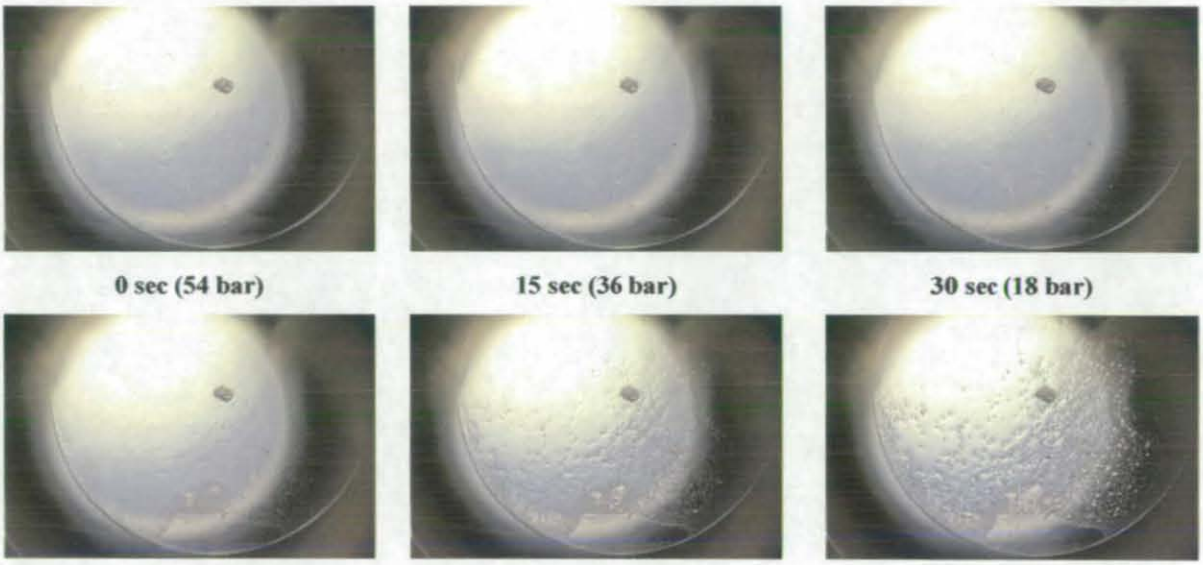

0 sec (54 bar) **15 sec (36 bar)** **30 sec (18 bar)**

45 sec (8. 4 bar) **60 sec (3. 7 bar)** **75 sec (1. 6 bar)**

Figure 6 - 18: Photographs of sample of PS (1 mm thick x 20 mm diameter) during depressurisation after holding at 54 bar and 100 °C (scale of images is 25 x 25 mm).

6.2.6 Bubble Growth - Effect of Impingement

During the analysis of the bubble growth data it was found that bubbles in the samples grow at different rates according to the proximity of other bubbles. One sample has been selected as an example, 25 bar and 100 °C, to illustrate this effect. The following photo has been taken after 600 second at 0 bar, and shows four bubbles, one of which is "free" and the others which are touching each other.

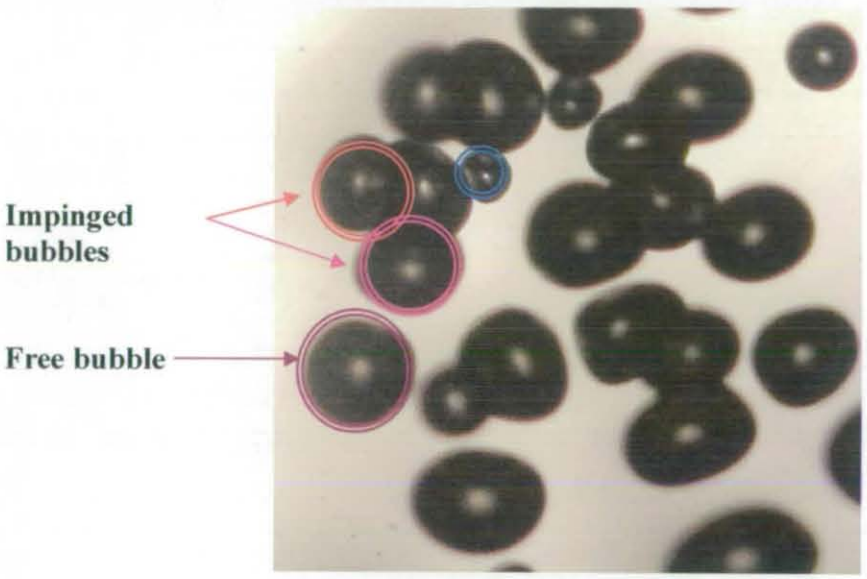

Figure 6 - 19: Photograph of a PS (1 mm thick x 20 mm diameter) sample 600 sec after the onset of depressurisation after holding at 24 bar (CO_2 pressure) and 100 °C for 2 hours, the photograph shows the location of three impinged bubbles and one free bubble that are considered here (scale of images is 6 x 6 mm).

The following figure presents the radius values of these bubbles versus time.

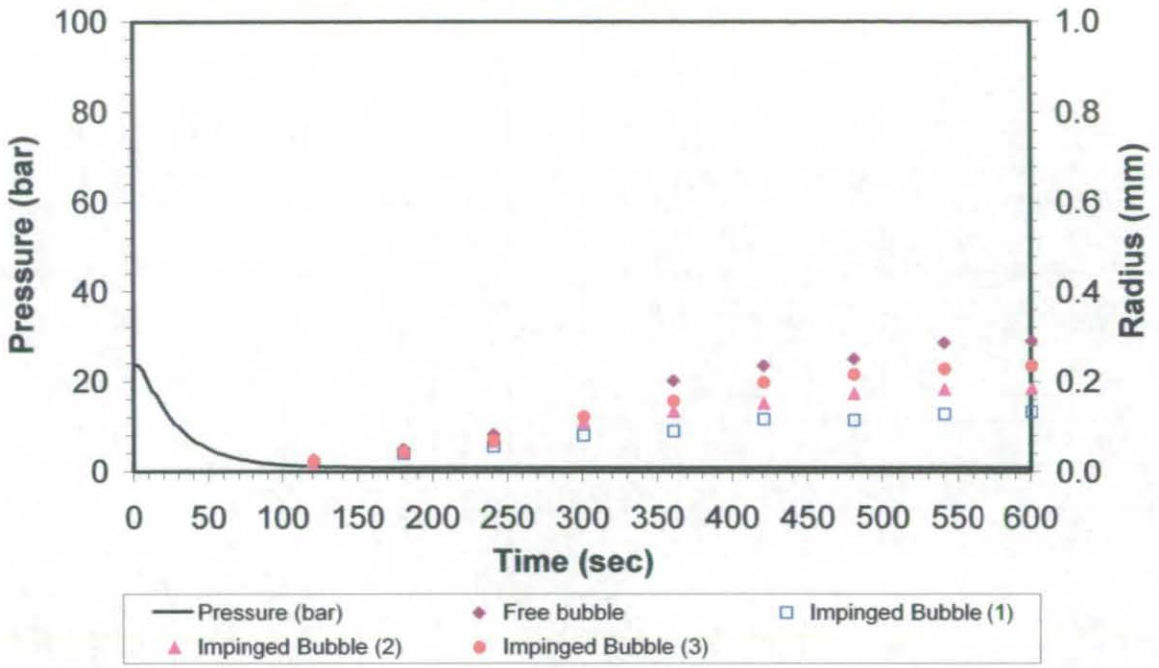

Figure 6 - 20: Bubble radius for of the four selected bubbles during depressurisation after holding at 24 bar and 100 °C for 2 hours. The graph shows the free bubble grows at a faster rate.

It is clear that the free bubble grows at the fastest rate compared to the other bubbles. This is likely to be due to a greater availability of CO_2 in the polymer immediately surrounding the free bubble compared to the impinged bubbles which "compete" for the same CO_2. Subsequent analysis has concentrated on the least impinged bubbles wherever possible.

6.2.7 Experimental Plan

Experiments were carried out according to the plan showing in Table 6-1. Three main operating temperatures were selected (50, 70 and 100 °C) each over a range of pressures from 24 to 120 bar. For the 100°C experiments the polymer will be in the rubbery state at the onset of depressurisation and much of the subsequent time period. However, most of the 50 °C experiments (below 100 bar) and 70 °C experiments (below 63 bar) will be with the polymer entirely within the glassy state.

These conditions coincided with those for which literature data for diffusivity and Henry's law constants were available. This was so that these data could be directly used in the models presented in section 6.3.

Table 6 - 1: Isothermal Operation Conditions.

Pressure (bar)	Temperature (°C)		
	50	70	100
24	✓	✓	✓
44	✓	✓	✓
63	✓	✓	✓
83	✓	✓	✓
100	✓	✓	✓
120	✓	✓	✓

6.2.8 Polymer Foaming Results and Discussion

As shown in the experimental plan the experiments will be divided into set of groups at 50, 70 and 100 °C with varying pressures of 24 to 120 bar. These investigations will focus in bubble growth before and after the ambient pressure was reached. Each group will be discussed in more detail:

6.2.8.1 Results from Experiments at 50 °C

Images taken 600 second after the onset of depressurisation are shown in Figures 6-20 to 6-23 for initial conditions of 50 °C and pressure up to 83 bar. These correspond to conditions below the T_g of PS. Perhaps unsurprisingly the images show no sign of any bubble formation as foaming is unlikely to occur if the polymer is unable to deform easily as stated in the literature review (see chapter 2, Figure 2-20).

Figure 6 - 21: Photograph of a 1 mm thick PS sample at various times after the onset of depressurisation after holding at 24 bar (in CO_2) and 50 °C for 2 hours. No bubbles are seen in any of the images. This photo has been taken at 600 sec and 0 bar (scale of images is 6 x 6 mm).

Figure 6 - 22: Photograph of a 1 mm thick PS sample at various times after the onset of depressurisation after holding at 44 bar (in CO_2) and 50 °C for 2 hours. No bubbles are seen in any of the images. This photo has been taken at 600 sec and 0 bar (scale of images is 6 x 6 mm).

Figure 6 - 23: Photograph of a 1 mm thick PS sample at various times after the onset of depressurisation after holding at 63 bar (in CO_2) and 50 °C for 2 hours. No bubbles are seen in any of the images. This photo has been taken at 600 sec and 0 bar (scale of images is 6 x 6 mm).

Figure 6 - 24: Photograph of a 1 mm thick PS sample at various times after the onset of depressurisation after holding at 83 bar (in CO_2) and 50 °C for 2 hours. No bubbles are seen in any of the images. This photo has been taken at 600 sec and 0 bar (scale of images is 6 x 6 mm).

Further experiments were performed at high pressures (100 and 120 bar). The bubble nucleation starts to appear after 30 to 60 sec. The resulting photographs (Figure 6-24 and 6-25) do show bubble formation after 30 to 60 second.

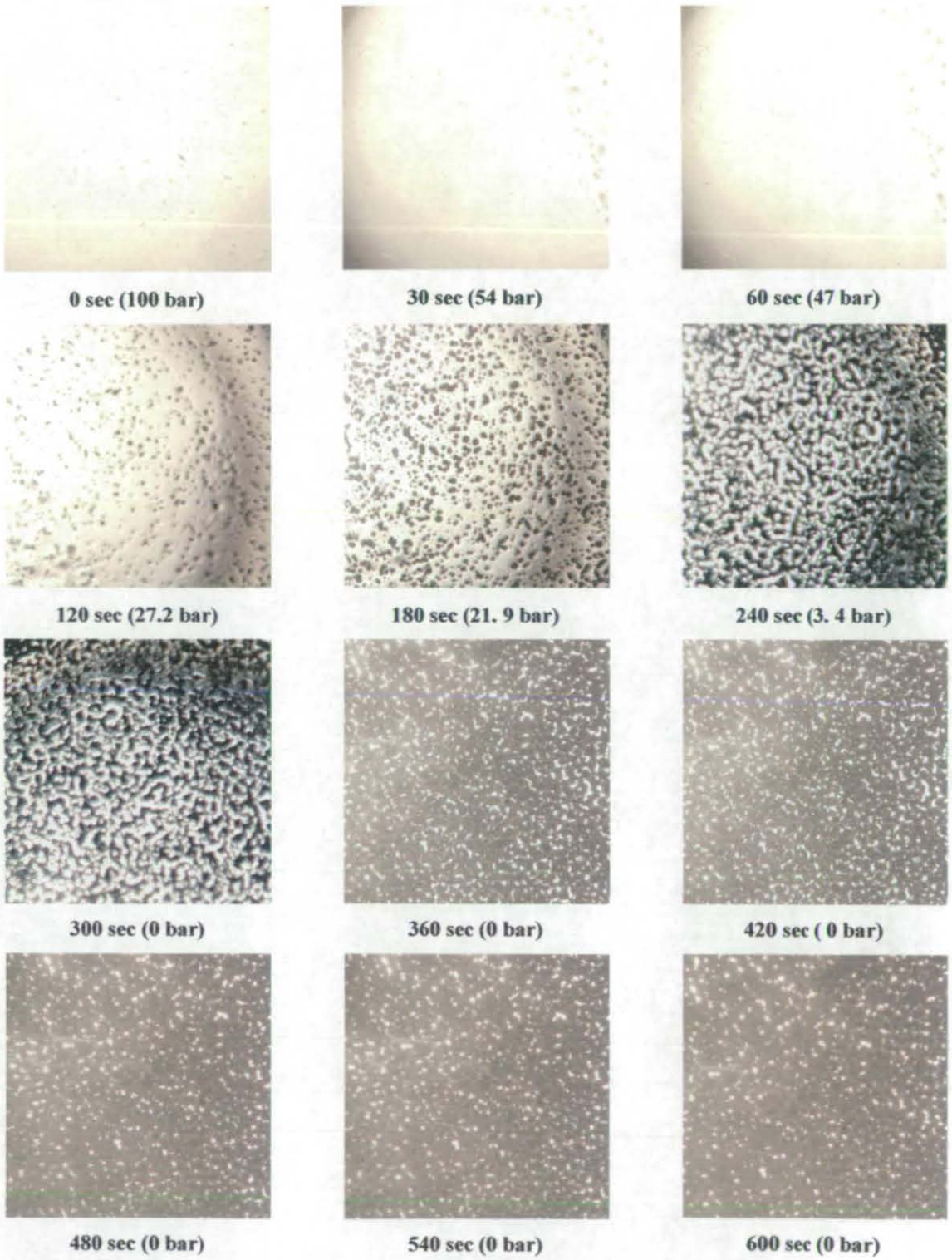

Figure 6 - 25: : Photographs of a 1 mm thick PS sample at various times after the onset of depressurisation after holding at 100 bar (in CO_2) and 50 °C for 2 hours (scale of images is 6 x 6 mm).

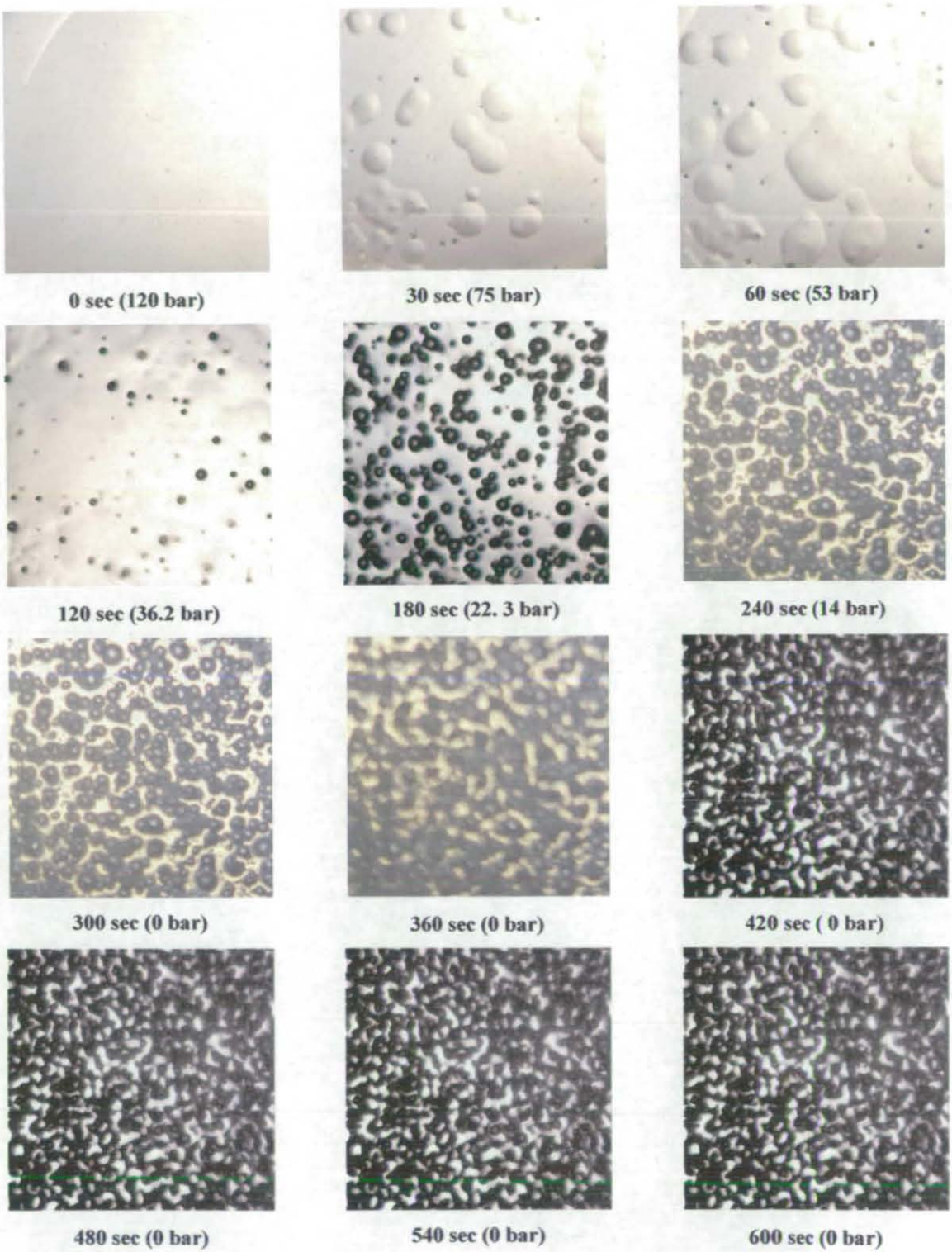

Figure 6 - 26: Photographs of a 1 mm thick PS sample at various times after the onset of depressurisation after holding at 120 bar (in CO_2) and 50 °C for 2 hours (scale of images is 6 x 6 mm).

The photographs in Figure 6-25 after 30 second (75 bar) and 60 second (63 bar) show large "blisters" which are different in appearance to other bubble forming. These are not apparent at lower pressures. At 50 °C CO_2 is a liquid at pressures above 31 bar so these "blisters" can be attributed to drops of liquid CO_2. The following Figure (Figure 6-26) illustrates the bubble radius of 100 and 120 bar at 50 °C.

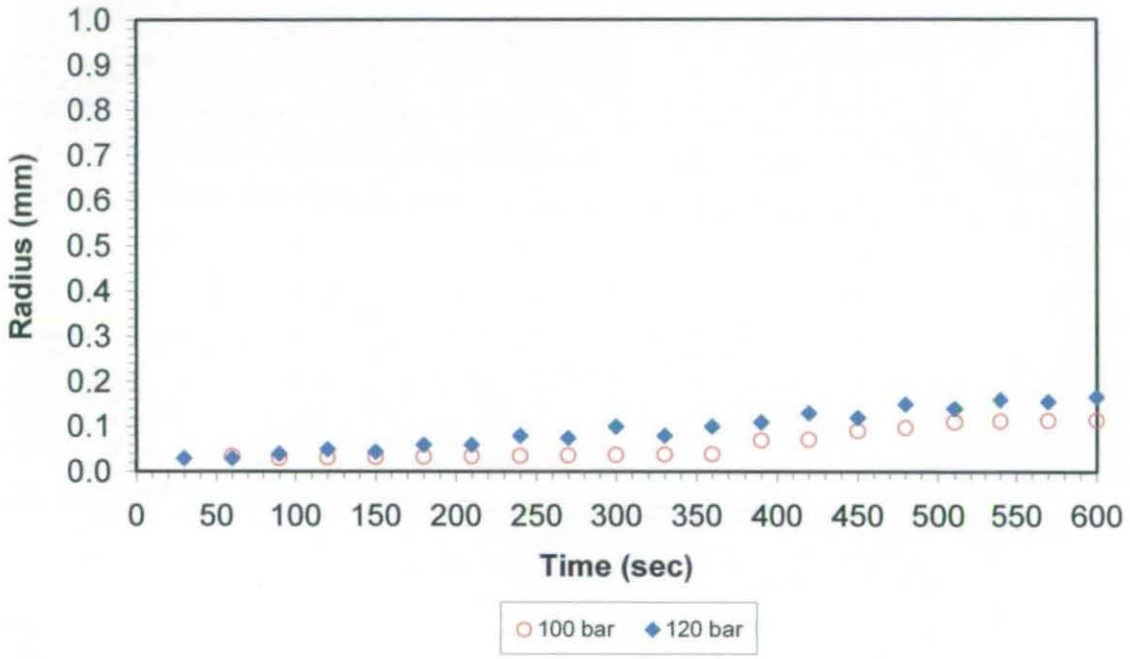

Figure 6 - 27: Bubble radius for of PS/CO_2 during depressurisation after holding at 100 and 120 bar at 50 °C for 2 hours.

The following table summarise and illustrate the starting and the final bubble size:

Table 6 - 2: Data analysis and the bubble starting point of 50 °C and pressure ranges of 24 to 120 bar.

Pressure	Temperature	Bubbles Start Time		Maximum Radius
(bar)	(° C)	Time (sec)	Pressure (bar)	(mm)
24	50	-	-	No bubbles
44	50	-	-	No bubbles
63	50	-	-	No bubbles
83	50	-	-	No bubbles
100	50	60	47	0.02 – 0.11
120	50	30	75	0.02 – 0.16

6.2.8.2 Results from Experiments at 70 °C

Images taken 600 seconds after the onset of during depressurisation are shown in Figures 6-27 and 6-28 for initial conditions over the pressure range (24 to 44 bar) and 70 °C. The images show no sign of any bubble. This again corresponds to conditions below the T_g of PS.

Figure 6 - 28: Photograph of a 1 mm thick PS sample at various times after the onset of depressurisation after holding at 24 bar (in CO_2) and 70 °C for 2 hours. No bubbles are seen in any of the images. This photo has been taken at 600 sec and 0 bar (scale of images is 6 x 6 mm).

Figure 6 - 29: Photograph of a 1 mm thick PS sample at various times after the onset of depressurisation after holding at 44 bar (in CO_2) and 70 °C for 2 hours. No bubbles are seen in any of the images. This photo has been taken at 600 sec and 0 bar (scale of images is 6 x 6 mm).

The following measurements were performed at higher pressures (63 to 120 bar) and at the same temperature (70 °C). See the following images (Figures 6-29 to 6-32):

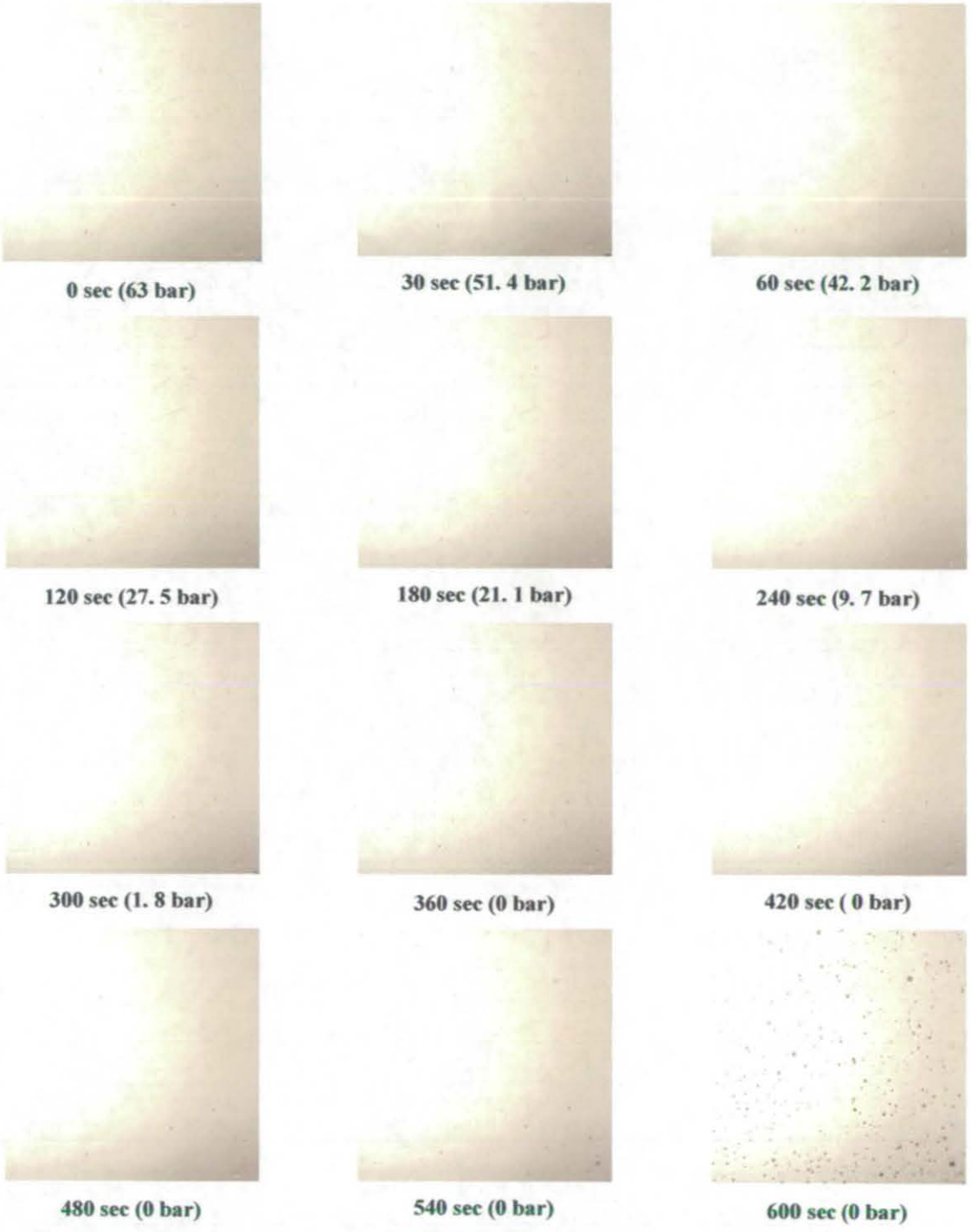

Figure 6 - 30: Photographs of a 1 mm thick PS sample at various times after the onset of depressurisation after holding at 63 bar (in CO_2) and 70 °C for 2 hours (scale of images is 6 x 6 mm).

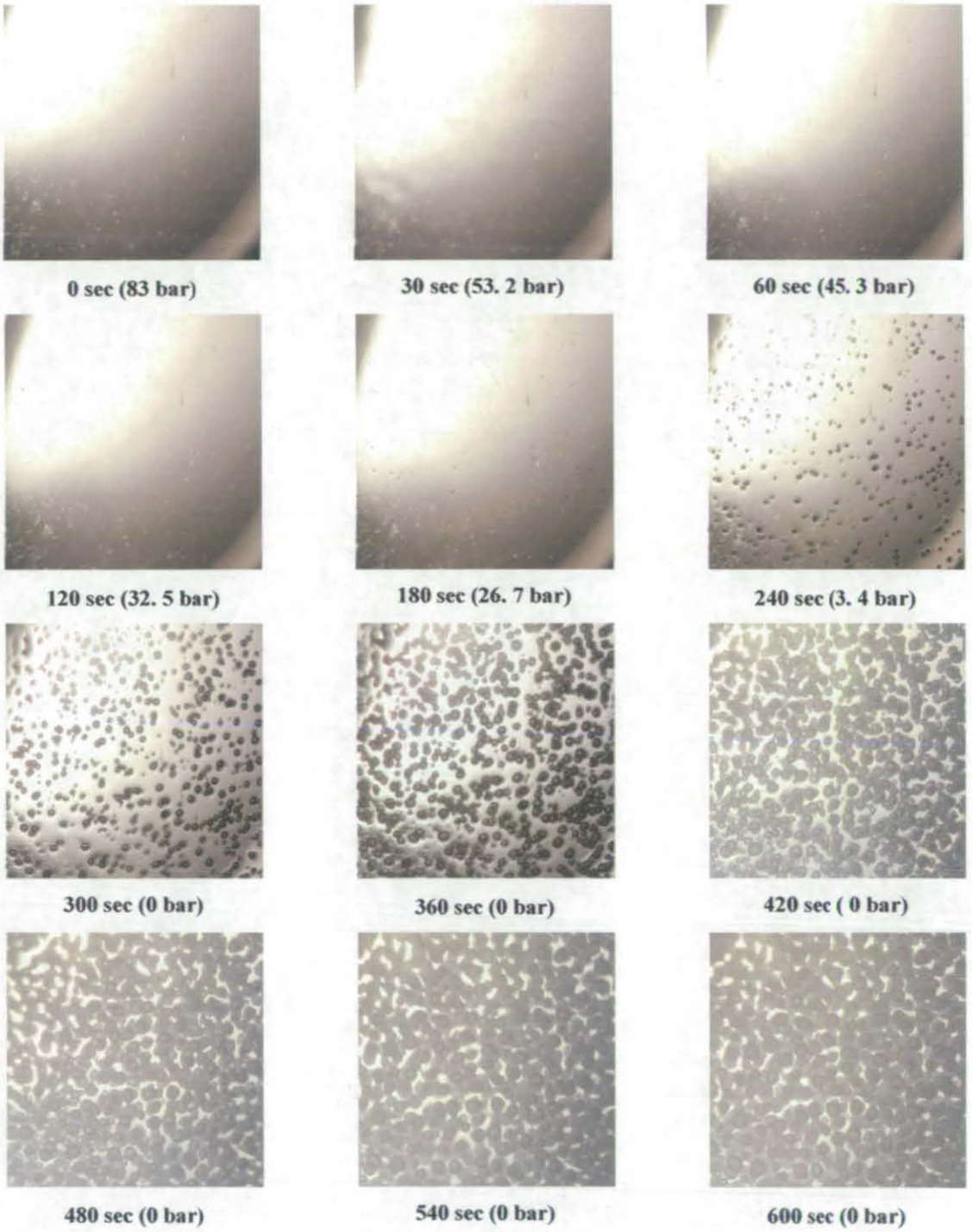

Figure 6 - 31: Photographs of a 1 mm thick PS sample at various times after the onset of depressurisation after holding at 83 bar (in CO_2) and 70 °C for 2 hours (scale of images is 6 x 6 mm).

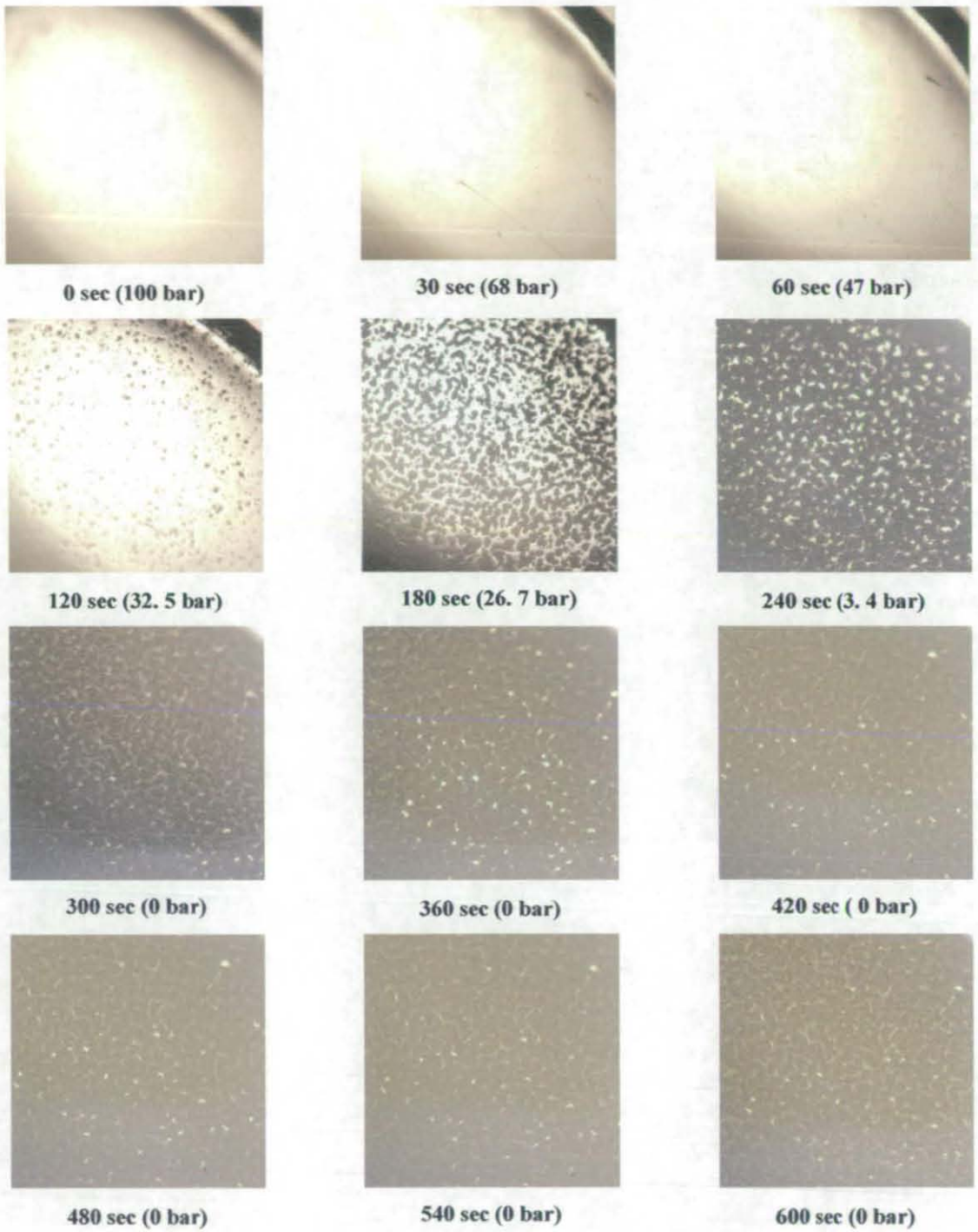

Figure 6 - 32: Photographs of a 1 mm thick PS sample at various times after the onset of depressurisation after holding at 100 bar (in CO_2) and 70 °C for 2 hours (scale of images is 6 x 6 mm).

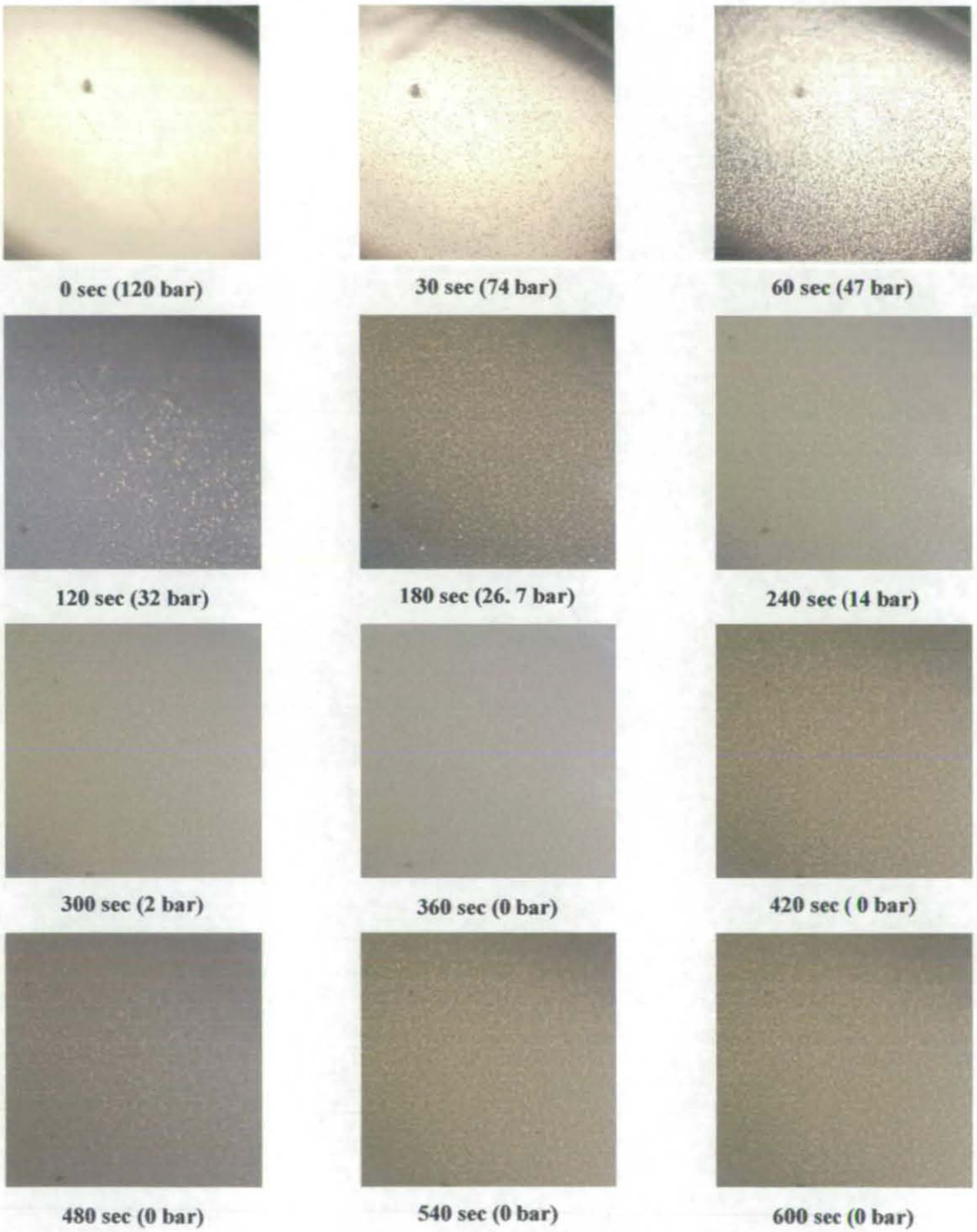

Figure 6 - 33: Photographs of a 1 mm thick PS sample at various times after the onset of depressurisation after holding at 120 bar (in CO_2) and 70 °C for 2 hours (scale of images is 6 x 6 mm).

It can be clearly seen in Figures (6-29 and 6-32) (63 bar and 83 bar initial pressure) the bubbles keep growing even after pressure has reached 0 bar. Some bubbles start to appear even after this long time (but with small diameter) in the interstices between the bubble. The following figure (Figure 6-33) presents the bubble radius growth for these experiments.

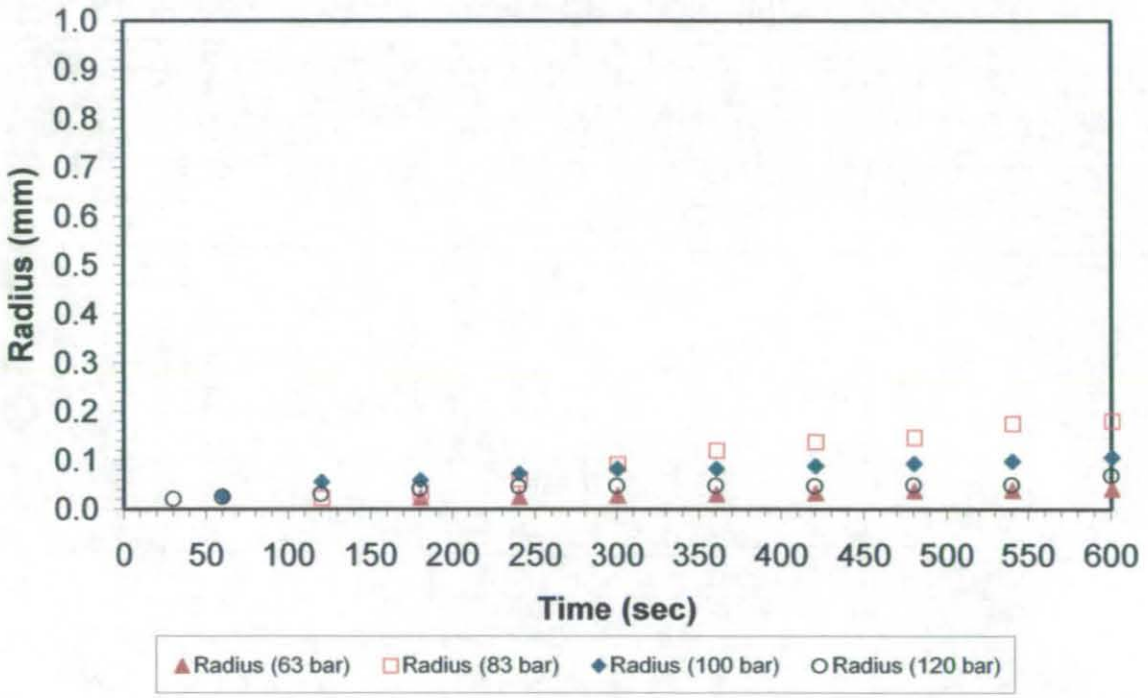

Figure 6 - 34: Bubble radius of PS/CO_2 during depressurisation after holding at 63 to 120 bar at 70 °C for 2 hours.

As we can see the bubbles start to grow at around 30 second at the highest pressure (120 bar) and at around 180 sec for the lowest pressure (63 bar). This is likely to be due to a faster increase in supersaturation at the higher initial pressures. The following table summarises these investigations and illustrates the starting and the final bubble point after the gas pressure reached 0 bar.

Table 6 - 3: Data analysis and the bubble starting point of 70 °C and pressure ranges of 24 to 120 bar.

Pressure (bar)	Temperature (°C)	Bubbles Start Time		Maximum Radius (mm)
		Time (sec)	Pressure (bar)	
24	70	-	-	No bubbles
44	70	-	-	No bubbles
63	70	180	21	0.02 – 0.04
83	70	120	32	0.02 – 0.18
100	70	60	47	0.02 – 0.10
120	70	30	74	0.02 – 0.07

6.2.8.3 Results from Experiments at 100 °C

These measurements were performed at a higher temperature (100 °C) with the same pressure ranges (24 to 120 bar) that were used in the previous measurements at 50 and 70 °C. Thus all samples are initially in the rubbery state (above T_g). Bubbles appeared in all the experiments without exception. The nucleation appeared to occur randomly leading to subsequent bubble growth from these sites. With time, more bubbles nucleate and grow, and the bubbles initially appear to be circular. As more bubbles form and grow in close proximity to each other, their shape is influenced by the impingement of surrounding neighbours leading to polygon shaped bubbles towards the end, with each bubble separated from the neighbouring bubble by a thin film of polymer. The following images present these investigations, see Figure 6-34 to 6-39.

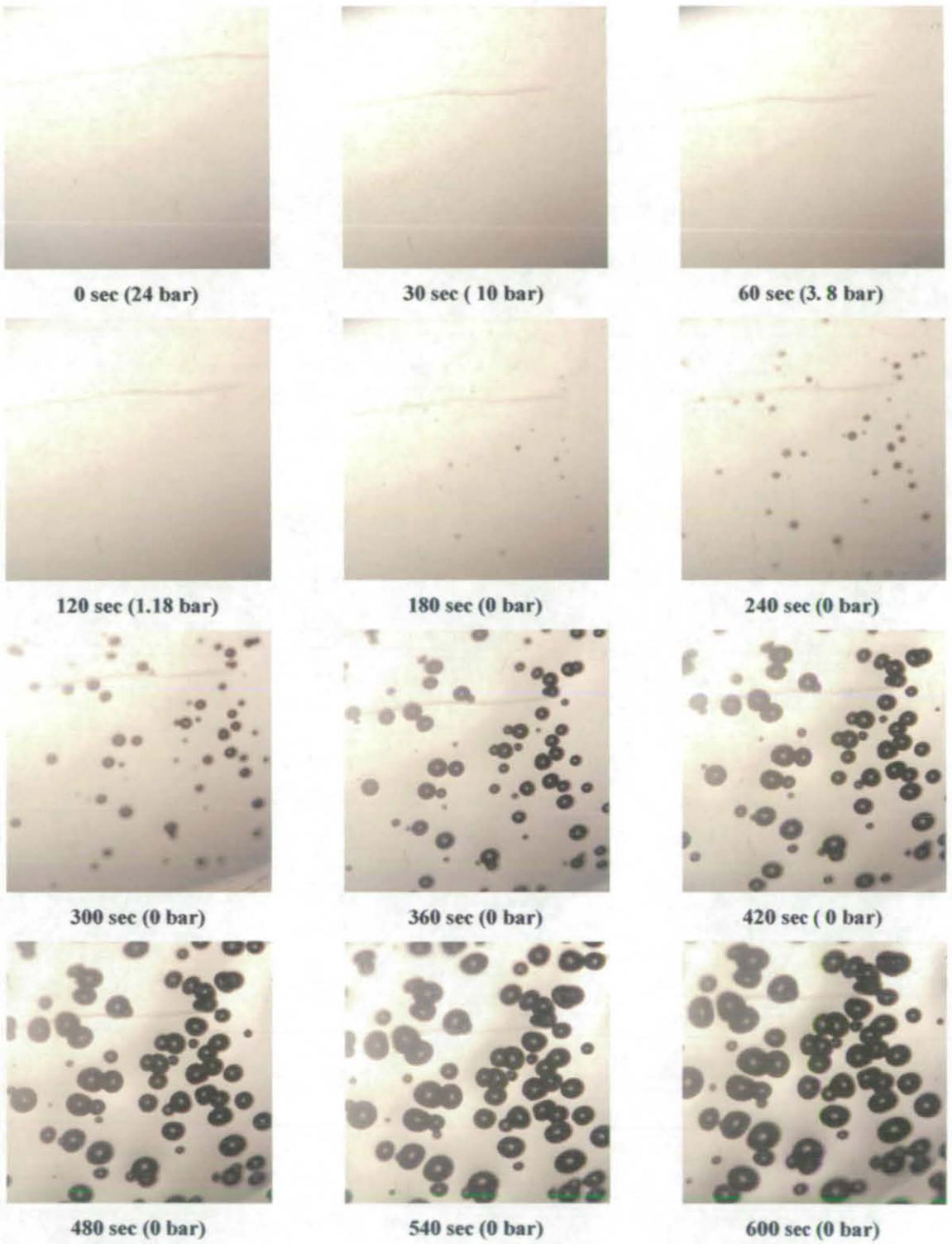

Figure 6 - 35: Photographs of a 1 mm thick PS sample at various times after the onset of depressurisation after holding at 24 bar (in CO_2) and 100 °C for 2 hours (scale of images is 6 x 6 mm).

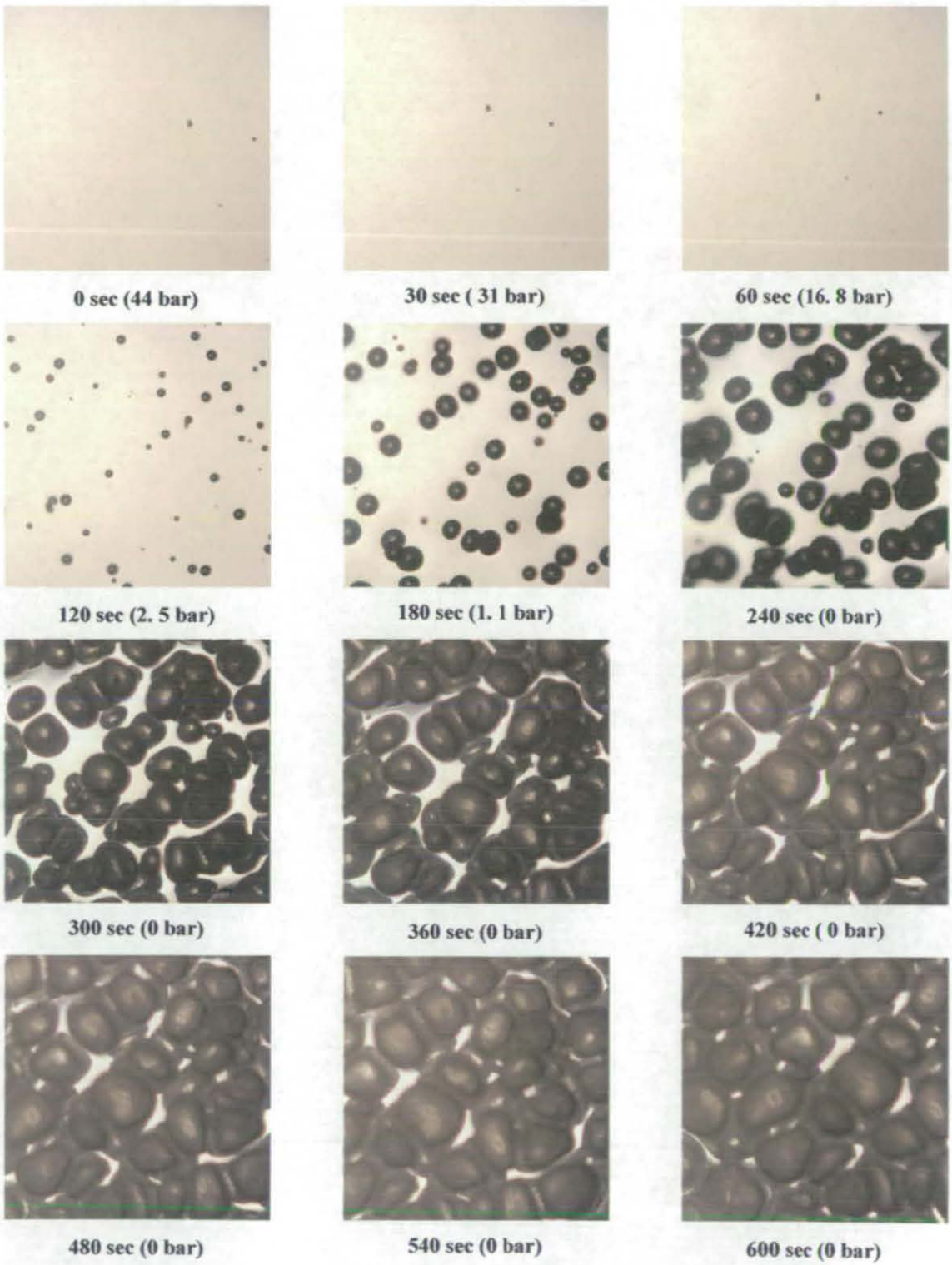

Figure 6 - 36: Photographs of a 1 mm thick PS sample at various times after the onset of depressurisation after holding at 44 bar (in CO_2) and 100 °C for 2 hours (scale of images is 6 x 6 mm).

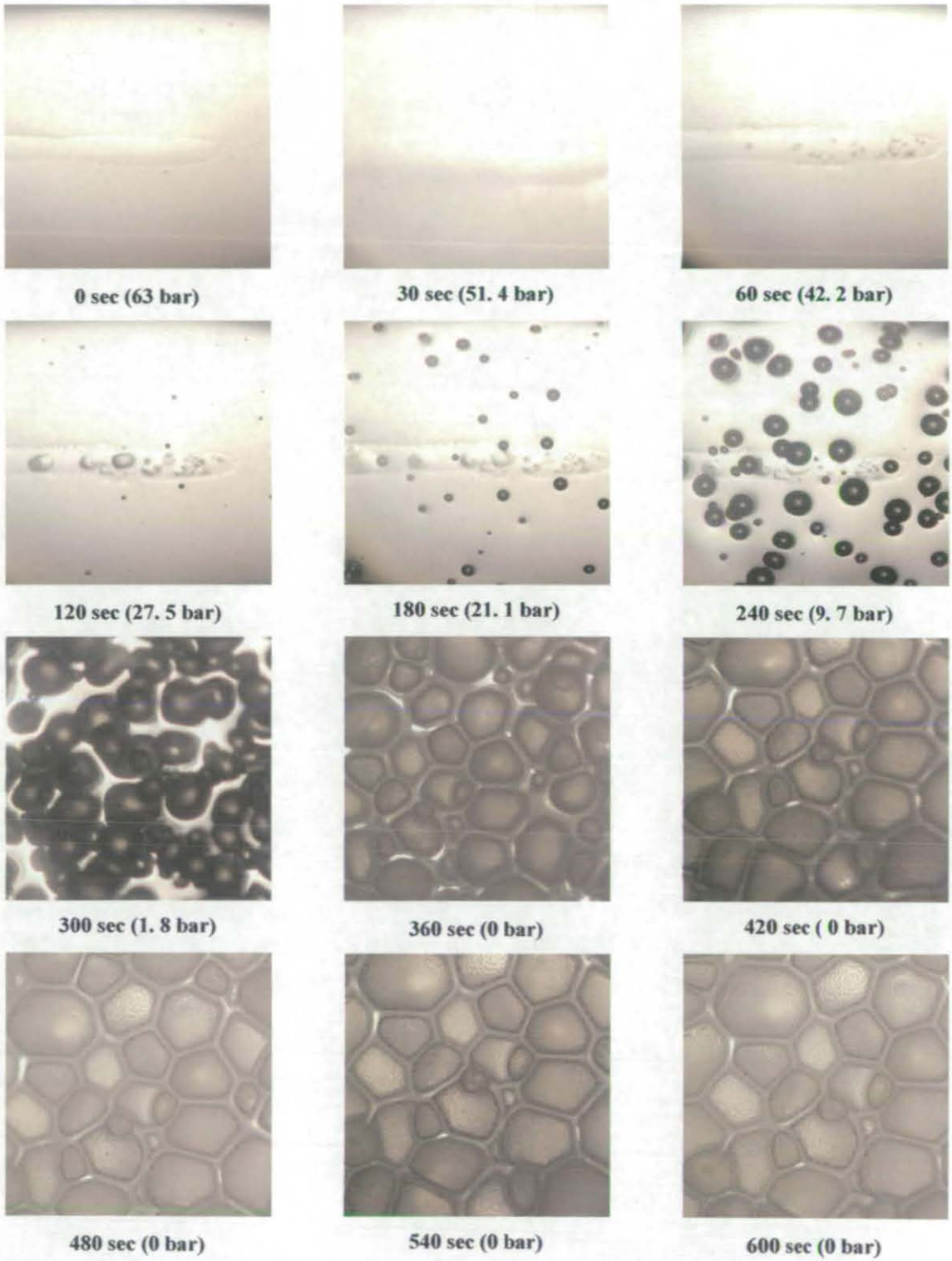

Figure 6 - 37: Photographs of a 1 mm thick PS sample at various times after the onset of depressurisation after holding at 63 bar (in CO_2) and 100 °C for 2 hours (scale of images is 6 x 6 mm).

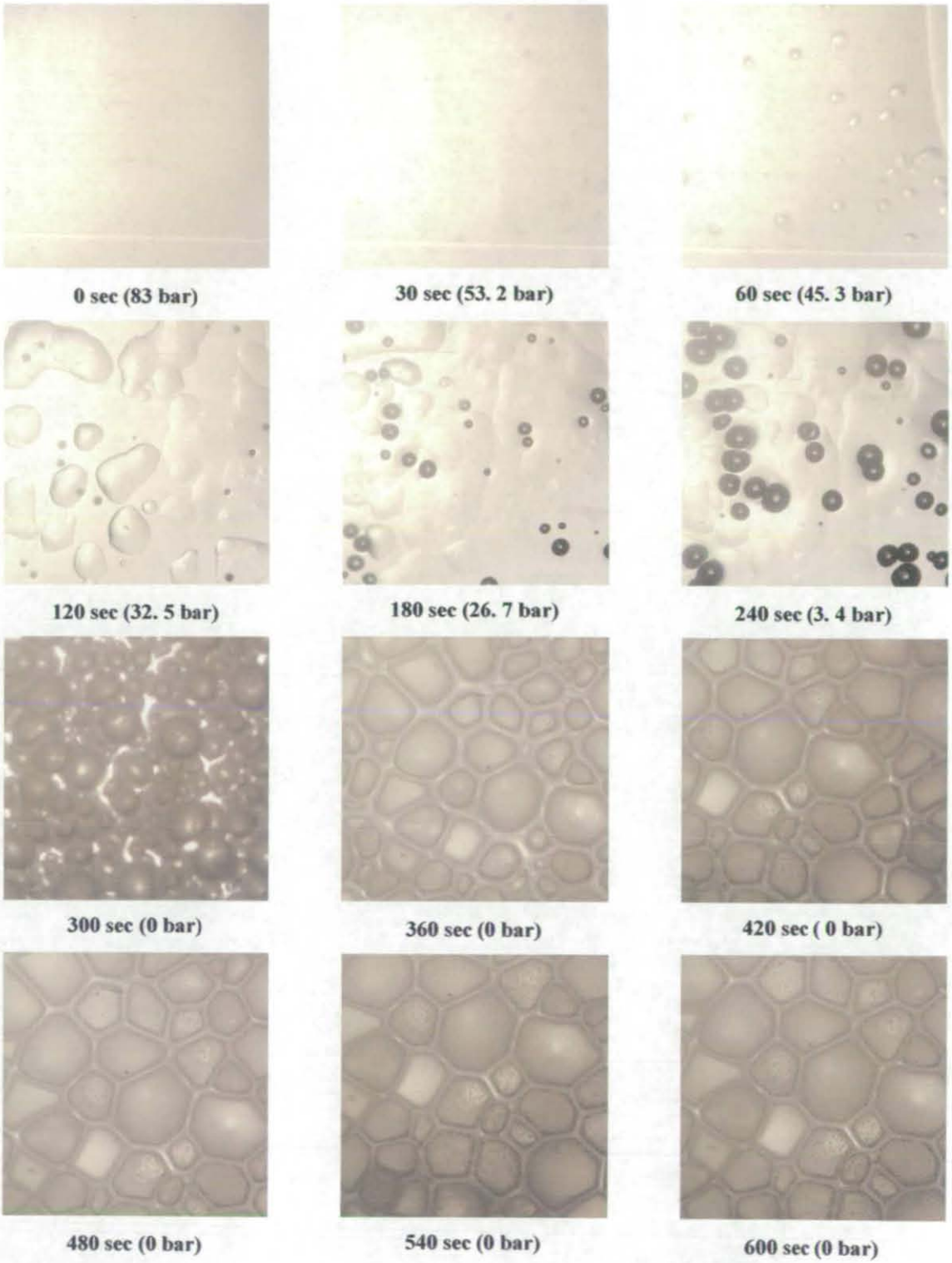

Figure 6 - 38: Photographs of a 1 mm thick PS sample at various times after the onset of depressurisation after holding at 83 bar (in CO_2) and 100 °C for 2 hours (scale of images is 6 x 6 mm).

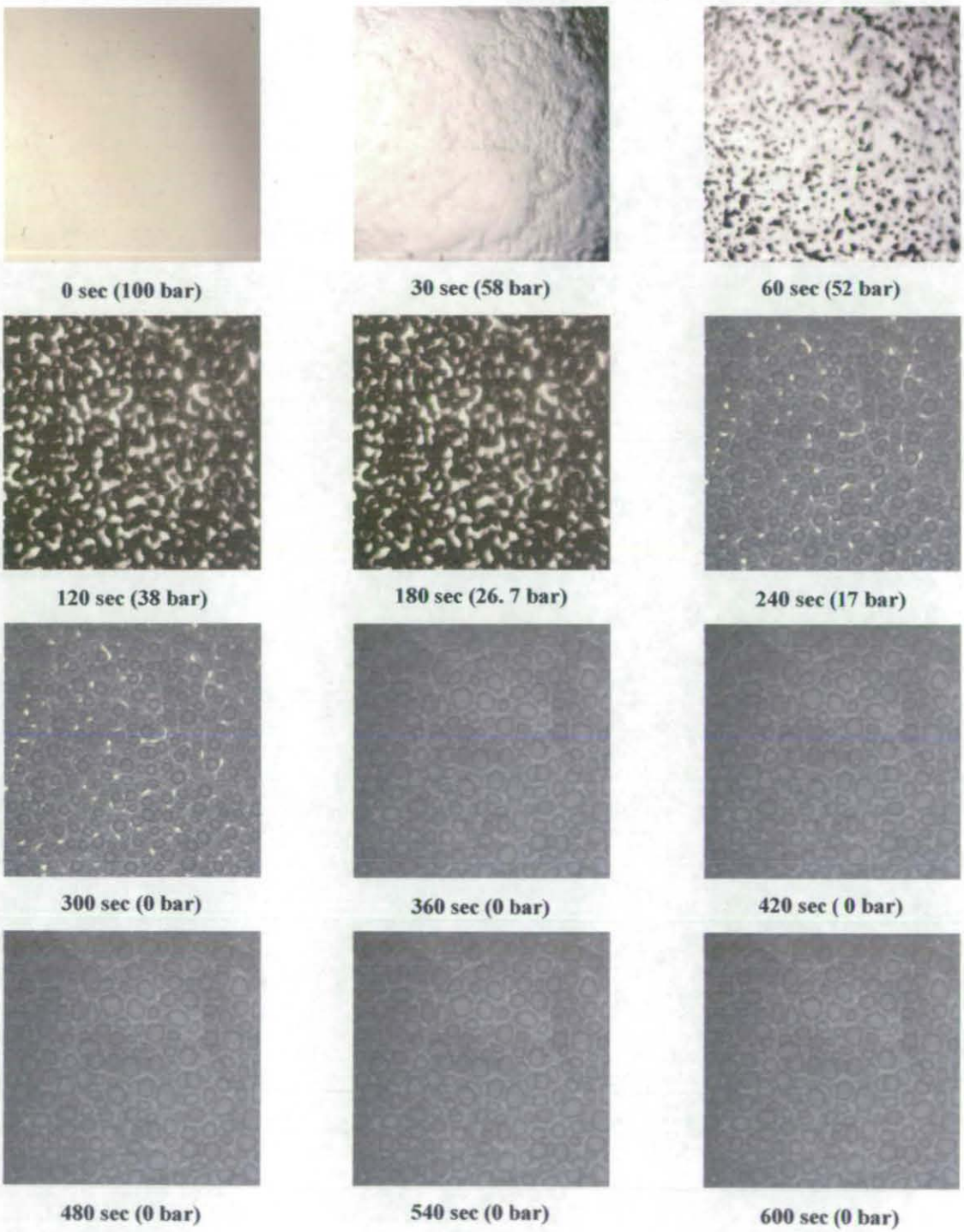

Figure 6 - 39: Photographs of a 1 mm thick PS sample at various times after the onset of depressurisation after holding at 100 bar (in CO_2) and 100 °C for 2 hours (scale of images is 6 x 6 mm).

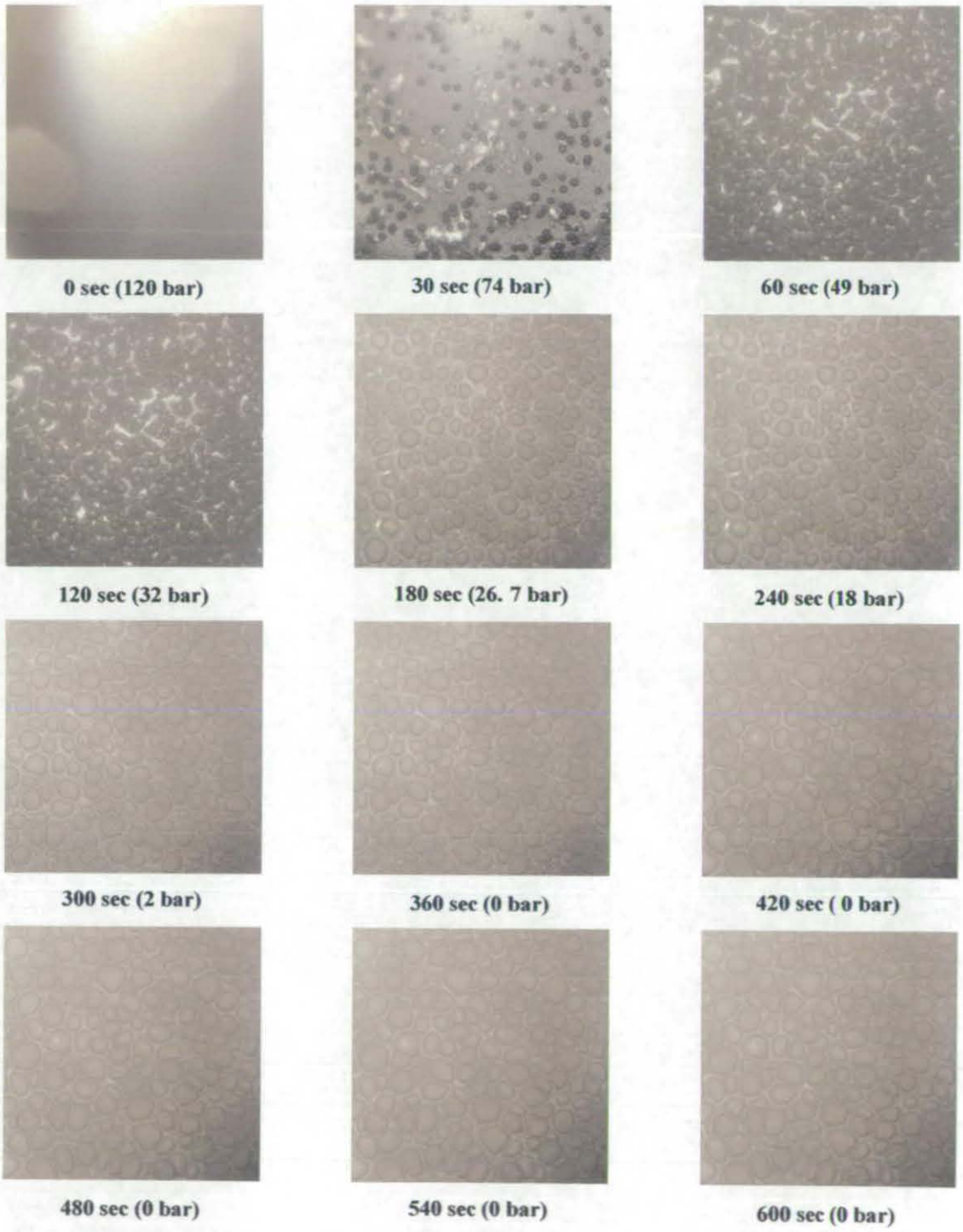

Figure 6 - 40: Photograph of a 1 mm thick PS sample at various times after the onset of depressurisation after holding at 120 bar (in CO_2) and 100 °C for 2 hours, (scale of images is 6 x 6 mm).

The following figure illustrates the depressurization curves for all the experiments performed at 100 °C (see Figure 6-40).

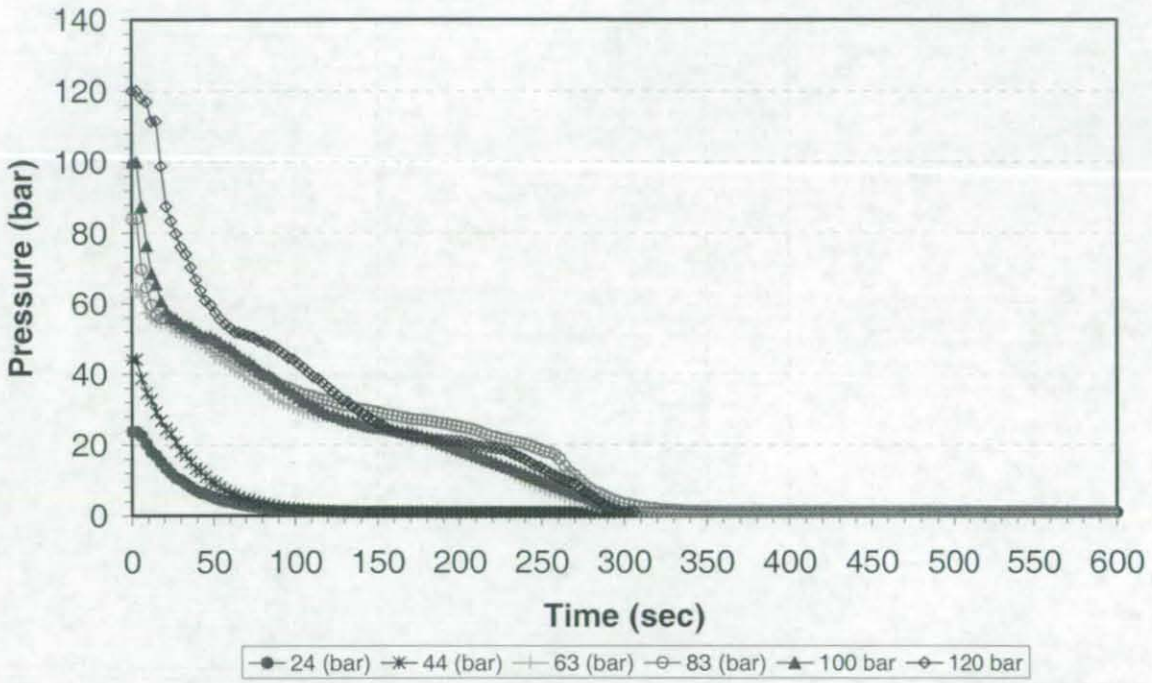

Figure 6 - 41: Depressurization time period for all the applying pressure (24 to 120 bar) performed at 100 °C.

As shown in Figure 6-40, all the experiments reached 0 bar before 300 sec of depressurisation. With low pressure (24 to 44 bar) the time to reach 0 bar was between 175 to 200 sec and for the high pressure (85 to 120 bar) it was around 275 to 300 sec. This is because the low pressure experiments have less gas to evacuate from the cell.

We can see from all the previous Figures (6-34 to 6-39) that the bubbles keep growing even when the cell pressure has reached 0 bar, and some bubbles start to appear even after this time in the interstices between the bubbles. This trend happens at all pressures but it can be seen more clearly with the higher pressures (see Figure 6-36 and 6-37). This shows that the CO_2 in the polymer, in the bubbles, and in the surrounding gas is not in equilibrium. In these experiments the temperature is above the glass transition, therefore the polymer is in the rubbery phase and the bubbles can grow very easily which made the bubbles very big compared with the earlier investigations in this work.

These investigations will give direct help to develop the bubble growth models. The following figure (Figure 6-41) presents the bubble radius for these pressure and temperature experiments.

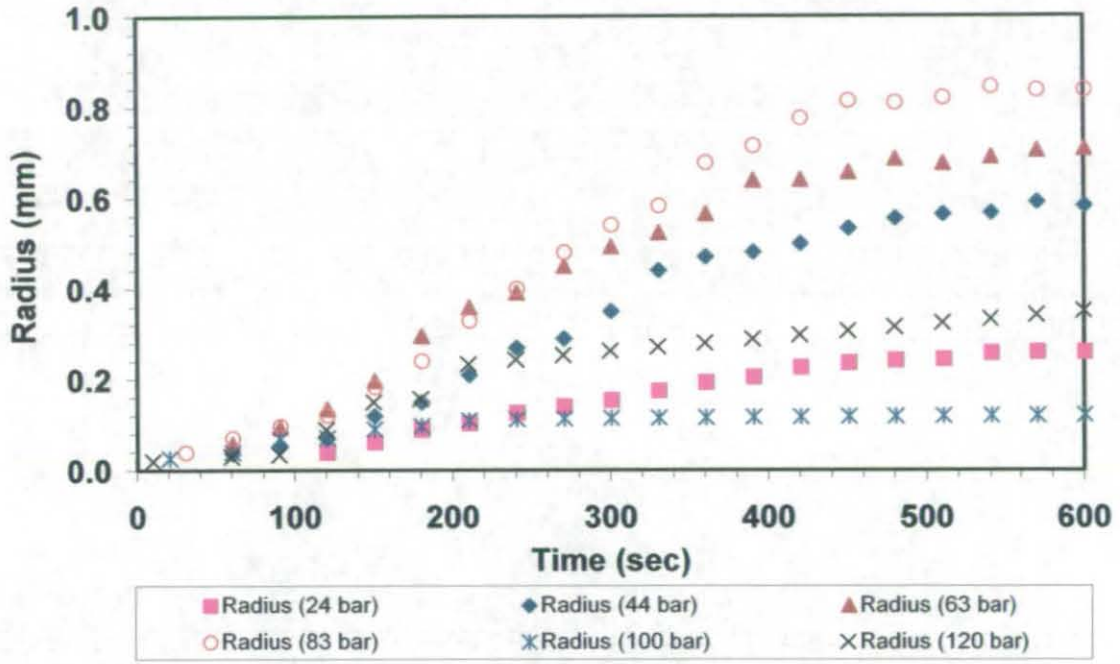

Figure 6 - 42: Bubble radius of PS/CO_2 during depressurisation after holding at 24 to 120 bar at 100 °C for 2 hours.

As we can see the bubbles appear before 30 sec for the high pressures (83 to 120 bar) and after 60 second for the lower pressures (24 and 63 bar). The following table summarises these investigations and illustrates the starting bubble point.

Table 6 - 4: Data analysis and the bubble starting point of 100 °C and pressure ranges of 24 to 120 bar.

Pressure	Temperature	Bubbles Start Time		Maximum Radius
(bar)	(°C)	Time (sec)	Pressure (bar)	(mm)
24	100	120	1.2	0.02 - 0.28
44	100	60	17	0.02 - 0.58
63	100	30	48	0.02 - 0.70
83	100	30	53	0.02 - 0.83
100	100	20	68	0.02 – 0.21
120	100	10	110	0.02 – 0.32

As shown in the table 6-4, the low pressure needed a longer time for nucleation to occur (around 120 sec) compared with higher pressures (10 sec). Again, this is probably because the amount of CO_2 dissolved in the PS is much greater at the higher pressure.

6.2.9 Incidence of Bubble Formation

As shown in the previous images, no signs of bubble formation were observed during depressurisation at 50 °C and initial pressures up to 83 bar, and at 70 °C and initial pressures up 44 bar. These correspond to conditions below the T_g of PS. However, at high pressures and temperatures above the T_g nucleation occurred. The following figure illustrates these incidents of bubble formation for all the operating conditions. It can be clearly seen that bubbles form only when the polymer has been in the rubbery state.

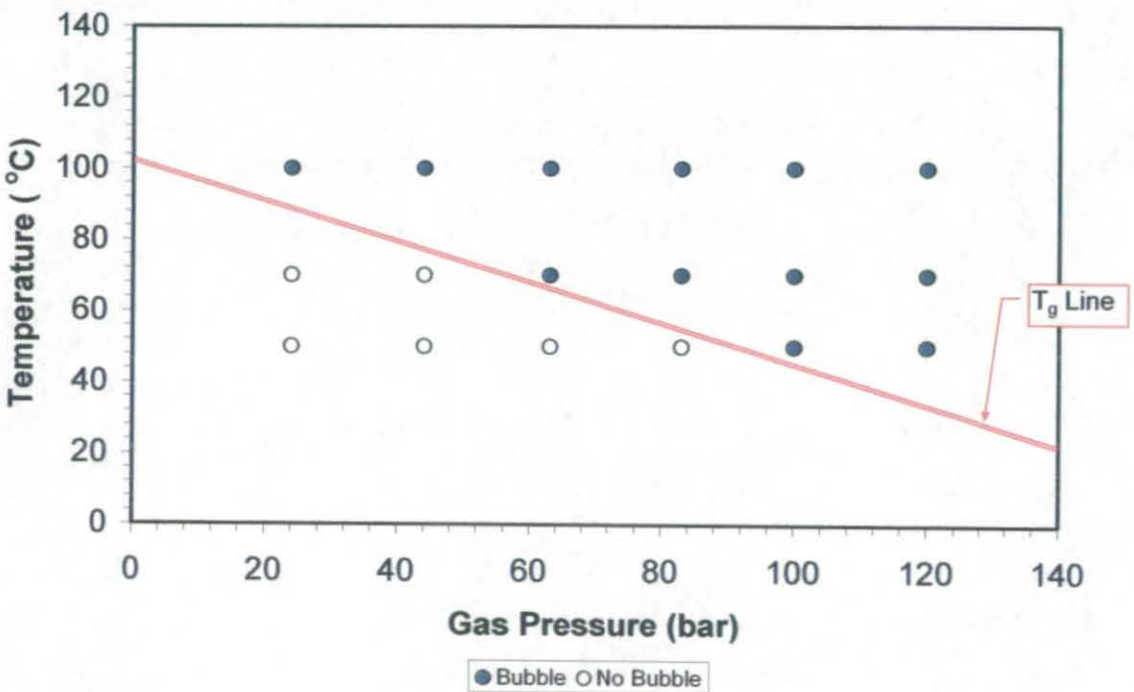

Figure 6 - 43: Incident of bubble formation and T_g line.

6.2.10 Possible Influence of the Glass Transition on Bubble Growth

It has been noted from the previous investigation in this work that the T_g has the biggest influence on bubble growth. In the previous images (Figure 6-34) (at the experimental condition of 24 bar and 100 °C) it can be seen that the bubbles grow very freely without impinging, but that the growth stops after 480 second before impingement occurred, which indicate that the growth here is not limited by impingement.

Another experiment also showed that the solubility of CO_2 cannot on its own be used as a predictor of bubble growth. At the experimental conditions at 83 bar and the two different temperatures of 70 °C (Figure 6-30) and 100 °C (Figure 6-37) it was found that the bubble diameter at 70 °C are much smaller than at 100°C. As solubility increases as temperature decreases (see Figure 2-20), solubility considerations alone would predict the opposite trend.

It also obvious that bubbles do not expand freely such that the CO_2 bubble pressure equilibrates with the cell pressure as this would result in much larger foam volumes than are observed. It is thus likely that bubble growth reduces as the polymer (at some point) passes from the rubbery to the glassy state.

6.2.11 Final Thickness of Samples

So far only the top view of the polymer samples during depressurisation has been shown, but no information about the thickness of the samples. All the experiments started with a 1 mm thick sample, but in many cases this increased dramatically. One example is the sample conditioned at 120 bar and 100 °C. Figure 6-43 shows that the thickness of the sample increased from 1mm to a maximum of 4 mm.

Figure 6 - 44: Thickness increases from 1 to 4 mm (120 bar and 100 °C).

6.2.12 Comparison of Bubble Radius with Literature Values

Only a few experimental investigations have addressed bubble growth in CO_2 / PS system as mentioned earlier in chapter 2 (see section 2.5.4). Most of these have been performed near the melting point of the PS (140 to 200 °C). Han and Yoo (1981) worked at molten temperature of 200 °C during mould filling and an injection pressure of 20.6 bar. They were able to observe bubble sizes down to 0.03 mm, and found that the bubbles were spherical. Another experimental investigation was preformed in 2005 by Tuladhar and Mackley on the foaming of PS using an in house developed Multipass Rheometer (MPR), at 140°C and 92 bar. The following Figure shows a comparison of bubble radius versus time data from these two studies and the work reported in this thesis.

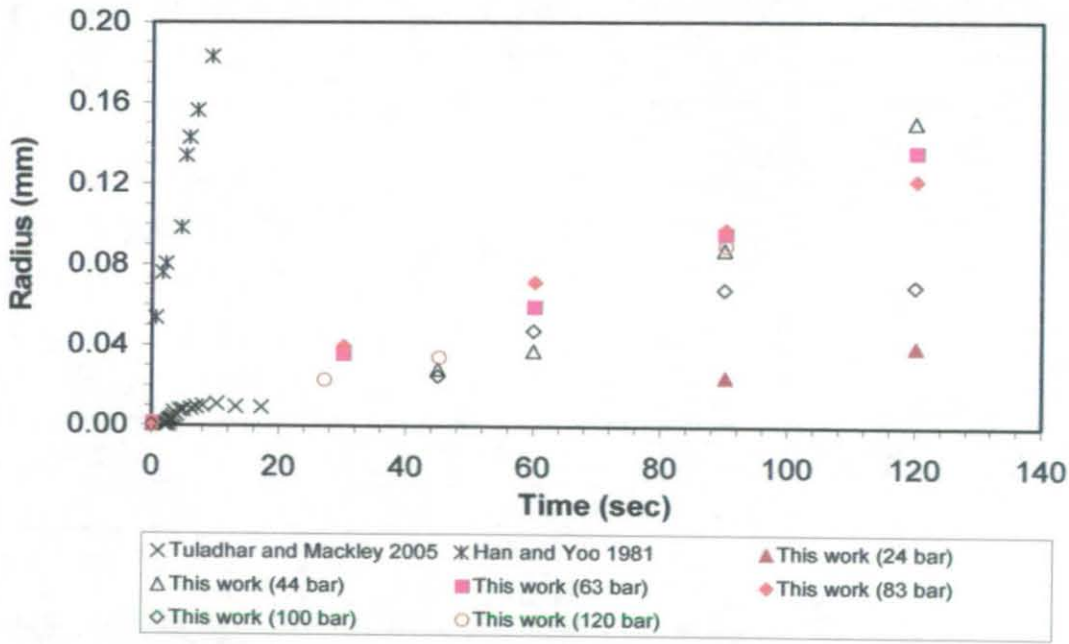

Figure 6 - 45: Comparison of bubble growth data with the literature (this work at 100 °C).

As we can see the data from this work lies in between the literature data, but it is very difficult to make direct comparisons. Han and Yoo (1981) used molten polymer at 200°C and reduced the pressure suddenly which produced very rapid foaming. Tuladhar and Mackley (2005) also shocked the polymer (at 140°C) with a very fast drop in the pressure (from 90 to 10 bar) in a very short time (about 10 sec). In contrast our work is starting from the semi-solid or just rubbery state. The bubble sizes reported by Han & Yoo (1981) were fairly similar to our work (0.02 – 0.8 mm), whilst those determined by Tuladhar & Mackley (2005) were much smaller (0.5 – 10 μm).

6.3 Bubble Growth Modelling

In this section the mathematical models described in chapter 4 section 4.3 are used to fit to the experimental data of bubble growth presented in section 6.2. The set of experiments used to test these models were those with pressure of 24, 44, 63, and 83 bar and at a temperature of 100°C. All these experimental data were logged for 600 sec during depressurisation.

Each bubble was assumed to be spherical with an initial radius of 0.02 mm and surrounded by a finite volume of polymer. Three bubble growth models were used based on diffusion control only (Model A); constant viscosity and diffusivity (Model B); and varying diffusivity and viscosity according to the WLF equation (Model C).

In the models time zero is taken at the onset of nucleation, which is often some time after depressurisation has commenced and so the starting cell pressure for the model is usually lower than the equilibration pressure (which determines the initial concentration of CO_2 in the polymer). Most of the parameter values such as c_o, ρ, γ, μ, D and T are either provided or calculated.

6.3.1 Diffusion Control (Model A)

The general model parameter values are shown in the following table:

Table 6 - 5: Model A general parameters values.

Parameters	Values	Source
Initial radius of polymer sphere, $R_{polymer}$ (mm)	1	Assumed
Initial radius of gas bubble, R_{bubble} (mm)	0.02	Measured
Initial pressure, P_i (bar)	24 to 83	Measured
Final Pressure, P_f (bar)	1	Measured
Temperature , T (°C)	100	Measured
Density of CO_2 in bubble, ρ (kmol/m^3)	0.032	Calculated
Henry's Constant, H (bar)	1628.2	[Sato et al 1996]

According to Sato et al.'s (2001) data each pressure has a different diffusivity as listed in the following table. Thus all the parameters in Model A are pre-set and there are no fitting parameters. See the following table:

Table 6 - 6: Model A diffusivity values.

Initial Pressure, P_i (bar)	Diffusion coefficient , D (10^{-10} m^2/s) [Sato et al 2001]
24	0.81
44	1.14
63	1.46
83	1.67

The following figure (Figure 6-45) compares the model A prediction with the experimental data of 100 °C for different initial pressures (24, 44, 63, and 83 bar). The model fit, however, significantly overpredicts bubble growth rates.

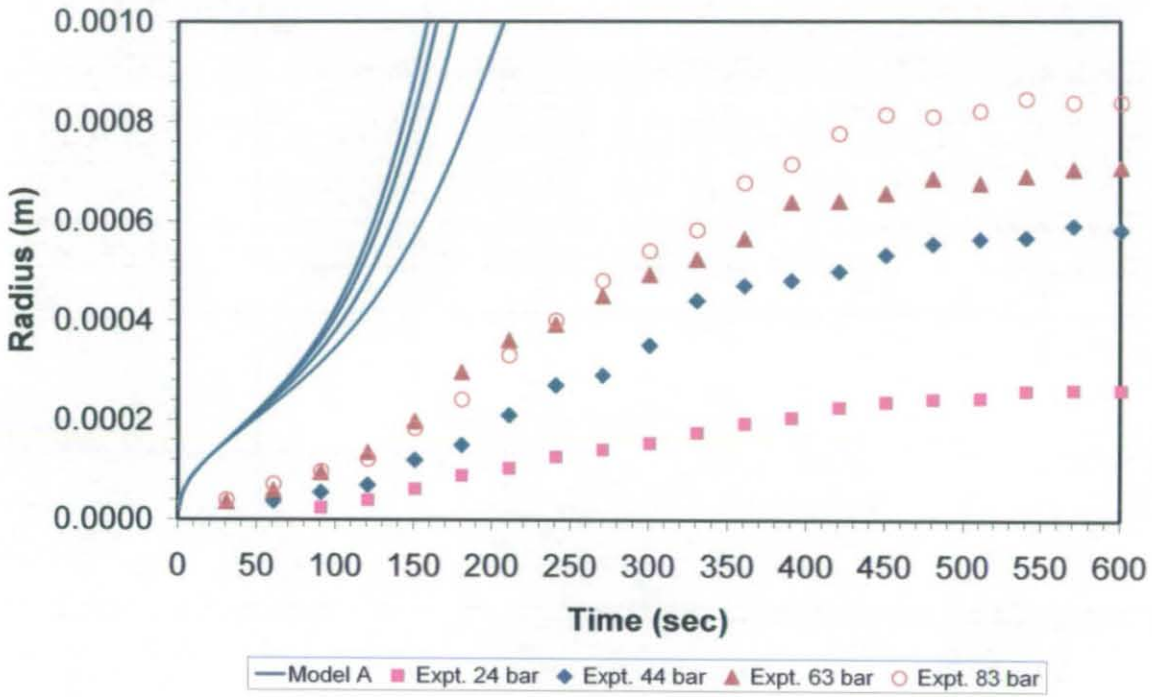

Figure 6 - 46: Model A versus experimental data for bubble growth at 100 °C.

As we know that model A assumes that the growth is controlled by diffusion only which lets the growth happen very quickly without any viscous resistance. Therefore model B was applied to assess whether a viscous model with surface tension can predict bubble the growth with better accuracy.

6.3.2 Constant Diffusivity and Viscosity (Model B)

The general model parameter values are shown in the following table:

Table 6 - 7: Model B general parameters values.

Parameters	Values	Source
Initial radius of polymer sphere, $R_{polymer}$ (mm)	1	Assumed
Initial radius of gas bubble, R_{bubble} (mm)	0.02	Measured
Initial pressure, P_i (bar)	24 to 83	Measured
Final Pressure, P_f (bar)	1	Measured
Temperature , T (°C)	100	Measured
Surface tension, γ (mNm^{-1}) , at 1 bar and 200°C	27.7	[Chen et al 2006]
Henry's Constant, H (bar)	1628.2	[Sato et al 1996]

Each pressure has a different diffusivity (again provided by Sato et al. (2001). As there are no literature values for viscosity this is a fitted parameter. See the following table:

Table 6 - 8: Model B diffusivity values and best fit of shear viscosity.

P_i (bar)	Diffusion coefficient D (10^{-10} m^2 s^{-1}) [Sato et al 2001]	Best fit of shear viscosity μ (10^7 Pa.s)
24	0.81	9
44	1.14	7
63	1.46	8
83	1.67	8

The following figure compares model B prediction for experimental data of 24 to 83 bar with 100 °C.

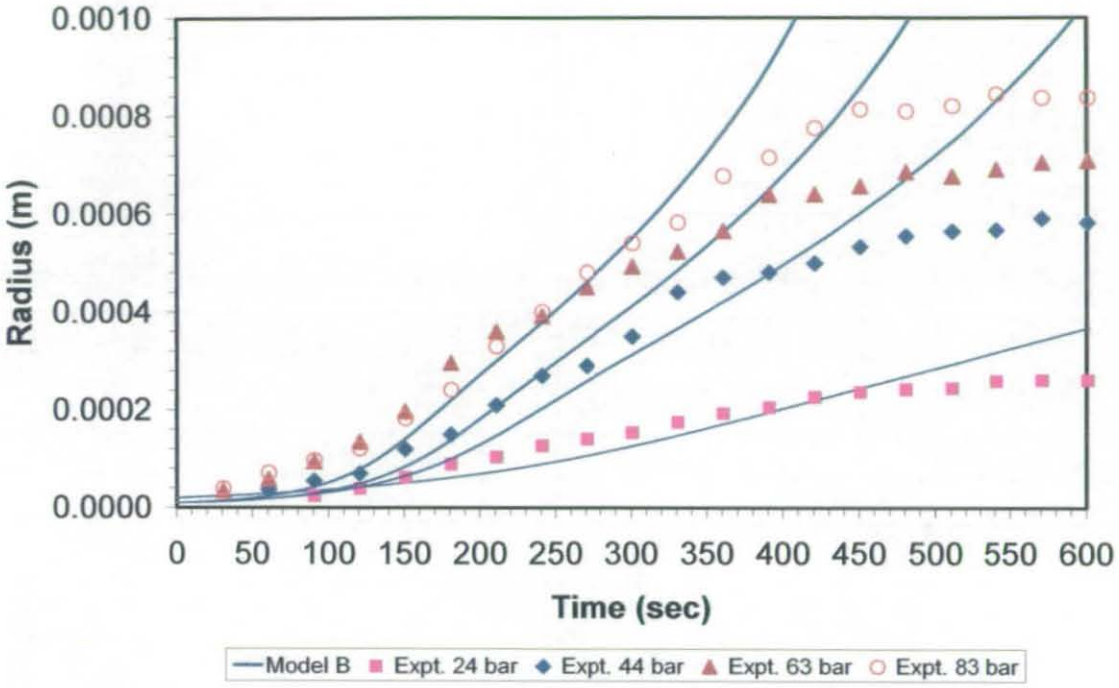

Figure 6 - 47: Model B versus experimental data for bubble growth at 100 °C.

As we can see model B is better than model A for our experimental data. This is because model B controls the growth by including viscosity and surface tension, but still the model fit is not good as it predicts a continuously increasing rate of bubble growth. To get better fits an "experiment" was performed in which the diffusivity values were reduced by a factor of 100 as shown in the following table (Table 6 -10). With the reduced diffusivity the model does show a better fit as shown in figure 6 – 47.

Table 6 - 9: Model B best fit of diffusivity and shear viscosity values.

P_i (bar)	Best fit of diffusion coefficient D (10^{-10} m^2 s^{-1})	Best fit of shear viscosity μ (10^7 Pa.s)
24	0.0081	9
44	0.0114	6
63	0.0146	6
83	0.0167	6

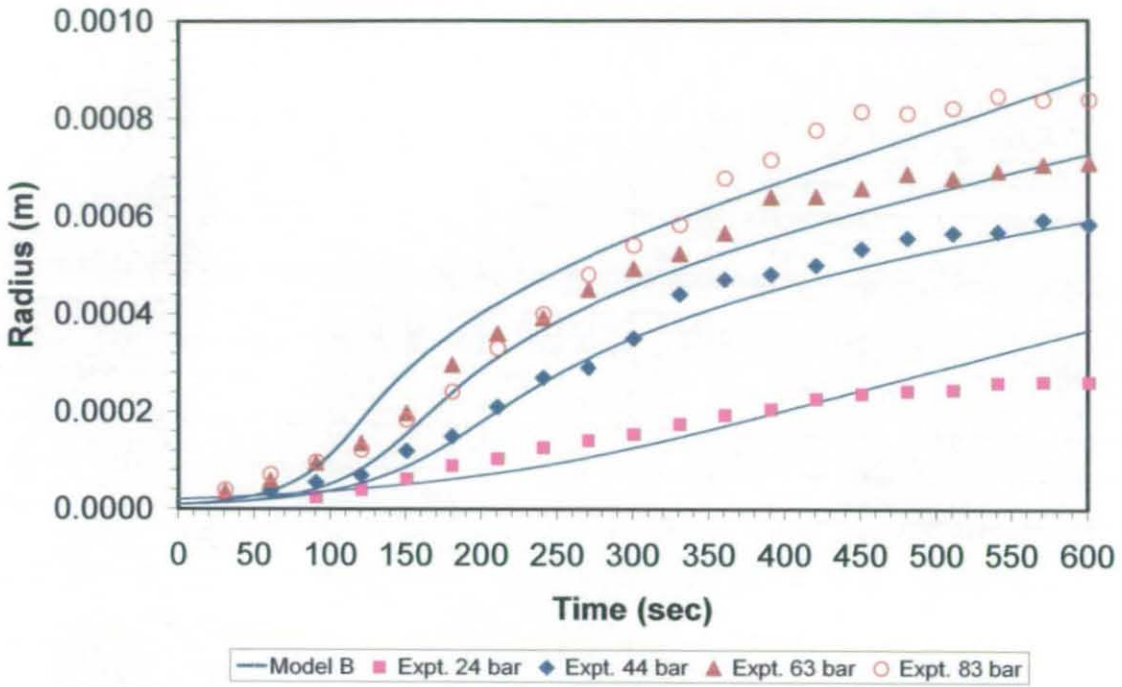

Figure 6 - 48: Model B versus experimental data for bubble growth at 100 °C (by *D*/100).

However this fit did require an adjusted diffusion coefficient. This may well reflect the possibility that at the end of the experiment the diffusivity will be smaller as the concentration of CO_2 in the polymer will be lower. Model C was then applied to determine whether a better prediction could be achieved using a varying viscosity and diffusivity model based on the WLF equation.

6.3.3 Diffusivity and Viscosity Varying According to WLF Equation (Model C)

The parameter values used in Model C are shown in the following table:

Table 6 - 10: Model C general parameters values.

Parameters	Values	Source
Initial radius of polymer sphere, $R_{polymer}$ (mm)	1	Assumed
Initial radius of gas bubble, R_{bubble} (mm)	0.01	Measured
Initial pressure, P_i (bar)	24 to 83	Measured
Final Pressure, P_f (bar)	1	Measured
Temperature , T (°C)	100	Measured
Surface tension, γ (mNm^{-1}), at 1 bar and 200 °C	27.7	[Chen et al 2006]
Henry's Constant, H (bar)	1628.2	[Sato et al 1996]
"Universal" constant of WLF equation c_1	17.4	[Williams et al 1955]
"Universal" constant of WLF equation c_2 , (K)	51.6	[Williams et al 1955]

Each pressure has different diffusivity and shear viscosity according to the WLF equation, see the following table:

Table 6 - 11: Model C diffusivity values and best fit of shear viscosity (F is the WLF equation).

P_i	Diffusion coefficient		Best fit of shear viscosity	
(bar)	Initial D (10^{-10} m^2 s^{-1}) [Sato et al 2001]	D_o (m^2 s^{-1}) ($D = D_o / F$)	Initial μ (10^7 Pa.s)	μ_o (Pa.s) ($\mu = F * \mu_o$)
24	0.81	2.72×10^{-16}	2.2	6.54×10^{12}
44	1.14	6.04×10^{-19}	2.5	4.72×10^{15}
63	1.46	1.66×10^{-20}	1.5	1.32×10^{17}
83	1.67	1.18×10^{-21}	1.5	2.11×10^{18}

The following figure compares the model C prediction with experimental data of 100 °C and different pressures (24, 44, 63 and 83 bar) (see Figure 6 - 48).

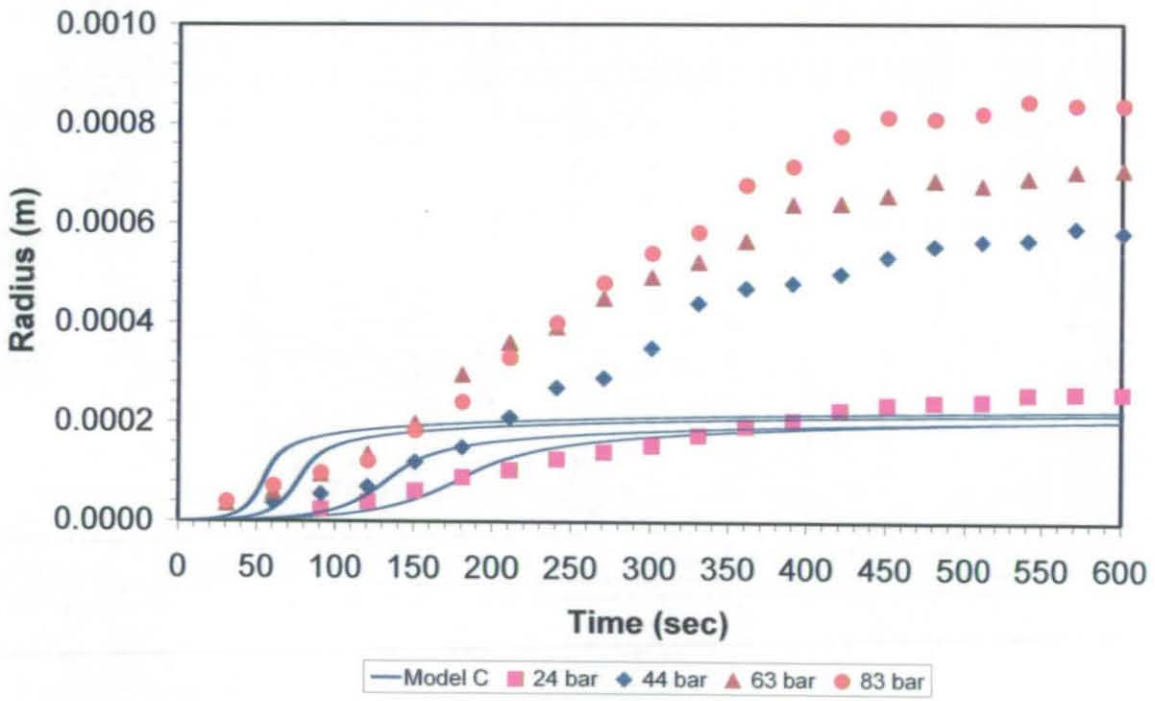

Figure 6 - 49: Model C versus experimental data for bubble growth at 100 °C (varying diffusivity and viscosity).

The model shows rapid bubble growth until reaches 150 sec, and then does not show any indication of growth. Therefore the model was improved by fitting the WLF equation to Sato et al.'s (2001) data for diffusivity at 100 °C (see Table 2-4). This is achieved for each pressure by plotting the diffusivity against concentration (obtained from the pressure value using Henry's law). The following figure illustrates theses fitted.

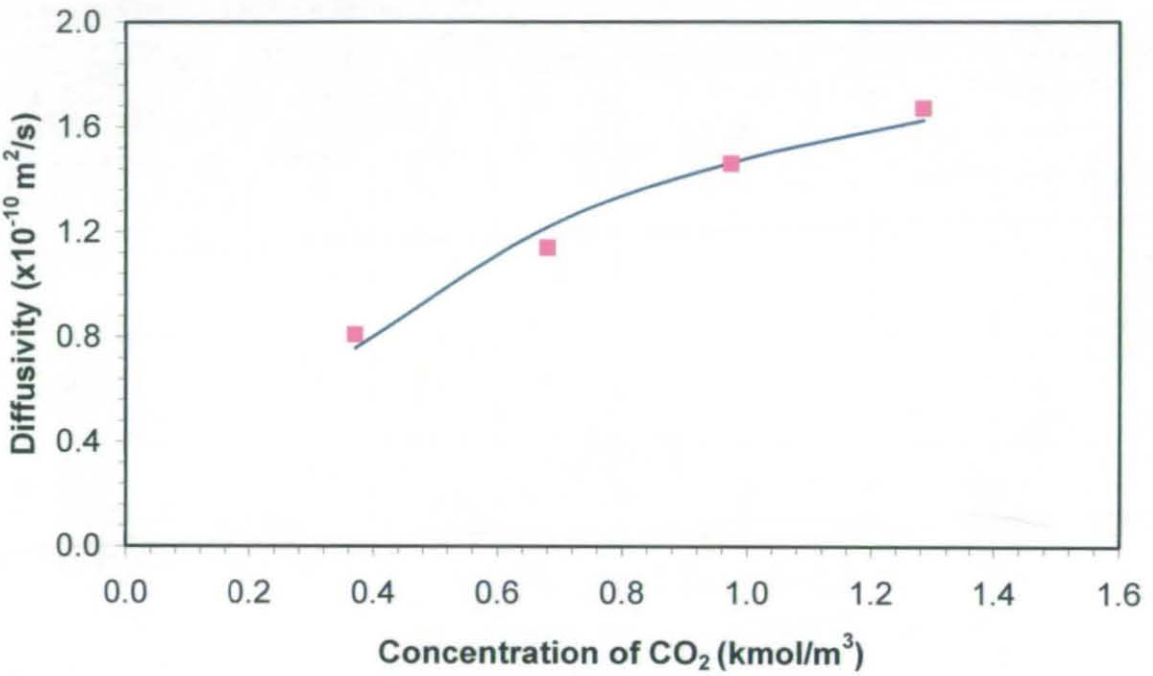

Figure 6 - 50: Fit (solid line) of the WLF equation to Sato et al.'s (2001) data for diffusivity at 100°C (■).

The following table (Table 6 -12) shows theses parameter values, and by keeping the same initial conditions showed in the previous Table 6-11:

Table 6 - 12: New parameter values based on a fit of the WLF equation to diffusivity data been used in the model calculated from Sato et al (2001).

Parameters	Values
D_o (x 10^{-12} m^2/s)	1.65
Constant of WLF equation c_1	2.14
Constant of WLF equation c_2, (K)	6.81

Table 6 – 13 shows the best fit of shear viscosity

Table 6 - 13: Model C best fit of shear viscosity values and Sato et al (2001) diffusivity values.

P_i	Diffusion coefficient [Sato et al 2001]		Best fitted of shear viscosity	
(bar)	Initial D (10^{-10} m^2 s^{-1})	D_o (x 10^{-12} m^2 s^{-1}) ($D = D_o / F$)	Initial μ (10^7 Pa.s)	μ_o (x 10^9 Pa.s) ($\mu = F * \mu_o$)
24	0.81	1.65	3.28	1.5
44	1.14	1.65	3.67	2.7
63	1.46	1.65	4.53	3.5
83	1.67	1.65	5.61	5.5

The model shows a very reasonable fit with our data by using realistic parameter values. The following figure compares the model C prediction with the experimental data of 100 °C and different pressures (24, 44, 63 and 83 bar) (see Figure 6 - 49).

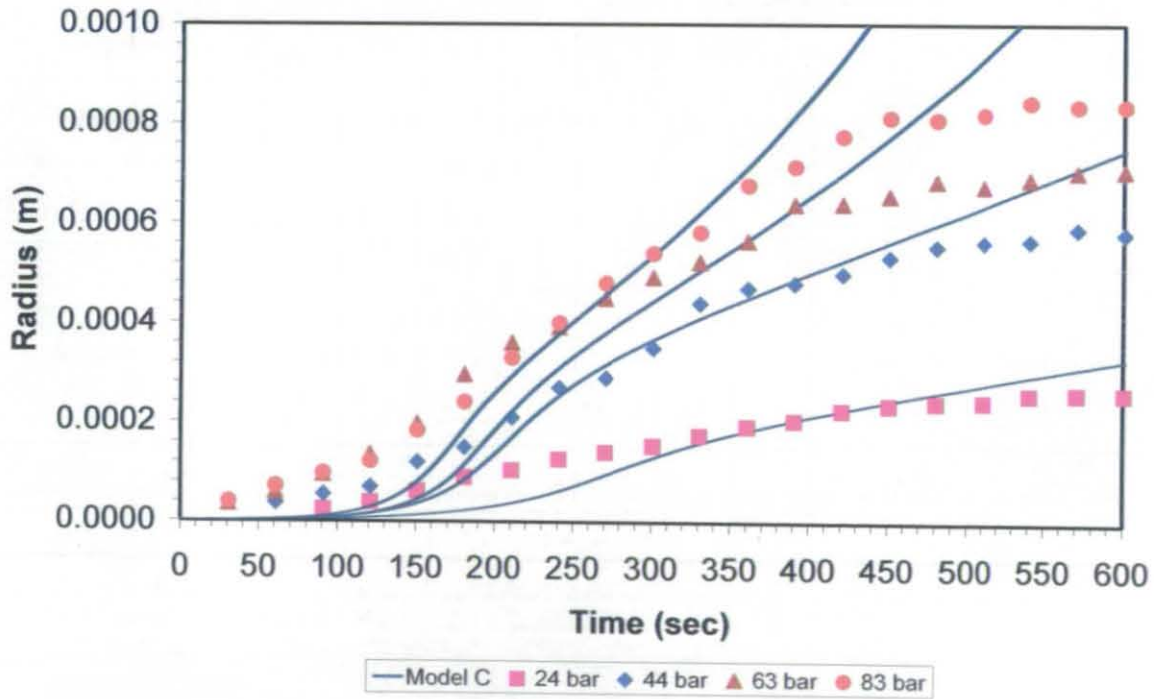

Figure 6 - 51: Model C versus experimental data for bubble growth at 100 °C.

6.4 Conclusion

The foaming behaviour of the polymer samples was measured on de-pressurization of the system. Generally, a higher percent swelling resulted from a higher pressure at the start of the depressurization. At higher initial pressures, more CO_2 is absorbed into the sample and thus the volume of bubbles is liable to be greater. When the bubble number was calculated for the all polymer, it was noted that all the polymers have the same trend, showing a big increase in the bubbles number with the increase in the gas pressure and this is because of the greater supersaturation.

To understand the process of bubble foaming and growth, experiments were performed in which these processes could be observed as they occur. These experiments were carried out in a high pressure view cell. Photographs of specimens during different stages of the experiment were analysed using image analysis software to provide data for bubble radius versus time. In these set of experiments only one polymer (PS) was tested to enable a more extensive study of the effect of process variables to be made. Different thicknesses (1 – 5 mm) of PS sample were tested under operation conditions of 100°C and 54 bar for 30 minutes. It was noted that with the thinnest (1mm) specimen it was easiest to observe individual bubbles.

To assess the time required for CO_2 to satisfactorily equilibrate in the sample, experiments were performed with different conditioning times of 30 to 180 minutes. As the conditioning time is increased up to 180 minutes it was seen that the radius of the foamed sample increased and there was less interstitial space between the bubbles. It can be seen that although the 180 minute sample gave the largest size it was only slightly larger than the 120 minute sample. Thus it was decided that the 120 minute conditioning time was sufficient for our experiments.

For the "in-house" prepared polymer samples where the majority of the surface was rough but a small amount was smooth and it was formed that bubble formation occurred preferentially where the surface was rough. This may be due to greater nucleation sites or faster diffusion into the rougher region. As such sample heterogeneity is undesirable in a

systematic study it was decided to perform future experiments using commercially bought samples (PS) of 1 mm thickness.

Three set of experiments were carried out at operating temperatures of 50, 70 and 100 °C each over a range of pressures from 24 to 120 bar. These conditions were chosen to coincide with literature data for diffusivity and Henry's law constant for use with the models. For the 100°C experiments the polymer will be in the rubbery state at the onset of depressurisation and much of the subsequent time period. However, most of the 50 °C experiments (below 100 bar) will be with the polymer entirely within the glassy state. These investigations will focus in bubble growth before and after the ambient pressure was reached.

Images during depressurisation at 50°C and with initial pressure up to 83 bar and at 70 °C at initial pressure up to 44 bar show no sign of any bubble formation. These correspond to conditions below the T_g of PS. However, at higher pressures bubbles start to appear after 30 sec, with maximum radius of 0.02 - 0.16 for 50 °C and 0.02 - 0.18 mm. The third set of experiments was performed at a higher temperature (100 °C) (above the T_g of PS) up to 120 bar. The nucleation appeared to occur randomly leading to subsequent bubble growth from these sites, with maximum radius of 0.02 - 0.83 mm. With more time the bubbles nucleate and grow, and the bubbles initially appear to be circular. As more bubbles form and grow in close proximity to each other, their shape is influenced by the impingement of surrounding neighbours leading to polygon shaped bubbles towards the end.

Only a few experimental investigations have addressed the bubble growth in polymer (CO_2/PS). These have been performed above the melting point of the polymer around 200°C and 20.6 bar [Han and Yoo 1981], 140 °C and 92 bar [Tuladhar and Mackley 2005]. Therefore only these two studies were compared with this work. The comparison shows that the growth rates in this work below the literature data, but it is very difficult to make direct comparisons because all the literature data used molten polymer and reduced the pressure suddenly, which resulted in much shorter experimental timescales about 10 sec.

Systematic foaming experiments were carried out by decompression of PS with CO_2 under controlled pressure and temperature. Foam microstructure and bubble size depended on the homogeneous mixing of polymer and gas in the compressed state and the pressure release rate during decompression. Three models were applied on the foaming experimental data. Model A assumes the growth is controlled by diffusion only which lets the growth happen very quickly without any viscous resistance, the fit is not good as the bubble is predicted to continue growing with increasing rapid bubble growth. Therefore model B and C were applied to assess whether a viscous model with surface tension can predict the growth.

Model B does not show good fit using the literature values of diffusivity, therefore reduced the diffusivity values did improve the model fit. The model (Model B) then showed reasonable fit, for the reduced diffusivity values, with our experimental data. Model C was then applied to assess whether a varying viscosity and diffusivity model with the WLF equation gave a better fit. Unfortunately, this model also does not show good fit. Therefore the model was further improved by fitting the WLF equation to Sato et al`s (2001) data for diffusivity at 100 °C. The model show very good agreement by using realistic parameter values.

Chapter 7 Conclusions & Recommendations

7.1 Conclusions

Two different aspects of polymer behaviour in the presence of high-pressure carbon dioxide have been investigated: softening and foaming.

7.1.1 Mechanical Measurement of Polymer Softening - Experimental Findings

The first study the glass transition (softening) temperature of four 2-3 mm thick polymer samples was mechanically measured, using a novel high pressure mechanical 3-point bend test rig equipped with a linear variable displacement transducer (LVDT) (with flat tip) to measure the central deflection whilst exposed to CO_2 at pressures of up to 120 bar. A stainless steel flat tip LVDT was initially used and while it is less sensitive to the surface softening than a sharp tip, it provides a good indication of the bending of a strip. However, the stainless steel LVDT is not the right material, because of the metal tip can heat up quickly, and this can result in a fast softening and melting of the polymer material conduct heat too quickly to the sample and cause localised heating which may cause spurious results. But with new improving this was improved in a second experimental setup, which used a nonconductive material (ceramic) with a pointed tip, which will not heat the polymer surface, and therefore will be better for identifying the T_g of a sample if scanning is used.

The nominal glass transition temperature was recorded as the onset temperature where the central deflection suddenly begins to increase. Significant reductions in the bending onset temperatures were observed on the application of carbon dioxide for polycarbonate (*Mw* 29 400, T_g 151.8 °C), poly(methyl-methacrylate) (Syndiotactic, *Mw* 179 000, T_g 110.8°C), Glycol modified poly(ethylene-terepthalate) (*Mw* 128 000, T_g 81 °C) and polystyrene (*Mw* 184 000, T_g 102.6 °C), of typically 50-100°C over the range of pressures applied (24 to120 bar). These polymer samples were chosen from all of the thermoplastic type. Their molecular weights were determined by the solution viscosity method, and T_g values by DSC. The polymers were supplied in sheets of different thickness: PC strips were 3 mm thick whereas PS, PETG and PMMA strips were 2 mm

thick.

This LVDT technique was able to detect surface softening temperatures which were similar to glass transition temperatures reported in the literature, this because of the new LVDT with ceramic pointed tip and the new conditions such as different scanning rates (0.2, and 0.5 °C/min) and isothermal tests.

7.1.2 Optical Measurement of Polymer Foaming - Experimental Findings

In a second system (Polymer foaming) specially constructed cylindrical view cell with 2 optical widows was used to take photographs of specimens during different stages of depressurisation. The photographs were analysed using image analysis software (Image J) to provide data for bubble radius versus time. In these set of experiments only one polymer (PS) was tested to enable a more extensive study of the effect of different process variables to be made. Different thicknesses (1 – 5 mm) of PS sample were tested under operation conditions of 100 °C and 54 bar for 30 minutes. It was noted that with the thinnest (1mm) specimen it was easiest to observe individual bubbles. It was also found that two hours was sufficient time for CO_2 to equilibrate with the polymer before depressurisation.

These investigations focussed on bubble growth both before and after ambient pressure were reached in the cell. Three sets of experiments were carried out according at three main operating temperatures (50, 70 and 100 °C) each over a range of pressures from 24 up to 120 bar. These conditions were chosen to coincide with conditions for which literature data for CO_2 diffusivity and the Henry's law constant for CO_2 solubility in PS were available to assist with the later modelling exercise. Images taken during depressurisation at 50 °C (from initial pressure up to 83 bar) and 70°C (from initial pressures up to 44 bar) showed no sign of any bubble formation. This corresponds to temperatures below the T_g of PS corresponding at the initial holding pressure of CO_2. However, at higher temperatures and high pressures bubbles appeared after 30 seconds, with maximum radii of 0.02 - 0.16 mm for 50 °C and 0.02 - 0.18 mm for 70 °C.

In the experiments at 100 °C (above the T_g line of PS) with pressures ranging from 24 to 120 bar the polymer will be in the rubbery state at the onset of depressurisation and much of the subsequent time period. The nucleation appeared to occur randomly leading to subsequent bubble growth from these sites. With time the bubbles grow, and the bubbles initially appear to be circular (with a maximum radius 0.02 mm). As more bubbles form and grow in close proximity to each other, their shape is influenced by the impingement of surrounding neighbours leading to polygon shaped bubbles towards the end with maximum radius of 0.83 mm.

In many cases bubbles were observed to keep growing even after the cell headspace had reached ambient pressure. This shows that the carbon dioxide pressure within the bubbles is higher than outside the polymer and so are not in equilibrium. In addition; it appears that bubble growth is influenced by three main factors forces; bubble impingement, amount of initial CO_2 in the polymer and the temperature in relation to the glass transition temperature (T_g). However, it appears that the glass transition is the most important factor as bubble growth at 100 °C was faster than at 70 °C even though more CO_2 is absorbed at 70 °C.

Only two previous experimental investigations have addressed bubble growth in the CO_2 / PS system. Therefore only these two studies were compared with this work. Both of these were performed near the melting point of the polymer around 200 °C and 20.6 bar [Han and Yoo 1981] and 140°C and 92 bar [Tuladhar and Mackley 2005]. It is very difficult to make direct comparisons with these studies as they foamed very quickly (about 10 sec) due to the higher temperatures used.

7.1.3 Insights Gained from Mathematical Modelling

Three mathematical models were used to interpret the data measured in this work:

(i) Diffusion coefficient can be estimated from temperature measured of onset of softening (T_A) and complete softening (T_B).

(ii) Polymer deflection is predicted as a function of line assuming it is a diffusion controlled process.

(iii) Bubble growth in polymer is predicted as a function of time based on three sets of assumption. These are:

  (a) Diffusion control (Model A)

  (b) Constant diffusivity and viscosity (Model B)

  (c) Diffusivity and viscosity varying in accordance with the Williams–Landel–Ferry (WLF) equation (Model C).

7.1.3.1 Diffusion Coefficient Estimation

Estimation of models for the diffusion of CO_2 in polymer strips have successfully been used to calculate the diffusivity of CO_2 into the polymers in both non-isothermal and isothermal experiments. In non-isothermal experiments diffusion coefficients were estimated by comparing the ratio of the decrease in the softening point by method T_B (gross softening) compared to that by method T_A (surface softening). The diffusivity average values of PC, PS, PETG and PMMA were found to be 0.73 x 10^{-10} m^2 /s, 0.82 x 10^{-10} m^2 /s, 0.68 x 10^{-10} m^2 /s, and 0.23 x 10^{-10} m^2/s respectively (at 20 to 120 bar and 25 to 160 °C). The average values of different scanning rate (0.2, 0.5, 1 °C/minute) of PS were found to be 2.03 x 10^{-10} m^2 /s, 1.9 x 10^{-10} m^2 /s, and 1.9 x 10^{-10} m^2 /s respectively (at 20 to 120 bar and 25 to 160 °C).

Further experiments were also performed to monitor the central deflection of the polymer strips with time at isothermal conditions. The average values of diffusivity for isothermal experiments at 50, 70 and 90 °C were found to be 7.6 x 10^{-10} m^2 /s, 5.6 x 10^{-10} m^2 /s and 7.0 x 10^{-10} m^2 /s respectively (at 20 to 120 bar).

Diffusion models for both non-isothermal and isothermal data provide realistic estimates of diffusion coefficients which suggest that diffusion is the major influence governing the softening of these polymer strips. However the variations of D formed suggest that the models are not complete description and that the viscous resistance of the polymers to sagging may also be an important factor. Variations in calculated diffusivity may also arise if the diffusivity varies with CO_2 concentration.

7.1.3.2 Deflection Model

The second model was an isothermal deflection model and it was successfully used to fit our experimental data. The model worked very well with longer times, but with at shorter times the model has small intervals but its faraway from the starting softening point (T_A), which we still can express the deflection. The resulting curves could be satisfaction by fitted to a deflection versus time model assuming that the stiffness of the strip is only significantly contributed to be the un-plasticised interior region, the size of which gradually reduces as diffusion proceeds.

7.1.3.3 Bubble Growth Model

Systematic foaming experiments were carried out by decompression of PS with CO_2 under controlled pressure and temperature. Foam microstructure and bubble size depended on the homogeneous mixing of polymer and gas in the compressed state and the pressure release rate during decompression. Three models were compared to apply on the foaming experimental data. Model A assumes the growth is controlled by diffusion only which lets the growth happen without any viscous resistance. Perhaps unsurprisingly the severely overpredicted bubble growth rates. Therefore model B was applied to assess whether a viscous model with surface tension can predict the growth more better accuracy.

Model B did indeed work better than model A with our experimental data. This is because model B was able to restrict growth by the viscosity and surface tension, but still the model fit was not good as it keep increasing and still overpredicted bubble growth.

It was found that better fits could be achieved if the diffusivity values were reduced, suggestion that diffusivity values might fall during foaming. Model C was applied to assess whether a viscous model by WLF equation with surface tension can better predict the bubble growth (following Chen et al 2006). Unfortunately, this model (Model C) also does not show good fit, because of the diffusivity and viscosity varying (WLF), which control the growth and need further work (see recommendation section). This model reduces both diffusivity and viscosity as the concentration of CO_2 falls. However, fits using the "Universal" WLF values for c_1 and c_2 did not produce good results. Therefore the model was then improved further by fitting the WLF equation to Sato et al`s (2001) data for diffusivity at 100°C. The model show reasonable agreement by using realistic parameter values It did not quite predict the final bubble sizes. This can be adjusted by varying the volume of polymer associated with each bubble, but this depends on bubble nucleation and is a difficult parameter to predict.

7.2 Recommendations

The isothermal deflection model can be further improved by:

i. Adding a viscous flow factor into the deflection model.

ii. Test the deflection model with different thickness of polymer strips when undergoing isothermal tests.

Further improvement to the bubble growth model by:

i. Predicting the volume of polymer per bubble by examining bubble nucleation.

ii. Make the extensional viscosity parameter extension thickening. However, this would add yet further parameters to the model.

References

ALESSI, P., CORTESI, A., KIKIC, I. and VECCHIONE, F., 2003. Plasticization of polymers with supercritical carbon dioxide: Experimental determination of glass-transition temperatures. *Journal of Applied Polymer Science,* **88**(9), pp. 2189-2193.

AMON, M. and DENSON, C.D., 1984. A Study of the Dynamics of Foam Growth - Analysis of the Growth of Closely Spaced Spherical Bubbles. *Polymer Engineering and Science,* **24**(13), pp. 1026-1034.

ARORA, K.A., LESSER, A.J. and MCCARTHY, T.J., 1998. Preparation and Characterization of Microcellular Polystyrene Foams Processed in Supercritical Carbon Dioxide. *Macromolecules,* **31**(14), pp. 4614-4620.

AUBERT, J.H., 1998. Solubility of carbon dioxide in polymers by the quartz crystal microbalance technique. *The Journal of Supercritical Fluids,* **11**(3), pp. 163-172.

BANERJEE, T. and LIPSCOMB, G.C., 1998. Direct measurement of the carbon dioxide-induced glass transition depression in a family of substituted polycarbonates. *Journal of Applied Polymer Science,* **68**(9), pp. 1441-1449.

BARLOW, E.J. and LANGLOIS, W.E., 1962. Diffusion of Gas from a Liquid into an Expanding Bubble. *IBM J,* **6**, pp. 329–337.

BERENS, A.R., HUVARD, G.S., KORSMEYER, R.W. and KUNIG, F.W., 1992. Application of Compressed Carbon-Dioxide in the Incorporation of Additives into Polymers. *Journal of Applied Polymer Science,* **46**(2), pp. 231-242.

BIRD, R.B., STEWART, W.E. and LIGHTFOOT, E.N., 1960. Transport phenomena.

BRANDRUP, J., IMMERGUT, E.H. and GRULKE, E.A. 1999. *Polymer Handbook.* 4th edn. New York ; Chichester : Wiley.

BROWN, M.E., GALLAGHER, P.K. and KEMP, R.B., 1998. Handbook of Thermal Analysis and Calorimetry. Elsevier.

BROWN, M.E., 2001. Introduction to Thermal Analysis : Techniques and Applications. 2nd edn. Springer: Dordrecht.

CALVERT, J.R. and FARRAR, R.A., 1999. An Engineering Data Book. New York, USA: Palgrave.

CHEN, X.P., FENG, J.J. and BERTELO, C.A., 2006. Plasticization effects on bubble growth during polymer foaming. *Polymer Engineering and Science,* **46**(1), pp. 97-107.

CHIOU, J.S., BARLOW, J.W. and PAUL, D.R., 1985. Plasticization of Glassy-Polymers by CO2. *Journal of Applied Polymer Science,* **30**(6), pp. 2633-2642.

CHRISTIAN, P., HOWDLE, S.M., GUEGEL, A., MANNERS, I. and MASSEY, J., 1997. Thermal Ring Opening Polymerization of a Silicon-bridged [1] Ferrocenophane in Supercritical Carbon Dioxide. *POLYMER PREPRINTS-AMERICA-,* **38**, pp. 434-435.

CLIFFORD, A., 1998. Fundamentals of supercritical fluids. Oxford.

COMYN, J., 1985. Polymer permeability. Elsevier Applied Science edn. London, UK.

CONDO, P.D. and JOHNSTON, K.P., 1992. Retrograde Vitrification of Polymers with Compressed Fluid Diluents - Experimental Confirmation. *Macromolecules,* **25**(24), pp. 6730-6732.

CRANK, J., 1975. The mathematics of diffusion. 2nd edn. Oxford, UK: Clarendon Press.

EAVES, D., 2004. Handbook of polymer foams. Shawbury: Rapra Technology.

EVERITT, S.L., HARLEN, O.G. and WILSON, H.J., 2006. Competition and interaction of polydisperse bubbles in polymer foams. *Journal of Non-Newtonian Fluid Mechanics,* **137**(1-3), pp. 60-71.

FENG, J.J. and BERTELO, C.A., 2004. Prediction of bubble growth and size distribution in polymer foaming based on a new heterogeneous nucleation model. *Journal of Rheology,* **48**(2), pp. 439-462.

FLICHY, N.M.B., KAZARIAN, S.G., LAWRENCE, C.J. and BRISCOE, B.J., 2001. Indentation of poly(methyl methacrylate) under high-pressure gases. *Journal of Polymer Science Part B-Polymer Physics,* **39**(23), pp. 3020-3028.

FRIED, J.R., LIU, H.C. and ZHANG, C., 1989. Effect of Sorbed Carbon-Dioxide on the Dynamic Mechanical-Properties of Glassy-Polymers. *Journal of Polymer Science Part C-Polymer Letters,* **27**(10), pp. 385-392.

GILBERT, M., 2005. *Course Handout.* Loughborough University, UK: Institute of Polymer Technology and Materials Engineering.

GLASSTONE, S. and LEWIS, D., 1960. Elements of physical chemistry. 2nd edn. Macmillan.

GOEL, S.K. and BECKMAN, E.J., 1995. Nucleation and Growth in Microcellular Materials - Supercritical CO2 as Foaming Agent. *AICHE Journal,* **41**(2), pp. 357-367.

GOEL, S.K. and BECKMAN, E.J., 1994. Generation of Microcellular Polymeric Foams using Supercritical Carbon-Dioxide .1. Effect of Pressure and Temperature on Nucleation. *Polymer Engineering and Science,* **34**(14), pp. 1137-1147.

GOOIJER, JESSE M. DE, 2002. Polymer modification in supercritical and subcritical fluids. Eindhoven: Proefschrift.

HAINES, P.J., 2002. Principles of Thermal Analysis and Calorimetry. Royal Society of Chemistry.

HAN, C.D. and YOO, H.J., 1981. Studies on Structural Foam Processing .4. Bubble-Growth during Mold Filling. *Polymer Engineering and Science,* **21**(9), pp. 518-533.

HANDA, Y.P., KRUUS, P. and ONEILL, M., 1996. High-pressure calorimetric study of plasticization of poly(methyl methacrylate) by methane, ethylene, and carbon dioxide. *Journal of Polymer Science Part B-Polymer Physics,* **34**(15), pp. 2635-2639.

HANDA, Y.P., ZHANG, Z.Y. and WONG, B., 1997. Effect of compressed CO_2 on phase transitions and polymorphism in syndiotactic polystyrene. *Macromolecules,* **30**(26), pp. 8499-8504.

IMAGE, J. Image processing and analysis in java [Homepage of Disclaimer], [Online]. Available: http://rsb.info.nih.gov/ij/ [12/1, 2006].

KAZARIAN, S.G., 2000. Polymer processing with supercritical fluids. *Polymer Science, Series C: Chemistry Reviews(USA),* **42**(1), pp. 78-101.

KAZARIAN, S.G., BRANTLEY, N.H., WEST, B.L., VINCENT, M.F. and ECKERT, C.A., 1997. In Situ Spectroscopy of Polymers Subjected to Supercritical CO_2: Plasticization and Dye Impregnation. *Applied Spectroscopy,* **51**(4), pp. 491-494.

KAZARIAN, S.G., BRANTLEY, N.H., WEST, B.L., VINCENT, M.F. and ECKERT, C.A., 1997. In situ spectroscopy of polymers subjected to supercritical CO2: Plasticization and dye impregnation. *Applied Spectroscopy,* **51**(4), pp. 491-494.

KENDALL, J.L., CANELAS, D.A., YOUNG, J.L. and DESIMONE, J.M., 1999. Polymerizations in supercritical carbon dioxide. *Chemical reviews,* **99**(2), pp. 543-563.

KLEMPNER, D. and FRISCH, K.C., 1991. Handbook of polymeric foams and foam technology. Hanser.

KOKTURK, G. and HOWDLE, S.M., 2002. 7th International Workshop on Polymer Reaction Engineering, 2002, Wiley-VCH.

LIANG, M.T. and WANG, C.M., 2000. Production of engineering plastics foams by supercritical CO2. *Industrial & Engineering Chemistry Research,* **39**(12), pp. 4622-4626.

MACKLEY, M.R., MARSHALL, R.T.J. and SMEULDERS, J.B.A.F., 1995. The Multipass Rheometer. *Journal of Rheology,* **39**(6), pp. 1293-1309.

MARTINACHE, J.D., ROYER, J.R., SIRIPURAPU, S., HENON, F.E., GENZER, J. and KHAN, S., 2001. Processing of polyamide 11 with supercritical carbon dioxide. *Industrial and Engineering Chemistry Research(USA),* **40**(23), pp. 5570-5577.

MARTINACHE, J.D., ROYER, J.R., SIRIPURAPU, S., HENON, F.E., GENZER, J., KHAN, S.A. and CARBONELL, R.G., 2001. Processing of polyamide 11 with supercritical carbon dioxide. *Industrial & Engineering Chemistry Research,* **40**(23), pp. 5570-5577.

MI, Y.L. and ZHENG, S.X., 1998. A new study of glass transition of polymers by high pressure DSC. *Polymer,* **39**(16), pp. 3709-3712.

MIYOSHI, T., TAKEGOSHI, K. and TERAO, T., 1997. C-13 high-pressure CPMAS NMR characterization of the molecular motion of polystyrene plasticized by CO_2 gas. *Macromolecules,* **30**(21), pp. 6582-6585.

MOREL, G. and PAUL, D.R., 1982. CO_2 Sorption and Transport in Miscible Poly(phenylene Oxide)-Polystyrene Blends. *Journal of Membrane Science,* **10**(2-3), pp. 273-282.

NEMEC, L. and KLOUZEK, J., 2003. Modelling of glass refining kinetics Part 1. Single bubbles. *Ceramics-Silikaty,* **47**(3), pp. 81-87.

NIKITIN, L.N., GALLYAMOV, M.O., VINOKUR, R.A., NIKOLAEC, A.Y., SAID-GALIYEV, E.E., KHOKHLOV, A.R., JESPERSEN, H.T. and SCHAUMBURG, K., 2003. Swelling and impregnation of polystyrene using supercritical carbon dioxide. *Journal of Supercritical Fluids,* **26**(3), pp. 263-273.

PANTOULA, M. and PANAYIOTOU, C., 2006. Sorption and swelling in glassy polymer. *Journal of Supercritical Fluids,* **37**(2), pp. 254-262.

POPE, M.I. and JUDD, M.D., 1977. Differential thermal analysis: a guide to the technique and its applications. London: Heyden.

RAMESH, N.S., RASMUSSEN, D.H. and CAMPBELL, G.A., 1994. The Heterogeneous Nucleation of Microcellular Foams Assisted by the Survival of Microvoids in Polymers Containing Low Glass-Transition Particles .1. Mathematical-Modeling and Numerical-Simulation. *Polymer Engineering and Science,* **34**(22), pp. 1685-1697.

ROTHMAN, L.B., ROBEY, R.J., ALI, M.K., MOUNT, D.J., IEEE and IEEE, 2002. Supercritical fluid processes for semiconductor device fabrication. 2002 *Ieee/semi Advanced Semiconductor Manufacturing Conference and Workshop,* , pp. 372-375.

ROYER, J.R., DESIMONE, J.M. and KHAN, S.A., 1999. Carbon dioxide-induced swelling of poly(dimethylsiloxane). *Macromolecules,* **32**(26), pp. 8965-8973.

SATO, Y., TAKIKAWA, T., TAKISHIMA, S. and MASUOKA, H., 2001. Solubilities and diffusion coefficients of carbon dioxide in poly(vinyl acetate) and polystyrene. *Journal of Supercritical Fluids,* **19**(2), pp. 187-198.

SATO, Y., YURUGI, M., FUJIWARA, K., TAKISHIMA, S. and MASUOKA, H., 1996. Solubilities of carbon dioxide and nitrogen in polystyrene under high temperature and pressure. *Fluid Phase Equilibria,* **125**(1-2), pp. 129-138.

SHENOY, S.L., FUJIWARA, T. and WYNNE, K.J., 2003. Quantifying plasticization and melting behavior of poly(vinylidene fluoride) in supercritical CO_2 utilizing a linear variable differential transformer. *Macromolecules,* **36**(9), pp. 3380-3385.

SHIEH, Y.T., SU, J.H., MANIVANNAN, G., LEE, P.H.C., SAWAN, S.P. and SPALL, W.D., 1996. Interaction of supercritical carbon dioxide with polymers. I. Crystalline polymers. *Journal of Applied Polymer Science,* **59**(4), pp. 695-705.

SHIEH, Y.T., SU, J.H., MANIVANNAN, G., LEE, P.H.C., SAWAN, S.P. and SPALL, W.D., 1996. Interaction of Supercritical Carbon-Dioxide with Polymers. II. Amorphous Polymers. *Journal of Applied Polymer Science*, **59**(4), pp. 707-717.

SHIM, J., CHANG, S. and PARK, S., 1997. Phase equilibria of supercritical fluid polymer systems, 1997, pp463–466.

SIRIPURAPU, S., GAY, Y.J., ROYER, J.R., DESIMONE, J.M., SPONTAK, R.J. and KHAN, S.A., 2002. Generation of microcellular foams of PVDF and its blends using supercritical carbon dioxide in a continuous process. *Polymer*, **43**(20), pp. 5511-5520.

STONG, C.L., 1973-last update, blowing plastic bubble [Homepage of the Amateur Scientist], [Online]. Available: http://www.sas.org/E-Bulletin/2003-12-19/labNotesAS/body.html [12/19, 2005].

TANG, M., DU, T.B. and CHEN, Y.P., 2004. Sorption and diffusion of supercritical carbon dioxide in polycarbonate. *Journal of Supercritical Fluids*, **28**(2-3), pp. 207-218.

TAYLOR, L.T., 1996. Supercritical fluid extraction. New York: Wiley.

THRONE, J.L., 1999. Understanding Thermoforming. Munich: Hanser.

TOMASKO, D.L., LI, H.B., LIU, D.H., HAN, X.M., WINGERT, M.J., LEE, L.J. and KOELLING, K.W., 2003. A review of CO_2 applications in the processing of polymers. *Industrial & Engineering Chemistry Research*, **42**(25), pp. 6431-6456.

TREYBAL, R.E., 1980. Mass-transfer operations. 3rd edn. New York ; London: McGraw-Hill.

TULADHAR, T.R. and MACKLEY, M.R., 2005. The development of polymer foam microstructure: experimental observations and matching modelling for polystyrene foams using different blowing agents, 10-14 July 2005 2005, Institution of Chemical Engineers (IChemE).

TULADHAR, T.R. and MACKLEY, M.R., 2004. Experimental observations and modelling relating to foaming and bubble growth from pentane loaded polystyrene melts. *Chemical Engineering Science*, **59**(24), pp. 5997-6014.

UGURAL, A.C., 1999. Stress in plates and shells. 2nd edn. New York ; London: McGraw-Hill.

VIETH, W.R., 1991. Diffusion in and through polymers : principles and applications. Munich: Hanser.

VOGT, B.D., RAMACHANDRARAO, V.S., GUPTA, R.R., LAVERY, K.A., FRANCIS, T.J., RUSSELL, T.P. and WATKINS, J.J., 2003. Phase behavior of polystyrene-block-poly(n-alkyl methacrylate)s dilated with carbon dioxide. *Macromolecules,* **36**(11), pp. 4029-4036.

WACS, Fourier Transform Infrared Spectroscopy (FTIR) - Introduction. Available: http://www.wcaslab.com/tech/tech2.htm [8 June 2006, 2006].

WANG, L.S. and GMEHLING, J., 1999. Improvement of SRK equation of state for vapor-liquid equilibria of petroleum fluids. *AICHE Journal,* **45**(5), pp. 1125-1134.

WANG, W.C.V., KRAMER, E.J. and SACHSE, W.H., 1982. Effects of High-Pressure CO_2 on the Glass-Transition Temperature and Mechanical-Properties of Polystyrene. *Journal of Polymer Science Part B-Polymer Physics,* **20**(8), pp. 1371-1384.

WEBB, K.F. and TEJA, A.S., 1999. Solubility and diffusion of carbon dioxide in polymers. *Fluid Phase Equilibria,* **158**, pp. 1029-1034.

WILLIAMS, M.L., LANDEL, R.F. and FERRY, J.D., 1955. Mechanical Properties of Substances of High Molecular Weight .19. the Temperature Dependence of Relaxation Mechanisms in Amorphous Polymers and Other Glass-Forming Liquids. *Journal of the American Chemical Society,* **77**(14), pp. 3701-3707.

WISSINGER, R.G. and PAULAITIS, M.E., 1991. Glass Transitions in Polymer CO_2 Mixtures at Elevated Pressures. *Journal of Polymer Science Part B-Polymer Physics,* **29**(5), pp. 631-633.

WISSINGER, R.G. and PAULAITIS, M.E., 1987. Swelling and Sorption in Polymer-CO_2 Mixtures at Elevated Pressures. *Journal of Polymer Science Part B-Polymer Physics,* **25**(12), pp. 2497-2510.

YOON, J.D. and CHA, S.W., 2001. Change of glass transition temperature of polymers containing gas. *Polymer Testing,* **20**(3), pp. 287-293.

ZHANG, Z.Y. and HANDA, Y.P., 1998. An in situ study of plasticization of polymers by high-pressure gases. *Journal of Polymer Science Part B-Polymer Physics,* **36**(6), pp. 977-982.

Nomenclature

b	width of the sample strips, (m)
c	concentration of CO_2 (at time t and distance x into the slab, (g/ml)
c_i	initial concentration of CO_2 in slab, (g/ml)
c_e	equilibrium concentration in slab (corresponding to infinite time), (g/ml)
c_g	concentration when the glass transition temperature (T_g) happens, (g/ml)
D	diffusion coefficient, (m^2/s)
D_o	coefficient in WLF equation for diffusivity (Eq. 4 – 49), (m^2/s)
d	thickness of the strip, (m)
E	modulus of elasticity (young's modulus)
E_a	activated energy, (K J/ kmol)
E'	storage modulus
E''	loss modulus
f	fraction of polymer volume inside the nodal radius
F_{Net}	rod net force on the sample, (N)
$F_{bouyancy}$	rod buoyancy, (N)
g	standard gravitational intensity, (N/kg)
H	Henry's constant, (bar)
I	moment of inertia, (m^4)
L	overall length, (m)
M	moles of CO_2
Mw	molecular weight of the polymer, (kg/kmol)
Mw_{CO2}	molecular weight of the carbon dioxide, (mol/m^3)
m	mass of the specimen, and mass of the rod, (N)
N_B:	number of bubbles
P	pressure, (bar)
P_c	absolute pressure, (Mpa)
P_i	initial pressure, (bar)
P_f	final pressure, (bar)
$\Re$	gas constant, (8.3145 J/mol K)
r	radius of a representative bubble, (m)

S	swelling ratio
t	time, (sec)
T_A	first softening point, (°C)
T_B	second softening point, (°C)
T_c	absolute temperature, (°C)
T_g	glass transition temperature, (°C)
$V_{polymer}$	polymer volume ($V_{Polymer}$), (m^3)
V_{bub}	volume of the bubble, (m^3)
V_{Rod}	rod volume, (m^3)
V_{Sphere}	volume of a representative bubble, (m^3)
V_i	volume of the specimen before foaming, (m^3)
V_f	volume of the specimen after foaming, (m^3)
ΔV	the different in the volume
V	molar volume, (m^3)
W	point load, (N)
x	depth of the strip, (m)
y	distance from surface, (m)
z	$1 / r^3$, (m^{-3})

Greek Letter

β	side group transition
$tan\ \delta$	representing the energy loss
δ	the phase difference
ρ	polymer density, (kg/m^3 , k mol/m^3)
ρ_{CO2}	Carbon dioxide density, (kg/m^3 , kg/mol)
μ	viscosity (shear viscosity), (Pa.s)
μ_o	viscosity in WLF equation for viscosity (Eq. 4 – 50), (Pa.s)
μ_{ext}	extensional viscosity, (Pa.s)
γ	surface tension (external stress), (N/m)
$\dot{\varepsilon}$	external strain rate
σ	stress
ε_{max}	strain

Appendix

Chapter 1

1.1 Experimental Setup

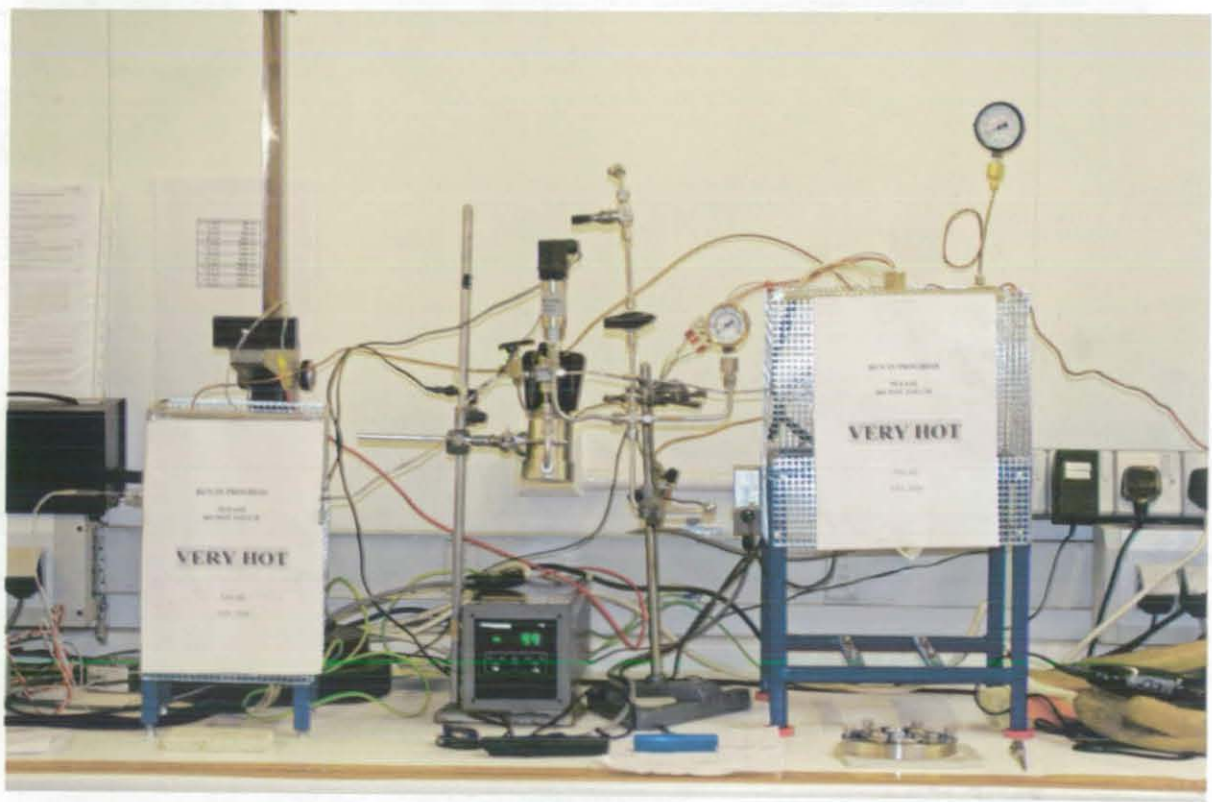

1.2 Polymer Softening and Polymer Foaming Units

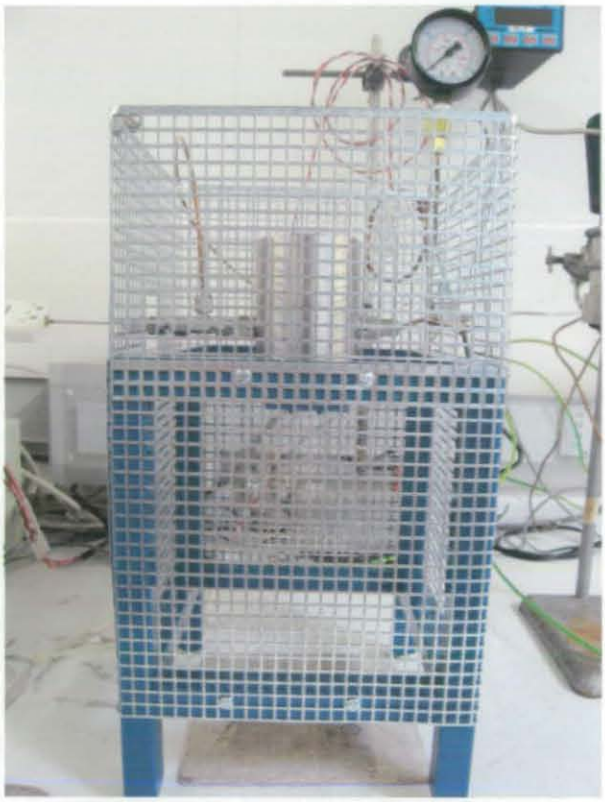

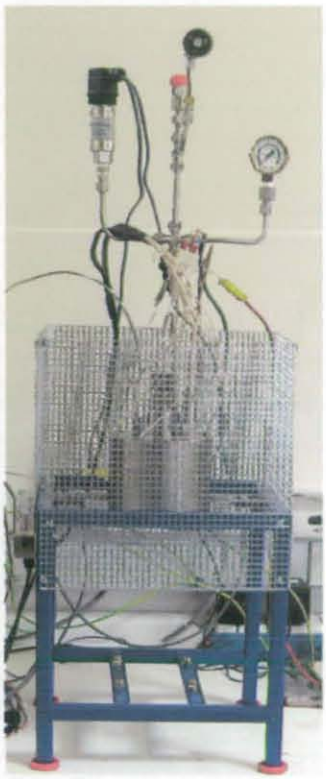

1.3 Pressure Control System

Chapter 2

2.1 Solubility of CO_2 in Polymers

2.1.1 Pressure Decay Method

The pressure decay method uses two chambers connected by a valve; one of the chambers contains a polymer sample. The test starts by charging the empty chamber with carbon dioxide to a measured pressure, and the chamber is then isolated. The next step is to open the value in between the two chambers for short time. The pressure in both chambers is measured over time. Knowing the volume of the two chambers it is possible to calculate the gas absorbed into the polymer sample from the variation of pressure in the two chambers.

Advantages:

(i) Is popular because
(ii) Simple and requires relatively simple equipment
(iii) Construction cost is not expensive.
(iv) Sensitive as the time available for the test

Disadvantages:

(i) Difficult to apply at high pressure especially for polymer melts (Because pressure sensors have suitable accuracy and small inner volumes are not available).
(ii) Need a large amount of sample (5 g) which result in long measurement times in the molten state.

2.1.2 Quartz Spring Method

The quartz spring balance is used to study the sorption by suspending the sample from the quartz spring in the view cell, which was then placed in the constant temperature bath and evacuated for 3 - 6 h. After the initial spring extension was measured, CO_2 was added to the cell, and the spring extension was measured periodically until the pressure stabilized and the spring extension reached a constant value.

2.1.3 Optically Monitoring Method

Another technique was presented for measuring the swelling and solubility of $scCO_2$ in polymer melts based on optically monitoring polymer swelling in real time. This provides information on the swelling kinetics, swelling equilibrium, and rates of CO_2 diffusion.

2.1.4 Gravimetric Measurements

Is performed to calculate the equilibrium sorption of polymer, the procedure is fellow:

(i) Sample is weighted before the run.

(ii) Sample placed inside the high pressure cell.

(iii) Charge the cell with CO_2 up to 90 bar.

(iv) Heat the cell up to 38 °C.

(v) Keep the sample under this condition until reaching the equilibrium.

(vi) Quick depressurisation (< 10 sec)

(vii) Transfer the sample to analytical balance (< 5 sec)

(viii) Recording the mass decrease due to desorption of CO_2 at room temperature.

(ix) Calculation then done by following equation of diffusion in both slab.

$$\frac{M_{(t)}}{M_0} = \frac{8}{\pi^2} \sum_{n=0}^{\infty} \frac{1}{(2n+1)^2} \exp\left(\frac{-(2n+1)^2 \pi^2 Dt}{l^2}\right.$$

where; $M_{(t)}$ is the sorption mass time, M_0 is the saturation amount of CO_2, D is the diffusivity and l is the thickness.

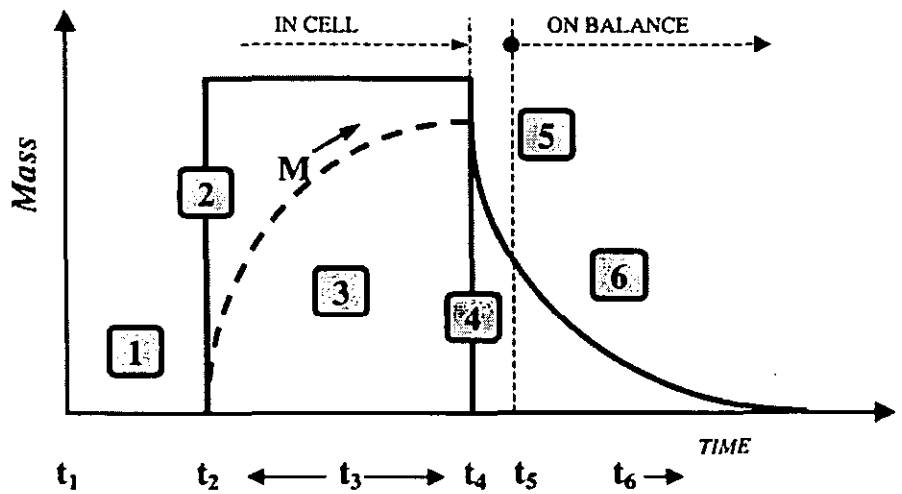

Gravimetric technique for polymer sorption and desorption processes. (1) Load film sample into high-pressure vessel (t_1); (2) apply CO_2 pressure (t_2 - the beginning of pressure increase); (3) process at polymer sorption of CO_2 (t_3); (4) rapid pressure release (t_4*/the finishing of pressure action); (5) transfer sample to balance (t_5 - the beginning of weighting process); (6) record weight during CO_2 desorption (t_6).

Advantages

(i) Temperature of the balance can be controlled independently

(ii) Can be proposing for solubility measured of high temperature.

Disadvantages

(i) Only used for gases tolerable (low) density

(ii) Study polymer melt with dense CO2 in supercritical state would be difficult.

2.1.5 Mass-Loss Analysis

Procedure:

(i) Wight the polymer sample

(ii) Place the sample in the cell

(iii) Charge the cell with CO2 pressure for equilibrium time.

(iv) Release the pressure very quickly.

(v) Weight the sample

(vi) Calculate the mass-loss by the following equation:

$$\frac{M_s}{M_\infty} = 1 - \frac{8}{\pi^2}\exp\left(\frac{-D_s\pi^2 t_s}{l^2}\right)$$

$$\frac{M_d}{M_\infty} = -\frac{4}{l}\sqrt{\frac{D_d t_d}{\pi}}$$

D_s *by plotting* $lin(1-\frac{M_s}{M_\infty})\ \alpha\ \left(\frac{t_s}{l^2}\right)$

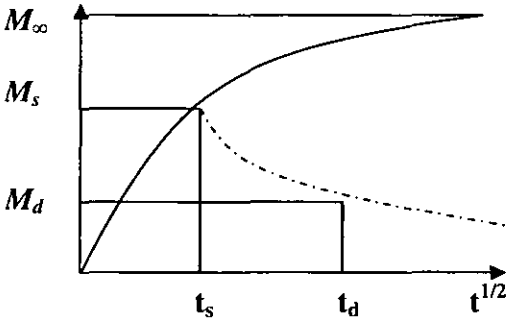

where: M_s is the sorption at t_s, M_∞ is the saturated sorption amount at large sorption time and M_d is the measured percentage weight loss during the desorption process.

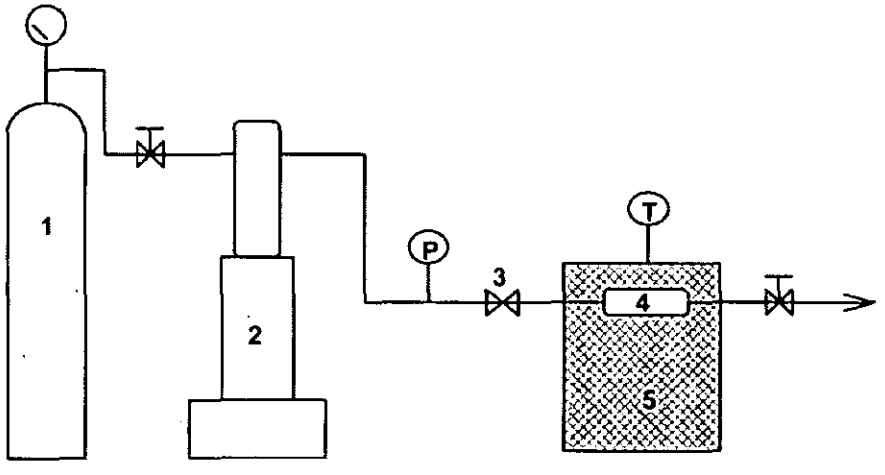

1: CO_2 tank

2: high pressure syringe pump (ISCO 100DX)

3: non-return valve

4: high pressure column

5: thermostatted vessel (ISCO SFX 2-10)

2.1.6 Electrobalance Method:

Advantages:

(i) Small amount of sample needed (short measurement times).
(ii) High sensitivity
(iii) Popular in solubility measurement at near room temperature.
(iv) Can use (placed) in the pressure vessel.

Disadvantages:

(i) Measurement is limited to temperature below 125°C due to the microbalance operating condition.

2.2 Diffusivity of CO_2 in Polymers

2.2.1 Mass-Loss Analysis

(See Solubility section)

2.2.2 Gravimetric Method

(See Solubility section)

2.2.3 Magnetic Suspension Balance (MSB)

Advantages:

(i) Similar to microbalance advantages.
(ii) Accurate for measurement of fluid densities.
(iii) The sample and the balance are isolated.
(iv) Suitable for measurement of gas solubility & diffusivity in polymer at high temperature and high pressure.
(v) Can use for gas in solid polymer.
(vi) Pressure up to 350 bar and temperature up to 250°C.
(vii) Can be calibrated during measurement.

Procedure:

(i) An electronically controlled magnetic suspension coupling is used to transmit the measurement force from the sample enclosed in a pressure vessel to a microbalance.
(ii) Suspension magnet is used for the transmitting the force consists of a permanent magnet, a sensor core and a device for decoupling the measuring load.
(iii) Electromagnet which is attached underfloor weighting hook of balance.
(iv) Using magnetic suspension coupling, the measuring force is transmitted contactless from the measuring champer to the microbalance, which is located outside the champer under ambient atmospheric conditions.

$$\frac{W_{g(t)} - W_{g(0)}}{W_{g(\infty)} - W_{g(0)}} = 1 - \frac{8}{\pi^2} \sum_{n=0}^{\infty} \frac{1}{(2n+1)^2} \exp\left[\frac{-(2n+1)^2 \pi^2 D t}{4 l^2}\right]$$

where; $W_{g(t)}$ amount of the gas in polymer at time t

2.2.4 Time Absorption Method

Is performed to calculate the equilibrium sorption of polymer, the procedure is fellow:

(i) Loaded the polymer sample to the vessel.

(ii) Charge the vessel by CO_2 for a specified time period.

(iii) Maintains the temperature to 40 °C and pressure up to 105 bar.

(iv) Depressurised the vessel very quickly

(v) Transfer the polymer sample to a balance

(vi) The weight loss is monitoring as function of time.

(vii) Weight loss and the time data recorded until no further weight loss.

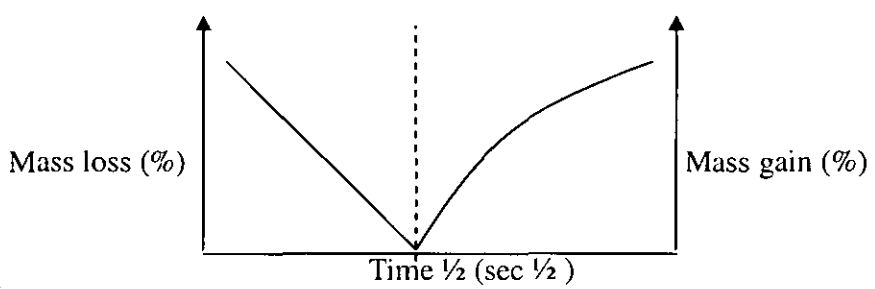

(viii) Calculate the diffusion by Fickian equation through a flat plate

$$\frac{M_{(t)}}{M_{(\infty)}} = 4\left(\frac{Dt}{\pi l^2}\right)^{1/2}$$

where; $M_{(t)}$ is the mass gain, $M_{(\infty)}$ maximum mass gain, D diffusivity, t is the time and l is the thickness.

2.3 Plasticisation of CO_2 in Polymers

2.3.1 Creep Compliance

Measuring the strain of the sample by applying weight load

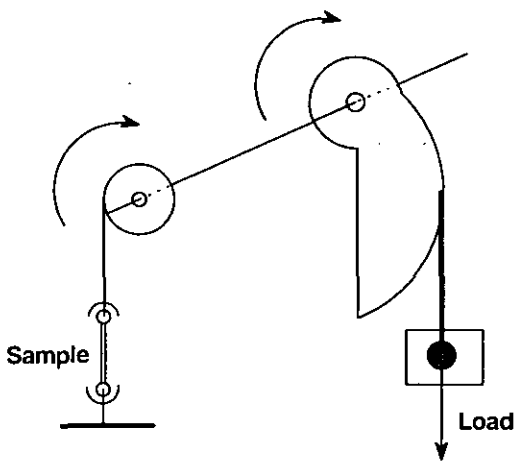

The creep compliance of a polymer $J_{(t)}$ in the presence of CO_2, at constant temperature and pressure, is time dependent as reported in the following equation: $J(t) = \frac{\varepsilon_{(t)}}{\sigma_0}$ where; σ_0 is the applied tensile stress and $\varepsilon_{(t)}$ is the strain at the time t. Wang et al (1982), a nonmagnetic screw rod is connected at end of the movable part and a linear variable differential transformer (LVDT) is connected to the other end. The lower core is used for measuring the strain of the PS sample by monitoring the displacement of the movable part of the strain frame after the top has been released.

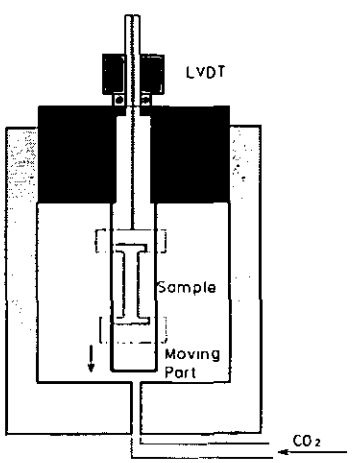

2.3.2 Inverse Gas Chromatography (IGC)

First used by Guillet in 1969. These days is presented as suitable techniques for study the plasticisation of CO_2 on polymers. IGC is technique based on the partition of a volatile solute between a mobile gas phase and stationary phase, liquid or solid.

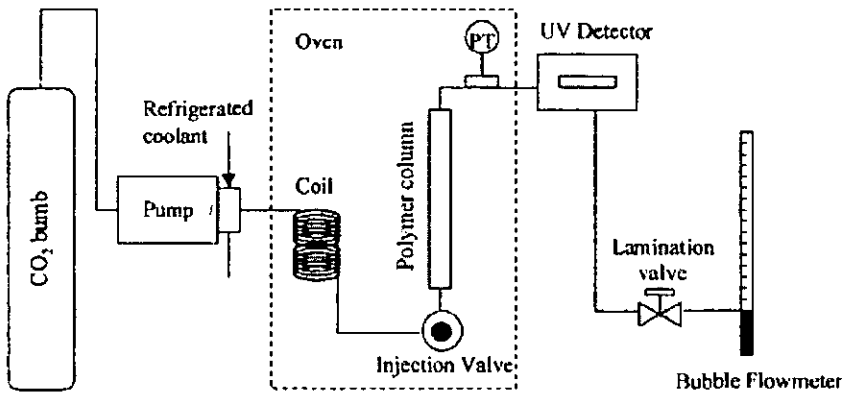

Analysis gas Chromatography

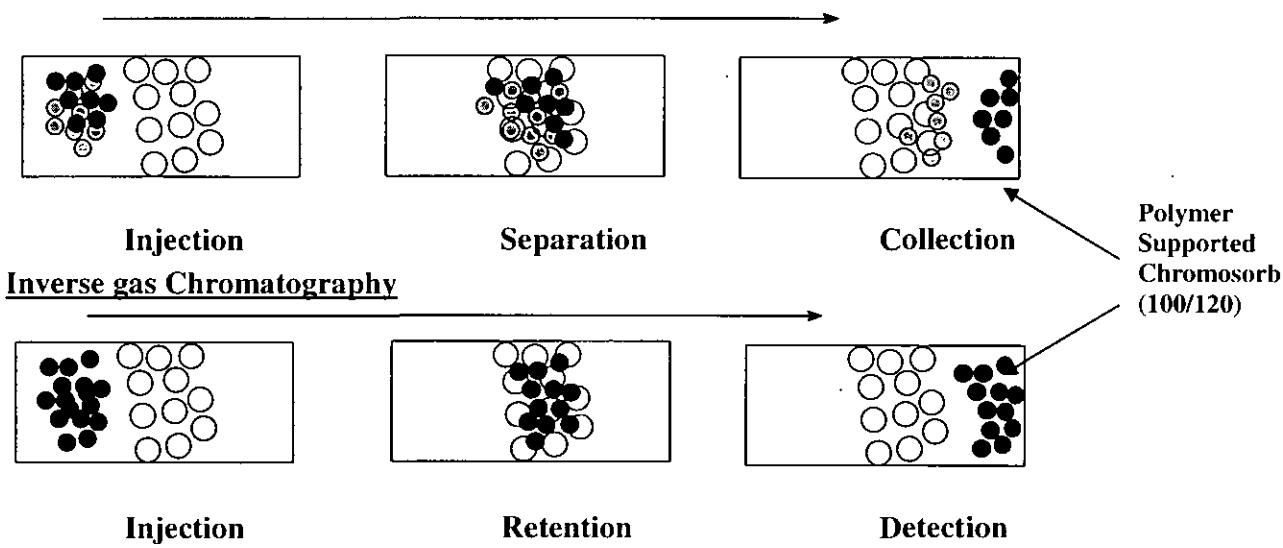

Partition coefficient, $K_s = \frac{V_N}{W_S}$ where V_N is the retention volume and W_s is the mass of sample.

Specific retention volume of injected, $V_g = \frac{F_m}{w} j \frac{P_0 - P_{H2O}}{760} \frac{273}{T_a}(t_R - T_a)$

where; F_m is mobile gas phase, w stationary phase weight, P_0 outside column pressure, T_a flow meter temperature, (T_g and T_m also can characteristic), P_{H2O} water vapour pressure, t_a inter retention time and j is the James Martin factor

2.3.3 Hardness of Polymers

Tests are used to determine the resistance of materials to deformation (twist or bend). There are three type of hardness:

(i) Scratch hardness: resistance to plastic deformation due to frication from a sharp object.

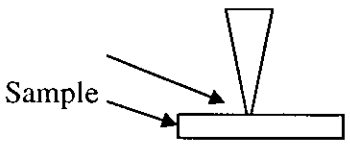

(ii) **Indentation** (groove) **hardness**: resistance to plastic deformation due to a constant load from a sharp object.

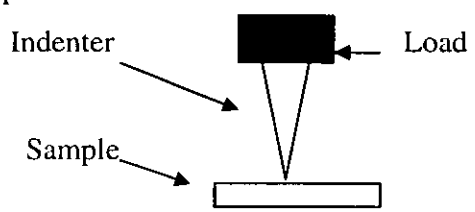

(iii) Rebound (jump back) hardness: high of the bounce of on object dropped on the materials.

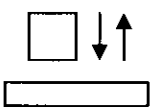

Deformation – Change in the shape due to an applied force.

2.3.4 Polymer Configuration Types

Isotactic

In isotactic macromolecules all the substituents are located on the same side of the macromolecular backbone. Isotactic polymers are usually semicrystalline and often form a helix configuration.

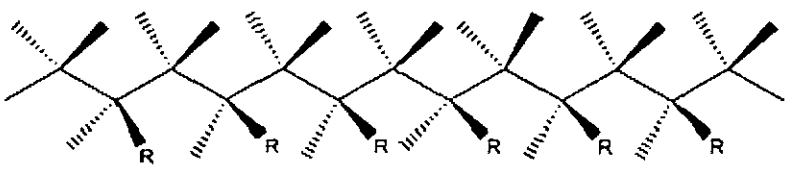

Syndiotactic

In syndiotactic or syntactic macromolecules the substituents have alternate positions along the chain.

Atactic

In atactic macromolecules the substituents are placed randomly along the chain.

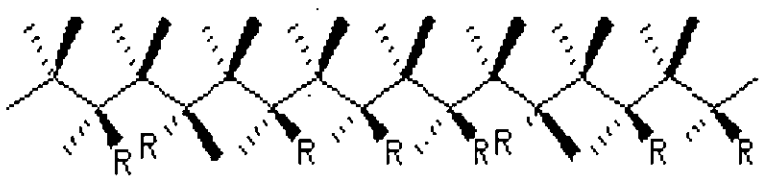

Cis and Trans

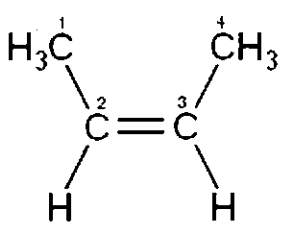

Cis

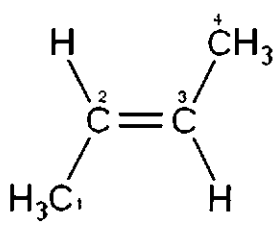

Trans

2.3.5 Stress and Strain

Stress;
measure the average amount of force exerted per unit area.

$$\sigma_0 = \frac{F}{A} \text{ (Pa)}$$

where; σ is the average stress, F is the force and A is the area.

Strain;
is the geometrical expression of deformation caused by the action of stress on physical body.

$$\varepsilon = \frac{\partial l}{l_0} = \frac{l - l_0}{l_0}$$

where ε is the strain in measured direction, l is the current length of the material and l_0 is the original length of the material

Chapter 3

3.1 Temperature Controller - Eurotherm (Type 812)

Programmer Parameters:

Parameters	Code	Setting Ranges	Setting Values
Ramp Rate 1	r_1	0.1 - 999.9 unit/min	**0.1**
Level 1	L_1	1 – 200 °C	**120**
Dwell 1	d_1	0 – 999.9 min	**0.1**
Ramp Rate 2	r_2	0.1 - 999.9 unit/min	**0.1**
Level 2	L_2	1 – 200 °C	**120**
Dwell 2	d_2	0 – 999.9 min	**1.0**
Loop Counter	L_C	1 - 100	**1.0**

Controller Parameters:

Parameters	Code	Setting Ranges	Setting Values
Alarm	A_L	1 - 50 °C	**50**
Proportional Band	P_b	0.5 – 50 %	**2.5**
Integral Time (sec)	t_1	Off – 1700 sec	**Off**
Derivative Time (sec)	t_d	Off – 180 sec	**Off**
Cycle Time	H_C	0.3 – 80 sec	**20**
Maximum Power	H_L	0 – 100 %	**100**

3.2 LVDT Calibration (Type sm3)

Displacment (mm)	Tranducer Voltage (10^3 mV)	
12	2337.16	2.33716
12.5	1868.62	1.86862
13	1293.7	1.2937
13.5	780.9	0.7809
14	248.26	0.24826
14.5	-220.57	-0.22057
15	-933.93	-0.93393
15.5	-1418.25	-1.41825
16	-1821.89	-1.82189
16.5	-2247.12	-2.24712

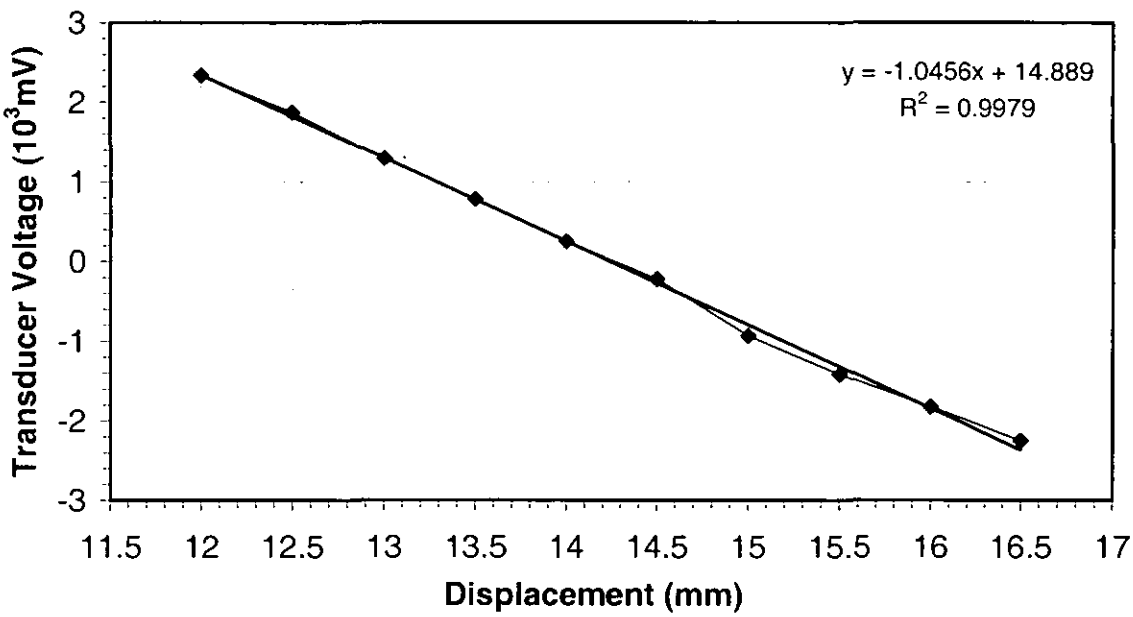

3.3 LVDT Calibration (New Type mach 1)

Transducer Voltage (mv)	(10^3mv)	Digital Calliper (mm)
2.67	0.00267	16.97
87.08	0.08708	16.48
146.1	0.1461	16.19
366.02	0.36602	15.03
522.13	0.52213	14.15
637.52	0.63752	13.56
847.28	0.84728	12.56
1022.01	1.02201	11.52
1237.66	1.23766	10.5
1423.55	1.42355	9.52
1708.4	1.7084	8.06
1909.17	1.90917	7.06
2133.676	2.133676	5.924
2358.182	2.358182	4.788
2457.5	2.4575	3.97

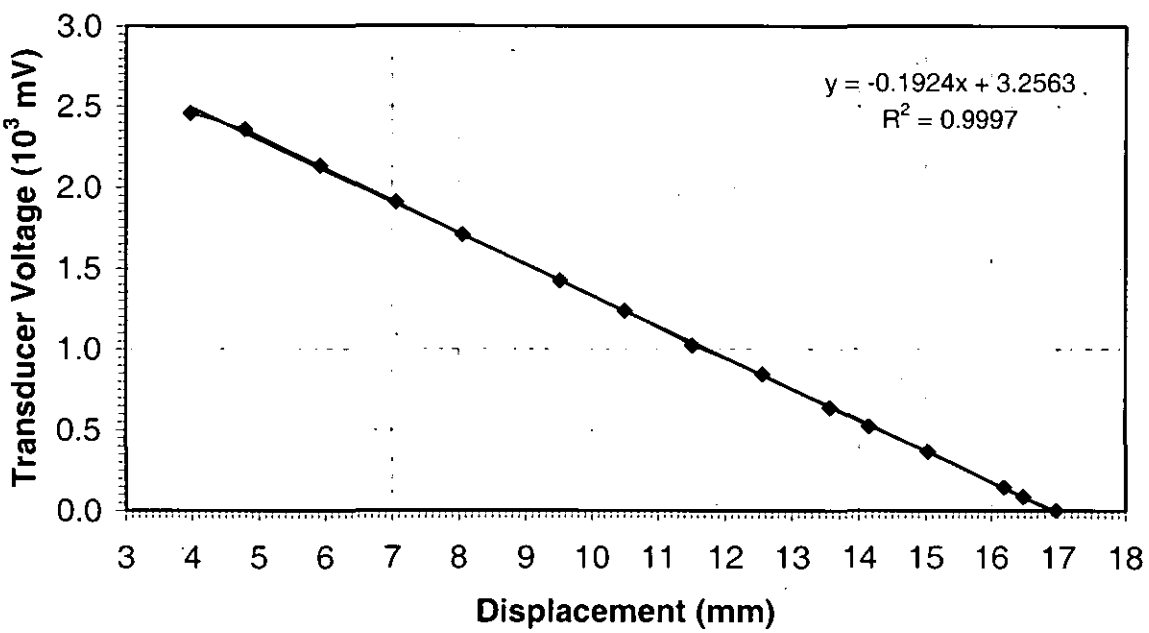

3.4 LVDT Core Net Force

3.4.1 CO_2 Molar Density Calculation

Soave Redlich Kwong

Pc (Pa)	7382000	w	0.2373
Tc (K)	304.2	m	0.8436
R (J/kmolK)	8314		
a	266766		
b	0.02968		

Temp (°C)	Desired pressure (bar)	Temp (K)	IG molar volume	Molar volume (m3/kmol)	Actual pressure (Pa)	Mass density (kg/m3)
150	149.9991	423.15	0.3426062	**0.1977682**	1.5E+07	222.483

Molar density (kmol/m^3)

Temperature (°C)		Pressure	1	21	41	55	71	86	101	121
20	293.15		0.04124508	0.978068565	2.279484604	3.828111	15.48554	16.3113	16.93546	17.59809
25	298.15		0.04054188	0.9537801	2.182699592	3.497944	13.85633	15.14608	15.97351	16.7891
30	303.15		0.03986265	0.931046163	2.098233188	3.263015	6.249421	13.67125	14.86753	15.90428
35	308.15		0.03920609	0.909641586	2.023324136	3.079637	5.061524	11.47633	13.55084	14.9275
40	313.15		0.03857107	0.889434918	1.956112723	2.929078	4.542943	7.895625	11.91367	13.84071
45	318.15		0.03792247	0.87031296	1.895217645	2.80139	4.197748	6.336749	9.923317	12.63275
50	323.15		0.03733374	0.852177618	1.839606167	2.690681	3.937764	5.609009	8.178863	11.3293
55	328.15		0.03676332	0.834943311	1.788481129	2.593021	3.729204	5.138311	7.085834	10.04112
60	333.15		0.03621039	0.818534933	1.741213764	2.505769	3.555213	4.79178	6.381941	8.926844
65	338.15		0.03567417	0.802886184	1.697299022	2.426998	3.406295	4.518535	5.880776	8.051594
70	343.15		0.03515394	0.787938354	1.656324895	2.355279	3.276208	4.293643	5.49726	7.379604
75	348.15		0.034649	0.773639071	1.617913313	2.289515	3.160928	4.103093	5.189167	6.854134
80	353.15		0.03415872	0.759941508	1.581868671	2.22885	3.057557	3.938054	4.933104	6.431495
85	358.15		0.03368249	0.746832434	1.547893313	2.172597	2.963977	3.792887	4.71492	6.08239
90	363.15		0.03321971	0.734199571	1.515783409	2.1202	2.878593	3.663509	4.525356	5.787462
95	368.15		0.0327345	0.722042502	1.485363546	2.071176	2.800164	3.547003	4.358319	5.533648
100	373.15		0.0322939	0.710378531	1.456481599	2.025207	2.727714	3.441184	4.209308	5.311838
105	378.15		0.03186505	0.699129225	1.429004775	1.981929	2.660421	3.344379	4.075062	5.115597
110	383.15		0.03144748	0.68828468	1.402816496	1.941072	2.59773	3.255272	3.953117	4.940114
115	388.15		0.03104076	0.677820515	1.377828268	1.902402	2.539049	3.172791	3.841568	4.781791
120	393.15		0.03064448	0.667714743	1.353892089	1.865719	2.483937	3.096146	3.738914	4.637862
125	398.15		0.03025823	0.657947099	1.330982912	1.830841	2.432022	3.024591	3.643951	4.506131
130	403.15		0.02988164	0.648498946	1.309024684	1.797635	2.382972	2.957548	3.5557	4.384939
135	408.15		0.02951436	0.639353109	1.28794948	1.765946	2.336551	2.894531	3.473353	4.272827
140	413.15		0.02915604	0.630493726	1.267696335	1.735634	2.292485	2.835125	3.39624	4.168662
145	418.15		0.02880636	0.621909399	1.248210523	1.706699	2.250569	2.778977	3.323744	4.071465
150	423.15		0.02846502	0.613568531	1.229409218	1.678863	2.210651	2.725781	3.255465	3.980552
155	428.15		0.02813173	0.605477238	1.211283867	1.652221	2.172541	2.675268	3.190956	3.89512
160	433.15		0.02780619	0.597620338	1.193792732	1.626596	2.136107	2.627187	3.129862	3.814703

3.4.2 LVDT Core net Force Calculation

$F_{net} = M \cdot g - F_{Buoyancy}$

$F_{Buoyancy} = \rho_{CO2} \times Mw_{CO2} \times V_{Road} \times g$

Mw_{CO2}	44	g/mol		
M_{Rod}	6	g		
g	0.009806	N/g	9.806	N/kg
F = M . g				
F	0.058836	N		
$V_{Road} = \pi r^2 L$				
r	0.0048	m		
L	0.06	m		
V	4.34294E-06	m^3	4.34294E-06	
ρ_{CO2}	16.31	mol/m^3	at 1 bar and 25 °C	
$F_{Buoyancy}$	3.0562E-05	N		
F_{net}	0.058805438	N	at 1 bar and 25 °C	

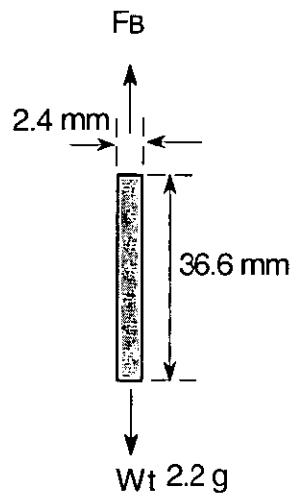

The density of CO_2 which present in the table is calculated by th SRK equation (equation of the state) at 25 °C

ρ ($kmol/m^3$)	0.041245082	0.978068565	2.279484604	3.8281	15.4855	16.311	16.935	17.598093
ρ (mol/m^3)	41.24508167	978.068565	2279.484604	3828.1	15485.5	16311	16935	17598.093

P (bar)	ρ (mol/m^3)	$F_{buoyancy}$ (N)	F_{Net} wet (N)
0	41.24	7.72764E-05	0.058758724
20	978.06	0.00183271	0.05700329
40	2279.48	0.004271338	0.054564662
54	3828.11	0.007173194	0.051662806
70	15485.54	0.029017134	0.029818866
85	16311.3	0.030564461	0.028271539
100	16935.46	0.031734025	0.027101975
120	17598.09	0.032975675	0.025860325

0.0329 0.0329

3.5 Materials Characterisation – Molecular Weight (*Mw*)

3.5.1 Polycarbonate:

PC

Dichloromethane η_o @ 20 °C (0.44 cP) = 0.00044 kg/m.s supplier **Fisher Scientific UK**
http://www.fisher.co.uk/index.htm

K = 0.0299 l/kg
α = 0.74 1/α 1.35135135

$$\frac{\eta}{\eta_0} = \frac{t}{t_0} \qquad \frac{\eta_{sp}}{c} = KM^{a} \qquad \frac{(\eta/\eta_0)-1}{c} = KM^{a}$$

or $$[\eta] = \frac{\eta - \eta_0}{\eta_0 c} \qquad \frac{\eta - \eta_0}{\eta_0 c} = KM^{a}$$

Dichloromethane
η_o (kg/m.s) 0.00044
time (sec), t_o 32

Randrup J, et al Polymer Handbook 4th edition 1999

Polymer (PC)	0.3g/100ml	0.5g/100ml	0.7g/100ml	1g/100ml
c (kg/l)	0.00309	0.00517	0.00708	0.0101
time (sec)	38	42	46	52
	38	42	46	51
	38	42	46	52
time (sec)	38	42	46	51.6666667

η (kg/m.s)	0.0005225	0.0005775	0.0006325	0.00071042
η_{sp} (kg/m.s)	0.1875	0.3125	0.4375	0.61458333
η_{sp}/c	60.67961165	60.44487427	61.7937853	60.849835

0.3	0.3
0.5	0.5
0.7	0.7
1	1
	Mean

c	η_{sp}/c
0.3	60.679612
0.5	60.444874
0.7	61.793785
1	60.849835
Mean	60.53

M	29374.6214

$$M = \left(\frac{\eta_{sp}}{c}\frac{1}{K}\right)^{1/a}$$

29472.779

3.5.2 Polystyrene:

PS

The proposed value for the viscosity of liquid toluene at 298.15 K and 0.1 MPa is =554.2±3.3 μPa.s Santos et al 2006

Toluene η_o @ 25 °C = **0.000554** kg/m.s | 0.00059542 from sheet 2 Asseal 1999

Glasstone S. and Lewis D.Elements of physical chemistry, p.597.196(

K (m3/kg) = 3.70E-05 **0.037 l/kg**

α **0.62** 1/α = **1.61290323**

$$\frac{\eta}{\eta_0} = \frac{t}{t_0} \qquad \eta_{sp} = \frac{\eta - \eta_0}{\eta_0} \qquad \frac{\eta_{sp}}{c} = KM^{a}$$

Toluene

η_o (kg/m.s) **0.000554**

time (sec), t_o **55**

Polymer (PS)	**0.3g/100ml**	**0.5g/100ml**	**0.7g/100ml**	**1g/100ml**
c (kg/l)	0.003	0.005	0.007	0.01
time (sec)	66.6	73.2	81.6	93.6
η (g/cm.s)	0.000670844	0.000737324	0.00082193	0.00094281
η_{sp} (g/cm.s)	0.210909091	0.330909091	0.48363636	0.70181818
η_{sp} / c	70.3030303	66.18181818	69.0909091	70.1818182

c	η_{sp} / c
0.003	70.30303
0.005	66.181818
0.007	69.090909
0.01	70.181818
Mean	68.054

M	**184317.9508**

$$M = \left(\frac{\eta_{sp}}{c}\frac{1}{K}\right)^{1/a}$$

3.5.3 Glycol modified poly(ethylene-terephthalate):

PETG

Dichloromethane η_o @ 45 °C (0.834 cP) = 0.000834 kg/m.s supplier **Fisher Scientific UK**
http://www.fisher.co.uk/index.htm

K = 0.4 l/kg
α = 0.5 1/α 2 **Randrup J, et al Polymer Handbook 4th edition 1999**

$$\frac{\eta}{\eta_0} = \frac{t}{t_0} \qquad \frac{\eta_{sp}}{c} = KM^{a} \qquad \text{or}$$

$$\frac{(\eta/\eta_0)-1}{c} = KM^{a} \qquad [\eta] = \frac{\eta - \eta_0}{\eta_0 c} \qquad \frac{\eta - \eta_0}{\eta_0 c} = KM^{a}$$

Dichloroacetic acid

η_o (kg/m.s)	0.000834
mint	1.38
time (sec), t_o	82.8

Polymer (PC)	0.3g/100ml	0.5g/100ml	0.7g/100ml	1g/100ml
c (kg/l)	0.00318	0.00517	0.00708	0.0101
time (sec)	120	42	150	201
	121.2	42	141	200.4
	120	42	140.4	200.4
time (sec)	120.4	145	168	200

η (kg/m.s)	0.001212725	0.001460507	0.00169217	0.00201449
η_{sp} (kg/m.s)	0.45410628	0.751207729	1.02898551	1.41545894
η_{sp} / c	142.800717	145.3013016	145.336936	140.144449

c	η_{sp} / c
0.00318	142.80072
0.00517	145.3013
0.00708	145.33694
0.0101	140.14445
Mean	143.39585

M	128514.813

$$M = \left(\frac{\eta_{sp}}{c}\frac{1}{K}\right)^{1/a}$$

3.5.4 Poly(methyl-methacrylate):

PMMA

Acetone η_o @ 25 ^{0}C (0.31 cP) = **0.00031** kg/m.s

PRESS. Handbook of Chemistry and Physics 1980.pp F52.

K = **0.0053** l/kg

α = 0.73 1/α **1.36986301**

Randrup J, et al Polymer Handbook 4th edition 1999, pp VII-68

$$\frac{\eta}{\eta_0} = \frac{t}{t_0} \qquad \frac{\eta_{sp}}{c} = KM^{a}$$

$$\frac{(\eta/\eta_0)-1}{c} = KM^{a} \qquad [\eta] = \frac{\eta - \eta_0}{\eta_0 c} \qquad \frac{\eta - \eta_0}{\eta_0 c} = KM^{a}$$

Acetone

η_o (kg/m.s)	**0.00031**
time (sec), t_o	**37**

Polymer (PMMA)	**0.3g/100ml**	**0.5g/100ml**	**0.7g/100ml**	**1g/100ml**
c (kg/l)	**0.003**	**0.005**	**0.007**	**0.01**
time (sec)	41	43	46	49
	41	43	45	49
	41	43	46	49
time (sec)	**41**	**43**	**46**	**49**

c	**η_{sp} / c**
0.003	36.036036
0.005	32.432432
0.007	34.749035
0.01	32.432432
Mean	**36.243**

η (kg/m.s)	0.000343514	0.00036027	0.00038541	0.00041054
η_{sp} (kg/m.s)	0.108108108	0.162162162	0.24324324	0.32432432
η_{sp} / c	36.03603604	32.43243243	34.7490347	32.4324324

M	**179206.5148**

$$M = \left(\frac{\eta_{sp}}{c}\frac{1}{K}\right)^{1/a}$$

Solvent	****Solvent Viscosity (cP)**	**T (^{o}C)**	***K (L / kg)**	***α**	**Polymer**	**M w**	**T_g (DSC)**
Dichloromethane	**0.44**	**20**	**0.0299**	**0.68**	**PC**	**29400**	**149.9 °C**
Toluene	**0.554**	**25**	**0.037**	**0.62**	**PS**	**184 000**	**102.56 °C**
Dichloroacetic Acid	**0.834**	**45**	**0.4**	**0.5**	**PETG**	**128 000**	**80.57 °C**
Acetone	**0.31**	**20**	**0.053**	**0.73**	**PMMA**	**179 000**	**110.83 °C**

****Fisher Scientific UK** http://www.fisher.co.uk/index.htm

****PRESS. Handbook of Chemistry and Physics 1980.pp F52.**

***Randrup J, et al Polymer Handbook 4th edition, Wiley 1999**

3.5.5 Polymers Densities

Reference Calibration (7.796 g/cc)

Absolute Density by Micromeritics 9200 Helium Pycnometer

Calculation for 150cc cell only. 5cc and 35cc cells on sheets 1 & 2

Cell volume (cc)	142.2475
Expansion volume (cc)	70.6253
Calibration date (mrk)	02/09/2005

Mass of sample = 396.2 **g**

	P1	P2	P1/P2	Density (g/cc)
Run 1	19.514	11.01	1.772388738	7.797678579
Run 2	19.476	10.989	1.772317772	7.798968199
Run 3	19.58	11.048	1.772266474	7.799900842
Run 4	19.596	11.055	1.772591588	7.793995929
Run 5	19.566	11.038	1.772603733	7.793775613

Average **7.796**

Polymers Densities

Polymer	Weight (g)	Volume (cc)	Density (g/cc)
Polycarbonate	**5.3**	**4.46**	**1.18**
Polystyrene	**3.1**	**3.19**	**0.97**
Poly(methyl-methacrylate)	**4.4**	**3.67**	**1.19**
Glycol modified Poly(ethylene-terephthalate)	**3.7**	**3.32**	**1.11**

Chapter 4

4.1 Diffusivity Estimation of CO_2/ Polymers

General Assumption:

(i) Constant Diffusivity
(ii) Purely elastic (No viscosity)
(iii) Diffusivity is perpendicular on the temperature

4.2 Deflection Model of CO_2/ Polymers

General Assumption:

(i) Constant Diffusivity
(ii) Purely elastic (No viscosity)
(iii) Diffusivity is perpendicular on the temperature

4.3 Bubble Growth Model

General Assumption:

(i) Constant Diffusivity (Model A & B only).
(ii) Purely elastic (No viscosity) (Model A & B only).
(iii) Diffusivity is perpendicular on the temperature.
(iv) Model C is applying WLF equations.

Chapter 5

5.1 T_A, T_B & Diffusivity of CO_2 / Polymers (20 to 120 bar, 1 °C/min)

PC

Time (sec)	P (bar)	T_B (°C)	Time (sec)	T_A(°C)	TA	TB	TB/ TA	Diffusivity($m^2 s^{-1}$)
10040	0	161.1	9370	156	0	0	0	0
7720	20	154.7	6340	135	21	6.4	0.304761905	7.14707E-11
7960	40	147.9	6430	114	42	13.2	0.314285714	7.08959E-11
8930	54	140.5	6620	99.3	56.7	20.6	0.363315697	7.07707E-11
8030	70	132.7	4440	82.5	73.5	28.4	0.386394558	8.28955E-11
8000	85	129.2	3750	66.75	89.25	31.9	0.357422969	7.79476E-11
7520	100	134.9	2140	51	105	26.2	0.24952381	6.41006E-11
7130	120	125.4	560	30	126	35.7	0.283333333	7.35023E-11
							av	7.30833E-11
							st dev	5.96572E-12

PS

Time (sec)	P (bar)	T_B (°C)	Time (sec)	T_A(°C)	TA	TB	TB/ TA	Diffusivity($m^2 s^{-1}$)
6120	0	101.2	6180	104	0	0	0	0
4190	20	89.4	3010	81	23	11.8	0.513043478	9.29683E-11
3950	40	83.6	2790	58	46	17.6	0.382608696	7.42663E-11
2500	54	90		53	51	11.2	0.219607843	7.93585E-11
4120	70	74.9	1490	30	74	26.3	0.355405405	6.69603E-11
3410	85	73.2	950	30	74	28	0.378378378	8.52154E-11
3650	100	65.4	1270	30	74	35.8	0.483783784	1.00243E-10
3820	120	71.4	800	30	74	29.8	0.402702703	8.03042E-11
							av	8.27595E-11
							st dev	1.12197E-11

PETG

Time (sec)	P (bar)	T_B (°C)	Time (sec)	T_A(°C)	TA	TB	TB/ TA	Diffusivity($m^2 s^{-1}$)
6770	0	111.2	6310	104	0	0		0
4890	20	98.7	2120	81	23	12.5	0.543478261	8.5009E-11
4650	40	93.7	1210	58	46	17.5	0.380434783	6.27801E-11
5260	54	87.8	2140	41.9	62.1	23.4	0.376811594	5.50502E-11
3900	70	80.2	570	23.5	80.5	31	0.385093168	7.56375E-11
4180	85	78.8	1570	6.25	97.75	32.4	0.331457801	6.24624E-11
4040	100	77.4	950	-11	115	33.8	0.293913043	5.91456E-11
4530	120	76.9	1030	-34	138	34.3	0.248550725	4.71773E-11
							av	6.38946E-11
							st dev	1.26968E-11

PMMA

Time (sec)	P (bar)	T_B (°C)	Time (sec)	T_A(°C)	TA	TB	TB/ TA	Diffusivity($m^2 s^{-1}$)
6560	0	105.5	5340	92.5	0	0		0
5930	20	105.2	4410	70.1	22.4	0.3	0.013392857	1.74312E-11
5180	40	105	3140	47.7	44.8	0.5	0.011160714	1.97782E-11
6480	54	101.2	3230	32.02	60.48	4.3	0.071097884	1.97211E-11
6540	70	103	3160	14.1	78.4	2.5	0.031887755	1.69781E-11
5850	85	95.8	2180	-2.7	95.2	9.7	0.101890756	2.41805E-11
5290	100	91.8	1960	-19.5	112	13.7	0.122321429	2.85032E-11
4840	120	85.1	430	-41.9	134.4	20.4	0.151785714	3.40126E-11
							av	2.29436E-11
							st dev	6.3422E-12

5.2 T_A & T_B Repeated of CO_2 / Polymers (20 to 120 bar, 1°C/min)

PC

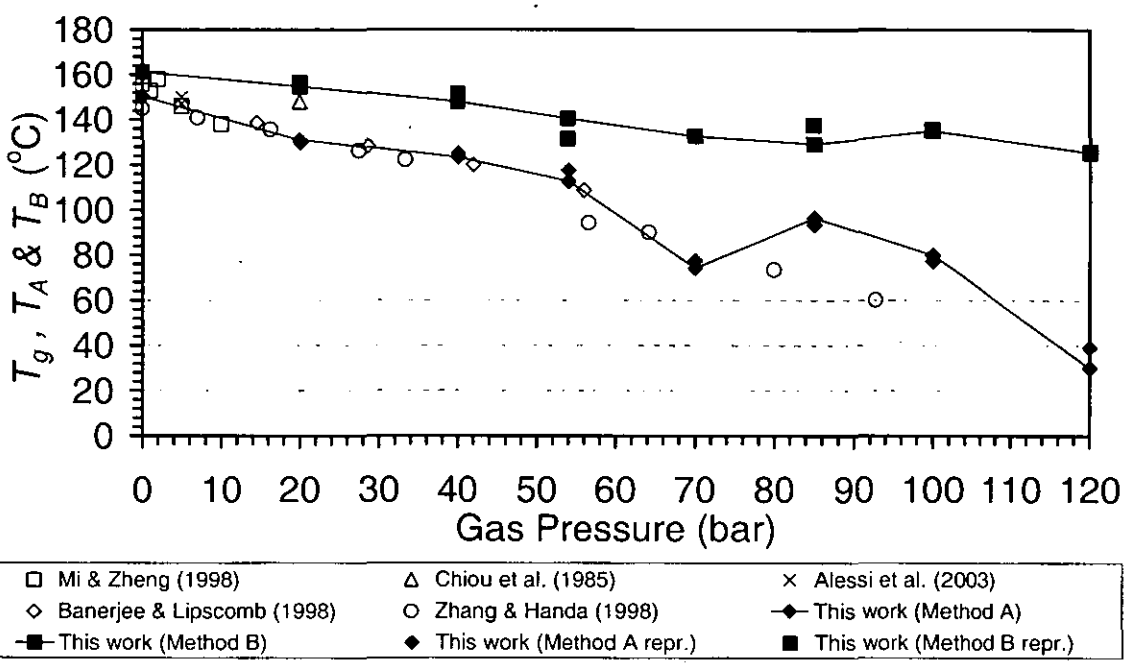

PS

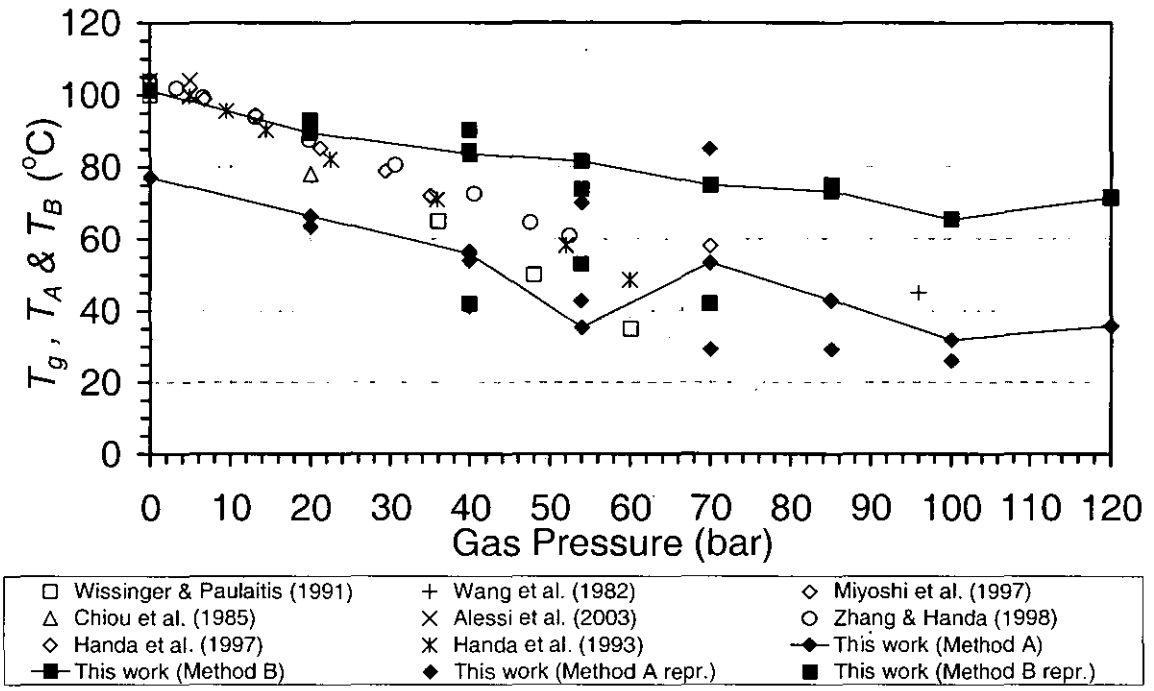
120
100
80
60
40
20
0
T_g, T_A & T_B (°C)
0 10 20 30 40 50 60 70 80 90 100 110 120
Gas Pressure (bar)
Wissinger & Paulaitis (1991)
Wang et al. (1982)
Miyoshi et al. (1997)
Chiou et al. (1985)
Alessi et al. (2003)
Zhang & Handa (1998)
Handa et al. (1997)
Handa et al. (1993)
This work (Method A)
This work (Method B)
This work (Method A repr.)
This work (Method B repr.)

PMMA

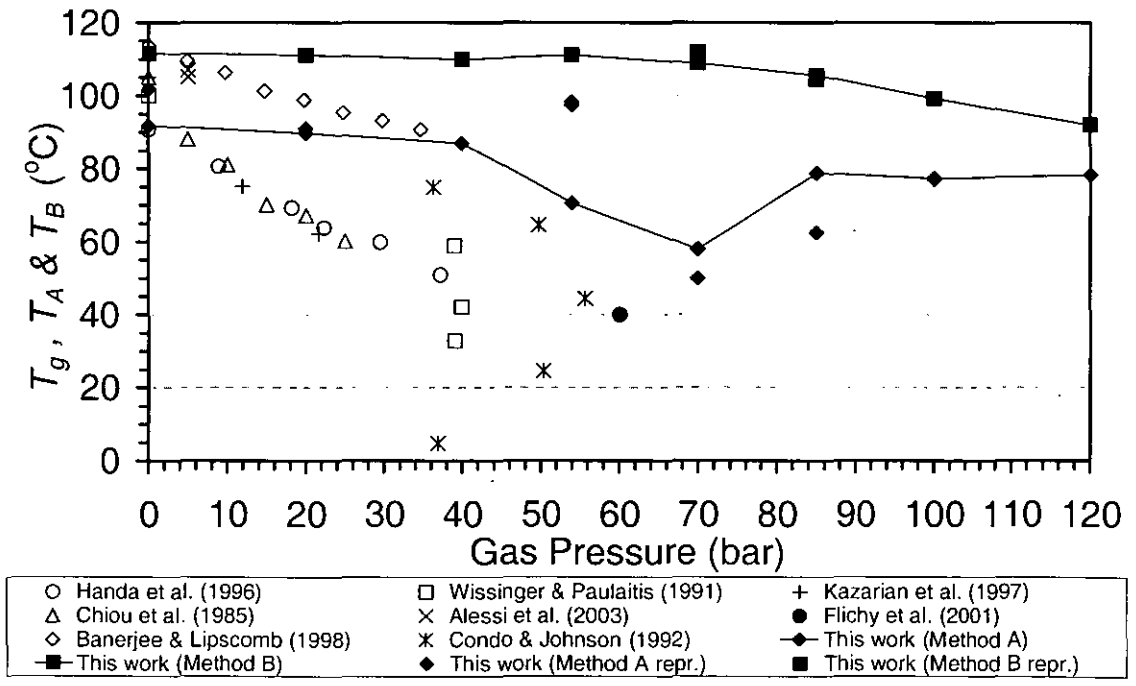
120
100
80
60
40
20
0
T_g, T_A & T_B (°C)
0 10 20 30 40 50 60 70 80 90 100 110 120
Gas Pressure (bar)
Handa et al. (1996)
Wissinger & Paulaitis (1991)
Kazarian et al. (1997)
Chiou et al. (1985)
Alessi et al. (2003)
Flichy et al. (2001)
Banerjee & Lipscomb (1998)
Condo & Johnson (1992)
This work (Method A)
This work (Method B)
This work (Method A repr.)
This work (Method B repr.)

5.3 T_A, T_B & Diffusivity of CO_2 / PS (20 to 120 bar, 1°C/min) – After Modification

PS

Time (sec)	P (bar)	T_B (°C)	Time (sec)	T_A(°C)	TA	TB	TB/ TA	Diffusivity($m^2 s^{-1}$)
3880	0	108	97	0	0	0	0	0
3230	20	97	82	15	11	0.73333333	1.96158E-10	1.961578511
2740	40	93	71	26	15	0.57692308	1.62967E-10	1.629667284
2580	54	90	54	43	18	0.41860465	1.23139E-10	1.23138818
2480	70	86	48	49	22	0.44897959	1.36873E-10	1.368731376
1390	85	76	51	46	32	0.69565217	4.17282E-10	4.172824871
1780	100	77	43	54	31	0.57407407	2.49331E-10	2.49330783
1290	120	72	49	48	36	0.75	5.11431E-10	5.114312685
							av	2.567401534
							st dev	1.502095163

5.4 Diffusivity of CO_2 / PS (20 to 120 bar, 0.2 - 1°C/min) – After Modification

0.2 (°C/min)

P (bar)	Time (sec)	T_B (°C)	T_A(°C)	∪TA	∪TB	∪TB/∪TA	Diffusivity($m^2 s^{-1}$)
0	3880	105.9	95.1	0	0	0	0
20	3770	83.9	68	27.1	22	0.81180812	2.0553E-10
40	3910	73.4	53	42.1	32.5	0.7719715	1.78268E-10
54	3390	69.8	52.4	42.7	36.1	0.84543326	2.52101E-10
70	4340	57.78	38.3	56.8	48.12	0.8471831	1.97981E-10
						av	2.0847E-10
						st dev	3.12755E-11

0.5 (°C/min)

P (bar)	Time (sec)	T_B (°C)	T_A(°C)	∪TA	∪TB	∪TB/∪TA	Diffusivity($m^2 s^{-1}$)
0	3880	105.9	95.1	0	0	0	0
20	3700	92.3	80.6	14.5	13.6	0.93793103	3.30918E-10
40	2600	87.2	59	36.1	18.7	0.51800554	1.51419E-10
54	3730	85.4	59.2	35.9	20.5	0.57103064	1.1821E-10
70	2720	82.47	57.54	37.56	23.43	0.62380192	1.81664E-10
						av	1.95552E-10
						st dev	9.38905E-11

1(°C/min)

P (bar)	Time (sec)	T_B (°C)	T_A(°C)	∪TA	∪TB	∪TB/∪TA	Diffusivity($m^2 s^{-1}$)
0	3880	105.9	95.1	0	0	0	0
20	3230	92.3	80	15.1	13.6	0.90066225	2.66443E-10
40	2740	87.2	63.7	31.4	18.7	0.5955414	1.69624E-10
54	2580	85.4	56.17	38.93	20.5	0.52658618	1.55414E-10
70	2480	82.6	57.5	37.6	23.3	0.61968085	1.97463E-10
						av	1.97236E-10
						st dev	2.13897E-11

5.5 Calculation of Deflection Model

5.5.1 Calculation of "Z" Factor & Activation Energy

Temperature (°C)	Pressure (bar)	c_e (g/100 g)	c_g (g/100 g)	Diffusivity (10^{-10} m^2/s)	Young's modulus (10^5 N/m^2)
50	70	8.0	8.0	15.1	2.8
	85	10.0		8.6	13.4
	100	11.2		4.6	4.1
	120	14.0		2.4	2.1
70	54	5.2	4.4	17.1	2.9
	70	7.1		3.9	4.5
	85	8.8		2.5	3.2
	100	10.4		3.2	4.1
	120	12.4		1.6	0.72
90	20	1.0	1.8	19.1	1.1
	40	2.8		13.1	2.2
	54	4.0		3.7	0.66
	70	5.4		3.4	1.1
	85	7.0		2.9	1.1
	100	8.4		3.3	0.98
	120	10.4		3.5	0.52

T (K)	1/T	x1000	LnD	Av. 1/T	Av. (Ln D)
323.15	0.003095	3.094538	-20.31780073	3.094538	-21.21051657
323.15	0.003095	3.094538	-20.87408873		
323.15	0.003095	3.094538	-21.49979463		
323.15	0.003095	3.094538	-22.15038219		
343.15	0.002914	2.914177	-20.17514443	2.914177	-21.66202802
343.15	0.002914	2.914177	-21.64708484		
343.15	0.002914	2.914177	-22.1095602		
343.15	0.002914	2.914177	-21.84719593		
343.15	0.002914	2.914177	-22.53115469		
363.15	0.002754	2.753683	-22.34275409	2.753683	-22.01855396
363.15	0.002754	2.753683	-22.75582379		
363.15	0.002754	2.753683	-21.70409509		
363.15	0.002754	2.753683	-21.79913864		
363.15	0.002754	2.753683	-21.95769785		
363.15	0.002754	2.753683	-21.81988012		
363.15	0.002754	2.753683	-21.75048813		

Nair KC, Kumar S, Thomas S, Schit S, Ramamurthy. Young Modulus (Mpa) = 3.60E+08
Rhelogical of short sisal fiber-reinforced polystyrene composites.
Composites Part A; Applied scince and manufacturing 2000: 1231 - 1240

$$D = D_o e^{-\frac{E}{RT}}$$

$$Ln(D) = -\frac{E}{RT} + Ln(D_o)$$

y = -1.9002x - 16.106 Slope of 1/T vs Ln(D) y = Ln D
y = mx + c x = 1/ T
R 8.314 kJ / kmol K c = Ln D_o = -16.106

Slope = $-\frac{E_a}{R}$ ⟹ m = - E_a / R = - 1.9002

Slop = 1.9002

kJ/kmol

Activation Energy =	15.7982628

5.5.2 Isothermal Test of 50 °C (70 – 120 bar)

70 bar

A	2.79E-10	**E**	2.86E+05	Max time	8500			
B	1.74E-05	**D**	1.53789E-09 m2/s		2.1693			
							Dt	10 s
A	2.79E+00				Sum	6.916637101	L	0.08 m
B	1.7429318						W	0.02 N
	Measured			**Fitted**		**Difference Sq.**		
							b	0.02 m
							do	0.002 m
	Time Seconds	Displacement mm					Cg	**0.08** g
	0	0		0		0	Ce	**0.09** g
	10	0.002		0.003055		1.11259E-06		
	20	0.004		0.004425		1.80238E-07		
	30	0.005		0.005521		2.71E-07		
	40	0.005		0.006476		2.17979E-06		
	50	0.007		0.007344		1.18079E-07		
	60	0.007		0.008149		1.31932E-06		
	70	0.008		0.008907		8.22681E-07		
	80	0.009		0.009629		3.95642E-07		
	90	0.009		0.010322		1.74665E-06		
	100	0.01		0.01099		9.80038E-07		

85 bar

A	5.98E-11	**E**	1.34E+06	Max time	5010			
B	2.35E-05	**D**	8.63217E-10		2.8256			
							Dt	30 s
A	5.98E-01				Sum	0.068918688	L	0.08 m
B	2.350445						W	0.02 N
	Measured			**Fitted**		**Difference Sq.**	E	2.00E+09
							b	0.02 m
							do	0.002 m
	Time Seconds	Displacement mm					D	2.40E-10 m2/s
	0	0		0		0	Cg	**0.08** g
	30	0		0.001652		2.72946E-06	Ce	**0.1** g
	60	0		0.002479		6.1473E-06		
	90	0		0.003183		1.01328E-05		
	120	0.001		0.003829		8.00323E-06		
	150	0.001		0.004442		1.18465E-05		
	180	0.001		0.005035		1.62786E-05		
	210	0.002		0.005615		1.30683E-05		
	240	0.002		0.006188		1.75382E-05		
	270	0.002		0.006757		2.26265E-05		
	300	0.003		0.007324		1.86988E-05		

100 bar

A	1.99E-10	**E**	4.02E+05	Max time	4500
B	2.45E-05	**D**	4.61256E-10		2.98142

A	1.99E+00	Sum	2.306482959
B	2.4545001		

	Measured			**Fitted**	**Difference Sq.**
Time Seconds	Displacement mm				
0	10.67549	0	0		0
10	10.67533	0	0.003134		9.82139E-06
20	10.67531	0	0.004587		2.10363E-05
30	10.67527	0.001	0.00577		2.27536E-05
40	10.67561	0.002	0.006818		2.32093E-05
50	10.67565	0.003	0.00778		2.28527E-05
60	10.67565	0.003	0.008685		3.23171E-05
70	10.67571	0.004	0.009546		3.07602E-05
80	10.67579	0.004	0.010375		4.06361E-05
90	10.67577	0.005	0.011177		3.81571E-05
100	10.67581	0.005	0.011959		4.84242E-05

Dt	10 s
L	0.08 m
W	0.02 N
E	2.00E+09
b	0.02 m
do	0.002 m
D	2.40E-10 m2/s
Cg	**0.08** g
Ce	**0.112** g

120 bar

A	3.82E-10	**E**	2.09E+05	Max time	3300
B	2.70E-05	**D**	2.48765E-10		3.48155

A	3.82E+00	Sum	1.907017845
B	2.703819		

	Measured			**Fitted**	**Difference Sq.**
Time Seconds	Displacement mm				
0	10.67549	0	0		0
10	10.67533	0.004	0.006696		7.26795E-06
20	10.67531	0.005	0.009836		2.33894E-05
30	10.67527	0.007	0.012411		2.92838E-05
40	10.67561	0.01	0.014703		2.21175E-05
50	10.67565	0.012	0.016819		2.32235E-05
60	10.67565	0.013	0.018815		3.38167E-05
70	10.67571	0.015	0.020724		3.27649E-05
80	10.67579	0.017	0.022567		3.09899E-05
90	10.67577	0.019	0.024358		2.87114E-05
100	10.67581	0.02	0.026109		3.73208E-05

Dt	10 s
L	0.08 m
W	0.02 N
E	2.00E+09
b	0.02 m
do	0.002 m
D	2.40E-10 m2/s
Cg	**0.08** g
Ce	**0.14** g

5.5.3 Isothermal Test of 70 °C (54 – 120 bar)

54 bar

A	2.75E-10	**E**	2.91E+05	Max time	3500
B	2.56E-05	**D**	1.73524E-09		3.38062

A	2.75E+00			Sum	0.187940132
B	2.5634615				

	Measured		**Fitted**	**Difference Sq.**
	Time Seconds	Displacement mm		
	0	0	0	0
	10	0.001	0.004535	1.24978E-05
	20	0.001	0.006648	3.19021E-05
	30	0.002	0.008375	4.06354E-05
	40	0.002	0.009906	6.25074E-05
	50	0.003	0.011317	6.91691E-05
	60	0.004	0.012644	7.47225E-05
	70	0.004	0.013911	9.82225E-05
	80	0.005	0.015131	0.000102634
	90	0.006	0.016315	0.000106389
	100	0.006	0.017469	0.000131541

Dt	10	s
L	0.08	m
W	0.02	N
E	2.00E+09	
b	0.02	m
do	0.002	m
D	2.40E-10	m2/s
Cg	**0.044**	g
Ce	**0.052**	g

70 bar

A	1.74E-10	**E**	4.59E+05	Max time	2600
B	3.03E-05	**D**	3.97595E-10		3.92232

A	1.74E+00			Sum	0.133577722
B	3.0330933				

	Measured		**Fitted**	**Difference Sq.**
	Time Seconds	Displacement mm		
	0	0	0	0
	13	0.005	0.004005	9.90262E-07
	26	0.008	0.005952	4.19513E-06
	39	0.012	0.007581	1.95308E-05
	52	0.018	0.009054	8.00256E-05
	65	0.022	0.010435	0.00013374
	78	0.024	0.011756	0.000149918
	91	0.026	0.013035	0.000168101
	104	0.027	0.014284	0.000161699
	117	0.029	0.015512	0.00018192
	130	0.03	0.016726	0.000176202

Dt	13	s
L	0.08	m
W	0.02	N
E	2.00E+09	
b	0.02	m
do	0.002	m
D	2.40E-10	m2/s
Cg	**0.044**	g
Ce	**0.071**	g

85 bar

A	2.50E-10	**E**	3.19E+05	Max time	2200
B	3.17E-05	**D**	2.51505E-10		4.26401

A	2.50E+00			Sum	0.181468914
B	3.1717793				

Measured		Fitted	Difference Sq.
Time Seconds	Displacement mm		
0	0	0	0
10	0.003	0.005226	4.95294E-06
20	0.006	0.007731	2.99731E-06
30	0.009	0.009812	6.58677E-07
40	0.011	0.011682	4.64751E-07
50	0.014	0.013424	3.31232E-07
60	0.016	0.015082	8.42649E-07
70	0.018	0.016679	1.744E-06
80	0.021	0.018233	7.65769E-06
90	0.023	0.019753	1.05408E-05
100	0.026	0.021249	2.25687E-05

Dt	10	s	
L	0.08	m	
W	0.02	N	
E	2.00E+09		
b	0.02	m	
do	0.002	m	
D	2.40E-10	m2/s	
Cg	**0.044**	g	
Ce	**0.088**	g	

100 bar

A	1.99E-10	**E**	4.02E+05	Max time	1500
B	4.16E-05	**D**	3.25045E-10		5.16398

A	1.99E+00			Sum	0.303569386
B	4.1605389				

Measured		Fitted	Difference Sq.
Time Seconds	Displacement mm		
0	0	0	0
10	0.006	0.005636	1.32388E-07
20	0.011	0.008471	6.3975E-06
30	0.014	0.010888	9.68294E-06
40	0.017	0.013111	1.51231E-05
50	0.021	0.015225	3.33535E-05
60	0.024	0.017273	4.52575E-05
70	0.027	0.019281	5.95871E-05
80	0.029	0.021266	5.9814E-05
90	0.031	0.023241	6.02093E-05
100	0.033	0.025213	6.06366E-05

Dt	10	s	
L	0.08	m	
W	0.02	N	
E	2.00E+09		
b	0.02	m	
do	0.002	m	
D	2.40E-10	m2/s	
Cg	**0.044**	g	
Ce	**0.104**	g	

120 bar

A	1.10E-09	**E**	7.28E+04	Max time	1500			
B	3.31E-05	**D**	1.64569E-10		5.16398			
							Dt	10 s
A	1.10E+01				Sum	1.894610045	L	0.08 m
B	3.3105697						W	0.02 N
	Measured			**Fitted**		**Difference Sq.**	E	2.00E+09
							b	0.02 m
							do	0.002 m
	Time	Displacement					D	2.40E-10 m2/s
	Seconds	mm					Cg	**0.044** g
	0	0		0		0	Ce	**0.124** g
	10	0.002		0.024043		0.0004859		
	21	0.006		0.036678		0.000941127		
	30	0.009		0.04532		0.001319158		
	40	0.014		0.054041		0.001603296		
	50	0.017		0.06219		0.002042171		
	60	0.022		0.069961		0.002300239		
	70	0.025		0.077467		0.002752739		
	80	0.029		0.084782		0.003111607		
	90	0.033		0.091958		0.003476042		
	100	0.037		0.099033		0.003848044		

5.5.4 Isothermal Test of 90°C (20 – 120 bar)

20 bar

A	7.38E-10	**E**	1.08E+05	Max time	1000			
B	4.51E-05	**D**	1.98922E-10		6.32456			
							Dt	10 s
A	7.38E+00				Sum	1.300228222	L	0.08 m
B	4.5132704						W	0.02 N
	Measured			**Fitted**		**Difference Sq.**	E	2.00E+09
							b	0.02 m
							do	0.002 m
	Time	Displacement					D	2.40E-10 m2/s
	Seconds	mm					Cg	**0.018** g
	0	0		0		0	Ce	**0.01** g
	10	0.001		0.022952		0.00048191		
	20	0.003		0.034696		0.001004664		
	30	0.004		0.044813		0.001665692		
	40	0.006		0.054193		0.002322561		
	50	0.008		0.063179		0.003044739		
	60	0.011		0.071947		0.0037.14533		
	70	0.013		0.080601		0.004569941		
	80	0.016		0.089212		0.005359939		
	90	0.019		0.097827		0.00621371		
	100	0.023		0.106485		0.006969728		

40 bar

A	3.62E-10	**E**	2.21E+05	Max time	900				
B	5.18E-05	**D**	1.31375E-09		6.66667				
								Dt	10 s
A	3.62E+00				Sum	1.077848403		L	0.08 m
B	5.1779546							W	0.02 N
	Measured			**Fitted**		**Difference Sq.**		E	2.00E+09
								b	0.02 m
								do	0.002 m
	Time	Displacement						D	2.40E-10 m2/s
	Seconds	mm						Cg	0.018 g
	0	0		0		0		Ce	0.028 g
	10	0.003		0.013201		0.000104067			
	20	0.005		0.020182		0.000230481			
	30	0.007		0.026311		0.000372912			
	40	0.009		0.032087		0.00053303			
	50	0.011		0.037704		0.000713078			
	60	0.013		0.043259		0.0009156			
	70	0.015		0.048814		0.001143406			
	80	0.017		0.054411		0.001399584			
	90	0.019		0.060079		0.001687522			
	100	0.021		0.065844		0.002010941			

54 bar

A	1.21E-09	**E**	6.61E+04	Max time	1000				
B	4.26E-05	**D**	3.75751E-10		6.32456				
								Dt	10 s
A	1.21E+01				Sum	4.851151886		L	0.08 m
B	4.2645476							W	0.02 N
	Measured			**Fitted**		**Difference Sq.**		E	2.00E+09
								b	0.02 m
								do	0.002 m
	Time	Displacement						D	2.40E-10 m2/s
	Seconds	mm						Cg	**0.018** g
	0	0		0		0		Ce	**0.04** g
	10	0.007		0.035236		0.00079729			
	20	0.011		0.053047		0.001767984			
	30	0.014		0.068283		0.002946631			
	40	0.019		0.082326		0.004010166			
	50	0.022		0.095708		0.005432821			
	60	0.026		0.1087		0.006839274			
	70	0.031		0.121464		0.008183782			
	80	0.035		0.134107		0.009822191			
	90	0.039		0.146703		0.011599923			
	100	0.044		0.159308		0.013295918			

70 bar

A	7.03E-10	**E**	1.14E+05	Max time	800				
B	4.93E-05	**D**	3.41745E-10		7.07107				
								Dt	10 s
A	7.03E+00				Sum	2.018338187		L	0.08 m
B	4.929694							W	0.02 N
	Measured			**Fitted**		**Difference Sq.**		E	2.00E+09
								b	0.02 m
								do	0.002 m
	Time	Displacement						D	2.40E-10 m2/s
	Seconds	mm						Cg	**0.018** g
	0	0		0		0		Ce	**0.054** g
	10	0.003		0.024213		0.000450002			
	20	0.006		0.036859		0.000952296			
	30	0.009		0.047884		0.001511937			
	40	0.013		0.05821		0.002043902			
	50	0.017		0.068193		0.002620696			
	60	0.021		0.078017		0.003250892			
	70	0.025		0.087792		0.00394282			
	80	0.029		0.097593		0.004704989			
	90	0.034		0.107474		0.005398374			
	100	0.039		0.117476		0.006158417			

85 bar

A	7.54E-10	**E**	1.06E+05	Max time	800				
B	5.07E-05	**D**	2.91352E-10		7.07107				
								Dt	10 s
A	7.54E+00				Sum	1.580425284		L	0.08 m
B	5.0719413							W	0.02 N
	Measured			**Fitted**		**Difference Sq.**		E	2.00E+09
								b	0.02 m
								do	0.002 m
	Time	Displacement						D	2.40E-10 m2/s
	Seconds	mm						Cg	**0.018** g
	0	0		0		0		Ce	**0.07** g
	10	0.003		0.026864		0.000569467			
	20	0.006		0.040993		0.001224515			
	30	0.01		0.053362		0.001880238			
	40	0.013		0.064988		0.00270271			
	50	0.017		0.076264		0.003512166			
	60	0.022		0.087393		0.004276189			
	70	0.026		0.098498		0.005255957			
	80	0.031		0.109663		0.006187867			
	90	0.036		0.120949		0.007216253			
	100	0.042		0.132402		0.008172531			

100 bar

A	8.72E-10	**E**	9.18E+04	Max time	600
B	5.74E-05	**D**	3.34009E-10		8.16497

A	8.72E+00			Sum	0.902710545
B	5.7438585				
	Measured		**Fitted**		**Difference Sq.**

Time Seconds	Displacement mm		
0	0	0	0
10	0.005	0.036018	0.000962126
20	0.011	0.055611	0.001990131
30	0.017	0.073107	0.003147982
40	0.024	0.089835	0.004334272
50	0.033	0.106314	0.005374936
60	0.041	0.122817	0.006693979
70	0.05	0.139515	0.008012952
80	0.061	0.15653	0.009126009
90	0.073	0.173955	0.010191998
100	0.084	0.191868	0.011635588

Dt	10	s
L	0.08	m
W	0.02	N
E	2.00E+09	
b	0.02	m
do	0.002	m
D	2.40E-10	m2/s
Cg	**0.018**	g
Ce	**0.084**	g

120 bar

A	1.56E-09	**E**	5.12E+04	Max time	400
B	6.26E-05	**D**	3.58241E-10		10

A	1.56E+01			Sum	1.382176141
B	6.2605495				
	Measured		**Fitted**		**Difference Sq.**

Time Seconds	Displacement mm		
0	0	0	0
10	0.018	0.071716	0.002885395
20	0.042	0.111763	0.004866926
30	0.065	0.148094	0.006904554
40	0.094	0.183306	0.007975645
50	0.12	0.21843	0.009688532
60	0.154	0.254023	0.010004629
70	0.185	0.290449	0.011119408
80	0.226	0.327976	0.010399186
90	0.262	0.366826	0.010988594
100	0.309	0.407192	0.009641609

Dt	10	s
L	0.08	m
W	0.02	N
E	2.00E+09	
b	0.02	m
do	0.002	m
D	2.40E-10	m2/s
Cg	**0.018**	g
Ce	**0.104**	g

Chapter 6

6.1 Result from LVDT – Bubble number and Swelling Ratio

PC 600 = 0.6 mm = 0.0006 m (microscop)

P (bar)	Bubbles D. (mm)	r (mm)	r (m)	V_{sphere} (m3)
0	0	0	0	0
0	0.178723404	0	0	0
20	0.312765957	0.1564	0.000156	1.60198E-11
40	0.482553191	0.2413	0.000241	5.88348E-11
54	0.45	0.225	0.000225	4.77129E-11
70	0.439361702	0.2197	0.00022	4.44084E-11
85	0.41106383	0.2055	0.000206	3.63686E-11
100	0.399148936	0.1996	0.0002	3.32969E-11
120	0.589787234	0.2949	0.000295	1.0742E-10

Measured		Caculated					
(g/cc)	wight (g)	V(cc)	V (m^3)	?V	No.Bubbles	x 10^4	Percent Swelling
1.186	5.3	4.4688	4.47E-06	0	0	0	0
1.147	5.3	4.6207	4.62E-06	1.51947E-07	0	0	0
1.15	5.3	4.6087	4.61E-06	1.39893E-07	8732.503899	0.87325	0.031304348
1.142	5.3	4.641	4.64E-06	1.72178E-07	2926.46648	0.292647	0.038528897
1.09	5.3	4.8624	4.86E-06	3.93583E-07	8248.97053	0.824897	0.088073394
1.05	5.3	5.0476	5.05E-06	5.78816E-07	13033.93568	1.303394	0.12952381
0.942	5.3	5.6263	5.63E-06	1.15752E-06	31827.5852	3.182759	0.259023355
0.485	5.3	10.928	1.09E-05	6.45903E-06	193983.1062	19.39831	1.445360825
0.357	5.3	14.846	1.48E-05	1.03771E-05	96603.47937	9.660348	2.322128852

	Diameter			Radius
	47	1.4	mm	mm
0 bar	8	0.2383		0.119148936
	7	0.2085		0.104255319
	4	0.1191		0.059574468
	5	0.1489		0.074468085
Average		0.1787		0.089361702
20 bar	13	0.3872		0.193617021
	4	0.1191		0.059574468
	9	0.2681		0.134042553
	16	0.4766		0.238297872
		0.3128		0.156382979
85 bar	12	0.3574		0.178723404
	15	0.4468		0.223404255
	14	0.417		0.208510638
	13	0.3872		0.193617021
	15	0.4468		0.223404255
		0.4111		0.205531915
120 bar	22	0.6553		0.327659574
	14	0.417		0.208510638
	26	0.7745		0.387234043
	19	0.566		0.282978723
	18	0.5362		0.268085106
		0.5898		0.294893617
40 bar	25	0.744681		0.372340426
	16	0.476596		0.238297872
	7	0.208511		0.104255319
	11	0.32766		0.163829787
	22	0.655319		0.327659574
		0.482553		0.241276596
70 bar	16	0.476596		0.238297872
	14	0.417021		0.208510638
	17	0.506383		0.253191489
	12	0.357447		0.178723404
		0.439362		0.219680851
100 bar	18	0.53617		0.268085106
	16	0.476596		0.238297872
	18	0.53617		0.268085106
	9	0.268085		0.134042553
	6	0.178723		0.089361702
		0.399149		0.199574468

PS 600 = 0.6 mm = 0.0006 m (microscop)

P (bar)	Bubbles D. (mm)	r (mm)	r (m)	V_{sphere} (m3)
0	0	0	0	0
0	0.029787234	0.0149	1.49E-05	1.38385E-14
20	0	0.54	0.00054	6.59584E-10
40	1.280851064	0.6404	0.00064	1.10026E-09
54	0.923404255	0.4617	0.000462	4.12263E-10
70	0.372340426	0.1862	0.000186	2.70283E-11
85	2.085106383	1.0426	0.001043	4.74661E-09
100	0.673191489	0.3366	0.000337	1.5974E-10
120	0.518297872	0.2591	0.000259	7.29016E-11

† (g/cc)	wight (g)	V(cc)	V (m^3)	?V	No.Bubbles	/1000	Percent Swelling
0.97	3.1	3.1959	3.2E-06	0	0	0	0
0.97	3.1	3.1959	3.2E-06	0	0	0	0
0.97	3.1	3.1959	3.2E-06	0	1	0.0001	0
0.88	3.1	3.5227	3.52E-06	3.26851E-07	297.0675911	0.029707	0.102272727
0.676	3.1	4.5858	4.59E-06	1.38992E-06	3371.447156	0.337145	0.434911243
0.29	3.1	10.69	1.07E-05	7.49378E-06	277256.4638	27.72565	2.344827586
0.104	3.1	29.808	2.98E-05	2.66118E-05	5606.492386	0.560649	8.326923077
0.104	3.1	29.808	2.98E-05	2.66118E-05	166594.2621	16.65943	8.326923077
0.109	3.1	28.44	2.84E-05	2.52445E-05	346281.837	34.62818	7.899082569

		Diameter		Radius
	47	1.4	mm	mm
0 bar	1	0.0298		0.014893617
	1	0.0298		0.014893617
	1	0.0298		0.014893617
	1	0.0298		0.014893617
Average		0.0298		0.014893617
40 bar	45	1.3404		0.670212766
	46	1.3702		0.685106383
	41	1.2213		0.610638298
	40	1.1915		0.595744681
		1.2809		0.640425532
85 bar	70	2.0851		1.042553191
	70	2.0851		1.042553191
	70	2.0851		1.042553191
	70	2.0851		1.042553191
	70	2.0851		1.042553191
		2.0851		1.042553191
120 bar	18	0.5362		0.268085106
	23	0.6851		0.342553191
	14	0.417		0.208510638
	10	0.2979		0.14893617
	22	0.6553		0.327659574
		0.5183		0.259148936

54 bar	47	1.4	0.7
	27	0.804255	0.40212766
	36	1.07234	0.536170213
	22	0.655319	0.327659574
	23	0.685106	0.342553191
		0.923404	0.461702128
70 bar	23	0.685106	0.342553191
	16	0.476596	0.238297872
	7	0.208511	0.104255319
	4	0.119149	0.059574468
		0.37234	0.186170213
100 bar	30	0.893617	0.446808511
	27	0.804255	0.40212766
	24	0.714894	0.357446809
	17	0.506383	0.253191489
	15	0.446809	0.223404255
		0.673191	0.336595745

PETG 600 = 0.6 mm = 0.0006 m (microscop)

P (bar)	Bubbles D. (mm)	r (mm)	r (m)	V_{sphere} (m3)
0	0	0	0	0
0	0.186170213	0	0	0
20	0.580851064	0.2904	0.00029	1.02611E-10
40	0.439361702	0.3	0.0003	1.13097E-10
54	0.82212766	0.4111	0.000411	2.90949E-10
70	1.10212766	0.5511	0.000551	7.00962E-10
85	1.25106383	0.6255	0.000626	1.02527E-09
100	0.42893617	0.2145	0.000214	4.13216E-11
120	0.375319149	0.1877	0.000188	2.76822E-11

(g/cc)	wight (g)	V(cc)	V (m^3)	?V	No.Bubbles	x10^5	Percent Swelling
1.27	4.4	3.4646	3.46E-06	0	0	0	0
1.263	4.4	3.4838	3.48E-06	1.92019E-08	0	0	0.005542359
1.163	4.4	3.7833	3.78E-06	3.18752E-07	3106.418964	0.031064	0.092003439
1.203	4.4	3.6575	3.66E-06	1.92956E-07	1706.105007	0.017061	0.055694098
0.911	4.4	4.8299	4.83E-06	1.36529E-06	4692.546938	0.046925	0.394072448
0.525	4.4	8.381	8.38E-06	4.91639E-06	7013.771244	0.070138	1.419047619
0.419	4.4	10.501	1.05E-05	7.03663E-06	6863.212818	0.068632	2.031026253
0.32	4.4	13.75	1.38E-05	1.02854E-05	248912.0667	2.489121	2.96875
0.299	4.4	14.716	1.47E-05	1.12512E-05	406439.7787	4.064398	3.247491639

		Diameter		Radius
	47	1.4	mm	mm
0 bar	13	0.387234		0.193617021
	4	0.119149		0.059574468
	3	0.089362		0.044680851
	5	0.148936		0.074468085
Average		0.18617		0.093085106
20 bar	25	0.744681		0.372340426
	14	0.417021		0.208510638
	25	0.744681		0.372340426
	14	0.417021		0.208510638
		0.580851		0.290425532
40 bar	14	0.417021		0.208510638
	24	0.714894		0.357446809
	4	0.119149		0.059574468
	17	0.506383		0.253191489
		0.439362		0.219680851
54 bar	34	1.012766		0.506382979
	36	1.07234		0.536170213
	23	0.685106		0.342553191
	22	0.655319		0.327659574
	23	0.685106		0.342553191
		0.822128		0.41106383
70 bar	40	1.19148936		0.595744681
	35	1.04255319		0.521276596
	42	1.25106383		0.625531915
	31	0.92340426		0.461702128
		1.10212766		0.55106383
85 bar	55	1.63829787		0.819148936
	20	0.59574468		0.29787234
	55	1.63829787		0.819148936
	25	0.74468085		0.372340426
	55	1.63829787		0.819148936
		1.25106383		0.625531915
100 bar	17	0.50638298		0.253191489
	22	0.65531915		0.327659574
	11	0.32765957		0.163829787
	18	0.53617021		0.268085106
	4	0.11914894		0.059574468
		0.42893617		0.214468085
120 bar	17	0.50638298		0.253191489
	15	0.44680851		0.223404255
	16	0.47659574		0.238297872
	10	0.29787234		0.14893617
	5	0.14893617		0.074468085
		0.37531915		0.187659574

PMMA 600 = 0.6 mm = 0.0006 m (microscop)

P (bar)	Bubbles D. (mm)	r (mm)	r (m)	V_{sphere} (m3)
0	0	0	0	0
0	0.0001	5E-05	5E-08	5.23599E-22
20	0.0002	0.0001	1E-07	4.18879E-21
40	0	0	0	0
54	0.911489362	0.4557	0.000456	3.96509E-10
70	0.99787234	0.4989	0.000499	5.20264E-10
85	0.762553191	0.3813	0.000381	2.32172E-10
100	0.357446809	0.1787	0.000179	2.39129E-11
120	0.184680851	0.0923	9.23E-05	3.2981E-12

) (g/cc)	wight (g)	V(cc)	V (m^3)	?V	No.Bubbles	$x10^3$	Percent Swelling
1.113	3.7	3.3243	3.32E-06	0	0	0	0
1.126	3.7	3.286	3.29E-06	-3.83806E-08	-7.33015E+13	0	-0.011545293
1.125	3.7	3.2889	3.29E-06	-3.54597E-08	-8.46538E+12	0	-0.010666667
1.101	3.7	3.3606	3.36E-06	3.62327E-08	#DIV/0!	0	0.010899183
0.373	3.7	9.9196	9.92E-06	6.59522E-06	16633.20778	0.166332	1.983914209
0.163	3.7	22.699	2.27E-05	1.9375E-05	37240.79847	0.372408	5.828220859
0.121	3.7	30.579	3.06E-05	2.72542E-05	117388.0288	1.17388	8.198347107
0.226	3.7	16.372	1.64E-05	1.30473E-05	545618.1978	5.456182	3.924778761
0.543	3.7	6.814	6.81E-06	3.48965E-06	1058077.214	10.58077	1.049723757

6.2 Results from Optical Measurements

i. 50 °C

100 bar + 50 °C

time (sec)	P (bar)	Area (Pixel2)	r (Pixel)	r (mm)	r(m)
45	49	44	3.74241	0.026732	2.67315E-05
60	27	96	5.527906	0.039485	3.9485E-05
90	20	300	9.77205	0.0698	6.98004E-05
120	7.3	316	10.02925	0.071638	7.16375E-05
150	1.22	508	12.71619	0.09083	9.08299E-05
180	0.9	586	13.65758	0.097554	9.75542E-05
240	0.9	750	15.45097	0.110364	0.000110364
260	0.9	780	15.75696	0.11255	0.00011255
280	0.9	800	15.95769	0.113984	0.000113984
300	0.9	810	16.05712	0.114694	0.000114694

120bar + 50°C

time (sec)	r (mm)
27	0.03
45	0.034216
90	0.069388
150	0.081502
180	0.105727
240	0.112335
260	0.132436
280	0.152532
300	0.166247
344	0.166247

ii. 70 °C

63 bar + 70 °C

time (sec)	Area (Pixel2)	r (Pixel)	r (mm)	r(m)
30				
60				
120	16	2.256758	0.01612	1.61E-05
180	35	3.337791	0.023841	2.38E-05
240	38	3.477898	0.024842	2.48E-05
300	48	3.90882	0.02792	2.79E-05
360	57	4.259538	0.030425	3.04E-05
420	67	4.618091	0.032986	3.3E-05
480	86	5.232079	0.037372	3.74E-05
540	92	5.411516	0.038654	3.87E-05
600	104	5.753627	0.041097	4.11E-05

83 bar + 70 °C

time (sec)	Area (Pixel2)	r (Pixel)	r (mm)	r(m)
30				
60				
120	31	3.141275	0.022438	2.24E-05
180	71	4.753946	0.033957	3.4E-05
240	225	8.462844	0.060449	6.04E-05
300	514	12.79106	0.091365	9.14E-05
360	884	16.77456	0.119818	0.00012
420	1164	19.24871	0.137491	0.000137
480	1313	20.4436	0.146026	0.000146
540	1880	24.46268	0.174733	0.000175
600	2014	25.31948	0.180853	0.000181

100 bar + 70 °C

time (sec)	Area (Pixel2)	r (Pixel)	r (mm)	r(m)
30				
60	44	3.74241	0.026732	2.67E-05
120	192	7.81764	0.05584	5.58E-05
180	216	8.29186	0.059228	5.92E-05
240	328	10.21791	0.072985	7.3E-05
300	413	11.46569	0.081898	8.19E-05
360	420	11.56245	0.082589	8.26E-05
420	480	12.36077	0.088291	8.83E-05
480	535	13.04974	0.093212	9.32E-05
540	592	13.72733	0.098052	9.81E-05
600	700	14.92705	0.106622	0.000107

120 bar + 70 °C

time (sec)	Area (Pixel2)	r (Pixel)	r (mm)	r(m)
30	26	2.876814	0.020549	2.05E-05
60	38	3.477898	0.024842	2.48E-05
120	57	4.259538	0.030425	3.04E-05
180	104	5.753627	0.041097	4.11E-05
240	133	6.506552	0.046475	4.65E-05
300	137	6.60367	0.047169	4.72E-05
360	141	6.69938	0.047853	4.79E-05
420	138	6.627727	0.047341	4.73E-05
480	148	6.863663	0.049026	4.9E-05
540	152	6.955796	0.049684	4.97E-05
600	240	8.740387	0.062431	6.24E-05

iii. 100 °C

24 bar + 100 °C		
P (bar)	r (mm)	r (m)
90	0.024513	2.45131E-05
120	0.03969	3.96902E-05
150	0.062171	6.21707E-05
180	0.089388	8.93881E-05
210	0.103609	0.000103609
240	0.126671	0.000126671
270	0.140759	0.000140759
300	0.153772	0.000153772
330	0.174733	0.000174733
360	0.192932	0.000192932
390	0.204695	0.000204695
420	0.225748	0.000225748
450	0.236155	0.000236155
480	0.241661	0.000241661
510	0.244102	0.000244102
540	0.258167	0.000258167
570	0.260266	0.000260266
600	0.260266	0.000260266

44 bar + 100 °C		
P (bar)	r (mm)	r (m)
60	0.037372	3.74E-05
90	0.055	0.000055
120	0.07	0.00007
150	0.12	0.00012
180	0.15	0.00015
210	0.21	0.00021
240	0.27	0.00027
270	0.29	0.00029
300	0.35	0.00035
330	0.44	0.00044
360	0.47	0.00047
390	0.48	0.00048
420	0.498777	0.000499
450	0.532042	0.000532
480	0.553994	0.000554
510	0.563354	0.000563
540	0.56633	0.000566
570	0.59	0.00059
600	0.581302	0.000581

63 bar + 100 °C		
P (bar)	r (mm)	r (m)
30	0.035819	3.58188E-05
60	0.059228	5.92276E-05
90	0.095195	9.5195E-05
120	0.135588	0.000135588
150	0.19759	0.00019759
180	0.296467	0.000296467
210	0.36	0.00036
240	0.392023	0.000392023
270	0.45	0.00045
300	0.492311	0.000492311
330	0.523053	0.000523053
360	0.564866	0.000564866
390	0.638486	0.000638486
420	0.639731	0.000639731
450	0.655925	0.000655925
480	0.685253	0.000685253
510	0.675743	0.000675743
540	0.69	0.00069
570	0.703969	0.000703969
600	0.707479	0.000707479

83 bar + 100 °C		
P (bar)	r (mm)	r (m)
30	0.03969	3.97E-05
60	0.071524	7.15E-05
90	0.097554	9.76E-05
120	0.121701	0.000122
150	0.183616	0.000184
180	0.241123	0.000241
210	0.33	0.00033
240	0.4	0.0004
270	0.48	0.00048
300	0.54	0.00054
330	0.582065	0.000582
360	0.676821	0.000677
390	0.714163	0.000714
420	0.775075	0.000775
450	0.812883	0.000813
480	0.808851	0.000809
510	0.819563	0.00082
540	0.843945	0.000844
570	0.83631	0.000836
600	0.83631	0.000836

100 bar + 50 °C

time (sec)	r (mm)
27	0.03
45	0.034215669
90	0.089388074
150	0.150246522
180	0.157270396
240	0.233527147
260	0.243558915
280	0.253193526
300	0.262474719
330	0.271438749
360	0.280116067
390	0.288984526
420	0.297805201
450	0.306625875
480	0.315446549
510	0.324267223
540	0.333087897
570	0.341908571
600	0.350729245

120bar + 50°C

time (sec)	P (bar)	ırea (Pixel2	r (Pixel)	r (mm)	r(m)
40	49	44	3.74241	0.026732	2.673E-05
60	27	96	5.527906	0.039485	3.949E-05
90	20	300	9.77205	0.0698	6.98E-05
120	7.3	316	10.02925	0.071638	7.164E-05
150	1.22	508	12.71619	0.09083	9.083E-05
180	0.9	586	13.65758	0.097554	9.755E-05
240	0.9	750	15.45097	0.110364	0.0001104
260	0.9	780	15.75696	0.11255	0.0001125
280	0.9	800	15.95769	0.113984	0.000114
300	0.9	810	16.05712	0.114694	0.0001147
330	0.9	820	16.15593	0.1154	0.0001154
360	0.9	830	16.25414	0.116101	0.0001161
390	0.9	840	16.35177	0.116798	0.0001168
420	0.9	850	16.44881	0.117492	0.0001175
450	0.9	860	16.54529	0.118181	0.0001182
480	0.9	870	16.6412	0.118866	0.0001189
510	0.9	880	16.73657	0.119547	0.0001195
540	0.9	890	16.83139	0.120224	0.0001202
570	0.9	900	16.92569	0.120898	0.0001209
600	0.9	910	17.01946	0.121568	0.0001216

6.3 Bubble Growth Models

6.3.1 Model A

24 bar

Diffusion into bubble constant diffusivity/constant pressure in bubble			
SI units		**Input here in familiar units**	
0.001	Initial radius of polymer sphere (m)	**1**	**mm**
0.00002	Initial radius of gas bubble (m)	**0.02**	**mm**
2400000	Initial pressure (Pa)	**24**	**bar**
100000	Final pressure (Pa)	**1**	**bar**
373.15	Temperature (K)	**100**	**C**
-1445.588	Arrhenius slope		
13.8	Arrhenius intercept		
1628.2	Henry's law constant p=Hc (bar.kgPS/kg CO2)		
6.47E+06	Henry's law constant p=Hc (Pa.m3/kmol)		
8.10E-11	Diffusion coefficient (m2/s)	**8.10E-11**	**m2/s**
0.016666667	Pressure decay constant (s-1)		
0.032292947	Density of C02 in bubble (kmol/m3)		
0.2	**Stability parameter**		
0.371185135	Initial concentration in polymer (kmol/m3)		
0.015466047	Final concentration in polymer (kmol/m3)		
4.18876E-09	Volume of polymer sphere (m3)		
4.61408E-08	Final bubble volume		
2.23E-03	Final bubble radius		
5.00E+00	Time period for smaller time steps		
0.5	Initial time step multiplier		

44 bar

Diffusion into bubble constant diffusivity/constant pressure in bubble			
SI units		**Input here in familiar units**	
0.001	Initial radius of polymer sphere (m)	**1**	**mm**
0.00002	Initial radius of gas bubble (m)	**0.02**	**mm**
4400000	Initial pressure (Pa)	**44**	**bar**
100000	Final pressure (Pa)	**1**	**bar**
373.15	Temperature (K)	**100**	**C**
-1445.588	Arrhenius slope		
13.8	Arrhenius intercept		
1628.2	Henry's law constant p=Hc (bar.kgPS/kg CO2)		
6.47E+06	Henry's law constant p=Hc (Pa.m3/kmol)		
1.14E-10	Diffusion coefficient (m2/s)	**1.14E-10**	**m2/s**
0.016666667	Pressure decay constant (s-1)		
0.032292947	Density of C02 in bubble (kmol/m3)		
0.2	**Stability parameter**		
0.68050608	Initial concentration in polymer (kmol/m3)		
0.015466047	Final concentration in polymer (kmol/m3)		
4.18876E-09	Volume of polymer sphere (m3)		
8.62632E-08	Final bubble volume		
2.74E-03	Final bubble radius		
5.00E+00	Time period for smaller time steps		
0.5	Initial time step multiplier		

63 bar

Diffusion into bubble constant diffusivity/constant pressure in bubble			
SI units		Input here in familiar units	
0.001	Initial radius of polymer sphere (m)	1	mm
0.00002	Initial radius of gas bubble (m)	0.02	mm
6300000	Initial pressure (Pa)	63	bar
100000	Final pressure (Pa)	1	bar
373.15	Temperature (K)	100	C
-1445.588	Arrhenius slope		
13.8	Arrhenius intercept		
1628.2	Henry's law constant p=Hc (bar.kgPS/kg CO2)		
6.47E+06	Henry's law constant p=Hc (Pa.m3/kmol)		
1.46E-10	Diffusion coefficient (m2/s)	1.46E-10	m2/s
0.016666667	Pressure decay constant (s-1)		
0.032292947	Density of C02 in bubble (kmol/m3)		
0.2	**Stability parameter**		
0.974360979	Initial concentration in polymer (kmol/m3)		
0.015466047	Final concentration in polymer (kmol/m3)		
4.18876E-09	Volume of polymer sphere (m3)		
1.2438E-07	Final bubble volume		
3.10E-03	Final bubble radius		
5.00E+00	Time period for smaller time steps		
0.5	Initial time step multiplier		

83 bar

Diffusion into bubble constant diffusivity/constant pressure in bubble			
SI units		Input here in familiar units	
0.001	Initial radius of polymer sphere (m)	1	mm
0.00002	Initial radius of gas bubble (m)	0.02	mm
8300000	Initial pressure (Pa)	83	bar
100000	Final pressure (Pa)	1	bar
373.15	Temperature (K)	100	C
-1445.588	Arrhenius slope		
13.8	Arrhenius intercept		
1628.2	Henry's law constant p=Hc (bar.kgPS/kg CO2)		
6.47E+06	Henry's law constant p=Hc (Pa.m3/kmol)		
1.67E-10	Diffusion coefficient (m2/s)	1.67E-10	m2/s
0.016666667	Pressure decay constant (s-1)		
0.032292947	Density of C02 in bubble (kmol/m3)		
0.2	**Stability parameter**		
1.283681924	Initial concentration in polymer (kmol/m3)		
0.015466047	Final concentration in polymer (kmol/m3)		
4.18876E-09	Volume of polymer sphere (m3)		
1.64502E-07	Final bubble volume		
3.40E-03	Final bubble radius		
5.00E+00	Time period for smaller time steps		
0.5	Initial time step multiplier		

6.3.2 Model B

- Model B with Diffusivity Published Value

24 bar

Diffusion into bubble constant diffusivity/constant pressure in bubble					
SI units				Input here	in familiar units
0.001	Initial radius of polymer sphere (m)			1	mm
0.00002	Initial radius of gas bubble (m)			0.02	mm
2400000	Initial pressure (Pa)			24	bar
200000	P_0 (Pa)	External pressure = (P_0-P_f) exp (-kt)+P_f		2	bar
100000	P_f (Pa)			1	bar
0.02	k (s^{-1})	(for constant external pressure enter k=0)		0.02	s^{-1}
373.15	Temperature (K)			100	°C
1628.2	**Henry's law constant p=Hc (bar.kgPS/kg CO2)**				
6465776	Henry's law constant p=Hc (Pa.m3/kmol)				
8.10E-11	Diffusion coefficient (m^2/s)			8.10E-11	m^2s^{-1}
0.80946	Initial density of CO2 in bubble (kmol/m3)				
0.06471	Final density of CO2 in bubble (kmol/m3)				
9.00E+07	**Shear viscosity (Pa.s)**			9.00E+07	
2.70E-04	Surface tension (Nm^{-1})			0.00027	Nm^{-1}
0.4000	Stability parameter			0.4	
0.3712	Initial concentration in polymer (kmol/m3)				
0.0155	Final concentration in polymer (kmol/m3)				
0.0000	Volume of polymer sphere (m^3)				
0.0000	Final bubble volume				
0.0018	Final bubble radius		1201925313		
5.0000	Time period for smaller time steps				
0.0100	Initial time step multiplier				
1.05E-10	volume of node a (m3)				
2.71E-14	Initial kmoles of CO2 in bubble (kmol)				
3.89E-11	Initial kmoles of CO2 in node a (kmol)				
1.55E-09	Initial kmoles of CO2 in polymer (kmol)				

44 bar

Diffusion into bubble constant diffusivity/constant pressure in bubble					
SI units				Input here	in familiar units
0.001	Initial radius of polymer sphere (m)			1	mm
0.00001	Initial radius of gas bubble (m)			0.01	mm
4400000	Initial pressure (Pa)			44	bar
2500000	P_0 (Pa)	External pressure = (P_0-P_f) exp (-kt)+P_f		25	bar
100000	P_f (Pa)			1	bar
0.02	k (s^{-1})	(for constant external pressure enter k=0)		0.02	s^{-1}
373.15	Temperature (K)			100	°C
1628.2	**Henry's law constant p=Hc (bar.kgPS/kg CO2)**				
6465776	Henry's law constant p=Hc (Pa.m3/kmol)				
1.14E-10	Diffusion coefficient (m^2/s)			1.14E-10	m^2s^{-1}
1.54264	Initial density of CO2 in bubble (kmol/m3)				
0.84481	Final density of CO2 in bubble (kmol/m3)				
7.00E+07	**Shear viscosity (Pa.s)**			7.00E+07	
2.70E-04	**Surface tension (Nm^{-1})**			0.00027	Nm^{-1}
0.4000	Stability parameter			0.4	
0.6805	Initial concentration in polymer (kmol/m3)				
0.0155	Final concentration in polymer (kmol/m3)				
0.0000	Volume of polymer sphere (m^3)				
0.0000	Final bubble volume				
0.0009	Final bubble radius		1201925313		
5.0000	Time period for smaller time steps				
0.0100	Initial time step multiplier				
1.05E-10	volume of node a (m3)				
6.46E-15	Initial kmoles of CO2 in bubble (kmol)				
7.13E-11	Initial kmoles of CO2 in node a (kmol)				
2.85E-09	Initial kmoles of CO2 in polymer (kmol)				

63 bar

Diffusion into bubble constant diffusivity/constant pressure in bubble														
SI units											Input here in familiar units			
0.001	Initial radius of polymer sphere (m)										1	mm		
0.00001	Initial radius of gas bubble (m)										0.01	mm		
6300000	Initial pressure (Pa)										63	bar		
5100000	P_0 (Pa)	External pressure = (P_0-P_0 exp (-kt)+P_t									51	bar		
100000	P_t (Pa)										1	bar		
0.02	k (s^{-1})	(for constant external pressure enter k=0)									0.02	s^{-1}		
373.15	Temperature (K)										100	°C		
1628.2	Henry's law constant p=Hc (bar.kgPS/kg CO2)													
6465776	Henry's law constant p=Hc (Pa.m3/kmol)													
1.46E-10	Diffusion coefficient (m^2/s)										1.46E-10	m^2s^{-1}		
2.29229	Initial density of C02 in bubble (kmol/m3)													
1.81268	Final density of C02 in bubble (kmol/m3)													
8.00E+07	Shear viscosity (Pa.s)										8.00E+07			
2.70E-04	Surface tension (Nm^{-1})										0.00027	Nm^{-1}		
0.4000	Stability parameter										0.4			
0.9744	Initial concentration in polymer (kmol/m3)													
0.0155	Final concentration in polymer (kmol/m3)													
0.0000	Volume of polymer sphere (m^3)													
0.0000	Final bubble volume													
0.0008	Final bubble radius									1201925313				
5.0000	Time period for smaller time steps													
0.0100	Initial time step multiplier													
1.05E-10	volume of node a (m3)													
9.60E-15	Initial kmoles of CO2 in bubble (kmol)													
1.02E-10	Initial kmoles of CO2 in node a (kmol)													
4.08E-09	Initial kmoles of CO2 in polymer (kmol)													

83 bar

Diffusion into bubble constant diffusivity/constant pressure in bubble														
SI units											Input here in familiar units			
0.001	Initial radius of polymer sphere (m)										1	mm		
0.00001	Initial radius of gas bubble (m)										0.01	mm		
8300000	Initial pressure (Pa)										83	bar		
5100000	P_0 (Pa)	External pressure = (P_0-P_0 exp (-kt)+P_t									51	bar		
100000	P_t (Pa)										1	bar		
0.02	k (s^{-1})	(for constant external pressure enter k=0)									0.02	s^{-1}		
373.15	Temperature (K)										100	°C		
1628.2	Henry's law constant p=Hc (bar.kgPS/kg CO2)													
6465776	Henry's law constant p=Hc (Pa.m3/kmol)													
1.67E-10	Diffusion coefficient (m^2/s)										1.67E-10	m^2s^{-1}		
3.13860	Initial density of C02 in bubble (kmol/m3)													
1.81268	Final density of C02 in bubble (kmol/m3)													
8.00E+07	Shear viscosity (Pa.s)										8.00E+07			
2.70E-04	Surface tension (Nm^{-1})										0.00027	Nm^{-1}		
0.4000	Stability parameter										0.4			
1.2837	Initial concentration in polymer (kmol/m3)													
0.0155	Final concentration in polymer (kmol/m3)													
0.0000	Volume of polymer sphere (m^3)													
0.0000	Final bubble volume													
0.0009	Final bubble radius									1201925313				
5.0000	Time period for smaller time steps													
0.0100	Initial time step multiplier													
1.05E-10	volume of node a (m3)													
1.31E-14	Initial kmoles of CO2 in bubble (kmol)													
1.34E-10	Initial kmoles of CO2 in node a (kmol)													
5.38E-09	Initial kmoles of CO2 in polymer (kmol)													

- Model B with best fit of Diffusivity values

24 bar

Diffusion into bubble constant diffusivity/constant pressure in bubble									
SI units							Input here in familiar units		
0.001	Initial radius of polymer sphere (m)						1	mm	
0.00002	Initial radius of gas bubble (m)						0.02	mm	
2400000	Initial pressure (Pa)						24	bar	
200000	P_o (Pa)	External pressure = (P_o-P_f) exp (-kt)+P_f					2	bar	
100000	P_f (Pa)						1	bar	
0.02	k (s^{-1})	(for constant external pressure enter k=0)					0.02	s^{-1}	
373.15	Temperature (K)						100	°C	
1628.2	**Henry's law constant p=Hc (bar.kgPS/kg CO2)**								
6465776	Henry's law constant p=Hc (Pa.m3/kmol)								
8.10E-11	Diffusion coefficient (m^2/s)						8.10E-11	m^2s^{-1}	
0.80946	Initial density of C02 in bubble (kmol/m3)								
0.06471	Final density of C02 in bubble (kmol/m3)								
9.00E+07	**Shear viscosity (Pa.s)**						9.00E+07		
2.70E-04	Surface tension (Nm^{-1})						0.00027	Nm^{-1}	
0.4000	Stability parameter						0.4		
0.3712	Initial concentration in polymer (kmol/m3)								
0.0155	Final concentration in polymer (kmol/m3)								
0.0000	Volume of polymer sphere (m^3)								
0.0000	Final bubble volume								
0.0018	Final bubble radius					1201925313			
5.0000	Time period for smaller time steps								
0.0100	Initial time step multiplier								
1.05E-10	volume of node a (m3)								
2.71E-14	Initial kmoles of CO2 in bubble (kmol)								
3.89E-11	Initial kmoles of CO2 in node a (kmol)								
1.55E-09	Initial kmoles of CO2 in polymer (kmol)								

44 bar

Diffusion into bubble constant diffusivity/constant pressure in bubble									
SI units							Input here in familiar units		
0.001	Initial radius of polymer sphere (m)						1	mm	
0.00001	Initial radius of gas bubble (m)						0.01	mm	
4400000	Initial pressure (Pa)						44	bar	
2500000	P_o (Pa)	External pressure = (P_o-P_f) exp (-kt)+P_f					25	bar	
100000	P_f (Pa)						1	bar	
0.02	k (s^{-1})	(for constant external pressure enter k=0)					0.02	s^{-1}	
373.15	Temperature (K)						100	°C	
1628.2	**Henry's law constant p=Hc (bar.kgPS/kg CO2)**								
6465776	Henry's law constant p=Hc (Pa.m3/kmol)								
1.14E-12	Diffusion coefficient (m^2/s)						1.14E-12	m^2s^{-1}	
1.54264	Initial density of C02 in bubble (kmol/m3)								
0.84481	Final density of C02 in bubble (kmol/m3)								
6.00E+07	**Shear viscosity (Pa.s)**						6.00E+07		
2.70E-04	**Surface tension (Nm^{-1})**						0.00027	Nm^{-1}	
0.0040	Stability parameter						0.004		
0.6805	Initial concentration in polymer (kmol/m3)								
0.0155	Final concentration in polymer (kmol/m3)								
0.0000	Volume of polymer sphere (m^3)								
0.0000	Final bubble volume								
0.0009	Final bubble radius					1201925313			
5.0000	Time period for smaller time steps								
0.0100	Initial time step multiplier								
1.05E-10	volume of node a (m3)								
6.46E-15	Initial kmoles of CO2 in bubble (kmol)								
7.13E-11	Initial kmoles of CO2 in node a (kmol)								
2.85E-09	Initial kmoles of CO2 in polymer (kmol)								

63 bar

Diffusion into bubble constant diffusivity/constant pressure in bubble												
SI units										Input here in familiar units		
0.001	Initial radius of polymer sphere (m)									1	mm	
0.00001	Initial radius of gas bubble (m)									0.01	mm	
6300000	Initial pressure (Pa)									63	bar	
5100000	P_0 (Pa)	External pressure = (P_0-P_f exp (-kt)+P_f								51	bar	
100000	P_f (Pa)									1	bar	
0.02	k (s^{-1})	(for constant external pressure enter k=0)								0.02	s^{-1}	
373.15	Temperature (K)									100	°C	
1628.2	Henry's law constant p=Hc (bar.kgPS/kg CO2)											
6465776	Henry's law constant p=Hc (Pa.m3/kmol)											
1.46E-12	Diffusion coefficient (m^2/s)									1.46E-12	m^2s^{-1}	
2.29229	Initial density of C02 in bubble (kmol/m3)											
1.81268	Final density of C02 in bubble (kmol/m3)											
6.00E+07	Shear viscosity (Pa.s)									6.00E+07		
2.70E-04	Surface tension (Nm^{-1})									0.00027	Nm^{-1}	
0.0040	Stability parameter									0.004		
0.9744	Initial concentration in polymer (kmol/m3)											
0.0155	Final concentration in polymer (kmol/m3)											
0.0000	Volume of polymer sphere (m^3)											
0.0000	Final bubble volume											
0.0008	Final bubble radius								1201925313			
5.0000	Time period for smaller time steps											
0.0100	Initial time step multiplier											
1.05E-10	volume of node a (m3)											
9.60E-15	Initial kmoles of CO2 in bubble (kmol)											
1.02E-10	Initial kmoles of CO2 in node a (kmol)											
4.08E-09	Initial kmoles of CO2 in polymer (kmol)											

83 bar

Diffusion into bubble constant diffusivity/constant pressure in bubble												
SI units										Input here in familiar units		
0.001	Initial radius of polymer sphere (m)									1	mm	
0.00001	Initial radius of gas bubble (m)									0.01	mm	
8300000	Initial pressure (Pa)									83	bar	
5100000	P_0 (Pa)	External pressure = (P_0-P_f exp (-kt)+P_f								51	bar	
100000	P_f (Pa)									1	bar	
0.02	k (s^{-1})	(for constant external pressure enter k=0)								0.02	s^{-1}	
373.15	Temperature (K)									100	°C	
1628.2	Henry's law constant p=Hc (bar.kgPS/kg CO2)											
6465776	Henry's law constant p=Hc (Pa.m3/kmol)											
1.67E-12	Diffusion coefficient (m^2/s)									1.67E-12	m^2s^{-1}	
3.13860	Initial density of C02 in bubble (kmol/m3)											
1.81268	Final density of C02 in bubble (kmol/m3)											
6.00E+07	Shear viscosity (Pa.s)									6.00E+07		
2.70E-04	Surface tension (Nm^{-1})									0.00027	Nm^{-1}	
0.0040	Stability parameter									0.004		
1.2837	Initial concentration in polymer (kmol/m3)											
0.0155	Final concentration in polymer (kmol/m3)											
0.0000	Volume of polymer sphere (m^3)											
0.0000	Final bubble volume											
0.0009	Final bubble radius								1201925313			
5.0000	Time period for smaller time steps											
0.0100	Initial time step multiplier											
1.05E-10	volume of node a (m3)											
1.31E-14	Initial kmoles of CO2 in bubble (kmol)											
1.34E-10	Initial kmoles of CO2 in node a (kmol)											
5.38E-09	Initial kmoles of CO2 in polymer (kmol)											

6.3.3 Model C

- Diffusivity and Viscosity Varying – WLF (Model C)

24 bar

Diffusion into bubble constant diffusivity/constant pressure in bubble										
SI units								Input here in familiar units		
0.001	Initial radius of polymer sphere (m)							1	mm	
0.000001	Initial radius of gas bubble (m)							0.001	mm	
2400000	Initial pressure (Pa)							24	bar	
200000	P_o (Pa)	External pressure = (P_o-P_n) exp (-kt)+P_i						2	bar	
100000	P_i (Pa)							1	bar	
0.02	k (s^{-1})	(for constant external pressure enter k=0)						0.02	s^{-1}	
373.15	Temperature (K)							100	°C	
1628	Henry's law constant p=Hc (bar.kgPS/kg CO2)									
6464982	Henry's law constant p=Hc (Pa.m3/kmol)									D (m^2/s)
2.72E-16	D_o (m^2/s)							2.72E-16	m^2s^{-1}	8.10E-11
0.80946	Initial density of C02 in bubble (kmol/m3)									
0.06471	Final density of C02 in bubble (kmol/m3)									(Pa.s)
6.54E+12	$_o$ (Pa.s)							6.54E+12		2.20E+07
2.70E-04	Surface tension (Nm^{-1})							0.00027	Nm^{-1}	
17.44	C_1	K	Willaims et al 1995							
51.6	C_2	K						10		
3.77E+02	T_{go}									
1.15E-05	m (K/Pa)									
7.43E+01	beta ($K.m^3$/kmol)									
0.3000	Stability parameter							0.02		
0.3712	Initial concentration in polymer (kmol/m3)									
0.0155	Final concentration in polymer (kmol/m3)									
0.0000	Volume of polymer sphere (m^3)									
0.0000	Final bubble volume									
0.0018	Final bubble radius						1201925313			
5.0000	Time period for smaller time steps									
0.1000	Initial time step multiplier									
1.05E-10	volume of node a (m3)									
3.39E-18	Initial kmoles of CO2 in bubble (kmol)									
3.89E-11	Initial kmoles of CO2 in node a (kmol)									
1.56E-09	Initial kmoles of CO2 in polymer (kmol)									

44 bar

Diffusion into bubble constant diffusivity/constant pressure in bubble										
SI units								Input here in familiar units		
0.001	Initial radius of polymer sphere (m)							1	mm	
0.000001	Initial radius of gas bubble (m)							0.001	mm	
4400000	Initial pressure (Pa)							44	bar	
2500000	P_o (Pa)	External pressure = (P_o-P_n) exp (-kt)+P_i						25	bar	
100000	P_i (Pa)							1	bar	
0.02	k (s^{-1})	(for constant external pressure enter k=0)						0.02	s^{-1}	
373.15	Temperature (K)							100	°C	
1628	Henry's law constant p=Hc (bar.kgPS/kg CO2)									
6464982	Henry's law constant p=Hc (Pa.m3/kmol)									
6.04E-19	D_o (m^2/s)							6.04E-19	m^2s^{-1}	1.14E-10
1.54264	Initial density of C02 in bubble (kmol/m3)									
0.84481	Final density of C02 in bubble (kmol/m3)									
4.72E+15	$_o$ (Pa.s)							4.72E+15		2.50E+07
2.70E-04	Surface tension (Nm^{-1})							0.00027	Nm^{-1}	
17.44	C_1	K	Willaims et al 1995							
51.6	C_2	K						10		
3.77E+02	T_{go}									
1.15E-05	m (K/Pa)									
7.43E+01	beta ($K.m^3$/kmol)									
0.3000	Stability parameter							0.02		
0.6806	Initial concentration in polymer (kmol/m3)									
0.0155	Final concentration in polymer (kmol/m3)									
0.0000	Volume of polymer sphere (m^3)									
0.0000	Final bubble volume									
0.0009	Final bubble radius						1201925313			
5.0000	Time period for smaller time steps									
0.1000	Initial time step multiplier									
1.05E-10	volume of node a (m3)									
6.46E-18	Initial kmoles of CO2 in bubble (kmol)									
7.13E-11	Initial kmoles of CO2 in node a (kmol)									
2.85E-09	Initial kmoles of CO2 in polymer (kmol)									

63 bar

Diffusion into bubble constant diffusivity/constant pressure in bubble										
SI units								Input here in familiar units		
0.001	Initial radius of polymer sphere (m)							1	mm	
0.000001	Initial radius of gas bubble (m)							0.001	mm	
6300000	Initial pressure (Pa)							63	bar	
5100000	P_o (Pa)	External pressure = (P_o-P_f) exp (-kt)+P_f						51	bar	
100000	P_i (Pa)							1	bar	
0.02	k (s^{-1})	(for constant external pressure enter k=0)						0.02	s^{-1}	
373.15	Temperature (K)							100	°C	
1628	Henry's law constant p=Hc (bar.kgPS/kg CO2)									
6464982	Henry's law constant p=Hc (Pa.m3/kmol)									
1.66E-20	D_o (m^2/s)							1.66E-20	m^2s^{-1}	1.46E-10
2.29229	Initial density of C02 in bubble (kmol/m3)									
1.81268	Final density of C02 in bubble (kmol/m3)									
1.32E+17	$_o$ (Pa.s)							1.32E+17		1.50E+07
2.70E-04	Surface tension (Nm^{-1})							0.00027	Nm^{-1}	
17.44	C_1	K	Willaims et al 1995							
51.6	C_2	K						10		
3.77E+02	T_{go}									
1.15E-05	m (K/Pa)									
7.43E+01	beta ($K.m^3$/kmol)									
0.3000	Stability parameter							0.02		
0.9745	Initial concentration in polymer (kmol/m3)									
0.0155	Final concentration in polymer (kmol/m3)									
0.0000	Volume of polymer sphere (m^3)									
0.0000	Final bubble volume									
0.0008	Final bubble radius						1201925313			
5.0000	Time period for smaller time steps									
0.1000	Initial time step multiplier									
1.05E-10	volume of node a (m3)									
9.60E-18	Initial kmoles of CO2 in bubble (kmol)									
1.02E-10	Initial kmoles of CO2 in node a (kmol)									
4.08E-09	Initial kmoles of CO2 in polymer (kmol)									

83 bar

Diffusion into bubble constant diffusivity/constant pressure in bubble										
SI units								Input here in familiar units		
0.001	Initial radius of polymer sphere (m)							1	mm	
0.000001	Initial radius of gas bubble (m)							0.001	mm	
8300000	Initial pressure (Pa)							83	bar	
5100000	P_o (Pa)	External pressure = (P_o-P_f) exp (-kt)+P_f						51	bar	
100000	P_i (Pa)							1	bar	
0.02	k (s^{-1})	(for constant external pressure enter k=0)						0.02	s^{-1}	
373.15	Temperature (K)							100	°C	
1628	Henry's law constant p=Hc (bar.kgPS/kg CO2)									
6464982	Henry's law constant p=Hc (Pa.m3/kmol)									
1.18E-21	D_o (m^2/s)							1.18E-21	m^2s^{-1}	1.67E-10
3.13860	Initial density of C02 in bubble (kmol/m3)									
1.81268	Final density of C02 in bubble (kmol/m3)									
2.11E+18	$_o$ (Pa.s)							2.11E+18		1.50E+07
2.70E-04	Surface tension (Nm^{-1})							0.00027	Nm^{-1}	
17.44	C_1	K	Willaims et al 1995							
51.6	C_2	K						10		
3.77E+02	T_{go}									
1.15E-05	m (K/Pa)									
7.43E+01	beta ($K.m^3$/kmol)									
0.3000	Stability parameter							0.02		
1.2838	Initial concentration in polymer (kmol/m3)									
0.0155	Final concentration in polymer (kmol/m3)									
0.0000	Volume of polymer sphere (m^3)									
0.0000	Final bubble volume									
0.0009	Final bubble radius						1201925313			
5.0000	Time period for smaller time steps									
0.1000	Initial time step multiplier									
1.05E-10	volume of node a (m3)									
1.31E-17	Initial kmoles of CO2 in bubble (kmol)									
1.34E-10	Initial kmoles of CO2 in node a (kmol)									
5.38E-09	Initial kmoles of CO2 in polymer (kmol)									

- WLF Constants Fitted to Sato et al (2001)

Sato et al 2001

p=Hc

1628	Henry's law constant p=Hc (bar.kgPS/kg CO_2)
6464982	Henry's law constant p=Hc (Pa.m^3/kmol)
64.649819	**Henry's law constant p=Hc (bar.m^3/kmol)**

p (bar)	c (kmol/m^3)	D Sato (x10^{-10} m2/s)	D fit (x10^{-10} m2/s)	error sq
24	0.371230735	0.81	0.757267767	0.002780688
44	0.680589681	1.14	1.219013558	0.006243142
63	0.974480679	1.46	1.46346894	1.20335E-05
83	1.283839625	1.67	1.624804673	0.002042618

Fit constants	
D_0	0.016490863
c_1	2.142182242
c_2	6.813288803
T (°C)	100

0.011078482	sum of squares

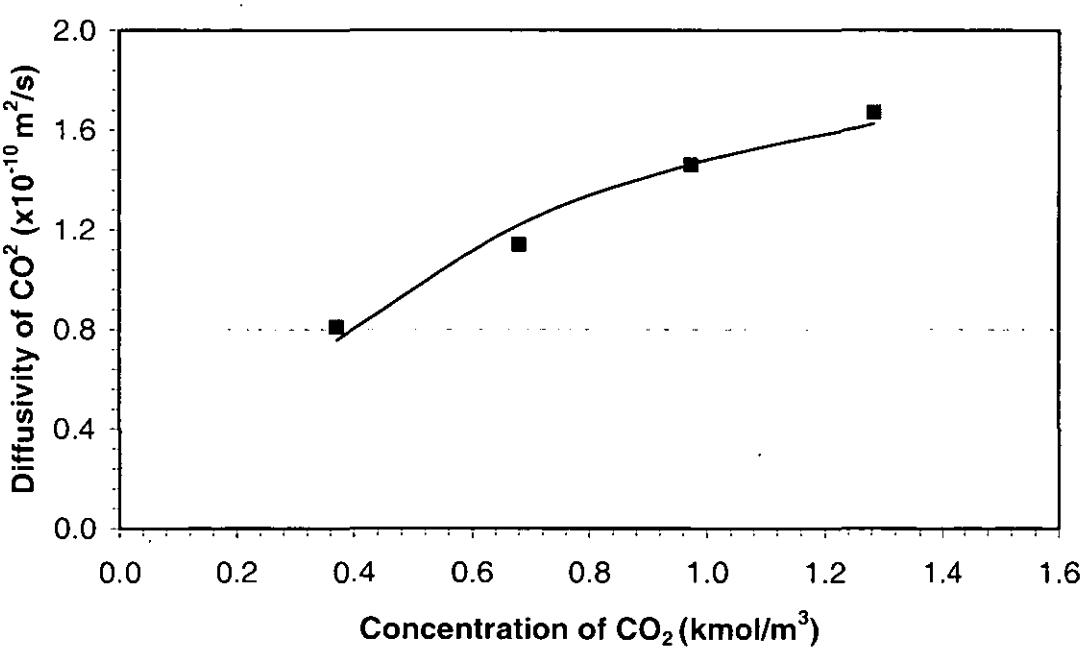

24 bar

Diffusion into bubble constant diffusivity/constant pressure in bubble										
SI units								Input here in familiar units		
0.00065	Initial radius of polymer sphere (m)							0.65	mm	
0.000001	Initial radius of gas bubble (m)							0.001	mm	
2400000	Initial pressure (Pa)							24	bar	
200000	P_0 (Pa)	External pressure = (P_0-P_f exp (-kt)+P_f						2	bar	
100000	P_f (Pa)							1	bar	
0.02	k (s^{-1})	(for constant external pressure enter k=0)						0.02	s^{-1}	
373.15	Temperature (K)							100	°C	
1628	Henry's law constant p=Hc (bar.kgPS/kg CO2)									
6464982	Henry's law constant p=Hc (Pa.m3/kmol)									D (m^2/s)
1.65E-12	D_0 (m^2/s)							1.65E-12	m^2s^{-1}	7.56E-11
0.80946	Initial density of C02 in bubble (kmol/m3)									
0.06471	Final density of C02 in bubble (kmol/m3)									
1.50E+09	μ_0 (Pa.s)							1.50E+09		3.28E+07
2.70E-04	Surface tension (Nm^{-1})							0.00027	Nm^{-1}	
2.14	C_1	K	Williams et al 1995							
6.81	C_2	K						10		
3.77E+02	T_{go}									
1.15E-05	m (K/Pa)									
7.43E+01	beta (K.m^3/kmol)									
0.3000	Stability parameter							0.02		
0.3712	Initial concentration in polymer (kmol/m3)									
0.0155	Final concentration in polymer (kmol/m3)									
0.0000	Volume of polymer sphere (m^3)									
0.0000	Final bubble volume									
0.0011	Final bubble radius						1201925313			
5.0000	Time period for smaller time steps									
0.1000	Initial time step multiplier									
2.88E-11	volume of node a (m3)									
3.39E-18	Initial kmoles of CO2 in bubble (kmol)									
1.07E-11	Initial kmoles of CO2 in node a (kmol)									
4.27E-10	Initial kmoles of CO2 in polymer (kmol)									

44 bar

Diffusion into bubble constant diffusivity/constant pressure in bubble										
SI units								Input here in familiar units		
0.001	Initial radius of polymer sphere (m)							1	mm	
0.000001	Initial radius of gas bubble (m)							0.001	mm	
4400000	Initial pressure (Pa)							44	bar	
2500000	P_0 (Pa)	External pressure = (P_0-P_f exp (-kt)+P_f						25	bar	
100000	P_f (Pa)							1	bar	
0.02	k (s^{-1})	(for constant external pressure enter k=0)						0.02	s^{-1}	
373.15	Temperature (K)							100	°C	
1628	Henry's law constant p=Hc (bar.kgPS/kg CO2)									
6464982	Henry's law constant p=Hc (Pa.m3/kmol)									
1.65E-12	D_0 (m^2/s)							1.65E-12	m^2s^{-1}	1.22E-10
1.54264	Initial density of C02 in bubble (kmol/m3)									
0.84481	Final density of C02 in bubble (kmol/m3)									
2.70E+09	μ_0 (Pa.s)							2.70E+09		3.67E+07
2.70E-04	Surface tension (Nm^{-1})							0.00027	Nm^{-1}	
2.14	C_1	K	Sato et al 2001							
6.81	C_2	K						10		
3.77E+02	T_{go}									
1.15E-05	m (K/Pa)									
7.43E+01	beta (K.m^3/kmol)									
0.3000	Stability parameter							0.02		
0.6806	Initial concentration in polymer (kmol/m3)									
0.0155	Final concentration in polymer (kmol/m3)									
0.0000	Volume of polymer sphere (m^3)									
0.0000	Final bubble volume									
0.0009	Final bubble radius						1201925313			
5.0000	Time period for smaller time steps									
0.1000	Initial time step multiplier									
1.05E-10	volume of node a (m3)									
6.46E-18	Initial kmoles of CO2 in bubble (kmol)									
7.13E-11	Initial kmoles of CO2 in node a (kmol)									
2.85E-09	Initial kmoles of CO2 in polymer (kmol)									

63 bar

Diffusion into bubble constant diffusivity/constant pressure in bubble											
SI units									Input here in familiar units		
0.001	Initial radius of polymer sphere (m)								1	mm	
0.000001	Initial radius of gas bubble (m)								0.001	mm	
6300000	Initial pressure (Pa)								63	bar	
5100000	P_0 (Pa)	External pressure = $(P_0-P_f)\exp(-kt)+P_f$							51	bar	
100000	P_f (Pa)								1	bar	
0.02	k (s^{-1})	(for constant external pressure enter k=0)							0.02	s^{-1}	
373.15	Temperature (K)								100	°C	
1628	Henry's law constant p=Hc (bar.kgPS/kg CO2)										
6464982	Henry's law constant p=Hc (Pa.m3/kmol)										
1.65E-12	**D_0 (m^2/s)**								1.65E-12	m^2s^{-1}	1.46E-10
2.29229	Initial density of C02 in bubble (kmol/m3)										
1.81268	Final density of C02 in bubble (kmol/m3)										
4.00E+09	**μ_0 (Pa.s)**								4.00E+09		4.53E+07
2.70E-04	Surface tension (Nm^{-1})								0.00027	Nm^{-1}	
2.14	**C_1**	K	Willaims et al 1995								
6.81	**C_2**	K							10		
3.77E+02	T_{g0}										
1.15E-05	m (K/Pa)										
7.43E+01	beta ($K.m^3/kmol$)										
0.3000	Stability parameter								0.02		
0.9745	Initial concentration in polymer (kmol/m3)										
0.0155	Final concentration in polymer (kmol/m3)										
0.0000	Volume of polymer sphere (m^3)										
0.0000	Final bubble volume										
0.0008	Final bubble radius							1201925313			
5.0000	Time period for smaller time steps										
0.1000	Initial time step multiplier										
1.05E-10	volume of node a (m3)										
9.60E-18	Initial kmoles of CO2 in bubble (kmol)										
1.02E-10	Initial kmoles of CO2 in node a (kmol)										
4.08E-09	Initial kmoles of CO2 in polymer (kmol)										

83 bar

Diffusion into bubble constant diffusivity/constant pressure in bubble											
SI units									Input here in familiar units		
0.001	Initial radius of polymer sphere (m)								1	mm	
0.000001	Initial radius of gas bubble (m)								0.001	mm	
8300000	Initial pressure (Pa)								83	bar	
5100000	P_0 (Pa)	External pressure = $(P_0-P_f)\exp(-kt)+P_f$							51	bar	
100000	P_f (Pa)								1	bar	
0.02	k (s^{-1})	(for constant external pressure enter k=0)							0.02	s^{-1}	
373.15	Temperature (K)								100	°C	
1628	Henry's law constant p=Hc (bar.kgPS/kg CO2)										
6464982	Henry's law constant p=Hc (Pa.m3/kmol)										
1.65E-12	**D_0 (m^2/s)**								1.65E-12	m^2s^{-1}	1.62E-10
3.13860	Initial density of C02 in bubble (kmol/m3)										
1.81268	Final density of C02 in bubble (kmol/m3)										
5.50E+09	**μ_0 (Pa.s)**								5.50E+09		5.61E+07
2.70E-04	Surface tension (Nm^{-1})								0.00027	Nm^{-1}	
2.14	**C_1**	K	Willaims et al 1995								
6.81	**C_2**	K							10		
3.77E+02	T_{g0}										
1.15E-05	m (K/Pa)										
7.43E+01	beta ($K.m^3/kmol$)										
0.3000	Stability parameter								0.02		
1.2838	Initial concentration in polymer (kmol/m3)										
0.0155	Final concentration in polymer (kmol/m3)										
0.0000	Volume of polymer sphere (m^3)										
0.0000	Final bubble volume										
0.0009	Final bubble radius							1201925313			
5.0000	Time period for smaller time steps										
0.1000	Initial time step multiplier										
1.05E-10	volume of node a (m3)										
1.31E-17	Initial kmoles of CO2 in bubble (kmol)										
1.34E-10	Initial kmoles of CO2 in node a (kmol)										
5.38E-09	Initial kmoles of CO2 in polymer (kmol)										

Publications

- The 7th World Congress of Chemical Engineering, Glasgow UK (10 - 13 July 2005).

Mechanical measurement of the plasticisation of polymers by high pressure carbon dioxide

S Al-Enezi [1], *K Hellgardt*, *AGF Stapley*
[1]Chemical Engineering, Loughborough University;

Plasticisers are commonly used in polymer processing as they lower the glass transition (softening) temperature of polymers to allow shape forming at lower temperatures. The ability of carbon dioxide at high pressure to act as a plasticiser of certain synthetic polymers has been well documented in the literature on the basis of evidence from FTIR spectroscopy. However, FTIR only measures conditions on the surface of polymers. Carbon dioxide is an environmentally attractive solvent and leaves virtually no residue in the polymer on return to ambient pressure, but if plasticisation is to be an effective for shape forming polymers the effect also needs to be demonstrated mechanically, which requires softening to occur throughout the sample. This paper presents results from 3-point bend test experiments on 2 mm thick polymer strips in a temperature controlled high pressure cell. This is equipped with a linear variable displacement transducer to measure the central deflection, and a platinum resistance probe located close to the sample in the cell to measure temperature. The nominal glass transition temperature was recorded as the onset temperature where the central deflection suddenly begins to increase. Significant reductions in glass transition temperature compared to ambient conditions were observed on the application of carbon dioxide at 1000 psig (69 bar) for the following samples: polycarbonate - from 157°C to 145°C, poly-methylmethacrylate - from 115°C to 75°C, poly-ethyleneterepthalate - from 88°C to 70°C and polystyrene - from 104°C to 64°C. Interesting effects were also observed to take place during depressurisation, as the carbon dioxide gas can expand within the material and create a foamed structure. Variations in bubble size and number were found to depend on depressurisation methods and this is the subject of ongoing investigations

Keywords: Glass transition temperature, softening, depressurization, supercritical fluids.

Mechanical Measurement of the Plasticisation of Polymers by High Pressure Carbon Dioxide

S. Al-Enezi, A.G.F. Stapley, K. Hellgardt

Department of Chemical Engineering, Loughborough University, Leicestershire, LE11 3TU, UK

Email: A.G.F.Stapley@Lboro.ac.uk

Introduction

Carbon dioxide at high pressure is a new and promising medium for polymer processing in areas as such as mechanical forming, dye impregnation and polymer foaming. It has been shown by FTIR that high pressure carbon dioxide reduces the glass transition temperature of polymers. However, this only measures surface effects. In this paper a novel mechanical measurement of Tg is made using a 3-point bend.

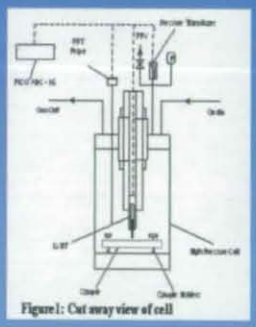

Figure 1: Cut away view of cell

Procedure

Four polymer materials were tested: polycarbonate (PC), polystyrene (PS), and glycol modified polyethylene-terephthalate (PETG), and polymethyl-methacrylate (PMMA). The polymer strips were cut from sheets of different thicknesses (2-3 mm). The polymer sample was placed in the cell in contact with the LVDT, and the cell sealed and placed in the oil bath at ambient temperature (1°C/min). Heating was then stopped and the cell depressurised over the course of 3 minutes.

Effect of Carbon Dioxide in Polymer Softening (Temperature vs. Displacement)

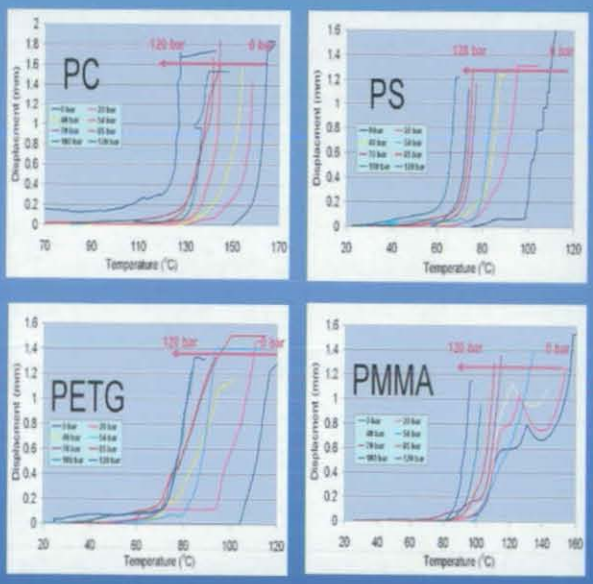

Effect of CO2 pressure on structure after Depressurization

Conclusions

Three-point bend testing of polymer strips in a high pressure cell has successfully been used to demonstrate the plasticisation of PC, PS, PETG and PMMA by carbon dioxide at high pressures. Samples typically showed a decrease on softening temperature of approximately 35K over an applied pressure range of 0 to 120 bar. The foaming behaviour of the polymer samples can also be tested on depressurization of the system.

Ref. Kazarian SG. Polymer Science, Ser. C 2000; 42:70-101

Loughborough University

- International Journal of Polymer Analysis and Characterization (Dec. 2006)

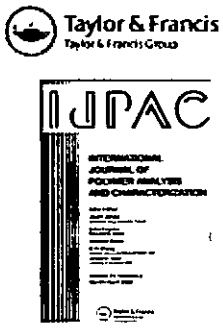

ISSN: 1023-666X

Mechanical Measurement of the Plasticisation of Polymers by High Pressure Carbon Dioxide

S. Al-Enezi, K. Hellgardt, A.G.F. Stapley

Department of Chemical Engineering, Loughborough University

Loughborough, Leicestershire, LE11 3TU, UK.

ABSTRACT

Plasticisers are commonly used in polymer processing as they lower the glass transition temperature of polymers to allow shape forming at lower temperatures. It is well established that CO_2 at high pressure acts as a plasticiser for certain synthetic polymers, but relatively few studies have demonstrated the effect mechanically. This paper presents results from 3-point bending tests on 2-3 mm thick polymer samples at pressures of up to 120 bar, using a linear variable displacement transducer (LVDT) to measure the central deflection. Significant reductions in the bending onset temperatures were observed on the application of CO_2 for polycarbonate (PC), polystyrene (PS), polymethyl-methacrylate (PMMA) and glycol modified polyethylene terephthalate (PETG) of typically 50-100 °C of pressures applied. Initial onset temperatures correlated reasonably well with literature values for T_g, but complete softening of the sample was influenced by the time taken for CO_2 to diffuse into the samples.

Keywords: *Glass transition, linear variable displacement transducer, softening, foaming, thermoplastics.*

- The 2nd Saudi Innovation Conference, Newcastle UK (11 – 12 May 2007)

ISBN: 978-0-955104-92-3

Measuring the Glass Transition of Polymers at High Pressure and Temperature by LVDT

S. Al-Enezi, K. Hellgardt, A.G.F. Stapley

Department of Chemical Engineering, Loughborough University
Loughborough, Leicestershire, LE11 3TU, UK.

Abstract

Plasticisers are commonly used in polymer processing as they lower the glass transition temperature of polymers to allow shape forming at lower temperatures. It is well established that CO_2 at high pressure acts as a plasticiser for certain synthetic polymers, but relatively few studies have demonstrated the effect mechanically. This paper presents results from 3-point bending tests on 2-3 mm thick polymer samples at pressures of up to 120 bar, using a linear variable displacement transducer (LVDT) to measure the central deflection. Significant reductions in the bending onset temperatures were observed on the application of CO_2 for polycarbonate, polystyrene, poly(methyl methacrylate) and glycol modified poly(ethylene terephthalate) of typically 50-100 K over the range of pressures applied. Initial onset temperatures correlated reasonably well with literature values for T_g, but complete softening of the sample was influenced by the time taken for CO_2 to diffuse into the samples.

Keywords: *Glass Transition, LVDT, Softening, Supercritical, Thermoplastics.*

- Saudi Innovation International Conference, Leeds UK (9 -10 June 2008)

ISBN: 978-0-9559241-2-5

Mechanical Measurement of Polystyrene Softening Under CO_2 at High-Pressure

S. Al-Enezi, K. Hellgardt, I. Cumming and A.G.F. Stapley

Department of Chemical Engineering, Loughborough University, Loughborough, Leicestershire, LE11 3TU, UK.

Abstract

This paper examines the effects derived from the ability of high pressure carbon dioxide to soften polystyrene. In this study the softening of polystyrene as a function of applied carbon dioxide pressure and temperature has been measured using a novel mechanical 3-point bend test rig. In initial experiments the temperature was slowly ramped upward and the nominal glass transition temperature was recorded as the temperature where the central deflection suddenly begins to increase. Significant reductions in the bending onset temperatures were observed on the application of carbon dioxide for polystyrene, of typically 60 °C over the range of pressures applied (24 to 120 bar). The temperatures at which large scale deflection occurred were significantly higher than the onset point and this was attributed to the time taken for CO_2 to diffuse into the polymer. A model was developed to use onset and full-scale bending temperature to estimate diffusion coefficients, assuming that full-scale bending corresponded to the centre of the strip being sufficiently plasticised by CO_2 to become rubbery.

Keywords: *Glass transition, linear variable displacement transducer, softening.*

- Saudi Innovation International Conference Leeds UK (9 -10 June 2008)

ISBN: 978-0-9559241-2-5

Foaming Behaviour of Polystyrene Containing Dissolved CO_2 during Depressurisation

S. Al-Enezi, K. Hellgardt, I. Cumming and A.G.F. Stapley

Department of Chemical Engineering, Loughborough University, Loughborough, Leicestershire, LE11 3TU, UK.

Abstract

This paper examines the effects derived from the ability of high pressure carbon dioxide to foam polystyrene. This has potential applications in the shape foaming of polymers at lower temperatures, dye impregnation and the foaming of polystyrene. This study was conducted in foaming behaviour of polystyrene containing dissolved CO_2 during depressurisation. In this study the polymer foaming was investigated using cylindrical high pressure view cell with 2 optical widows. This study differs from previous published work in that conditions were chosen to be near the glass transition temperature (T_g) of the polymer. Foaming was not observed when the polymer was initially at conditions below T_g, but was observed above the T_g. The radius of bubbles was measured with time and the results compared against models for bubble growth. Best fits were obtained with a viscous-diffusion model.

Keywords: *Foaming, CO_2, polystyrene, optical cell, bubble growth model.*

Awarded

- ***"This paper has awarded the prize of the best research work in UK by National Union of Kuwaiti Student (NUKS) and Kuwait Institute for Scientific Research (KISR) for the year of 2005-2006".***

Kuwait Institute for Scientific Research

Novel Processing of Polymers Using High Pressure Carbon Dioxide

Salah Al-Enezi

Department of Chemical Engineering, Loughborough University, Loughborough, Leicestershire, LE11 3TU, UK.

ملخـص البحـث

علم تلين أو تمييع المواد شائع الاستخدام في العمليات البولمرية ولذلك لما يعمل علي تقليل درجة ليونة البولمر وبالتالي يسهل التعامل مع هذه المواد عند درجات حرارة اقل وبصوره أفضل. مهارة وقدرة غاز ثاني أكسيد الكاربو ن علي العمل كملين لهذة المواد الصناعية عرض بشكل كامل وبإستئدال تفصيلي من احد اشهر الأجهزة المستخدمة (FTIR) في هذا المجال، بالرغم من انه من اشهر وأدق الأجهزة المستخدمة إلا انه يقيس فقط درجة ليونة سطح المادة. غاز ثاني أكسيد الكربون من أفضل أنواع الغازات المصاحبة للبيئة وذلك لعدم تركة أي مواد ضاره، ولكن لو أردنا دراسة درجه الليونه للمادة ككل من حيث السطح الخارجي وكذلك من داخل المادة نحتاج أن ندرس المادة ميكانيكيا للتأكد من ليونتها من الداخل والخارج. هذه الورقة العلمية تعرض نتائج من جهاز فحص ميكانيكي ثلاثي الضغط لسمكات مختلفة 2 ملم و 3 ملم لمواد صناعية بولمرية. هذا الجهاز مزود ب (LVDT) وذلك لقياس درجة الليونة وكذلك مزود بمقياس حراري بلاتنيمي (PRT) قريب من العينة لقياس الحرارة العينة. درجه التحول من الحالة الصلبة إلي الحالة شبه لينه هي الدرجة التي سجلت كحاله بداية التحول وهي بداية فقد العينة للحالة الصلبه (الزجاجيه) واكتسابها الحالة الشبه لينه (الربليه). تراجع ملحوظ في درجة الليونة إلي ما يقارب 40 درجة سيليزيه علي الضغط المستخدم والعينات التي تمت الدراسة عليها هي PS , PETG, PMMA , PC . وكذلك حدثت أمور مهمة عندما تم تفريغ الغاز من العينة وذلك أن الغاز يتمدد مع العينة ويحدث فقاعات ورغوه علي سطح العينة وكذلك لوحظ أن هناك اختلاف في حجم وكميه الفقاعات وذلك بسبب طريقه إفراغ الغاز والوقت الذي يتم تفريقه الغاز فيه وجاري الآن البحث والتحري في هذا المجال لإكتشاف المزيد.

ABSTRACT

Plasticisers are commonly used in polymer processing as they lower the glass transition (softening) temperature of polymers to allow shape forming at lower temperatures. The ability of carbon dioxide at high pressure to act as a plasticiser of certain synthetic polymers has been well documented in the literature on the basis of evidence from FTIR spectroscopy. However, FTIR only measures conditions on the surface of polymers. Carbon dioxide is an environmentally attractive solvent and leaves virtually no residue in the polymer on return to ambient pressure, but if plasticisation is to be an effective for shape forming polymers the effect also needs to be demonstrated mechanically, which requires softening to occur throughout the sample. This paper presents results from 3-point bend test experiments on 2 mm and 3 mm thick polymer strips in a temperature controlled high pressure cell. This is equipped with a linear variable displacement transducer (LVDT) to measure the central deflection, and a platinum resistance probe (PRT) located close to the sample in the cell to measure temperature. The nominal glass transition temperature was recorded as the onset temperature where the central deflection suddenly begins to increase. Significant reductions in the bending onset temperatures were observed on the application of carbon dioxide (typically 40 ^{0}C reductions for 120 bar applied pressure) for polycarbonate, polymethyl methacrylate, polyethylene terepthalate and polystyrene. Interesting effects were also observed to take place during de-pressurisation, as the carbon dioxide gas can expand within the material to create a foamed structure. Variations in bubble size and number were found to depend on de-pressurisation methods and this is the subject of ongoing investigations.

Keywords: *Glass transition temperature, softening, depressurization, supercritical fluids.*